INVESTIGATING AND ACCOUNTING FOR NON-STATIONARY DATA IN DESIGN RAINFALL AND FLOOD ESTIMATION:

CASE STUDY IN KWAZULU-NATAL, SOUTH AFRICA

Report to the
Water Research Commission

by

KA Johnson, JC Smithers and DV Mukansi

with contributions by

RE Schulze, TR Kjeldsen, S Schütte and JA du Plessis

School of Engineering and Centre for Water Resources Research
College of Agriculture, Engineering and Science
University of KwaZulu-Natal

WRC Report No. 3147/1/24
ISBN 978-0-6392-0626-4

May 2024

WATER
RESEARCH
COMMISSION

Obtainable from
Water Research Commission
Bloukrans Building, Lynnwood Bridge Office Park
4 Daventry Street
Lynnwood Manor
PRETORIA

orders@wrc.org.za or download from www.wrc.org.za

This is the final report of WRC project no. C2022/2023-00773.

EXECUTIVE SUMMARY

Introduction

Standard methods for frequency analysis of extreme rainfall and flood events assume a stationary climate, i.e. the statistics of the data do not change over time. However, the reported increase in the occurrence of extreme rainfalls leading to catastrophic flood events has raised the questions of whether changes in the magnitude and frequency of observed extreme rainfall events are already evident in South Africa, what the drivers of these changes are, and what the potential impacts on design rainfall estimation and consequently on flood risk assessment could be for in South Africa. Accurate estimations of design floods are required to limit the risk to loss of life and failure of, or over expenditure on, hydraulic structures. The needs to develop methods to account for non-stationary data, and to update design rainfall estimation methods to include possible trends in extreme rainfall events in a changing environment, have been identified as high priority research areas in the National Flood Studies Programme (NFSP) (Smithers *et al.*, 2016). The damage and loss of life caused by recent (2022) flooding across KwaZulu-Natal, and the realisation of possible increased rainfall variability in the future, highlight the fact that Design Flood Estimation (DFE) techniques currently used in South Africa are outdated and need revision.

The impact of a changing climate has become a key concern in South Africa, where temperatures shown a greater increase compared to observed global averages (Ziervogel *et al.*, 2014), and the highest recorded temperatures have been documented in recent years (Moyo and Nyoni (2021). Generally, heavy rainfalls are related to warmer atmospheric conditions. McBride *et al.* (2022) noted that the probability of significant extreme daily rainfall events occurring has increased for most parts of South Africa. Many observations of global climate trends have raised an increasing concern that the extreme rainfalls, including the Probable Maximum Precipitation (PMP) needed for the design of high-hazard hydraulic infrastructure, will change as a result of the influence of a changing climate (Rouhani, 2016). Johnson and Smithers (2020) revised the 1-day PMPs in South Africa using an updated rainfall database and a modernized methodology and highlighted that many of the extreme events noted in their study occurred after the previously estimated PMPs were published in HRU (1972). Hence, it is critical to update PMP estimates currently used in industry, which were derived on the

assumption of stationary data, and use this information to estimate the potential impacts of the changing climate on extreme rainfall estimation.

Internationally, numerous research institutions are investigating non-stationarity in flooding using modelled future climate data. With the increasing availability of climate model data through Global Circulation Models (GCMs), there is greater opportunity to use such data to determine the potential impacts of future climate scenarios on extreme rainfall and flood events using advanced statistical techniques, and to develop methods/tools to incorporate these trends in design rainfall and flood estimation.

Given the importance of flood risk management, the shortcomings of the methods currently used by practitioners for DFE and the potential impact of climate change, dealing with a non-stationary climate data series currently requires urgent attention in South Africa (Johnson *et al.*, 2021). A method to account for non-stationary data which incorporates the impacts of a changing climate in extreme design rainfall estimates in South Africa needs to be developed using regional approaches to detect trends in historical data.

Aims of the Project

Given the background provided above, the aims of this project are therefore to undertake the following for South Africa:

(a) To review and refine the updated 1-day PMP estimates;
(b) To develop and assess the performance of a method to account for the impacts of non-stationary data on PMP estimation;
(c) To develop and assess the performance of a method to account for the impacts of non-stationary data on design rainfall estimation; and
(d) To assess the trends in hydrological extremes and investigate the use of regional magnification factors.

Aims (a and b): Updating the 1-day PMP

The PMP is the theoretical upper limit of extreme rainfall and is widely used by engineers and hydrologists to determine the Probable Maximum Flood (PMF) which is critical for the design and risk management of high-hazard hydraulic structures. In South Africa, the PMP was last estimated over 50 years ago using approximately 30 years of data. Since then, numerous severe rainfall events have occurred which exceed presently available PMP estimates. Despite this, the outdated estimates are currently used in professional practice. In addition, modernised methods have been developed and applied globally to estimate the PMP, highlighting the need to update the PMP estimates for South Africa.

The aims (a) and (b) of this study were to present updated 1-day PMP estimates for South Africa using an updated database and modernised methods, accounting for possible impacts of non-stationarity. The objectives were to: (i) report on the collation of an updated hydro-meteorological database, (ii) estimate the PMP using appropriate hydro-meteorological methods prescribed by the WMO, (iii) to critically evaluate the newly derived PMP estimates, and (iv) disseminate the new knowledge on the updated 1-day PMP through a workshop.

Using updated rainfall records, compared to previous studies, and a storm maximisation and transposition approach, this Chapter of the report provides new 1-day PMP estimates for the country. The importance of revising the PMP to include new extreme rainfall events is highlighted as the majority of the events used in this study occurred after the publication of the previous estimates. The use of extended rainfall records and modernised methods produces generally larger PMP estimates compared to the previous estimates. It is noteworthy that the majority of the extreme events used in this analysis occurred after the publication of the previous studies and currently used guidelines. Continual revision of the PMP is recommend to include new extreme rainfall events.

Despite recent developments in PMP estimation in South Africa, there have been no formal or official changes to the guidelines used by practitioners. As such, a workshop was needed to inform practitioners of the new methods available to estimate the 1-day PMP in South Africa, and to provide supporting material to facilitate the use of the updated PMP estimates in

industry. The workshop was held on Thursday, 25 May 2023 at Stellenbosch University, both in-person and online, and was attended by a variety of academic researchers, industry practitioners and stakeholders. The presentation slides, journal article and booklet materials, as well as the gridded PMP database and all supporting materials can be accessed via the Water Research Observatory website.

Aim (c): Non-stationary Frequency Analysis of Extreme Rainfall Events on the East Coast of KwaZulu-Natal

Extreme flood events can damage hydrological structures such as dam walls, spillways, bridges, and culverts. Therefore, minimising the risk of failure of hydraulic structures requires design floods be estimated accurately. The underestimation of design floods and failure of hydraulic structures can lead to loss of life and significant economic losses, while overestimation may result in over-design which results in excessive construction and maintenance costs. Recent large floods include the events in 2019 and 2022 experienced along the eastern coast of South Africa and have been reported to have resulted in infrastructural damages of billions of Rands, with thousands of people affected (Singh, 2019; Pinto *et al*; 2022).

Traditional methods for frequency analysis of extreme events and most current risk assessment models are based on techniques and concepts developed nearly a century ago (e.g. Fuller, 1914) and are based on the assumption of climate stationarity. However, anthropogenically induced climate change has resulted in changes in extreme weather events, thus questioning the assumption of stationarity (Serinaldi and Kilsby, 2015). In recent years, the frequency and impacts of extremes have increased substantially in many parts of South Africa (Thoithi *et al.*, 2023). Hence, there is significant interest in understanding how extreme events may change into the future and how frequency analyses should be adapted to account for non-stationary data.

Aim (c) of the study, undertaken as a pilot study on the East Coast of KwaZulu-Natal, was to determine if any trends exist in observed extreme rainfall events in order to contribute to an understanding of the teleconnection patterns between various climate drivers and the annual

maximum daily extreme rainfall and to account for possible non-stationary climate data in the estimation of extreme design rainfall events in South Africa. The objectives of this component of the study were to: (i) investigate trends in annual maximum daily rainfall using parametric and non-parametric statistical tests, (ii) identify potential climate drivers of extreme rainfalls, (iii) perform stationary and non-stationary rainfall frequency analyses, (iv) critically evaluate the stationary vs non-stationary models, and (v) evaluate projected changes in rainfall using GCMs.

In terms of rainfall data analyses undertaken in this study, the annual maximum daily rainfall from 39 observational stations in KwaZulu-Natal, located along the east coast of South Africa, were analysed. The existence of temporal trends in the data series were investigated using non-parametric tests. The results indicate weak evidence that the annual maximum daily rainfalls have been increasing in magnitude over time. The trends detected varied across the sites, with approximately 40% of sites showing a positive trend, only one of which showed a statistically significant increasing trend. Non-stationary extreme value statistical analysis was used to explore the utility of rainfall relationships in KZN with various potential climate drivers to predict possible future impacts on extreme rainfall. Several non-stationary models, using time and various climate drivers as covariates (Southern Oscillation Index, Dipole Mode Index, CO_2, and Global Mean Temperature), were developed, and compared to the standard stationary models. Most rainfall records indicate that a stationary behaviour is dominant. The variability of the results of the trend and non-stationary analyses highlights the importance of understanding the trends and drivers of extreme rainfalls and the impacts on design rainfall and design flood estimation. To improve the study, the use of other physical covariates, as well as combinations of covariates, should be explored.

Changes in atmospheric CO_2 explain the largest proportion of variability in the rainfall data relative to other covariates considered in the study. The projected changes in rainfall were analysed using Global Circulation Models (GCMs) to derive possible climate change factors, or ratios, that could be applied to current design rainfall depths to design for future scenarios. The ratios of changes from the present to the near future climate periods, and from the present to the distant future climate periods for design rainfall were derived. Design rainfalls are projected to remain stable into the near future compared to the present, with increases of

approximately 10%, and ratios increasing with an increase in return period. Projected changes into the distant future show a 10-30% increase in design rainfalls in many locations in the study area. These results could vary elsewhere in the country. It is recommended that the use of projected trends in rainfalls from GCMs should be informed by the considerations based on the observed rainfall data trends.

Aim (d): Detecting Trends in Hydrological Extremes and Non-Stationary Extreme Value Analysis of Flood Data in KwaZulu-Natal

As with rainfall analysis, the current methods and models used to determine design flood estimates from flow data assume that hydrological processes and upstream land uses as well as river and dam abstractions remain stationary (Vogel *et al.*, 2011). However, the magnitude and frequency of extreme flood events is changing in many parts of the world (Vogel *et al.*, 2011; Prosdocimi *et al.*, 2014a; Hesarkazzazi *et al.*, 2021). Therefore, there is a need to investigate, and incorporate if necessary, non-stationary models in DFE in South Africa.

This section includes an analysis of trends in extreme floods along the East Coast of KwaZulu-Natal in South Africa. This study site was selected to complement and correspond to the rainfall analyses in Aim (c). The aims of this component of the study were to determine if any trends exist in observed extreme flood events on the East Coast of KwaZulu-Natal, and to evaluate the possible non-stationarity in observed flow data. The objectives were to: (i) collect, screen, and analyse streamflow data for trends, (ii) perform stationary and non-stationary flood frequency analyses, (iii) critically evaluate the stationary vs non-stationary models, and (iv) investigate regional magnification factors to detect trends.

The annual maximum streamflows from 19 stations in KwaZulu-Natal, along the East Coast of South Africa, were analysed. Non-parametric trends were investigated, and the results indicate that the annual maximum streamflow has been decreasing in magnitude and frequency in the majority of stations. Extreme value analysis was performed using both stationary and non-stationary models using time and rainfall as covariates. Similar to rainfall, the results show that the stationary models are superior to non-stationary models at most stations with time as a covariate. Where possible, streamflow stations were linked with rainfall stations to determine

the impact of rainfall on annual maximum streamflow. The results indicate that the non-stationary model incorporating observed rainfall as a covariate performed better than the stationary model as well as the non-stationary model with only time as a covariate. Therefore, incorporation of rainfall in DFE should be considered to account for non-stationary trends and to mitigate the risk of failure of hydraulic structures. Regional magnification factors to account for non-stationarity were thus not investigated further in this study as the majority of the stations showed a negative trend, which means application of a regional magnification factor would result in a reduction of the magnitude of the estimated design floods.

Conclusions

The outcomes presented in this report are sometimes contrary to the outputs from GCMs reported in international studies and to reported increases in extreme events in South Africa. These results may differ elsewhere in the country and this study has highlighted the need to investigate trends and non-stationarity in other parts of the country located in different climate zones and with up-to-date datasets. Further analysis of data for various event durations (e.g. sub-daily or multi-day events) are recommended. Given the generally weak positive trends in rainfall data and negative trends in the annual maximum flow data, alternative more detailed analysis methods, such as the peak over threshold approach, are recommended for future research.

Capacity Building Report

This project has contributed to the support for two postgraduate students. Of these, one student, being the project leader, has graduated with a PhD in Engineering. Another student has made progress towards his PhD research. In addition, the project leader is an early career researcher who has gained experience leading this project. This research has been shared at local and international conferences and has been presented at the annual NFSP workshops, attended by practitioners, stakeholders, and researchers.

ACKNOWLEDGEMENTS

The funding of the project by the Water Research Commission and the contribution of the members of the Reference Group members is acknowledged gratefully.

Mr W Nomquphu	Water Research Commission (Chair)
Ms P Jaca	Water Research Commission (Coordinator)
Mr CJ Brooker	CBA Consulting
Mr E Oakes	DWS
Dr OJ Gericke	CUT
Prof J Ndiritu	University of Witwatersrand
Prof SJ Van Vuuren	University of Stellenbosch
Dr P Wolski	UCT
Dr R Odoulami	UCT
Dr B Abiodun	UCT
Mr M Parak	SANRAL
Mr A Trollip	Anglo American
Prof B Hewitson	UCT
Prof A Görgens	Zutari

TABLE OF CONTENTS

Page

EXECUTIVE SUMMARY iii
ACKNOWLEDGEMENTS x
TABLE OF CONTENTS xi
LIST OF TABLES xiii
LIST OF FIGURES xiv
1. INTRODUCTION 1
2. UPDATING THE 1-DAY PMP ESTIMATES 6
2.1 Introduction 6
2.2 Study Area and Data 7
2.2.1 Homogeneous Rainfall Districts 7
2.2.2 Hydro-meteorological Data 8
2.3 Methodology – PMP Estimation Using the Generalised Estimation Method 10
2.3.1 Selection of extreme rainfall events 10
2.3.2 Moisture maximisation 11
2.3.3 Transposition 13
2.3.4 Isohyetal Patterns and Adjustment of the Interpolated Surface 14
2.4 Results and Discussion 15
2.4.1 Consideration of Extraordinary PMPs 16
2.4.2 Consideration of Large Moisture Maximisation Ratios 17
2.4.3 Comparison of New PMP Values to HRU PMP 18
2.4.4 Comparison to the 1:500-year and 1:1000-year Rainfalls 21
2.5 Knowledge Dissemination Workshop 22
2.5.1 Structure of the Workshop 23
2.5.2 Workshop materials 23
2.6 Conclusions 24
3. NON-STATIONARY FREQUENCY ANALYSIS OF EXTREME RAINFALL EVENTS ON THE EAST COAST OF KWAZULU-NATAL 26
3.1 Introduction 26
3.2 Materials and Methods 28
3.2.1 Data sources and case study site selection 28

3.2.2 Methodology 31
3.3 Results and Discussion 36
3.3.1 Trend detection 36
3.3.2 Analysis of stationary and non-stationary models 39
3.3.3 Projected changes in rainfall 44
3.4 Conclusions 47
4. DETECTING TRENDS IN HYDROLOGICAL EXTREMES AND NON-STATIONARY EXTREME VALUE ANALYSIS OF FLOOD DATA IN KWAZULU-NATAL 50
4.1 Introduction 50
4.2 Materials and Methods 51
4.2.1 Data sources and case study site selection 51
4.2.2 Data screening and assessment 52
4.2.3 Methodology 54
4.3 Results and Discussion 58
4.3.1 Homogeneity test 58
4.3.2 Trend detection 58
4.3.3 Analysis of stationary and non-stationary models 59
4.3.4 Linking rainfall to flow 63
4.4 Conclusions 68
5. DISCUSSIONS, CONCLUSIONS AND RECOMMENDATIONS 70
6. CAPACITY BUILDING 73
7. REFERENCES 74
8. APPENDIX A: Updating the 1-day PMP Estimates 86
9. APPENDIX B: Non-stationary Frequency Analysis of Extreme Rainfalls in KwaZulu-Natal 89
10. APPENDIX C: Non-stationary Frequency Analysis of Extreme Floods in KwaZulu-Natal 156

LIST OF TABLES

Page

Table 2.1 Comparison of the HRU approach and the new approach for estimating PMP 21

Table 3.1 Station information for case study sites 30

Table 3.2 Trends in KwaZulu-Natal extreme rainfall using the Mann-Kendall test 38

Table 3.3 The GEV statistical model performance criteria of selected sites in KwaZulu-Natal AMDR for time as a covariate 39

Table 3.4 Summary of best-fit models for all stationary and non-stationary cases 43

Table 4.1 Station information for case study sites along the East Coast of KwaZulu-Natal 53

Table 4.2 Summary of studies that made use of non-stationary models in design flood estimation (after Prosdocimi and Kjeldsen (2021) 57

Table 4.3 Homogenity test of DWS stations in the East Coast of KwaZulu-Natal 58

Table 4.4 Trends in annaul maximum streamflows at stations along the East Coast of KwaZulu-Natal using the Mann-Kendall test 59

Table 4.5 The LP3 statistical model selection criteria of selected sites in the East Coast of KwaZulu-Natal AMS for time as a covariate 60

Table 4.6 Summary of best-fit models for all stationary and non-stationary cases 64

Table 6.1 List of students involved in the project 73

Table 8.1 Critical analysis of selected stations with large moisture maximisation ratios 87

Table 9.1 The GEV statistical model performance criteria of KwaZulu-Natal AMDR for all covariates 94

Table 10.1 The LP3 statistical model performance criteria for all covariates 173

LIST OF FIGURES

Page

Figure 2.1 (a) Locations of selected rainfall stations with at least 40 years of daily record and (b) distribution of record lengths for selected rainfall stations 9
Figure 2.2 PMP estimation procedure 10
Figure 2.3 Locations of the 380 representative stations 11
Figure 2.4 Example of residual error in interpolated PMP surface 14
Figure 2.5 Technique for adjusting the residuals in the interpolated PMP surface 15
Figure 2.6 Map of 1-day PMP estimates for South Africa 16
Figure 2.7 Locations of selected stations with large moisture maximisation ratios 18
Figure 2.8 Comparison ratios of new PMP to HRU PMP 19
Figure 2.9 Comparison of the new PMP to the HRU PMP for Rainfall District 70 19
Figure 2.10 Comparison of the New PMP and HRU PMP derived from the same observed rainfall event 20
Figure 2.11 Comparison of the (a)1:500-year rainfall, (b) 1:1000-year rainfall and (c) PMP, and (d) summary of exceedances of the PMP 22
Figure 3.1 SASRI stations in KwaZulu-Natal selected for this study 29
Figure 3.2 Stationary and non-stationary design rainfall estimation procedures 32
Figure 3.3 Time series for Station 38 37
Figure 3.4 The GEV (a) stationary model, (b) non-stationary model considering time as a covariate, and (c) effective return period as a function of time for Station 38: Sezela – Illovo Sugar Estate 42
Figure 3.5 Best-fit distribution model, based on the AIC measure 43
Figure 3.6 Best-fit distribution model, based on the BIC measure 44
Figure 3.7 Projected changes from the present to the near future in design rainfalls for 1-day design rainfalls for the 2-, 10-, 50-, and 100-year return periods, derived from outputs from multiple GCMs 46
Figure 3.8 Projected changes from the present to the distant future in design rainfalls for 1-day design rainfalls for the 2-, 10-, 50-, and 100-year return period, derived from outputs from multiple GCMs 47
Figure 4.1 Selected DWS streamflow recording stations along the East Coast of KwaZulu-Natal 53

Figure 4.2 Stationary and non-stationary design flood estimation procedures 54
Figure 4.3 The LP3 (a) stationary model, (b) non-stationary model considering time as a covariate, and (c) effective return period as a function of time for Station W4H012 61
Figure 4.4 Best-fit distribution model, based on the AIC measure 62
Figure 4.5 Best-fit distribution model, based on the BIC measure 62
Figure 4.6 Time series for annual maximum streamflow and rainfall stations in the East Coast of KwaZulu-Natal 66
Figure 4.7 Best-fit distribution model, based on the AIC measure for flow stations linked with a rainfall station.....67
Figure 4.8 Best-fit distribution model, based on the BIC measure for flow stations linked with a rainfall station.....67
Figure 8.1 Homogeneous rainfall districts for South Africa 86
Figure 8.2 Map of Annual Maximum Daily Rainfalls for South Africa 86
Figure 9.1 Time series of all annual maximum rainfalls at all SASRI stations used in this research 93
Figure 9.2 The GEV (a) stationary model, (b) non-stationary model considering time as a covariate, (c) non-stationary model considering SOI as a covariate, (d) non-stationary model considering DMI as a covariate, (e) non-stationary model considering CO_2 as a covariate, (f) non-stationary model considering GMT as a covariate and (g) effective return period as a function of time for Station 6: Pongola – SASRI 96
Figure 9.3 The GEV (a) stationary model, (b) non-stationary model considering time as a covariate, (c) non-stationary model considering SOI as a covariate, (d) non-stationary model considering DMI as a covariate, (e) non-stationary model considering CO_2 as a covariate, (f) non-stationary model considering GMT as a covariate and (g) effective return period as a function of time for Station 8: Glen Park – St Lucia Farms 97

Figure 9.4 The GEV (a) stationary model, (b) non-stationary model considering time as a covariate, (c) non-stationary model considering SOI as a covariate, (d) non-stationary model considering DMI as a covariate, (e) non-stationary model considering CO_2 as a covariate, (f) non-stationary model considering GMT as a covariate and (g) effective return period as a function of time for Station 9: Mtubatuba – Riverview Sugar Mill 98

Figure 9.5 The GEV (a) stationary model, (b) non-stationary model considering time as a covariate, (c) non-stationary model considering SOI as a covariate, (d) non-stationary model considering DMI as a covariate, (e) non-stationary model considering CO_2 as a covariate, (f) non-stationary model considering GMT as a covariate and (g) effective return period as a function of time for Station 11: Mtunzini – ex SASRI 99

Figure 9.6 The GEV (a) stationary model, (b) non-stationary model considering time as a covariate, (c) non-stationary model considering SOI as a covariate, (d) non-stationary model considering DMI as a covariate, (e) non-stationary model considering CO_2 as a covariate, (f) non-stationary model considering GMT as a covariate and (g) effective return period as a function of time for Station 12: Melmoth – CA Leith & Sons 100

Figure 9.7 The GEV (a) stationary model, (b) non-stationary model considering time as a covariate, (c) non-stationary model considering SOI as a covariate, (d) non-stationary model considering DMI as a covariate, (e) non-stationary model considering CO_2 as a covariate, (f) non-stationary model considering GMT as a covariate and (g) effective return period as a function of time for Station 18: Glendale – Tenrith Farm 101

Figure 9.8 The GEV (a) stationary model, (b) non-stationary model considering time as a covariate, (c) non-stationary model considering SOI as a covariate, (d) non-stationary model considering DMI as a covariate, (e) non-stationary model considering CO_2 as a covariate, (f) non-stationary model considering GMT as a covariate and (g) effective return period as a function of time for Station 20: Tongaat – Klipfontein (THS) 102

Figure 9.9 The GEV (a) stationary model, (b) non-stationary model considering time as a covariate, (c) non-stationary model considering SOI as a covariate, (d) non-stationary model considering DMI as a covariate, (e) non-stationary model considering CO_2 as a covariate, (f) non-stationary model considering GMT as a covariate and (g) effective return period as a function of time for Station 22: Seven Oaks – Saw Mill 103

Figure 9.10 The GEV (a) stationary model, (b) non-stationary model considering time as a covariate, (c) non-stationary model considering SOI as a covariate, (d) non-stationary model considering DMI as a covariate, (e) non-stationary model considering CO_2 as a covariate, (f) non-stationary model considering GMT as a covariate and (g) effective return period as a function of time for Station 23: Noodsberg – Illovo Sugar Mill 104

Figure 9.11 The GEV (a) stationary model, (b) non-stationary model considering time as a covariate, (c) non-stationary model considering SOI as a covariate, (d) non-stationary model considering DMI as a covariate, (e) non-stationary model considering CO_2 as a covariate, (f) non-stationary model considering GMT as a covariate and (g) effective return period as a function of time for Station 26: Illovo – Sugar Estate 105

Figure 9.12 The GEV (a) stationary model, (b) non-stationary model considering time as a covariate, (c) non-stationary model considering SOI as a covariate, (d) non-stationary model considering DMI as a covariate, (e) non-stationary model considering CO_2 as a covariate, (f) non-stationary model considering GMT as a covariate and (g) effective return period as a function of time for Station 27: Vulamehlo – Esperanza 106

Figure 9.13 The GEV (a) stationary model, (b) non-stationary model considering time as a covariate, (c) non-stationary model considering SOI as a covariate, (d) non-stationary model considering DMI as a covariate, (e) non-stationary model considering CO_2 as a covariate, (f) non-stationary model considering GMT as a covariate and (g) effective return period as a function of time for Station 29: Mt Edgecombe – SASRI 107

Figure 9.14 The GEV (a) stationary model, (b) non-stationary model considering time as a covariate, (c) non-stationary model considering SOI as a covariate, (d) non-stationary model considering DMI as a covariate, (e) non-stationary model considering CO_2 as a covariate, (f) non-stationary model considering GMT as a covariate and (g) effective return period as a function of time for Station 38: Sezela – Illovo Sugar Estate 108
Figure 9.15 The GEV (a) stationary model, (b) non-stationary model considering time as a covariate, (c) non-stationary model considering SOI as a covariate, (d) non-stationary model considering DMI as a covariate, (e) non-stationary model considering CO_2 as a covariate, (f) non-stationary model considering GMT as a covariate and (g) effective return period as a function of time for Station 105: Oribi Flats – Minnehaha Farm.....109
Figure 9.16 The GEV (a) stationary model, (b) non-stationary model considering time as a covariate, (c) non-stationary model considering SOI as a covariate, (d) non-stationary model considering DMI as a covariate, (e) non-stationary model considering CO_2 as a covariate, (f) non-stationary model considering GMT as a covariate and (g) effective return period as a function of time for Station 110: Renishaw – Crooks Bros Estate.....110
Figure 9.17 The GEV (a) stationary model, (b) non-stationary model considering time as a covariate, (c) non-stationary model considering SOI as a covariate, (d) non-stationary model considering DMI as a covariate, (e) non-stationary model considering CO_2 as a covariate, (f) non-stationary model considering GMT as a covariate and (g) effective return period as a function of time for Station 111: Powerscourt – Roseleigh Estate.....111
Figure 9.18 The GEV (a) stationary model, (b) non-stationary model considering time as a covariate, (c) non-stationary model considering SOI as a covariate, (d) non-stationary model considering DMI as a covariate, (e) non-stationary model considering CO_2 as a covariate, (f) non-stationary model considering GMT as a covariate and (g) effective return period as a function of time for Station 114: Inanda – Farm 112

Figure 9.19 The GEV (a) stationary model, (b) non-stationary model considering time as a covariate, (c) non-stationary model considering SOI as a covariate, (d) non-stationary model considering DMI as a covariate, (e) non-stationary model considering CO_2 as a covariate, (f) non-stationary model considering GMT as a covariate and (g) effective return period as a function of time for Station 120: Inyaninga – THS 113
Figure 9.20 The GEV (a) stationary model, (b) non-stationary model considering time as a covariate, (c) non-stationary model considering SOI as a covariate, (d) non-stationary model considering DMI as a covariate, (e) non-stationary model considering CO_2 as a covariate, (f) non-stationary model considering GMT as a covariate and (g) effective return period as a function of time for Station 123: Maidstone – Sugar Mill (THS) 114
Figure 9.21 The GEV (a) stationary model, (b) non-stationary model considering time as a covariate, (c) non-stationary model considering SOI as a covariate, (d) non-stationary model considering DMI as a covariate, (e) non-stationary model considering CO_2 as a covariate, (f) non-stationary model considering GMT as a covariate and (g) effective return period as a function of time for Station 125: Sinembe – Spreyton Farm 115
Figure 9.22 The GEV (a) stationary model, (b) non-stationary model considering time as a covariate, (c) non-stationary model considering SOI as a covariate, (d) non-stationary model considering DMI as a covariate, (e) non-stationary model considering CO_2 as a covariate, (f) non-stationary model considering GMT as a covariate and (g) effective return period as a function of time for Station 126: Upper Tongaat – Barwon Farm 116
Figure 9.23 The GEV (a) stationary model, (b) non-stationary model considering time as a covariate, (c) non-stationary model considering SOI as a covariate, (d) non-stationary model considering DMI as a covariate, (e) non-stationary model considering CO_2 as a covariate, (f) non-stationary model considering GMT as a covariate and (g) effective return period as a function of time for Station 129: Kearsney – Ocean Lodge 117

Figure 9.24 The GEV (a) stationary model, (b) non-stationary model considering time as a covariate, (c) non-stationary model considering SOI as a covariate, (d) non-stationary model considering DMI as a covariate, (e) non-stationary model considering CO_2 as a covariate, (f) non-stationary model considering GMT as a covariate and (g) effective return period as a function of time for Station 130: Doornkop – Langespruit Farm 118
Figure 9.25 The GEV (a) stationary model, (b) non-stationary model considering time as a covariate, (c) non-stationary model considering SOI as a covariate, (d) non-stationary model considering DMI as a covariate, (e) non-stationary model considering CO_2 as a covariate, (f) non-stationary model considering GMT as a covariate and (g) effective return period as a function of time for Station 131: Darnall – Sugar Mill (THS) 119
Figure 9.26 The GEV (a) stationary model, (b) non-stationary model considering time as a covariate, (c) non-stationary model considering SOI as a covariate, (d) non-stationary model considering DMI as a covariate, (e) non-stationary model considering CO_2 as a covariate, (f) non-stationary model considering GMT as a covariate and (g) effective return period as a function of time for Station 132: Tugela Mouth – Wetherly Estate 120
Figure 9.27 The GEV (a) stationary model, (b) non-stationary model considering time as a covariate, (c) non-stationary model considering SOI as a covariate, (d) non-stationary model considering DMI as a covariate, (e) non-stationary model considering CO_2 as a covariate, (f) non-stationary model considering GMT as a covariate and (g) effective return period as a function of time for Station 136: Glenside – Misty Krantz Estate 121
Figure 9.28 The GEV (a) stationary model, (b) non-stationary model considering time as a covariate, (c) non-stationary model considering SOI as a covariate, (d) non-stationary model considering DMI as a covariate, (e) non-stationary model considering CO_2 as a covariate, (f) non-stationary model considering GMT as a covariate and (g) effective return period as a function of time for Station 138: Mandini – SAWS 122

Figure 9.29 The GEV (a) stationary model, (b) non-stationary model considering time as a covariate, (c) non-stationary model considering SOI as a covariate, (d) non-stationary model considering DMI as a covariate, (e) non-stationary model considering CO_2 as a covariate, (f) non-stationary model considering GMT as a covariate and (g) effective return period as a function of time for Station 139: Inyoni – Myrln Estate 123
Figure 9.30 The GEV (a) stationary model, (b) non-stationary model considering time as a covariate, (c) non-stationary model considering SOI as a covariate, (d) non-stationary model considering DMI as a covariate, (e) non-stationary model considering CO_2 as a covariate, (f) non-stationary model considering GMT as a covariate and (g) effective return period as a function of time for Station 142: Eshowe – Brocklee Farm 124
Figure 9.31 The GEV (a) stationary model, (b) non-stationary model considering time as a covariate, (c) non-stationary model considering SOI as a covariate, (d) non-stationary model considering DMI as a covariate, (e) non-stationary model considering CO_2 as a covariate, (f) non-stationary model considering GMT as a covariate and (g) effective return period as a function of time for Station 143: Nkwaleni – Zigagazi 125
Figure 9.32 The GEV (a) stationary model, (b) non-stationary model considering time as a covariate, (c) non-stationary model considering SOI as a covariate, (d) non-stationary model considering DMI as a covariate, (e) non-stationary model considering CO_2 as a covariate, (f) non-stationary model considering GMT as a covariate and (g) effective return period as a function of time for Station 144: Felixton – Sugar Mill (THS).....126
Figure 9.33 The GEV (a) stationary model, (b) non-stationary model considering time as a covariate, (c) non-stationary model considering SOI as a covariate, (d) non-stationary model considering DMI as a covariate, (e) non-stationary model considering CO_2 as a covariate, (f) non-stationary model considering GMT as a covariate and (g) effective return period as a function of time for Station 146: Kulu Halt – Honey Farm.....127

Figure 9.34 The GEV (a) stationary model, (b) non-stationary model considering time as a covariate, (c) non-stationary model considering SOI as a covariate, (d) non-stationary model considering DMI as a covariate, (e) non-stationary model considering CO_2 as a covariate, (f) non-stationary model considering GMT as a covariate and (g) effective return period as a function of time for Station 147: Ukulu Properties – Crystal Holdings 128

Figure 9.35 The GEV (a) stationary model, (b) non-stationary model considering time as a covariate, (c) non-stationary model considering SOI as a covariate, (d) non-stationary model considering DMI as a covariate, (e) non-stationary model considering CO_2 as a covariate, (f) non-stationary model considering GMT as a covariate and (g) effective return period as a function of time for Station 148: Mposa – Redcroft Farm 129

Figure 9.36 The GEV (a) stationary model, (b) non-stationary model considering time as a covariate, (c) non-stationary model considering SOI as a covariate, (d) non-stationary model considering DMI as a covariate, (e) non-stationary model considering CO_2 as a covariate, (f) non-stationary model considering GMT as a covariate and (g) effective return period as a function of time for Station 149: Kwambonambi – Mondi Forestry..... 130

Figure 9.37 The GEV (a) stationary model, (b) non-stationary model considering time as a covariate, (c) non-stationary model considering SOI as a covariate, (d) non-stationary model considering DMI as a covariate, (e) non-stationary model considering CO_2 as a covariate, (f) non-stationary model considering GMT as a covariate and (g) effective return period as a function of time for Station 151: ULOA – Mark & Ross Sugar Estate..... 131

Figure 9.38 The GEV (a) stationary model, (b) non-stationary model considering time as a covariate, (c) non-stationary model considering SOI as a covariate, (d) non-stationary model considering DMI as a covariate, (e) non-stationary model considering CO_2 as a covariate, (f) non-stationary model considering GMT as a covariate and (g) effective return period as a function of time for Station 152: Mtubatuba – Nyalazi River..... 132

Figure 9.39 The GEV (a) stationary model, (b) non-stationary model considering time as a covariate, (c) non-stationary model considering SOI as a covariate, (d) non-stationary model considering DMI as a covariate, (e) non-stationary model considering CO_2 as a covariate, (f) non-stationary model considering GMT as a covariate and (g) effective return period as a function of time for Station 154: Mkuze – Mkuze Estate.....133
Figure 9.40 The GEV (a) stationary model, (b) non-stationary model considering time as a covariate, (c) non-stationary model considering SOI as a covariate, (d) non-stationary model considering DMI as a covariate, (e) non-stationary model considering CO_2 as a covariate, (f) non-stationary model considering GMT as a covariate and (g) effective return period as a function of time for Station 155: Pongola – Impala Irrigation Board 134
Figure 9.41 Time series of annual maximum rainfall for SASRI station 6 and 6 GCMs for corresponding years.....135
Figure 9.42 Time series of annual maximum rainfall for SASRI station 8 and 6 GCMs for corresponding years.....135
Figure 9.43 Time series of annual maximum rainfall for SASRI station 9 and 6 GCMs for corresponding years.....135
Figure 9.44 Time series of annual maximum rainfall for SASRI station 11 and 6 GCMs for corresponding years.....136
Figure 9.45 Time series of annual maximum rainfall for SASRI station 12 and 6 GCMs for corresponding years.....136
Figure 9.46 Time series of annual maximum rainfall for SASRI station 18 and 6 GCMs for corresponding years.....136
Figure 9.47 Time series of annual maximum rainfall for SASRI station 20 and 6 GCMs for corresponding years.....137
Figure 9.48 Time series of annual maximum rainfall for SASRI station 22 and 6 GCMs for corresponding years.....137
Figure 9.49 Time series of annual maximum rainfall for SASRI station 23 and 6 GCMs for corresponding years.....137
Figure 9.50 Time series of annual maximum rainfall for SASRI station 26 and 6 GCMs for corresponding years.....138

Figure 9.51 Time series of annual maximum rainfall for SASRI station 27 and 6 GCMs for corresponding years....138
Figure 9.52 Time series of annual maximum rainfall for SASRI station 29 and 6 GCMs for corresponding years....138
Figure 9.53 Time series of annual maximum rainfall for SASRI station 38 and 6 GCMs for corresponding years....139
Figure 9.54 Time series of annual maximum rainfall for SASRI station 105 and 6 GCMs for corresponding years....139
Figure 9.55 Time series of annual maximum rainfall for SASRI station 110 and 6 GCMs for corresponding years....139
Figure 9.56 Time series of annual maximum rainfall for SASRI station 111 and 6 GCMs for corresponding years....140
Figure 9.57 Time series of annual maximum rainfall for SASRI station 114 and 6 GCMs for corresponding years....140
Figure 9.58 Time series of annual maximum rainfall for SASRI station 120 and 6 GCMs for corresponding years....140
Figure 9.59 Time series of annual maximum rainfall for SASRI station 123 and 6 GCMs for corresponding years....141
Figure 9.60 Time series of annual maximum rainfall for SASRI station 125 and 6 GCMs for corresponding years....141
Figure 9.61 Time series of annual maximum rainfall for SASRI station 126 and 6 GCMs for corresponding years....141
Figure 9.62 Time series of annual maximum rainfall for SASRI station 129 and 6 GCMs for corresponding years....142
Figure 9.63 Time series of annual maximum rainfall for SASRI station 130 and 6 GCMs for corresponding years....142
Figure 9.64 Time series of annual maximum rainfall for SASRI station 131 and 6 GCMs for corresponding years....142
Figure 9.65 Time series of annual maximum rainfall for SASRI station 132 and 6 GCMs for corresponding years....143
Figure 9.66 Time series of annual maximum rainfall for SASRI station 136 and 6 GCMs for corresponding years....143

Figure 9.67 Time series of annual maximum rainfall for SASRI station 138 and 6 GCMs for corresponding years....143
Figure 9.68 Time series of annual maximum rainfall for SASRI station 139 and 6 GCMs for corresponding years....144
Figure 9.69 Time series of annual maximum rainfall for SASRI station 142 and 6 GCMs for corresponding years....144
Figure 9.70 Time series of annual maximum rainfall for SASRI station 143 and 6 GCMs for corresponding years....144
Figure 9.71 Time series of annual maximum rainfall for SASRI station 146 and 6 GCMs for corresponding years....145
Figure 9.72 Time series of annual maximum rainfall for SASRI station 144 and 6 GCMs for corresponding years....145
Figure 9.73 Time series of annual maximum rainfall for SASRI station 147 and 6 GCMs for corresponding years....145
Figure 9.74 Time series of annual maximum rainfall for SASRI station 148 and 6 GCMs for corresponding years....146
Figure 9.75 Time series of annual maximum rainfall for SASRI station 149 and 6 GCMs for corresponding years....146
Figure 9.76 Time series of annual maximum rainfall for SASRI station 151 and 6 GCMs for corresponding years....146
Figure 9.77 Time series of annual maximum rainfall for SASRI station 152 and 6 GCMs for corresponding years....147
Figure 9.78 Time series of annual maximum rainfall for SASRI station 154 and 6 GCMs for corresponding years....147
Figure 9.79 Time series of annual maximum rainfall for SASRI station 155 and 6 GCMs for corresponding years....147
Figure 9.80 Projected changes from the present to the near future in design rainfalls for the 1-day 2-year Return Period derived from outputs from multiple GCMs....148
Figure 9.81 Projected changes from the present to the distant future in design rainfalls for the 1-day 2-year Return Period derived from outputs from multiple GCMs....149
Figure 9.82 Projected changes from the present to the near future in design rainfalls for the 1-day 10-year Return Period derived from outputs from multiple GCMs....150

Figure 9.83 Projected changes from the present to the distant future in design rainfalls for the 1-day 10-year Return Period derived from outputs from multiple GCMs....151
Figure 9.84 Projected changes from the present to the near future in design rainfalls for the 1-day 50-year Return Period derived from outputs from multiple GCMs....152
Figure 9.85 Projected changes from the present to the distant future in design rainfalls for the 1-day 50-year Return Period derived from outputs from multiple GCMs....153
Figure 9.86 Projected changes from the present to the near future in design rainfalls for the 1-day 100-year Return Period derived from outputs from multiple GCMs 154
Figure 9.87 Projected changes from the present to the distant future in design rainfalls for the 1-day 100-year Return Period derived from outputs from multiple GCMs 155
Figure 10.1 Time series of annual streamflows at stations along the East Coast of KwaZulu-Natal....158
Figure 10.2 The LP3 (a) stationary model, (b) non-stationary model considering time as a covariate, and (c) effective return period as a function of time for Station: T5H012 159
Figure 10.3 LP3 (a) stationary model, (b) non-stationary model considering time as a covariate, and (c) effective return period as a function of time for Station: U2H001....160
Figure 10.4 LP3 (a) stationary model, (b) non-stationary model considering time as a covariate, and (c) effective return period as a function of time for Station: U2H006....161
Figure 10.5 LP3 (a) stationary model, (b) non-stationary model considering time as a covariate, and (c) effective return period as a function of time for Station: U2H048....162
Figure 10.6 LP3 (a) stationary model, (b) non-stationary model considering time as a covariate, (c) non-stationary model considering rainfall as a covariate, and (d) effective return period as a function of time for Station:U3H001 163
Figure 10.7 LP3 (a) stationary model, (b) non-stationary model considering time as a covariate, (c) non-stationary model considering rainfall as a covariate, and (d) effective return period as a function of time for Station:U3H005 164

Figure 10.8 LP3 (a) stationary model, (b) non-stationary model considering time as a covariate, and (c) effective return period as a function of time for Station: U4H002 165
Figure 10.9 LP3 (a) stationary model, (b) non-stationary model considering time as a covariate, and (c) effective return period as a function of time for Station: U6H003 166
Figure 10.10 LP3 (a) stationary model, (b) non-stationary model considering time as a covariate, (c) non-stationary model considering rainfall as a covariate, and (d) effective return period as a function of time for Station:V5H002 167
Figure 10.11 LP3 (a) stationary model, (b) non-stationary model considering time as a covariate, and (c) effective return period as a function of time for Station: W1H004 168
Figure 10.12 LP3 (a) stationary model, (b) non-stationary model considering time as a covariate, (c) non-stationary model considering rainfall as a covariate, and (d) effective return period as a function of time for Station:W1H009..... 169
Figure 10.13 LP3 (a) stationary model, (b) non-stationary model considering time as a covariate, and (c) effective return period as a function of time for Station: W2H005 170
Figure 10.14 LP3 (a) stationary model, (b) non-stationary model considering time as a covariate, and (c) effective return period as a function of time for Station: W3H022 171
Figure 10.15 LP3 (a) stationary model, (b) non-stationary model considering time as a covariate, (c) non-stationary model considering rainfall as a covariate, and (d) effective return period as a function of time for Station:W4H012..... 172

This page was intentionally left blank

1. INTRODUCTION

Estimates of extreme design rainfall are needed routinely for Design Flood Estimation (DFE) to design and assess the flood risk of hydraulic structures such as dam spillways, culverts and stormwater drains. Standard methods for frequency analysis of extreme events are based on the assumption of a stationary climate (Prosdocimi *et al.*, 2014b), i.e. that the long-term attributes of climate do not change over time. However, it is postulated that anthropogenically induced climate change has resulted in changes in extreme weather events, thus questioning the assumption of stationarity (Serinaldi and Kilsby, 2015). As a consequence of a projected changing climate, the frequency and magnitude of extreme rainfall events is expected to increase in the future (Bates *et al.*, 2008), thus further exacerbating flood risk exposure of already vulnerable communities and hydraulic infrastructure. The possible non-stationarity in climate is projected to result in changes in rainfall and runoff characteristics, with potential impacts on the accuracy of current estimates of design rainfall and on the estimation of extreme rainfall quantities such as the Probable Maximum Precipitation (PMP). This may have significant consequences for the flood risk profiles of existing hydraulic infrastructure and on the design of new hydraulic infrastructure, and consequently also for the South African economy (Cullis *et al.*, 2015). It is therefore essential to account for possible trends and associated uncertainties associated with non-stationary climate data in the analysis of extreme rainfall events (Yilmaz *et al.*, 2014) in support of more reliable design of critical infrastructure and credible flood management interventions.

The damage and loss of life caused by recent (2022) flooding across the East Coast regions of KwaZulu-Natal, and the realisation of possible increased rainfall variability in the future, highlight the fact that DFE techniques currently used South Africa are outdated and need revision. As a consequence, a National Flood Studies Programme (NFSP) has been initiated to overhaul and modernise DFE procedures used in South Africa (Smithers *et al.*, 2016). The NFSP is a comprehensive plan covering all approaches to DFE, which includes updating and modernisations of the estimation of design rainfalls and floods under non-stationary climate conditions in South Africa. The need to develop methods to account for non-stationary data, and to update design rainfall estimation methods to include possible trends in extreme rainfall

events in a changing environment, have been identified as high priority research areas in the NFSP.

The impact of a changing climate has become a key concern in South Africa (Department of Environmental Affairs, 2014a; Department of Environmental Affairs, 2014b; Department of Environmental Affairs, 2017). In South Africa, over the past five decades the mean annual temperatures have increased by more than 1.5 times the observed global average increase (Ziervogel *et al.*, 2014). The Department of Environmental Affairs (2017) noted that the highest recorded temperatures up to that year since 1951 occurred in 2015. Moyo and Nyoni (2021) noted that South Africa is likely to be at least 3°C warmer by 2050 than the period from 1961-2000 under a "business-as-usual" scenario in greenhouse gas emissions. The Intergovernmental Panel on Climate Change (IPCC) note that severe and widespread impacts associated with such temperature increases are attributable to climate change (IPCC, 2018). Changes in temperature have a significant impact on extreme weather events (Pfahl *et al.*, 2017; IPCC, 2018) and, generally, warmer atmospheric conditions are more conducive to heavy rainfall events (IPCC, 2017a; Pfahl *et al.*, 2017). Over parts of South Africa, it has been noted that the frequency of extreme rainfall events has increased (Ziervogel *et al.* (2014).

The estimation of design floods is impacted by changes in rainfall and runoff distribution characteristics (Smithers, 2012b). Many observations of global climate trends have raised an increasing concern that the extreme rainfalls, including the PMP, needed for the design of high-hazard hydraulic infrastructure, will change due to the influence of a changing climate (Rouhani, 2016). The potential influences of climate change on key variables for PMP estimation, such as maximum moisture and precipitation efficiency, have been studied in some detail (Clark, 1987; Rastogi *et al.*, 2017). Results of that research suggest that changes in both atmospheric temperature and the maximum atmospheric moisture that can be held may increase PMP estimates by approximately 20% due to climate change (Clark, 1987; Rastogi *et al.*, 2017).

Johnson and Smithers (2020) revised the 1-day PMPs in South Africa using an updated rainfall database and a modernized methodology and highlighted that many of the extreme events noted in their study occurred after the previously estimated PMPs published in HRU (1972). This

indicates that there has been an increase in extreme rainfall events recorded compared to previous years. Hence it is critical to publish the updated PMP estimates, derived on the assumption of stationary data, and use this information to estimate the potential impacts of the changing climate on extreme rainfall estimation.

Dam safety management has conventionally been carried out assuming stationary climatic conditions (Ehsani *et al.*, 2017). However, researchers are increasingly taking the non-stationarity hypothesis in rainfall and flood frequency analysis into account to cater for the effects of climate change (Gregersen *et al.*, 2017; Sarhadi and Soulis, 2017; Fluixá-Sanmartín *et al.*, 2019; Pedretti and Irannezhad, 2019; Hesarkazzazi *et al.*, 2021). Moyo and Nyoni (2021) warn that most climate change scenarios for South Africa show potential detrimental impacts on dams and flood risk management. Warmer and drier climate is linked to increased risk of droughts which adversely impact on the reliability of water supply systems and the structural integrity of dams. Warmer and wetter scenarios are characterized by more frequent and severe extreme flood events which are directly linked to dam safety concerns as well as to increased sedimentation. Ultimately, any climate change scenario is highly likely to have an adverse impact on dam safety and flood risk management. Luxford and Faulkner (2020) recommend the development of a practical method of non-stationary flood frequency estimation in the UK, that includes investigating trends in extreme rainfall and incorporating non-stationarity and integrates the modelling of past trends and future expected climate change.

The importance of this research has recently been highlighted by the Water Research Commission (WRC) through a Webinar titled “Roadshow: Advancing Dam Safety in The Context of Climate Change in South Africa” held in May 2021. Dams are strategic assets for storing water to support life and socio-economic development. Their failure often results in the loss of life, extensive downstream damage to the environment and impacts on economic activities. In South Africa the Dam Safety Office, located within the Department of Water and Sanitation (DWS), is responsible for ensuring the safety of dams. In addition to normal ageing-related deterioration of dams, their safety is likely threatened by climate change. According to the erstwhile Department of Environmental Affairs (now DEFF), the biggest cost increase associated with climate change in the water sector will be in infrastructure damage due to

flooding, projected to rise from about R670 million per year to R3.5 billion per year (WRC, 2021).

Given the importance of flood risk management, the shortcomings of the methods currently used by practitioners for DFE and the potential impact of climate change, dealing with a non-stationary climate data series currently requires urgent attention in South Africa (Johnson *et al.*, 2021). Hattingh (2021) noted that to address the challenge of climate change and its impacts on dams, risk-based approaches need to be developed to account for uncertainty associated with a non-stationary climate, further highlighting the importance of this research in the South African context. With the increasing availability of climate model data through Global Circulation Models (GCMs), there is greater opportunity to use such data to determine the potential impacts of future climate scenarios on extreme rainfall and flood events using advanced statistical techniques, and to develop methods/tools to incorporate these trends in design rainfall and flood estimation. For example, numerous research institutions in the UK are involved in research on non-stationarity in flooding using climate model data (Luxford and Faulkner, 2020).

All DFE methods currently used in South Africa are based on the assumption of a stationary climate. The concept of regionally derived "magnification" adjustment factor to account for non-stationarity is a convenient method for linking trends due to non-stationary frequency analysis to estimates from methods based on the assumption of stationarity, as well as providing an intuitive means of communicating the effects of change on design floods. While many of the climate modelling studies reported in the literature indicate changes in the frequency and magnitude of extreme flood events, there does not seem to be consensus in the literature on the detection of trends in the observed data. This disparity could be attributed to the relatively short periods of observations available. Kjeldsen and Prosdocimi (2021a) presented a regional approach to magnification factors to allow a statistical assessment of the impact of non-stationary data on design floods in both gauged and ungauged locations, regardless of the causes (e.g. climate change, increased abstractions, changes in land cover) of non-stationary data. This approach can be used to allow more robust assessment of trends in regional series of hydrological extremes and changes in design rainfalls and floods across a specified region or pooling group in South Africa.

Given the above, a method to account for non-stationary data which incorporates the impacts of a changing climate in extreme design rainfall estimates in South Africa needs to be developed using regional approaches to detect trends in historical data.

Given the background provided above, the aims of this project are therefore to undertake the following for South Africa:

(a) To review and refine the updated 1-day PMP estimates;
(b) To develop and assess the performance of a method to account for the impacts of non-stationary data on PMP estimation;
(c) To develop and assess the performance of a method to account for the impacts of non-stationary data on design rainfall estimation; and
(d) To assess the trends in hydrological extremes and investigate the use of regional magnification factors.

The structure of this document is as follows:

The estimation of the updated 1-day PMP is presented in Chapter 2. Detecting trends in rainfall extremes and non-stationary extreme value analysis of rainfall data are presented in Chapter 3 and detecting trends in flood extremes and non-stationary extreme value analysis of peak discharge data is covered in Chapter 4. Chapter 5 contains discussions, conclusions and recommendations on this study. Chapter 6 presents a summary of the capacity building through the project. Chapter 7 lists the references used and Chapters 8, 9 and 10 contain the appendices.

2. UPDATING THE 1-DAY PMP ESTIMATES

KA Johnson and JC Smithers

2.1 Introduction

The Probable Maximum Precipitation (PMP) is an extreme rainfall quantity which represents the maximum depth of precipitation that could possibly occur in a specific area and for a specific duration (WMO, 2009). The PMP is commonly used to derive the Probable Maximum Flood (PMF), which is used by engineers and hydrologists in the planning, design and risk assessment of high-hazard hydraulic structures (Wang, 1984; Chavan and Srinivas, 2015). The South African National Committee on Large Dams (SANCOLD) Guidelines for the estimation of the PMF is dependent on the PMP (SANCOLD, 1991).

Numerous methods have been developed globally to estimate the PMP. In South Africa the PMP is currently determined using the Hydrological Research Unit (HRU) Report No. 1/72 (HRU, 1972), which was developed based on approximately 30 years of rainfall data from the 1930s to 1960s using a total of 170 storms across the country. For small-area storms the PMP is presented as an envelope of maximum observed storm values and for large-area storms the PMP is presented as Depth-Area-Duration (DAD) curves for meteorologically homogeneous regions (Cullis *et al.*, 2007). Since the publication of these guidelines there has been no update in the development of PMP estimation in South Africa and these guidelines are still used in professional practice today. Studies have shown that numerous extreme rainfall events have occurred since this publication, which have exceeded the PMP estimates (Cullis *et al.*, 2007; Görgens *et al.*, 2007). These PMP estimates may thus no longer be the best estimates of extreme rainfall and require urgent updating and modernisation (Smithers *et al.*, 2014). The use of outdated PMP estimates potentially affects the accuracy of PMF estimations, and consequently the design of high-hazard hydraulic structures.

The World Meteorological Organisation (WMO) has published a number of guidelines which describe methods for estimating the PMP. The latest WMO guideline published in 2009 provides two approaches for estimating the PMP: (i) hydro-meteorological methods which maximise rainfall events based on atmospheric moisture conditions and (ii) statistical methods

which can be used when sufficient meteorological data are not available (WMO, 2009). PMPs derived using hydro-meteorological methods produce reliable and precise estimates (WMO, 2009; Fattahi *et al.*, 2011; Salas *et al.*, 2014) and are most widely applied globally (Lee *et al.*, 2016). Johnson and Smithers (2019) provide a comprehensive review of various methods for estimating the PMP.

The aim of this Chapter is to present new PMP estimates for South Africa using an updated database and modernised methods. The objectives are to: (i) report on the collation of an updated hydro-meteorological database, (ii) estimate the PMP using appropriate hydro-meteorological methods prescribed by the WMO, (iii) to critically evaluate the newly derived PMP estimates, and (iv) disseminate the new knowledge on the PMP through a workshop.

2.2 Study Area and Data

This section contains a brief description of the rainfall characteristics of the study area and detailed information of the data used to derive the PMPs. This study focusses on the estimation of PMP for the entire country. South Africa is a semi-arid with an uneven spatial distribution of rainfall and most of the country receiving an average of less than 500 mm of rainfall annually. The countries latitudinal location lies between the tropical, subtropical and temperate pressure systems (Braun *et al.*, 2017), which results in three rainfall seasonality zones across the country: summer rainfall zone (October to March), winter rainfall zone (April to September) and year-round rainfall zone (Roffe *et al.*, 2019). Rainfall varies considerably across the country with the summer rainfall zones in the east experiencing the greatest rainfalls with a mean annual precipitation (MAP) in excess of 800 mm and gradually decreasing westward (Schulze, 2011).

2.2.1 Homogeneous Rainfall Districts

Homogeneous rainfall districts obtained from the South African Weather Service (SAWS) were used as a basis for this study. The development of these districts started in the 1930s where homogeneous regions were divided into rainfall districts based on the statistics of maximum rainfalls and the seasonal distribution of precipitation (Schumann and Hofmeyer, 1938) and calculations of district rainfall has continually improved over the years (South

African Weather Bureau, 1960; South African Weather Bureau, 1972; Landman *et al.*, 2006). The latest improvement occurred in 2016 and this entailed that at least 90% of the rainfall data of a month for a station should be available before the station is included in the calculations (de Jager, 2018, personal communication). Presently there are 94 homogeneous rainfall districts, as delineated in Figure 8.1 in Appendix A.

2.2.2 Hydro-meteorological Data

2.2.2.1 Rainfall

For estimating the PMP a high-quality database containing the most extreme rainfall events is required. Daily rainfall data from 1 629 stations across the country with at least 40 years of quality controlled daily records were selected for this study, as shown in Figure 2.1(a). The annual maximum daily rainfall data from Smithers and Schulze (2000b) was the primary source of data, the majority of which was contributed by the South African Weather Service (SAWS) and the Agricultural Research Council (ARC). The data record contained in the database was limited up to the year 2000 and additional SAWS station data were obtained from the University of Cape Town Climate Systems Analysis Group (CSAG) and used to extend approximately 50% of the existing database with data for the period 2000-2010. Thus, the end dates for the rainfall records used in this study range between 2000 and 2010. At the time of the study, funds were not available to purchase the full dataset from SAWS to update the database up to 2018. Figure 2.1(b) shows the distribution of the record lengths for the stations used in this study.

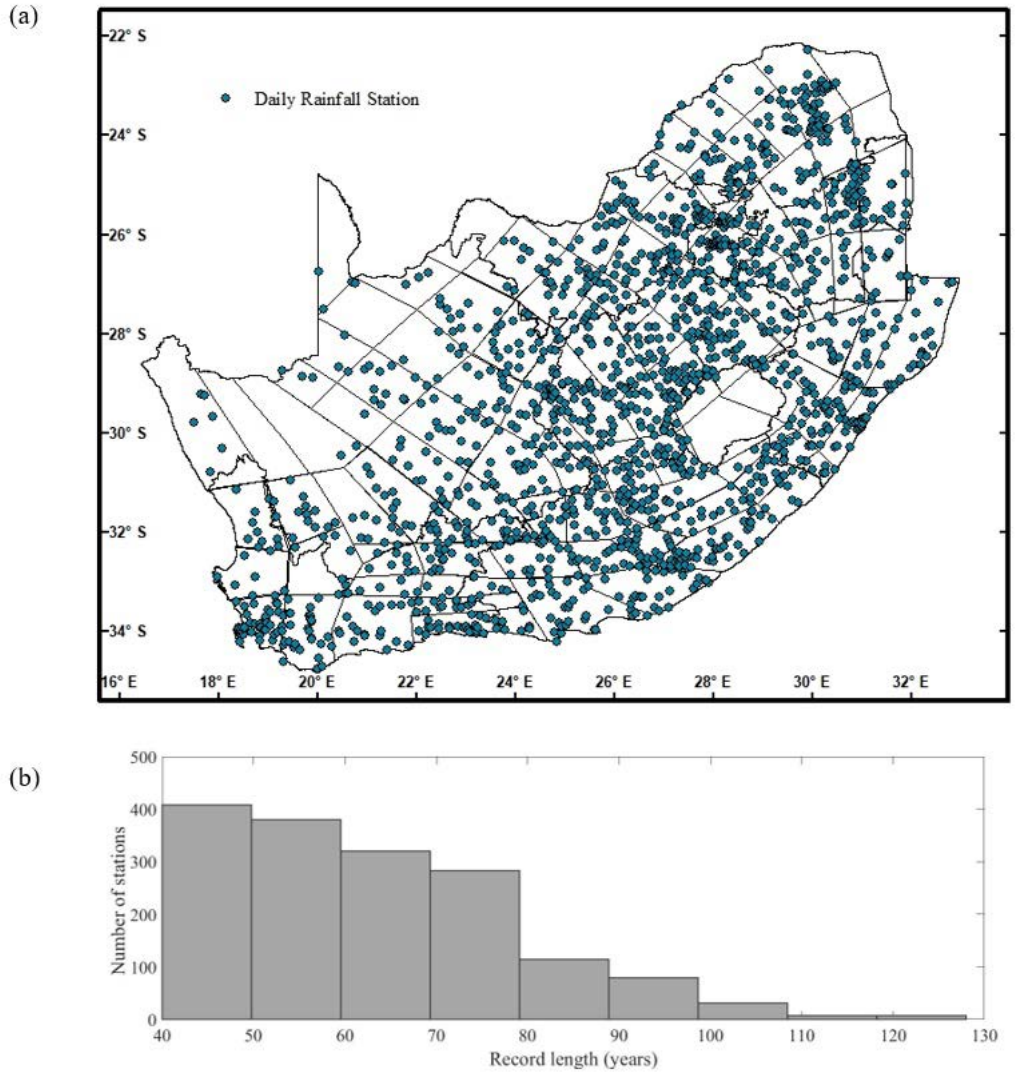

Figure 2.1 (a) Locations of selected rainfall stations with at least 40 years of daily record and (b) distribution of record lengths for selected rainfall stations

2.2.2.2 Temperature and relative humidity

Daily estimates of temperature (*T*) and relative humidity (*RH*) data were obtained from the gridded database developed by Schulze and Maharaj (2004) and were used to determine daily dew point temperatures (T_d) values for this study. However, the duration of *T* and *RH* data available through the gridded database is limited to the period 1950 to 2000. Data from other sources were not available at the time of the study and funds were not available to purchase these data from SAWS.

2.3 Methodology – PMP Estimation Using the Generalised Estimation Method

For this study, the generalised estimation method prescribed by WMO (2009), has been adopted to estimate the 1-day PMPs for South Africa. The generalised estimation method is a hydro-meteorological approach used for estimating the PMP for large meteorological homogeneous regions. It is a physical approach that requires site specific meteorological and geographical data. This method is one of the most commonly used and accepted methods for PMP estimation which provides more reliable estimates when compared to other methods (Fattahi *et al.*, 2011; Afzali-Gorouh *et al.*, 2018; Boota *et al.*, 2018). The basis of PMP estimation is the maximisation of observed extreme precipitation using the relationship between observed representative precipitable water content and the theoretical maximum precipitable water content, followed by the transposition of the maximised precipitations to ungauged regions. The main steps involved in this approach are summarised in Figure 2.2.

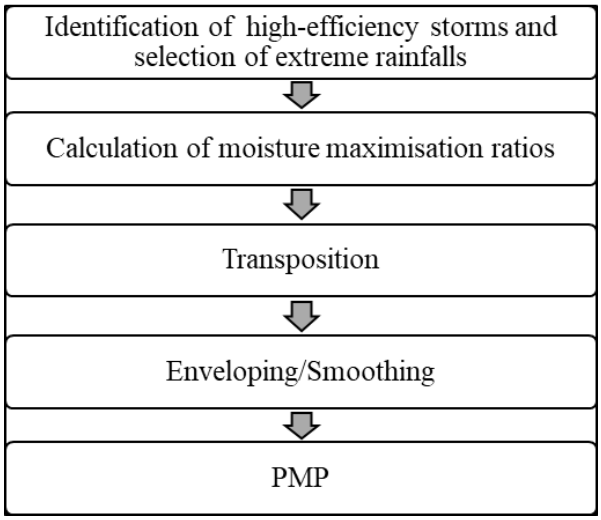

Figure 2.2 PMP estimation procedure

2.3.1 Selection of extreme rainfall events

Identification of a high-efficiency storm involves the analysis of observed rainfall data and the selection of major storm events, based on the assumption that the precipitations of the selected storms were operating at, or close to, maximum efficiency. From the daily rainfall data, the Annual Maximum Daily Rainfall (AMDR) values were analysed and the largest AMDR was selected as the most extreme rainfall event at each station. A map of the AMDR is provided in Figure 8.2 in Appendix A. Of the 1 629 available stations, 380 stations were selected as initial

representative stations for the 94 districts, with an average of 4 stations per district. These stations were selected based on the date of the occurrence of most extreme AMDR. Firstly, only stations where the greatest AMDR occurred between 1950 and 2000 were considered for the representative stations as the temperature and relative humidity data available for the maximisation of the storm events was limited to this period. Secondly, it was observed that often the most extreme AMDR values recorded at close neighbouring stations resulted from the same storm event. Based on this observation, where possible, only stations where unique storms resulted in the largest AMDR were chosen. As such, the stations selected represent a range of unique storm events within each district and are also well spatially distributed. The locations of the 380 representative stations are shown in Figure 2.3.

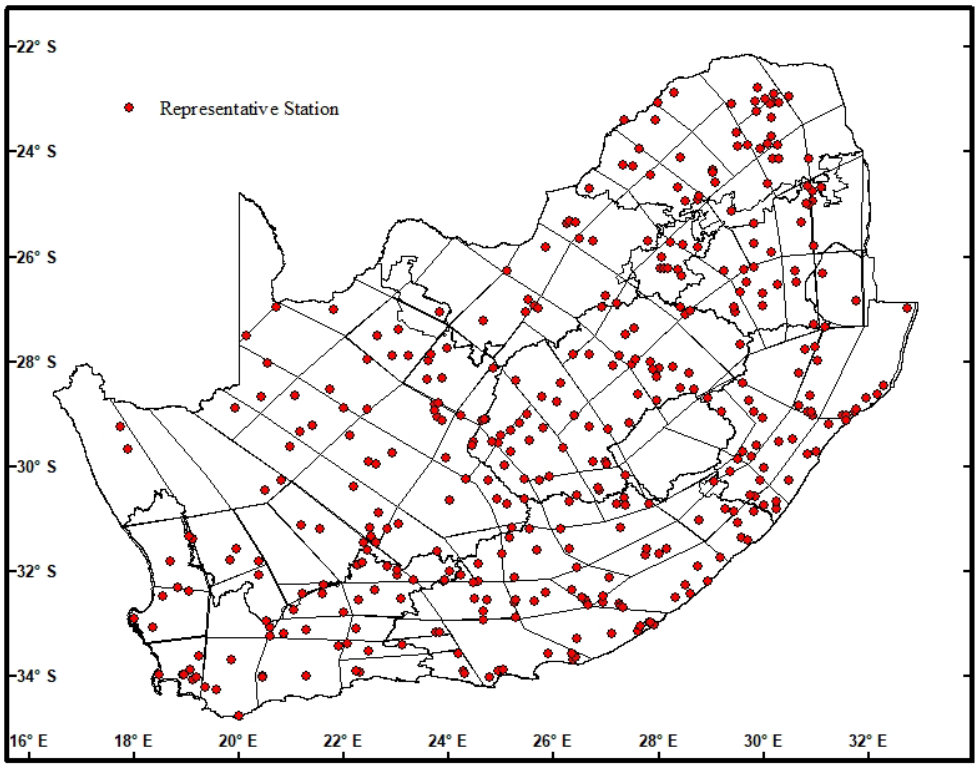

Figure 2.3 Locations of the 380 representative stations

2.3.2 Moisture maximisation

In this process the moisture factors of high-efficiency storms are adjusted to their theoretical maximum. Storm efficiency is linked to the precipitable water content in the atmosphere (Abbs,

1999; WMO, 2009). Precipitable water content is the quantity of water measured in a vertical column of the atmosphere that is potentially available for precipitation (NWS, 1980). Adjusting storms to their maximum efficiency is performed by multiplying the selected observed storm rainfall by the moisture maximisation ratio defined as: $R_m = W_m/W_s$, where W_m represents the maximum precipitable water content of the maximum persistent 12-hour 100 kPa dew point for the date of the storm occurrence or the 15 days before and 15 days after the storm, and W_s is the precipitable water content estimated for the actual storm for the persistent 12-hour 100 kPa dew point. The precipitable water content can be estimated from the surface dew point temperature, based on the assumption of a saturated atmosphere and a pseudo-adiabatic lapse rate during a storm event. Using the corresponding dew point temperatures, the precipitable water values are obtained from Table A.1.3 in WMO (2009). The table provides precipitable water content (mm) as a function of 100 kPa dew point temperature (°C). As dew point temperature is not measured directly, daily temperature (*T*) and relative humidity (*RH*) data were used to calculate daily maximum dew point temperatures (T_d) using Eq. 2.1 (Wanielista *et al.*, 1997). Based on the time scale of the available *T* and *RH* data, the daily (24-hour) T_d values were used as an alternative to the 12-hour values as they provide minimal differences for this application (WMO, 2009; Thuy *et al.*, 2019).

$$T_d = \left(\frac{RH}{100}\right)^{\frac{1}{8}} (112 + 0.9T) + 0.1T - 112 \qquad (2.1)$$

where

T_d = dew point temperature (°C),

RH = relative humidity (%), and

T = surface temperature (°C).

Moisture maximisation ratios were determined for the 380 representative stations and applied to the selected AMDR values to determine at-site PMP estimates. Due to the limitation of the duration of the *T* and *RH* database, many significant storm events that occurred outside of the 1950 to 2000 window could not be maximised in this way. Assuming that atmospheric moisture conditions associated with the drivers of similar storm events are translatable to adjacent locations within homogeneous rainfall districts, in order to maximise all the extreme rainfall

events, isolines of the moisture maximisation ratios calculated for the 380 representative stations were constructed by interpolation and spatially joined to the remaining stations to associate an R_m value with every AMDR. These ratios were then applied to the AMDRs at stations without *T* and *RH* data in order to maximise these events and generate at-site PMP estimates at all 1629 locations.

There are various suggestions for limiting the moisture maximisation ratios in PMP estimation. The concept of limiting the maximisation ratio is to maintain the original dynamics of a particular storm event (Hansen *et al.*, 1988) and setting upper boundaries may be recommended in order to not produce exaggerated PMP values (Lee *et al.*, 2016), however, there is no scientific justification for limiting the moisture maximisation ratio (Rouhani and Leconte, 2016) and a study by Papalexiou and Koutsoyiannis (2006) showed no evidence of upper bounds in atmospheric moisture or precipitation. In Australia, upper limits have been chosen based on the analysis of actual storm events where the largest ratios were observed (Minty *et al.*, 1996; Bureau of Meteorology, 2003; Walland *et al.*, 2003). The limits chosen for Australia have been adopted in other studies (Rousseau *et al.*, 2014; Lee *et al.*, 2016) although this decision was not based on the actual storm characteristics of the study areas. For this study the only limits placed on the moisture maximisation ratios are based on the R_m values determined at the representative stations such that interpolated R_m values applied to the remaining stations will not exceed the calculated values at the representative stations.

2.3.3 Transposition

Transposition of the maximised AMDR events translates the meteorological characteristics of observed extreme storm events from gauged locations to locations without adequate records of major storm events. Due to the spatial distribution of the stations used in this study, standard linear geo-statistical interpolation methods, such as Inverse Distance Weighting (IDW), performed poorly in translating the PMP estimates to ungauged locations and preserving the original sample point values. To overcome this, Multiquadric Radial Basis Functions (MRBF) which is a deterministic interpolation method widely used for interpolating meteorological data and often yields superior results (de Gaetano and Belcher, 2007) has been used to transpose the at-site PMP estimates to ungauged locations without compromising the at-site PMP values. MRBF provide a higher accuracy interpolation and are superior in preserving the original

sample point values when compared to other commonly used geo-statistical methods such as Kriging (Bronowicka-Mielniczuk *et al.*, 2019). Unlike Kriging, MRBF does not require variogram modelling, which requires numerous inputs and is dependent on the application of advanced statistical concepts and tools. A proper variographic study is difficult to perform in smaller data sets with irregular spatial distribution and inappropriate variogram modelling can yield highly inaccurate results (Rusu and Rusu, 2006). Using MRBF interpolation, the at-site PMP estimates were transposed across the country to generate a 5 x 5 km gridded database for the 1-day PMP.

2.3.4 Isohyetal Patterns and Adjustment of the Interpolated Surface

The use of the MRBF procedures aims to yield a model that will produce the smallest residual errors, *i.e.* a model that will fit the actual data points used in the interpolation the best. However, these discrepancies between the actual PMPs and the modelled values may result in different at-site PMP values to those determined through the moisture maximisation process being obtained. An example of such a case is depicted in Figure 2.4.

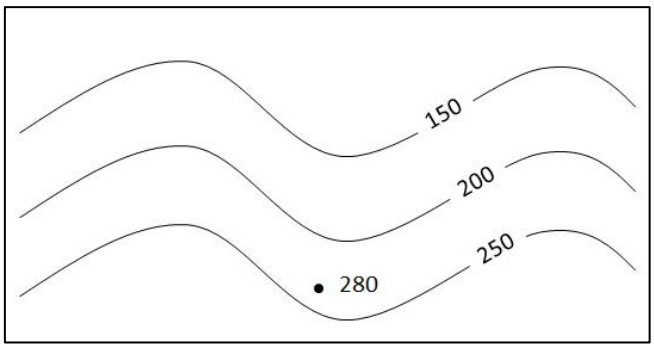

Figure 2.4 Example of residual error in interpolated PMP surface

The ratios of the PMP estimated using the MRBF to the observed PMP were determined as the residuals. The inverses of these residuals were then interpolated using the same approach used in the MRBF interpolation for the PMP estimates to generate a residual adjustment surface. This residual adjustment surface was then applied to the estimated PMP surface to adjust the PMP surface locally to fit the at-site values and globally to the ungauged locations. In this way, the surface was adjusted to fit the actual PMP values determined at the rainfall stations and the surrounding areas were adjusted according to the interpolated residual adjustment surface. A graphical explanation of the technique used to adjust the residuals in the interpolated PMP

surface is shown in Figure 2.5. Adjustment of the interpolated PMP estimates was vital as large differences between the at-site PMPs and the corresponding interpolated values would result in significant discrepancies in the PMP estimates. Residuals of as much as 30% were observed in the interpolated surface.

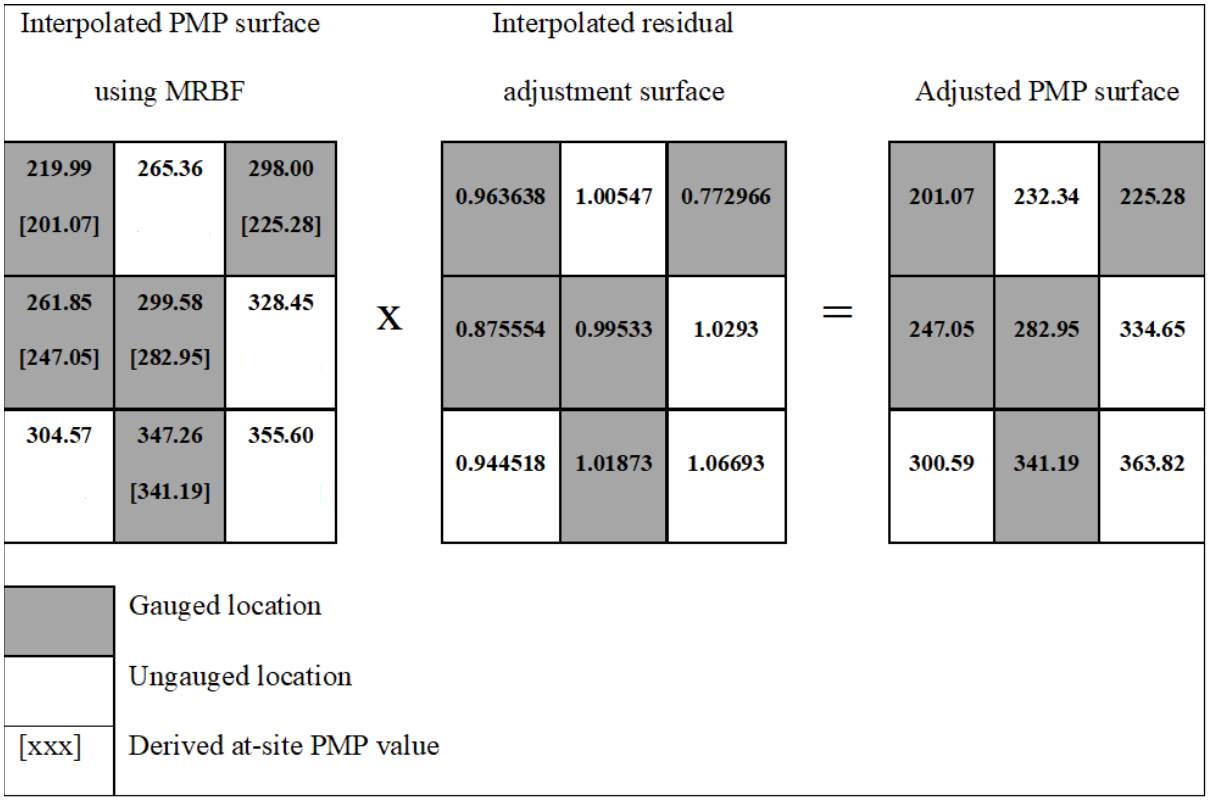

Figure 2.5 Technique for adjusting the residuals in the interpolated PMP surface

2.4 Results and Discussion

A storm maximisation and transposition approach was applied to daily rainfall data in South Africa in order to determine 1-day PMP estimates for the entire country, as shown in Figure 2.6. The estimates vary across the country due to the various rainfall seasonality zones and corresponding rainfall drivers.

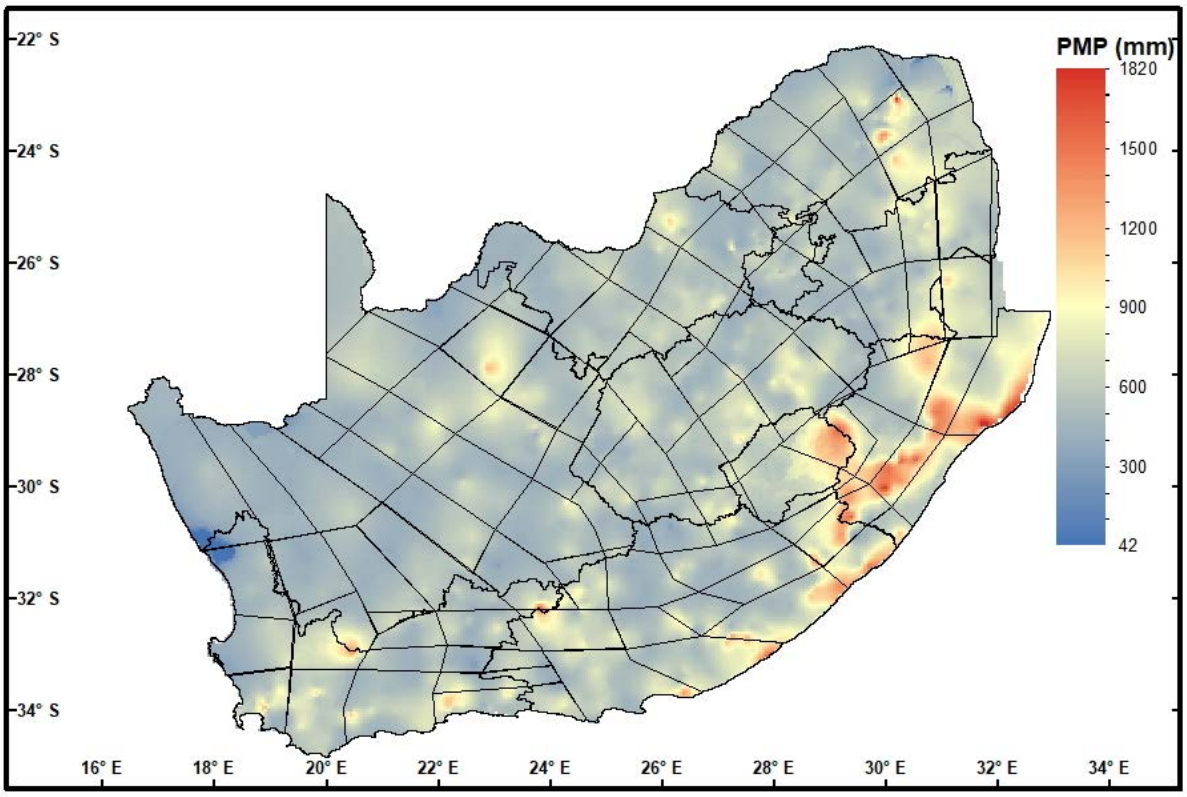

Figure 2.6 Map of 1-day PMP estimates for South Africa

2.4.1 Consideration of Extraordinary PMPs

Estimating the PMP using hydro-meteorological methods considers the physical atmospheric characteristics of specific storm events, however, taking into account atmospheric variables may result in unreasonably large PMPs. The selection of the high-efficiency storms is based on the assumption that the precipitation efficiencies of the selected storms were near or at the maximum. Further maximisation of such events by taking into account the maximum potential atmospheric moisture conditions increases the potential rainfall depth to what is atmospherically feasible. Although PMP estimates may seem uncharacteristically large in some parts, studies have shown that unprecedented extreme weather events in the order of magnitude of the PMP have occurred globally (Bureau of Meteorology, 2003; Micovic *et al.*, 2014; Kappel, 2019). While the method applied in this study assumes that the selected rainfall events have relatively high efficiencies, storms of greater efficiency may still occur in future.

Typically, extraordinary PMPs are shown to occur in high rainfall producing regions in the eastern parts of the country, and in instances where large PMPs occur in locations

uncharacteristic of the MAPs, such as the central interior and western parts, it is noted that the observed rainfall events that resulted in these PMPs were significantly greater than what is typical for these particular locations. Furthermore, these PMPs do not result from a single rainfall station but rather several neighbouring stations which, on analysis of the daily rainfall data, are likely to be affected by the same storm events and have similar storm dates and magnitudes. In addition, a discordancy test (Hosking and Wallis, 1997) was performed using the AMDR for each district and no discordant sites were identified.

The largest estimates are of particular interest for engineering design purposes. According to the daily rainfall records the largest recorded 1-day rainfall depth is 670 mm at a site in the north-eastern parts of the country with an MAP of around 1 100 mm. The maximisation of this event has yielded the highest PMP value for the country, with an R_m of 2.7 applied to 670 mm yielding a PMP estimate of 1 820 mm. The greatest recorded 24-hour point rainfall depth in the world is 1 825 mm which occurred in 1966 in La Réunion, an island east of South Africa (WMO, 1994). This island has an MAP of 860 mm, once more indicating that extraordinary events uncharacteristic of the MAP can occur.

2.4.2 Consideration of Large Moisture Maximisation Ratios

The limitation of the moisture maximisation ratio may be implemented in order to limit exaggerated PMP estimates. However, it is not known if the parameters that produce precipitation are upper-bounded, and if so, how closely PMP estimates approach the theoretical limit (Micovic *et al.*, 2014). Therefore, limiting the corresponding atmospheric moisture conditions without scientific justification is arbitrary. Hence, the moisture maximisation ratios were not limited arbitrarily for this study but rather based on the calculated values.

Understanding that large moisture maximisation ratios can yield excessively high PMPs, several AMDRs with associated R_m values greater than 3 were investigated. The AMDRs at 17 stations, as shown in Figure 2.7, were found to be associated with well-documented significant flooding events. Most of these stations were part of the 380 representative stations where the R_m values were calculated based on the actual storm event data. This indicates that the atmospheric moisture conditions associated with these types of rainfalls are possibly linked to flooding. Table 8.1 in Appendix A summarises the details of the flooding associated with the rainfall events with large moisture maximisation ratios.

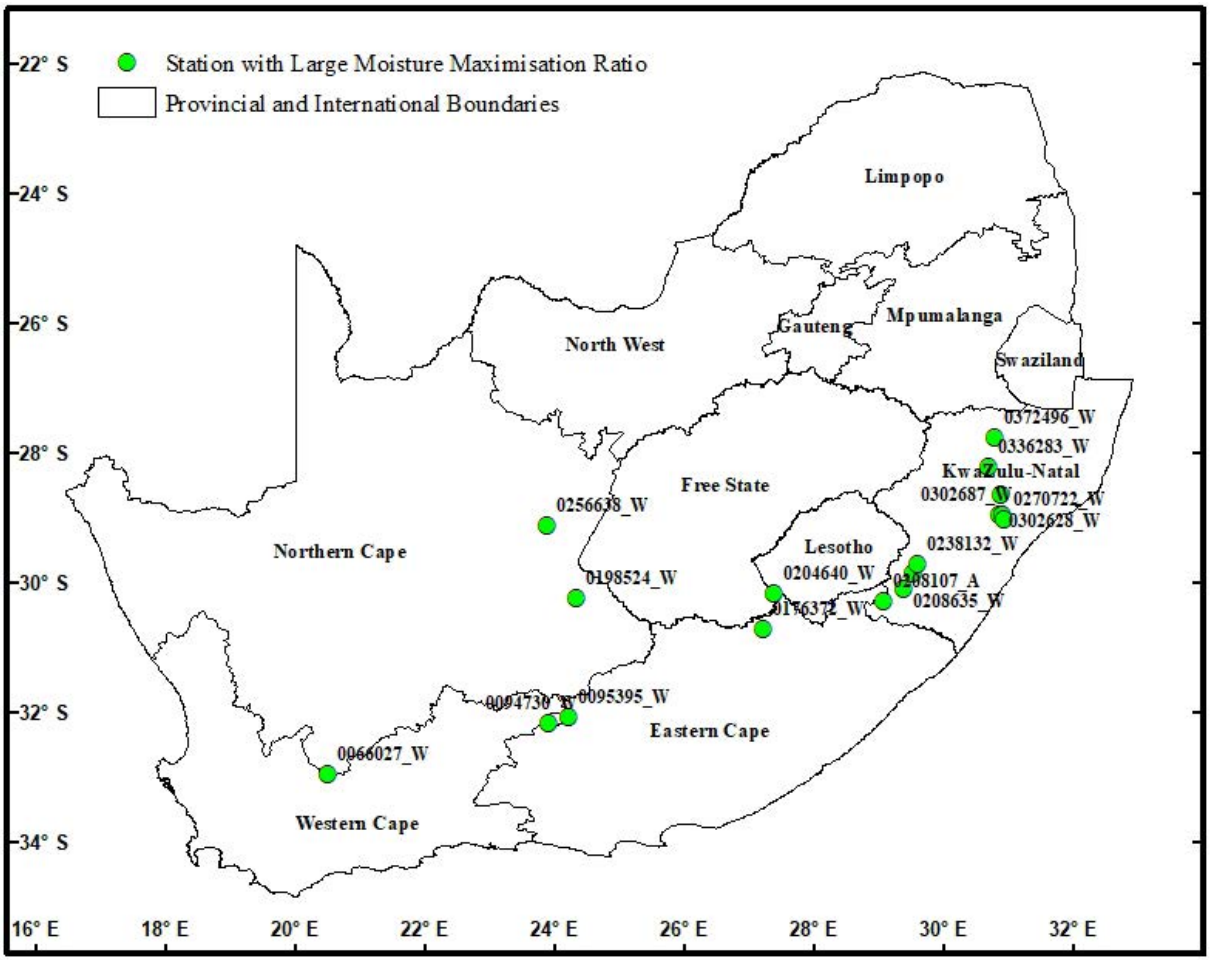

Figure 2.7 Locations of selected stations with large moisture maximisation ratios

2.4.3 Comparison of New PMP Values to HRU PMP

The HRU guidelines provide Depth-Area-Duration (DAD) curves for the PMP for each meteorologically homogeneous region as defined in HRU (1972), which are applicable at any location within the region. The locations of the 380 representative stations were matched to the corresponding HRU regions to make direct comparisons between the new 1-day PMPs and the 1-day HRU PMPs. A frequency distribution of the ratios of the newly derived PMPs to the corresponding HRU PMPs are depicted in Figure 2.8, where ratio of up to 1.1 indicates that the new PMP is equal to (within 10%) or less than the HRU estimate, and the upper limit ratios 2-6 indicate that the new PMP is greater than the HRU PMP. Approximately 80% of the new PMPs are greater than the corresponding HRU estimates, with some new estimates shown to be greater than 5 times the HRU estimates. It is noteworthy that at the particular sites where

the new PMP is at least 5 times larger, the most extreme events occurred after the period of record used for the HRU estimates, showing the impact of an updated record on PMP estimates.

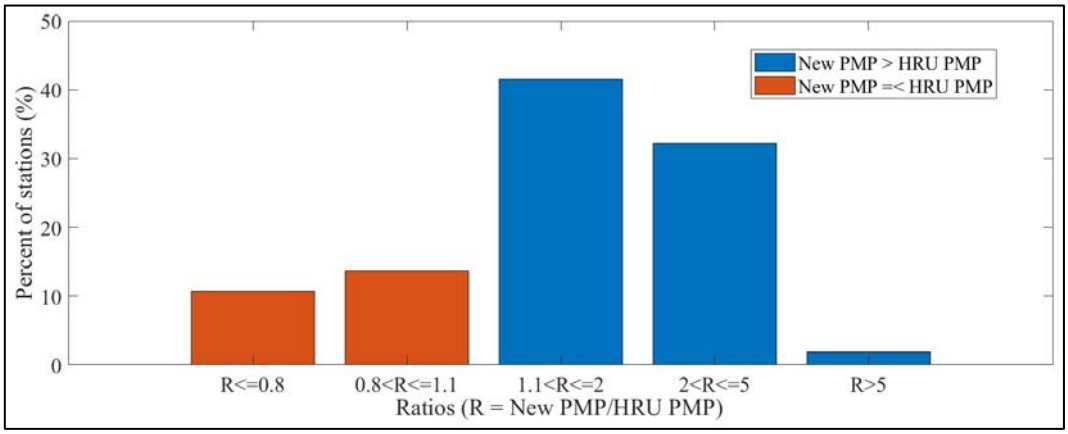

Figure 2.8 Comparison ratios of new PMP to HRU PMP

Although the HRU PMPs are applicable at any location within the region, in reality the PMP can vary with location within the same homogeneous region or rainfall district. As an example, the stations in rainfall District 70 all fall within the same HRU homogeneous region, and as such, a blanketed value for the HRU PMP is applied across the region. As depicted in Figure 2.9, PMP estimates can vary even within the same region or district and applying a blanket value can result in over- or under-estimation of the PMP.

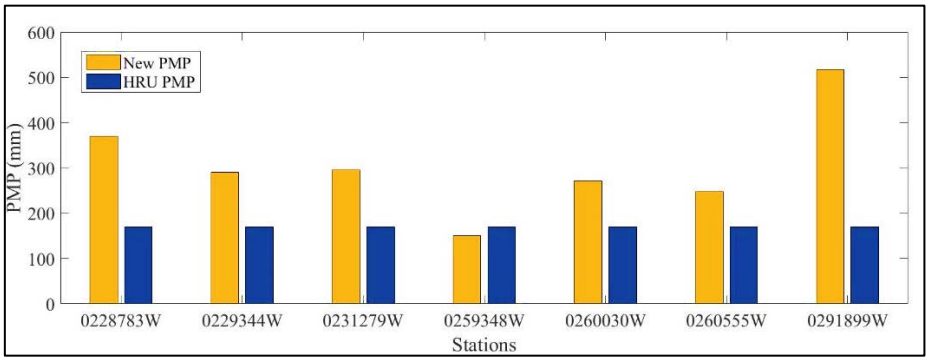

Figure 2.9 Comparison of the new PMP to the HRU PMP for Rainfall District 70

Furthermore, when the occurrence of the maximum AMDRs selected for this study were within an overlapping window with the data record used in HRU (1972), *i.e.* the 1950s, comparisons of the storm events were done to check if it were possible that the same events were used for both studies in order to compare the PMPs derived for the same storm events using two

different methods. Only 40 of the rainfall events were found to occur in the overlapping window. After analysing and comparing the rainfall depths for each of the 40 recorded storm events to the corresponding locations and rainfall depths in HRU (1972), it was assumed that events selected for these stations were common for both studies. Based on this, 75% of the newly derived PMPs were found to be larger than the HRU estimates, an example of four stations is shown in Figure 2.10. This indicates that even if the same storm events were analysed, the differences between the two approaches yield different results, with the newer approach in this study generally producing larger PMP estimates.

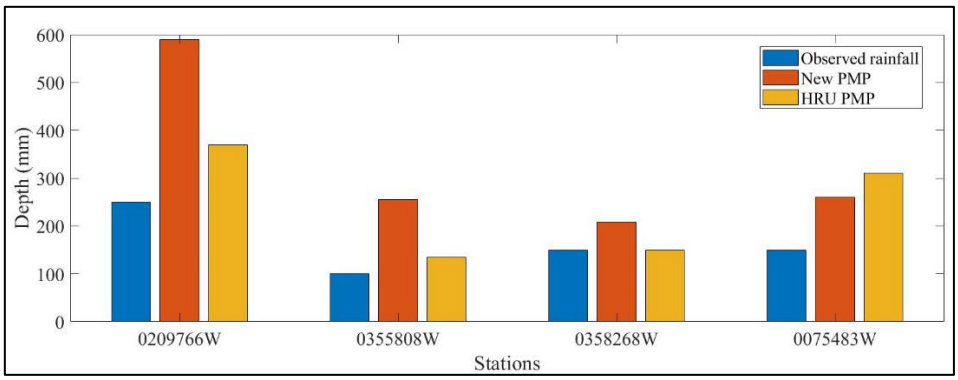

Figure 2.10 Comparison of the New PMP and HRU PMP derived from the same observed rainfall event

Approximately 70% of the most extreme storm events used in this study occurred after the 1960s. This highlights the importance of revising PMP estimates using updated and extended records. Overall, the approach used in this study provides larger PMP estimates when compared to the HRU estimates. This is likely due to the many differences used in the new approach. In instances where the new estimates are lower than the HRU estimates, this indicates that the previous PMP values may have been overestimated. A summary of the difference between the HRU methods and the methods used for this study is contained in Table 2.1. From the summary the shortcomings of the old methods and the advantages of the new approach are clear, and this gives an indication that the new approach undertaken in this study provides improved PMP estimates.

Table 2.1 Comparison of the HRU approach and the new approach for estimating PMP

	HRU PMP	New PMP
Rainfall records	30 years (1932-1961).	At least 40 years (end date ranging from 2000 to 2010).
Selection of extreme rainfall events	170 storms selected country-wide.	1629 stations used country-wide, and the most extreme rainfall event selected from each station.
Approach	Storm maximisation and transposition.	WMO generalised estimation method, storm maximisation and transposition.
Homogeneous regions	29	94
Maximisation	No data available. Procedures to calculate precipitable water content from surface temperature and pressure derived.	Daily T and RH data used to calculate T_d and corresponding precipitable water content obtained from WMO Table A.1.3.
Transposition/ interpolation	Isopercental procedure using percentages of the average MAP to draw isohyetal patterns.	Deterministic models using multiquadric RBFs.
Output	DAD curves for various durations applicable at any location within each region.	1-day PMP estimates on 5 x 5 km grid.

2.4.4 Comparison to the 1:500-year and 1:1000-year Rainfalls

The PMP defines the upper limit of extreme rainfall and is not associated with an exceedance probability, although it may be exceeded in the future with longer datasets and improved estimation methods. To evaluate if the estimated PMPs can be considered as an upper limit of extreme rainfalls, the PMP has been compared to the 1:500 and 1:1000-year rainfall estimates derived using the Generalised Extreme Value (GEV) distribution fitted to the 1-day AMDR data series using the method of L-moments (Hosking and Wallis, 1997). The GEV is the most appropriate distribution for extreme rainfall estimation in South Africa (Smithers, 1996; Smithers and Schulze, 2000a; Smithers and Schulze, 2000b). The maps of the 1:500 and

1:1000-year rainfalls compared with the PMP are shown in Figure 2.11(a-c). Generally, the PMP is greater than the 1:1000-year rainfall; however, occasionally the PMP is exceeded by the 1:500 and the 1:1000-year estimates as summarised in Figure 2.11(d). Further analysis to estimate the actual return period associated with the PMP is recommended for future research.

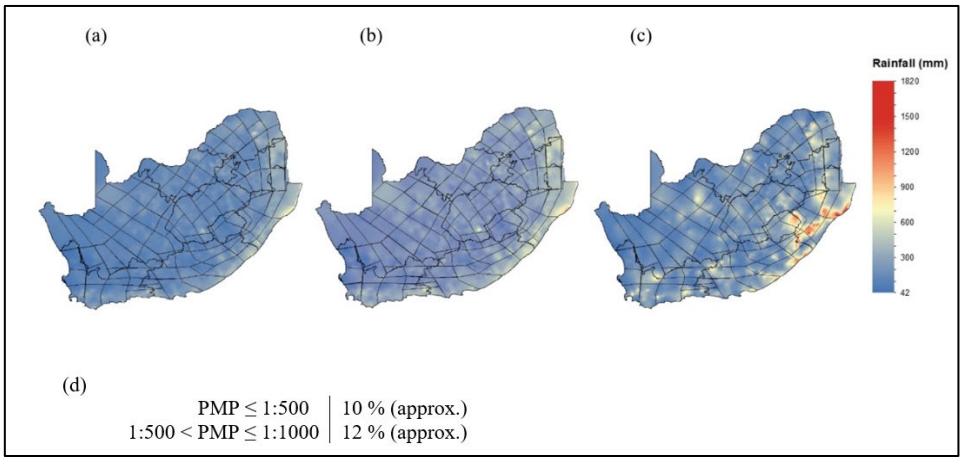

Figure 2.11 Comparison of the (a)1:500-year rainfall, (b) 1:1000-year rainfall and (c) PMP, and (d) summary of exceedances of the PMP.

2.5 Knowledge Dissemination Workshop

Despite recent developments in PMP estimation in South Africa, there have been no formal or official changes to the guidelines used by practitioners. As such, a workshop is needed to inform practitioners of the new methods available to estimate the 1-day PMP in South Africa, and to provide supporting material to facilitate the use of the updated PMP estimates in industry. The workshop was held on Thursday, 25 May 2023 at Stellenbosch University, both in-person and online, and was attended by a variety of academic researchers, industry practitioners and stakeholders. Approximately 50 participants joined the workshop either in-person or virtually.

2.5.1 Structure of the Workshop

The Workshop was conducted in 2 parts: firstly, a presentation by Ms Johnson, followed by an open discussion led by Ms Johnson and facilitated by Prof Jeff Smithers. The presentation on the updated 1-day PMP estimates provided a background to the concept of the PMP and a motivation for the importance of updating these estimates, particularly in the South African context. The current methods used in practice (HRU, 1972) were discussed, and the shortcomings of HRU estimates were highlighted. The data and methods used to update the 1-day PMP estimates in Johnson and Smithers (2020) were presented. A critical evaluation of the new PMP estimates was presented, including the consideration of extraordinarily high PMPs, a comparison of the HRU PMPs to the new PMPs, and a comparison of the new PMPs to high-return period rainfall estimates. A summary of the differences between the HRU method and new method developed by Johnson and Smithers (2020) was given to highlight the ways that the new method provides improved estimates based on the updated data and methodology. Finally, a gridded database of the new 1-day PMP estimates was presented. This database can be used to determine an at-site PMP value on a 5 x 5 km grid across South Africa.

After the presentation, an open discussion allowed practitioners to pose questions to the authors and to provide feedback on their experience of utilising PMP estimates in practice. The discussion yielded some suggestions for further improvement of the PMP estimates, *viz.*, developing regional estimates as opposed to point estimates, updating short and long duration estimates, and the inclusion of the effects of the changing climate and other meteorological factors in PMP estimates. The importance of data availability and accessibility to further revise PMP estimates in South Africa was highlighted. It was noted that the PMPs need continual revision to include newly occurring extreme events and the guidelines need to be revised.

2.5.2 Workshop materials

Workshop participants were provided with the following materials via the Water Research Observatory (WRO) online platform (WRC Project no. C2020/2021-00440):

- Workshop Presentation Slides,
- Journal Article of published 1-day PMPs (Johnson and Smithers, 2020),
- CSV file for shapefile of gridded database,

- Booklet of information on PMP estimation, and
- Authors contact details and background information.

The WRO aims to bring together important water-related datasets and information, including past research and current monitoring data, to enable big data analytics and the more sustainable management of water resources. Practitioners, researchers, academics, and stakeholders can now access the 1-day PMP dataset to use in practice and to provide feedback to the authors. The presentation slides, journal article and booklet materials, as well as the gridded PMP database and all supporting materials can be accessed via the link: https://data.waterresearchobservatory.org/metadata-form/updating-the-estimation-of-1-day-probable-maximum-precipitation-in-south-africa.

2.6 Conclusions

The PMP is an important consideration for engineering design, particularly for the design of high-hazard hydraulic structures. With the availability of an updated rainfall record and the development of new approaches globally there is an urgent need to update the PMP estimates for South Africa. A storm maximisation and transposition approach was used to estimate the 1-day PMP for South Africa. The use of an extended rainfall database and modernised methodology has produced improved PMPs compared to the previous estimates.

Large moisture maximisation ratios may also result in unusually large PMPs; however, these ratios are based on actual storm event data and indicate the realistic potential atmospheric moisture available to cause a PMP event. As the climate variables which cause precipitation are unbounded, imposing an upper bound or limit on the moisture maximisation ratio is not realistic and cannot be justified. Rouhani and Leconte (2016) propose that if such limits exit, they would be based on climate variables.

Transposition of the at-site maximised AMDR events was done using a deterministic interpolation method based only on the extreme rainfall data. However, these extreme events can be influenced by topographical gradients and elevation. To improve the transposition to ungauged locations, it recommended that these factors be considered in future research.

This study presents 1-day PMPs for South Africa; however, sub-daily and multi-day PMPs are also needed for engineering design. The limited availability of sub-daily rainfall data in South Africa prevents the estimation of reliable and accurate sub-daily PMPs. Multipliers for sub-daily storm durations may be applied to the 1-day PMPs to estimate sub-daily PMPs. Due to the limitation in the data available to maximise multi-day extreme rainfalls, it is not possible to determine multi-day PMPs using the methodology in this paper. Given current data availability policies, significant funds will be required to purchase large quantities of temperature and relative humidity, or dew point temperature data associated with multi-day rainfall events for all stations across the country. To address this, it is recommended that relationships between the 1-day PMP and 1-day high-return period design rainfall estimates be determined, and these relationships be used to investigate possible methods of obtaining multi-day PMPs. To gain insight to the possible exceedance probabilities of the PMP it is recommended that the relationships between the 1-day PMPs and 1-day high-return period design rainfall estimates may give an indication of the return period that could possibly be associated with the PMP.

A scientific basis to limit the moisture maximisation ratios should be investigated. Implementing thresholds on atmospheric moisture conditions should not be arbitrary but rather, site specific, time dependent and a function of storm characteristics.

3. NON-STATIONARY FREQUENCY ANALYSIS OF EXTREME RAINFALL EVENTS ON THE EAST COAST OF KWAZULU-NATAL

KA Johnson, JC Smithers, RE Schulze, TR Kjeldsen and S Schütte

3.1 Introduction

Extreme hydrological events such as floods are one of the deadliest hazards in South Africa (Pinto *et al.*, 2022). Extreme floods events can damage hydrological structures such as dams, spillways, bridges, and culverts. Design floods are estimated from past data based on a probability of occurrence and are required by engineers and hydrologists for the design of hydraulic structures and to quantify the risk of failure of these structures as a result of extreme hydro-climatic conditions. Therefore, minimising the risk of failure of hydraulic structures requires design floods be accurately estimated. The underestimation of design floods and failure of hydraulic structures can lead to loss of life and significant economic losses, while overestimation may result in over-design which results in excessive construction and maintenance costs. The trade-off between safety and costs is a delicate balancing act, especially for emerging economies with public budgets under pressure from competing demands. The South African Government has reported that the most common weather-related catastrophes in South Africa between the period 1900 to 2014 were floods, droughts and large storms (DFFE, 2016). Recent large floods include the event on the April 2022 experienced along the eastern coast of South Africa which was reported to have resulted in infrastructural damages to the value of 17 billion Rands and 435 casualties, 55 injured, and 54 people missing (Pinto *et al.*, 2022). Similarly, for an event in the same region in April 2019, Singh (2019) reported 650 million Rands damages to infrastructure and 60 deaths. These reported losses highlight the critical importance of flood management in the region and the absolute need for risk analysis to be supported by the best available information, data, and methods. This is particularly important as the magnitude and frequency of extreme weather events is expected to increase over time, combined with an increase in social vulnerability resulting from growing populations and associated economic activity.

Traditional methods for frequency analysis of extreme events and most current risk assessment models are based on techniques and concepts developed around a century ago (e.g. Fuller, 1914) and are based on the assumption of climate stationarity, i.e. that no temporal change is evident in the statistics of extreme events (Prosdocimi *et al.*, 2014b; Ragno *et al.*, 2019c). However, anthropogenically induced climate change has resulted in changes in extreme weather events, thus questioning the assumption of stationarity (Serinaldi and Kilsby, 2015). In recent years, the frequency and impacts of extremes have increased substantially in many parts of South Africa (Thoithi *et al.*, 2023). Hence, there is significant interest in understanding how extreme events may change into the future and how frequency analyses should be adapted to account for non-stationary data.

Statistical models used to analyse extreme events can be broadly categorised into two groups: stationary and non-stationary. In a stationary model, the observations are assumed to be drawn from a static/non-varying probability distribution function, which is assumed to represent the entire population of data, with constant parameters. Hence, the statistics of extreme events are assumed to not change over time or with respect to another variable or covariate. However, in a non-stationary model, the parameters of the underlying probability distribution function change over time or due to a selected covariate (Sadegh *et al.*, 2015). Several studies have promoted the idea of moving away from stationary models to ensure that the changing properties of extreme hydrological events are captured and accounted for in design estimates (Vasiliades *et al.*, 2015; Zhou *et al.*, 2016; Demaria *et al.*, 2017; Tan and Gan, 2017; Gao and Zheng, 2018; Ragno *et al.*, 2019b; Ouarda *et al.*, 2020; Song *et al.*, 2020; Hesarkazzazi *et al.*, 2021; Silva *et al.*, 2021).

Moyo and Nyoni (2021) warned that most climate change scenarios in South Africa show detrimental impacts on dams and flood risk management. Warmer and drier climate is linked to increased risk of droughts which adversely impact on the reliability of water supply systems and the structural integrity of dams. Warmer and wetter scenarios are characterised by more frequent and severe extreme flood events which are directly linked to dam safety concerns as well as to increased sedimentation. McBride *et al.* (2022) noted that, despite the total number of observed rain days having remained relatively constant over the past century, the probability of significant extreme daily rainfall events occurring has increased for most parts of South

Africa. Ultimately, many climate change scenarios are highly likely to have an adverse impact on dam safety and flood risk management. The impacts of climate change can be modelled using outputs from GCMs. These models can be used at a global scale or can be downscaled, and bias corrected for application at local scales.

Given the importance of water resources and flood risk management, the potential impact of climate change on the magnitude and frequency of extreme events requires urgent attention in South Africa to ensure that the best possible science is supporting operational hydrological decision-making and risk assessment (Smithers *et al.*, 2014; Johnson *et al.*, 2021). This urgency is supported by Hattingh (2021), who highlighted the need to address the challenge of climate change and its impacts on dams, including risk-based approaches, in order to account for uncertainty associated with a non-stationary climate, with this further highlighting the importance of this research in the South African context.

The aims of the study reported in this Chapter are to determine if any trends exist in observed extreme rainfall events along the East Coast of KwaZulu-Natal, to contribute an understanding of the teleconnection patterns between various climate drivers and the annual maximum daily extreme rainfall and to account for possible non-stationarity in climate data in the estimation of extreme design rainfall events in South Africa. The objectives of this chapter are to: (i) investigate trends in annual maximum daily rainfall using parametric and non-parametric statistical tests, (ii) identify potential climate drivers of extreme rainfalls, (iii) perform stationary and non-stationary rainfall frequency analyses, (iv) critically evaluate the stationary vs non-stationary models, and (v) evaluate projected changes in rainfall using GCMs.

3.2 Materials and Methods

3.2.1 Data sources and case study site selection

Given the lack of access to concurrent and up-to-date rainfall data at a national scale from the South African Weather Services (SAWS), the east coast of KwaZulu-Natal (KZN) in South Africa was selected for a case study to investigate how extreme rainfalls may have changed over time, as data were available for this region. Daily rainfall data were obtained from the South African Sugarcane Research Institute (SASRI), which provides open access to up-to-

date climate data over the sugarcane production region within South Africa. Approximately 100 stations with rainfall data up to the year 2020 were extracted from the SASRI database. The rainfall data were screened according to the following criteria:

a) the record length must be at least 40 years,
b) the record should be the most up-to-date, and
c) no more than three months of data should be missing.

The daily rainfall time series from each site was checked for missing data. To construct a time series of the Annual Maximum Daily Rainfall (AMDR) it is important that each year of the records be sufficiently complete so that the largest rainfall totals are likely to have been captured and to prevent seasonal bias. Based on the selection criteria, 39 sites were selected for this study. Figure 3.1depicts the SASRI station numbers and locations of the stations used in the study and Table 3.1 contains a summary of the station information.

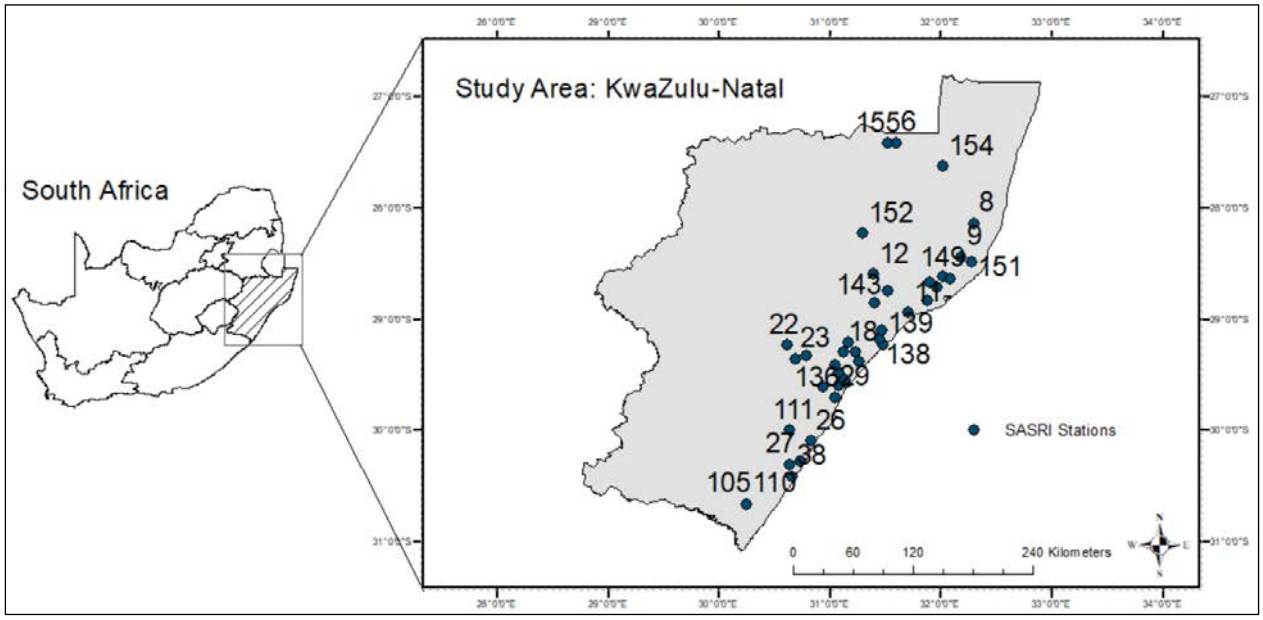

Figure 3.1 SASRI stations in KwaZulu-Natal selected for this study

Table 3.1 Station information for case study sites

Station Name	SASRI Station Number	Altitude (m)	Start Year	End Year	Total Years
Pongola – SASRI	6	308	1966	2014	48
Glen Park − St Lucia Farms	8	35	1966	2020	54
Mtubatuba – Riverview Sugar Mill	9	46	1966	2020	54
Mtunzini – ex SASRI	11	36	1966	2020	54
Melmoth – CA Leith & Sons	12	790	1967	2020	53
Glendale – Tenrith Farm	18	129	1966	2020	54
Tongaat – Klipfontein (THS)	20	72	1965	2020	55
Seven Oaks – Saw Mill	22	1067	1966	2020	54
Noodsberg – Illovo Sugar Mill	23	1008	1971	2020	49
Illovo – Sugar Estate	26	15	1966	2020	54
Vulamehlo – Esperanza	27	195	1968	2015	47
Mt Edgecombe – SASRI	29	96	1927	2020	93
Sezela – Illovo Sugar Estate	38	90	1976	2020	44
Oribi Flats – Minnehaha Farm	105	520	1965	2020	55
Renishaw – Crooks Bros Estate	110	61	1957	2020	63
Powerscourt – Roseleigh Estate	111	637	1957	2020	63
Inanda – Farm	114	556	1957	2020	63
Inyaninga – THS	120	107	1957	2019	62
Maidstone – Sugar Mill (THS)	123	46	1957	2020	63
Sinembe – Spreyton Farm	125	237	1957	2020	63
Upper Tongaat – Barwon Farm	126	457	1957	2020	63
Kearsney – Ocean Lodge	129	277	1957	2020	63
Doornkop – Langespruit Farm	130	545	1957	2020	63
Darnall – Sugar Mill (THS)	131	142	1957	2020	63
Tugela Mouth – Wetherly Estate	132	114	1957	2015	58
Glenside – Misty Krantz Estate	136	997	1974	2017	43
Mandini – SAWS	138	99	1957	2020	63
Inyoni – Myrln Estate	139	107	1957	2020	63
Eshowe – Brocklee Farm	142	549	1957	2020	63
Nkwaleni – Zigagazi	143	137	1957	2019	62
Felixton – Sugar Mill (THS)	144	46	1957	2020	63
Kulu Halt – Honey Farm	146	61	1957	2020	63
Ukulu Properties – Crystal Holdings	147	152	1957	2020	63
Mposa – Redcroft Farm	148	91	1957	2020	63
Kwambonambi – Mondi Forestry	149	30	1957	2020	63

Station Name	SASRI Station Number	Altitude (m)	Start Year	End Year	Total Years
ULOA – Mark & Ross Sugar Estate	151	15	1957	2015	58
Mtubatuba – Nyalazi River	152	34	1957	2015	58
Mkuze – Mkuze Estate	154	150	1957	2020	63
Pongola – Impala Irrigation Board	155	290	1957	2020	63

3.2.2 Methodology

The basic methodology applied in this study to determine extreme rainfall quantities at a given location, and how they may vary with respect to a selected covariate, is detailed in the following sections. The main steps involved in this approach are summarised in Figure 3.2

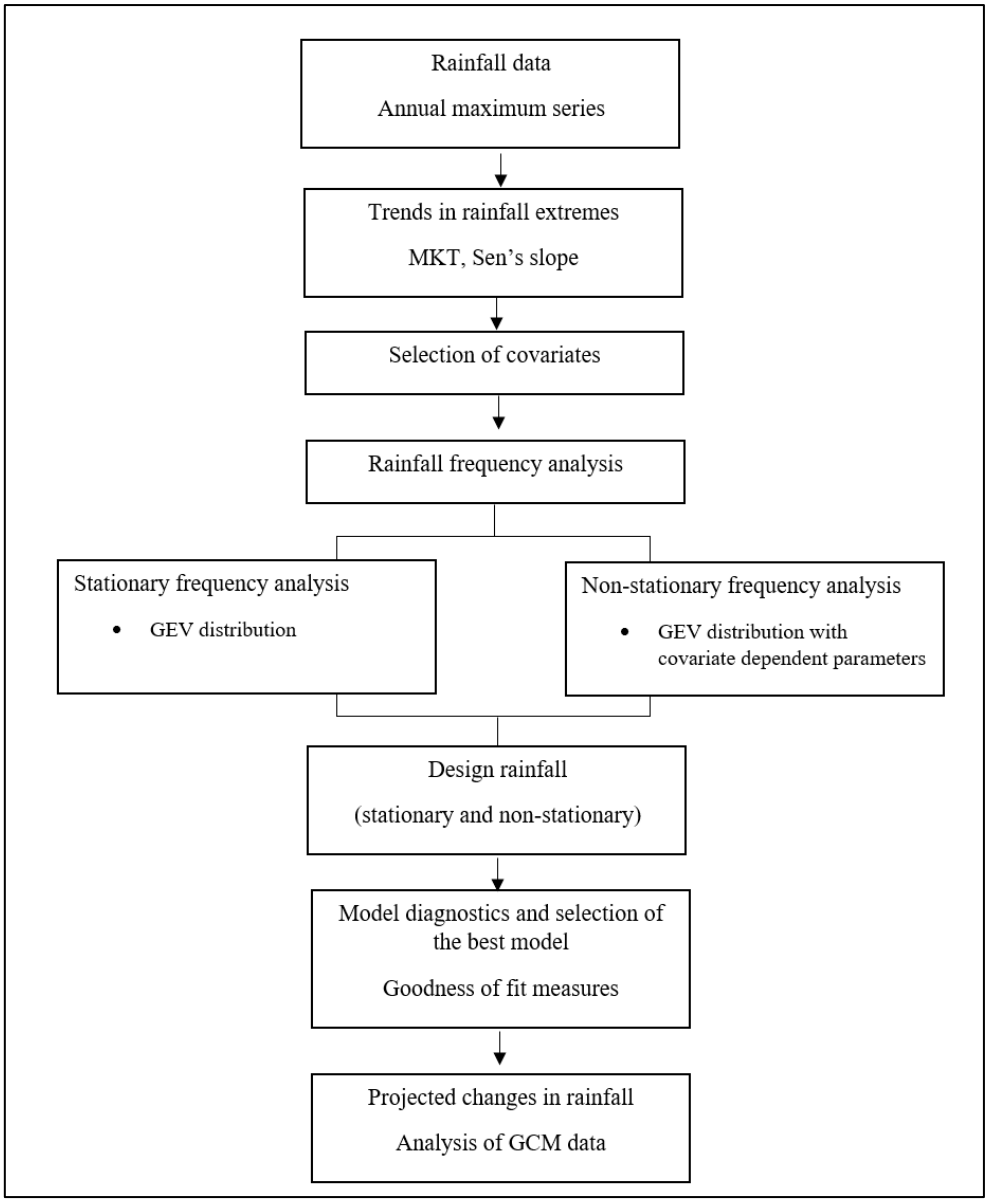

Figure 3.2 Stationary and non-stationary design rainfall estimation procedures

3.2.2.1 Trends in rainfall extremes

The existence or not of trends in hydrological extremes can be investigated using parametric or non-parametric methods. Parametric methods include using simple linear regression to investigate how annual maximum rainfall changes over time. However, this method can only be used on data that are normally distributed (Kundzewicz, 2019). The Mann-Kendall Test, MKT, (Mann, 1945; Kendall, 1962) is a non-parametric test often used to detect trends in hydrological extremes (Cheng *et al.*, 2014; Yilmaz and Perera, 2015; Agilan and Umamahesh,

2018; Ragno *et al.*, 2019b; Hesarkazzazi *et al.*, 2021). The term 'non-parametric' refers to the absence of assumptions about the distribution of the data in the method (Mathivha *et al.*, 2021). The MKT does not provide information on the magnitude of a trend, it only provides details about the existence, significance, and direction of a trend (Mangini *et al.*, 2018). In addition, the Sen's slope is a non-parametric method used to evaluate the linear trend of the data series (Sen, 1968). Hence, the MKT and Sen's slope were selected to detect and quantify trends in the AMDR data.

3.2.2.2 Frequency distribution and non-stationary models

The three-parameter Generalised Extreme Value (GEV) distribution is commonly applied to Annual Maximum Series (AMS) of rainfall data. The GEV has been determined to be a suitable distribution for design rainfall estimation in South Africa (Smithers, 1996; Smithers and Schulze, 2000b) and it allows the incorporation of non-stationarity through varying parameters. The GEV distribution was thus selected for use in this research to evaluate the non-stationarity of rainfall data over time.

The GEV distribution function is used to model time series of annual maximum series data or block maxima. The GEV cumulative distribution function is given as (Coles, 2001):

$$\Psi_{GEV}(x) = \exp\left\{-\left(1+\xi\cdot\left(\frac{x-\mu}{\sigma}\right)\right)^{-\frac{1}{\xi}}\right\} \tag{3.1}$$

for $1+\xi\cdot((x-\mu)/\sigma) > 0.\mu,\sigma$, and ξ are the parameters of the distribution: μ is the location parameter, $\sigma > 0$ is the scale parameter, and ξ is the shape parameter which defines the tail behaviour of the distribution. The stationary GEV model can be extended for dependent series by letting the parameters of the distribution be a function of a general covariate x_c, i.e. $\mu(x_c), \sigma(x_c), \xi(x_c)$ (Coles, 2001). Hence, the non-stationary form of Eq. (3.1) is described as:

$$\Psi_{GEV}(x \mid x_c) = \exp\left\{-\left(1+\xi(x_c)\cdot\left(\frac{x-\mu(x_c)}{\sigma(x_c)}\right)\right)^{-\frac{1}{\xi(x_c)}}\right\} \tag{3.2}$$

The concept of effective return period or effective design value is defined as q-quantile, Q, varying as a function of a given covariate, e.g. temporal and/or physical. Therefore, for a

constant value of $RP = 1/q$, where q is the annual exceedance probability, the effective return period is defined as:

$$\left(\left(x_c, Q_q(x_c)\right),\ q \in [0,1]\right) \tag{3.3}$$

where

x_c = the covariate, and

$Q_q(x_c)$ = the q-quantile.

The Process-informed Non-stationary Extreme Value Analysis (ProNEVA) is a tool in MATLAB developed by Ragno *et al.* (2019c) in which the non-stationary component is defined by a temporal or physical driver. This tool has been used to perform stationary and non-stationary rainfall frequency analysis for this study.

3.2.2.3 Selection of covariates

According to Agilan and Umamahesh (2017), the most suitable covariates for short-duration rainfall events (less than 24 hours) are local processes, e.g. local temperature changes and urbanisation, whilst the most suitable covariates for long-duration (1-day and greater) rainfall events are global processes, such as global temperature change, the El Niño-Southern Oscillation (ENSO) cycle, and the Indian Ocean Dipole (IOD) cycle. ENSO and IOD are significant drivers of the southern African climate during the austral summer rainy season and have thus been used in numerous studies to predict the occurrence of extremes (Gaughan *et al.*, 2016; Hoell *et al.*, 2021; Lüdecke *et al.*, 2021).

ENSO and IOD are related to sea surface variations and air pressure across the world, based on observed data. ENSO is represented by the Southern Oscillation Index (SOI), which is associated with warm Sea Surface Temperatures (SST) and is characterised by the variations between the Indonesian Low pressure system and the South Pacific Tropical High pressure system (de Silva and Hornberger, 2019). The IOD is an oscillation of SST in the equatorial Indian Ocean and is considered relevant to the climate of countries surrounded by the Indian Ocean. It is represented by the Dipole Mode Index (DMI). The effects of ENSO and IOD are

considered to be independent (de Silva and Hornberger, 2019), hence both phenomena are considered as potential significant covariates for this study.

As changes in temperature are linked to increased greenhouse gas concentrations (IPCC, 2017b), and these climate process behaviours and their associations are potentially non-stationary (Endris *et al.*, 2019), CO_2 concentrations for South Africa and Global Mean Temperatures (GMT) were included as potential significant covariates for this study.

The main purpose of this chapter is to contribute to an understanding of the teleconnection patterns between the Southern Oscillation Index (SOI), Dipole Mode Index (DMI), Carbon Dioxide (CO_2), and Global Mean Temperature (GMT) and annual maximum daily extreme rainfall in KZN, in identifying non-stationary patterns in the data. Data used for the analyses are SOI and DMI monthly data from 1928-2020 (Bureau of Meteorology, 2023), annual global carbon emissions data ($MtCO_2$) from 1960-2020 (Global Carbon Atlas, 2023), and global mean temperature data from 1928-2020 (National Aeronautics and Space Administration, 2023).

3.2.2.4 Model diagnostics and selection of the best model

The purpose of fitting a statistical model, whether it is stationary or non-stationary, is to characterise the population from which the data were drawn for further analysis. Hence, it is necessary to check the performance of the fitted model to the data (Coles, 2001). Several metrics are implemented to assess the Goodness of Fit (GOF) and support model selection, including: (1) the Akaike Information Criterion (AIC), (2) the Bayesian Information Criterion (BIC), and (3) the Root Mean Square Error (RMSE).

The Akaike Information Criterion, (AIC) (Akaike, 1974), is a GOF measure that compares the frequency models and represents how well each model fits the data relative to other models. The lower the AIC value, the better the model performance, in comparison to other models. The AIC is computed as follows:

$$AIC = 2 \cdot (D - \hat{L}) \tag{3.4}$$

where D is the number of parameters of the statistical model and $\hat{L}$ is the maximised log-likelihood function which is a measure of how well a particular model fits the data using the

probability density of observed data viewed as a function of the parameters of a statistical model.

The Bayesian Information Criterion (BIC) (Schwarz, 1978) is defined as:

$$BIC = D \cdot \ln(N) - 2 \cdot \hat{L}, \quad (3.5)$$

where N is the length of records. As with AIC, the model with lower BIC yields the best fit. The Root Mean Square Error (RMSE) is widely used in hydrology and climatology as a GOF measurement, and is given by

$$RMSE = \sqrt{\frac{\sum_{i=1}^{n}(y_i - Y_i)^2}{n}} \quad (3.6)$$

where

y_i = the actual value for the ith observation,

Y_i = the predicted value for the ith observation, and

n = the number of observations.

A perfect fit is associated with $RMSE = 0$, given $RMSE \in [0, \infty)$.

3.3 Results and Discussion

3.3.1 Trend detection

Table 3.2 contains a summary of results for the analyses of the AMS from 39 stations subjected to the MKT and Sen's slope test. The MKT was evaluated at the 5% significance level. Figure 9.1 in Appendix B contains the graphs depicting the time series plot for each station assessed. Based on the MKT and Sen's test, the results indicate that for the majority of the stations in the KZN study region no significant upward trend over time was detected, with approximately 40% of stations showing a positive trend and only one station (Station 38: Sezela – Illovo Sugar Estate), located on the south coast of the province, showing a significant positive trend, as shown in Figure 3.3. It is noteworthy that this station has one of the shortest record lengths, which could influence the results. These results highlight the difficulties in detecting significant trends in relatively short and highly variable at-site hydro-meteorological series, especially when using non-parametric tests with relatively low statistical power. The results are similar

to those found by Kibii (2021), who assessed seasonal and annual rainfall trends in South Africa and found that daily rainfall reflected insignificant trends.

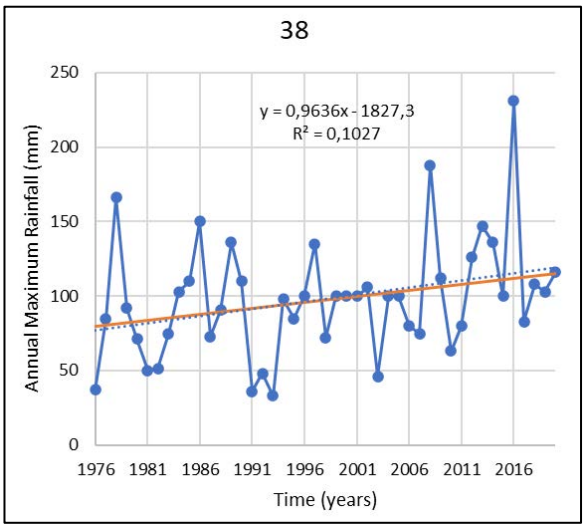

Figure 3.3 Time series for Station 38

Table 3.2 Trends in KwaZulu-Natal extreme rainfall using the Mann-Kendall test

Station Name	SASRI Station Number	p-value	Sen's Slope	Interpretation of Test
Pongola – SASRI	6	0.088	0.426	Insignificant positive trend
Glen Park – St Lucia Farms	8	0.147	-0.367	Insignificant negative trend
Mtubatuba – Riverview Sugar Mill	9	0.092	-0.609	Insignificant negative trend
Mtunzini – ex SASRI	11	0.674	-0.150	Insignificant negative trend
Melmoth – CA Leith & Sons	12	0.747	0.070	Insignificant positive trend
Glendale – Tenrith Farm	18	0.165	-0.396	Insignificant negative trend
Tongaat – Klipfontein (THS)	20	0.472	-0.244	Insignificant negative trend
Seven Oaks – Saw Mill	22	0.983	0.000	Insignificant trend
Noodsberg – Illovo Sugar Mill	23	0.604	0.073	Insignificant positive trend
Illovo – Sugar Estate	26	0.389	0.333	Insignificant positive trend
Vulamehlo – Esperanza	27	0.985	0.000	Insignificant positive trend
Mt Edgecombe – SASRI	29	0.075	0.250	Insignificant positive trend
Sezela – Illovo Sugar Estate	38	**0.023***	**0.810***	**Significant positive trend***
Oribi Flats – Minnehaha Farm	105	0.539	0.255	Insignificant positive trend
Renishaw – Crooks Bros Estate	110	0.070	0.613	Insignificant positive trend
Powerscourt – Roseleigh Estate	111	0.147	-0.344	Insignificant negative trend
Inanda – Farm	114	0.835	-0.062	Insignificant negative trend
Inyaninga – THS	120	0.585	-0.121	Insignificant negative trend
Maidstone – Sugar Mill (THS)	123	0.509	0.167	Insignificant positive trend
Sinembe – Spreyton Farm	125	0.138	0.323	Insignificant positive trend
Upper Tongaat – Barwon Farm	126	0.354	0.208	Insignificant positive trend
Kearsney – Ocean Lodge	129	0.461	-0.081	Insignificant negative trend
Doornkop – Langespruit Farm	130	0.780	-0.033	Insignificant negative trend
Darnall – Sugar Mill (THS)	131	0.672	0.092	Insignificant negative trend
Tugela Mouth – Wetherly Estate	132	0.468	-0.191	Insignificant negative trend
Glenside – Misty Krantz Estate	136	0.100	-0.448	Insignificant negative trend
Mandini – SAWS	138	0.206	0.401	Insignificant positive trend
Inyoni – Myrln Estate	139	0.147	0.359	Insignificant positive trend
Eshowe – Brocklee Farm	142	0.404	-0.195	Insignificant negative trend
Nkwaleni – Zigagazi	143	0.826	-0.039	Insignificant negative trend
Felixton – Sugar Mill (THS)	144	0.631	-0.136	Insignificant negative trend
Kulu Halt – Honey Farm	146	0.516	-0.176	Insignificant negative trend
Ukulu Properties – Crystal Holdings	147	0.655	-0.129	Insignificant negative trend
Mposa – Redcroft Farm	148	0.972	0.007	Insignificant positive trend
Kwambonambi – Mondi Forestry	149	0.242	-0.257	Insignificant negative trend
ULOA – Mark & Ross Sugar Estate	151	0.517	-0.203	Insignificant negative trend
Mtubatuba – Nyalazi River	152	0.367	-0.230	Insignificant negative trend
Mkuze – Mkuze Estate	154	0.839	-0.023	Insignificant negative trend
Pongola – Impala Irrigation Board	155	0.235	0.249	Insignificant positive trend

***Significant trends at 5% level identified**

3.3.2 Analysis of stationary and non-stationary models

Both stationary and non-stationary frequency analyses were undertaken using the GEV distribution for all stations in the study area. For the non-stationary frequency analysis, the location and scale parameters of the GEV distribution were modelled as linear functions of the selected covariates and the shape parameter was kept constant.

Firstly, the non-stationary models considering time as a covariate were compared to the stationary models for each station. Table 3.3 contains a summary of results for the AIC, BIC and RMSE tests considering time as a covariate at the 39 stations used in the study. The AIC and BIC and RMSE values of the stationary model are lower than those of the non-stationary model for most stations. Based on the AIC, the results indicate that 35 out of 39 stations in the KZN region are better modelled through the stationary model, as lower AIC, BIC, and RMSE values indicate a superior performing model (Ragno *et al.*, 2019b). The non-stationary models provided a better fit than the corresponding stationary model at only four stations (38, 136, 138 and 152). Using the BIC measure, the non-stationary models for only one station (138) were found to give a better fit of the data. Ouarda *et al.* (2020) found similar results considering time as covariate in the non-stationary model.

Table 3.3 The GEV statistical model performance criteria of selected sites in KwaZulu-Natal AMDR for time as a covariate

Station Name	**SASRI Station Number**	**Stationary**			**Non-Stationary**		
		AIC	**BIC**	**RMSE**	**AIC**	**BIC**	**RMSE**
Pongola – SASRI	6	460.81	466.49	1.62	462.90	474.25	1.29
Glen Park – St Lucia Farms	8	558.34	564.36	1.55	562.22	574.27	1.27
Mtubatuba – Riverview Sugar Mill	9	575.74	581.70	1.82	579.30	591.24	1.60
Mtunzini – ex SASRI	11	580.81	586.83	1.32	587.07	599.11	1.41
Melmoth – CA Leith & Sons	12	524.07	529.98	2.01	530.18	542.00	2.18
Glendale – Tenrith Farm	18	538.31	544.27	1.24	542.06	553.99	1.63
Tongaat – Klipfontein (THS)	20	549.95	555.97	1.24	553.22	565.27	1.66

Station Name	SASRI Station Number	Stationary			Non-Stationary		
		AIC	BIC	RMSE	AIC	BIC	RMSE
Seven Oaks – Saw Mill	22	493.72	499.74	4.30	495.97	508.02	3.57
Noodsberg – Illovo Sugar Mill	23	433.83	439.57	2.60	440.31	451.78	2.73
Illovo – Sugar Estate	26	531.30	537.10	1.76	536.26	547.85	1.35
Vulamehlo – Esperanza	27	504.05	509.60	1.88	508.19	519.30	1.58
Mt Edgecombe – SASRI	29	954.38	961.98	1.45	956.19	971.39	1.16
Sezela – Illovo Sugar Estate	38	449.01	454.36	1.79	**447.38***	456.30	**1.71***
Oribi Flats – Minnehaha Farm	105	597.12	603.20	1.22	600.91	613.06	0.99
Renishaw – Crooks Bros Estate	110	678.80	685.27	1.18	681.18	694.14	0.97
Powerscourt – Roseleigh Estate	111	650.68	657.16	1.71	654.17	667.12	1.47
Inanda – Farm	114	654.36	660.84	1.68	660.62	673.57	1.49
Inyaninga – THS	120	638.31	644.73	1.12	641.61	654.47	0.97
Maidstone – Sugar Mill (THS)	123	644.55	651.02	1.53	649.04	662.00	1.39
Sinembe – Spreyton Farm	125	646.42	652.90	1.87	647.89	660.84	2.15
Upper Tongaat – Barwon Farm	126	650.56	657.04	1.75	655.20	668.15	1.57
Kearsney – Ocean Lodge	129	624.55	631.03	2.60	627.67	640.62	2.11
Doornkop – Langespruit Farm	130	633.31	639.74	1.45	639.00	651.86	1.15
Darnall – Sugar Mill (THS)	131	644.40	650.87	1.62	650.88	663.84	1.88
Tugela Mouth – Wetherly Estate	132	582.99	589.23	1.38	587.49	599.96	0.96
Glenside – Misty Krantz Estate	136	449.30	454.65	5.50	**441.49***	450.41	**4.77***
Mandini – SAWS	138	669.56	676.04	3.14	**663.81***	**674.60***	**2.37***
Inyoni – Myrln Estate	139	655.28	661.76	1.53	658.52	671.47	1.26
Eshowe – Brocklee Farm	142	649.98	656.46	1.43	653.17	666.12	1.03
Nkwaleni – Zigagazi	143	639.43	645.91	1.86	644.96	657.91	1.61

Station Name	SASRI Station Number	Stationary			Non-Stationary		
		AIC	BIC	RMSE	AIC	BIC	RMSE
Felixton – Sugar Mill (THS)	144	658.45	664.92	1.53	662.85	675.80	1.41
Kulu Halt – Honey Farm	146	674.01	680.48	1.63	679.81	692.77	1.53
Ukulu Properties – Crystal Holdings	147	672.21	678.69	1.42	677.51	690.46	2.02
Mposa – Redcroft Farm	148	658.21	664.68	1.61	664.53	677.49	1.64
Kwambonambi – Mondi Forestry	149	656.35	662.82	2.01	664.71	677.66	2.00
ULOA – Mark & Ross Sugar Estate	151	639.67	645.90	3.13	645.48	657.94	2.83
Mtubatuba – Nyalazi River	152	578.80	585.03	2.13	**578.77***	591.24	**1.31***
Mkuze – Mkuze Estate	154	612.12	618.59	2.37	617.67	630.62	1.14
Pongola – Impala Irrigation Board	155	615.82	622.30	2.09	618.61	631.57	2.37

*** Non-stationary model performs better than stationary model overall**

Station 38 (Sezela – Illovo Sugar Estate) in Figure 3.4 was the only station to show a significant increase in rainfall over time and have the non-stationary time-model outperform the stationary model. This station also showed an increase in the effective return period of rainfall, which summarizes the impact of time on rainfall by describing return periods as functions of time (x-axis). Although Station 38 showed a positive trend in data and a corresponding increase in overall effective return periods, the trends of effective return periods vary for each station and a positive trend does not necessarily correlate to an increasing effective return period.

The effective return period for Station 38 is shown to increase as a function of time for all return periods. Figure 3.4 depicts the GEV for the: (a) stationary model, (b) non-stationary model, and (c) effective return period as a function of time for Station 38: Sezela (Illovo Sugar Estate). Appendix B (Figure 9.2 to Figure 9.40) contains the plots for the stationary and non-stationary frequency analyses for all covariates and effective return periods for all stations.

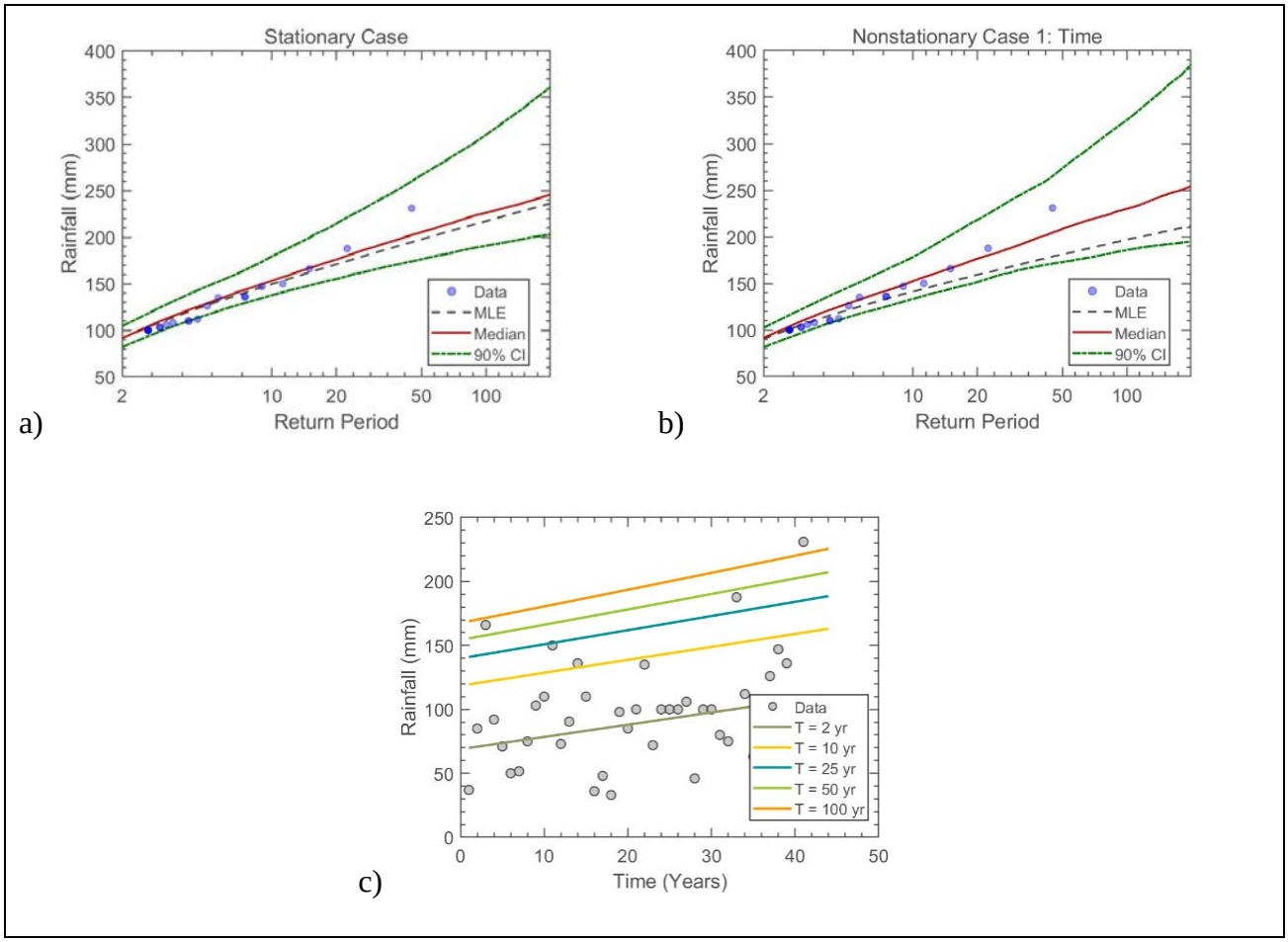

Figure 3.4 The GEV (a) stationary model, (b) non-stationary model considering time as a covariate, and (c) effective return period as a function of time for Station 38: Sezela – Illovo Sugar Estate

Secondly, the non-stationary models considering SOI, DMI, CO_2 and GMT as covariates were compared to the stationary models for each station. Table 2.4 summarises the best-fit models for the stationary and non-stationary cases based on AIC and BIC measures. The detailed results are presented in Table 9.1 in Appendix B. The stationary models perform better than the non-stationary models at 56% and 36% of stations, based on the AIC and BIC measures, respectively. Some non-stationarity is noted with respect to time; however, very little impact due to SOI and DMI is evident.

Most often the stations where the non-stationary CO_2 model outperformed the other models resulted in consistent trends for both AIC and BIC tests. This indicates that it may be argued

that climate driving factors, such as CO_2 changes, largely influence extreme rainfalls in KZN. None of the non-stationary models considering GMT as a covariate outperformed any other model.

Table 3.4 Summary of best-fit models for all stationary and non-stationary cases

AIC		BIC	
Model	**Number of best-fit models**	**Model**	**Number of best-fit models**
Stationary	22 (56%)	Stationary	14 (36%)
Non-stationary – Time	4 (10%)	Non-stationary – Time	2 (5%)
Non-stationary – SOI	4 (10%)	Non-stationary – SOI	0 (0%)
Non-stationary – DMI	1 (3%)	Non-stationary – DMI	0 (0%)
Non-stationary – CO_2	8 (21%)	Non-stationary – CO_2	23 (59%)
Non-stationary – GMT	0 (0%)	Non-stationary – GMT	0 (0%)

Figure 3.5 and Figure 3.6 show the locations of which models best fit the data based on AIC and BIC, respectively. No spatial patterns are evident based on the location of the best-fit non-stationary models.

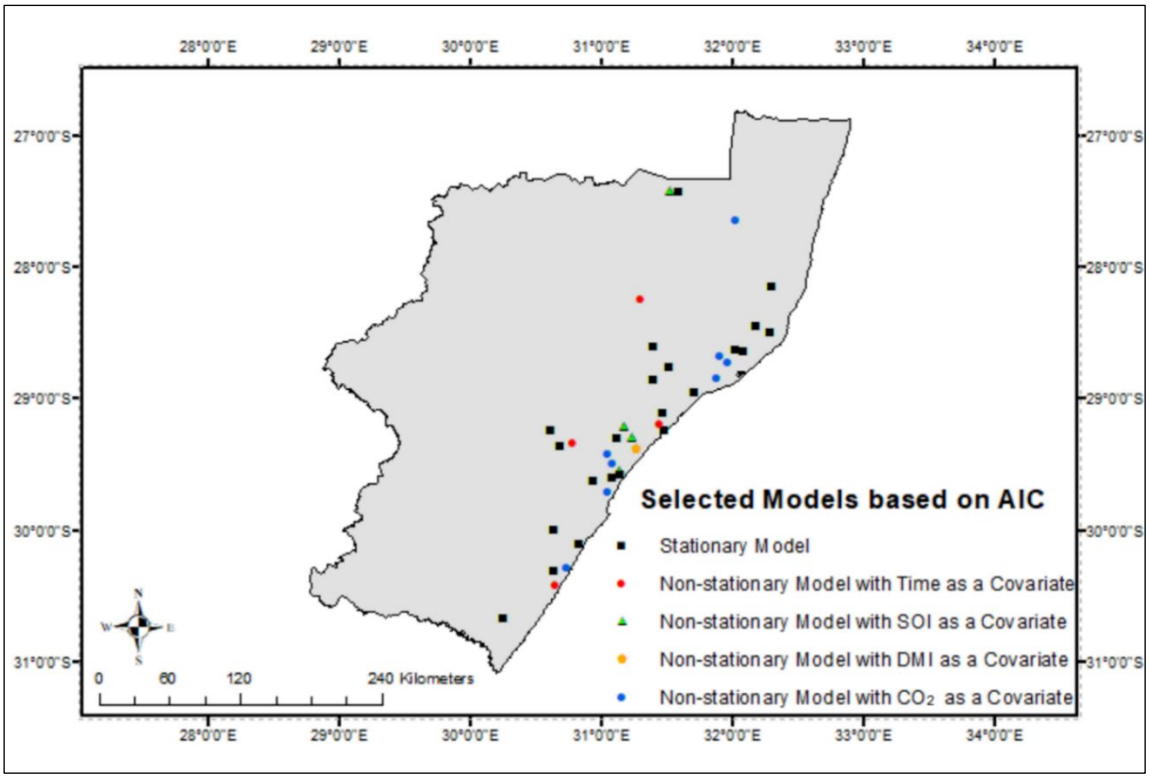

Figure 3.5 Best-fit distribution model, based on the AIC measure

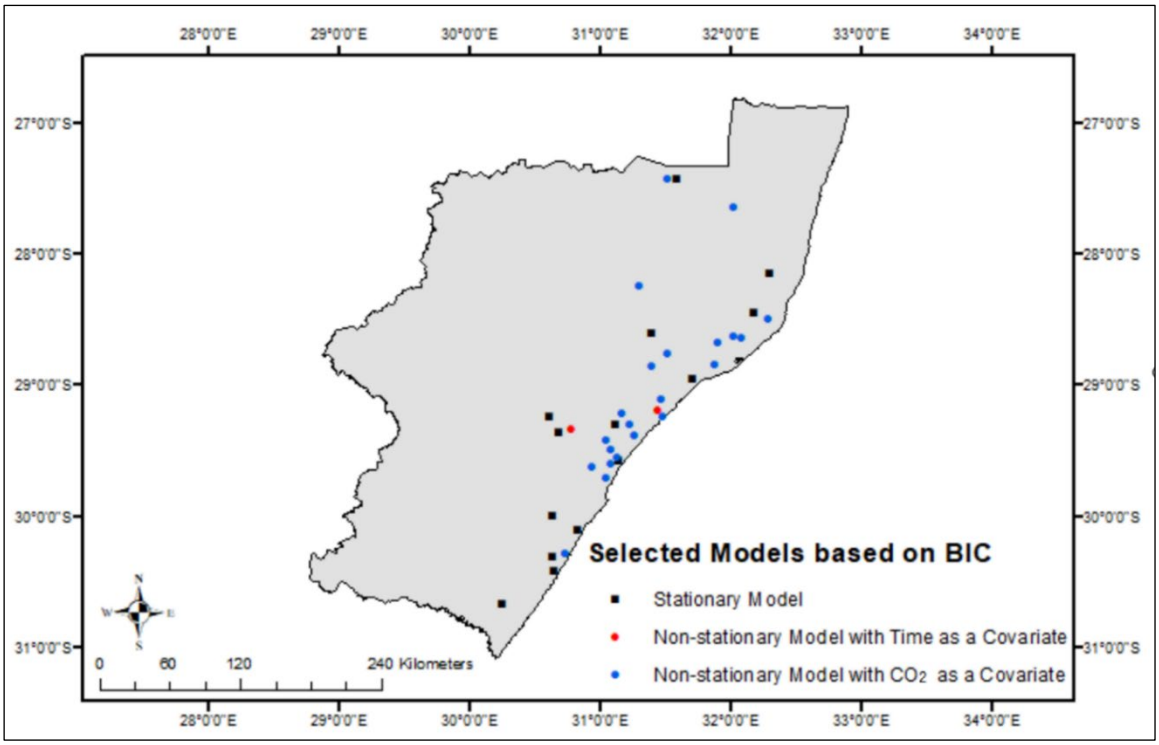

Figure 3.6 Best-fit distribution model, based on the BIC measure

3.3.3 Projected changes in rainfall

The results of the analysis of observed data in the previous sections mostly show insignificant changes in historical extreme rainfalls and design rainfalls. However, there is still a need to understand possible future scenarios for design purposes. To consider the projected changes in rainfall and the possible climate change factors, or ratios, that could be applied to current design rainfall depths to estimate design for future scenarios, an ensemble of very high-resolution climate model simulations of present-day climate as well as projections of future climate changes over South Africa was selected. These projections were produced by the CSIR using the CCAM regional climate model and were further bias-corrected to local observed temperature and rainfall data by Schütte *et al*. (2023). The data used in this study were sourced from Schütte *et al.* (2023) and contains outputs from six GCMs from the CMIP5 archive based on the Representative Concentration Pathway (RCP) Scenarios 8.5, i.e. the "business as usual" scenario of Greenhouse Gas emissions into the future. The simulations span the period 1961-2100.

The six GCMs are the:

• Australian Community Climate and Earth System Simulator (ACCESS1-0),

• Community Climate System Model (CCSM4),

• National Center for Meteorological Research Coupled Global Climate Model, v5 (CNRM-CM5),

• Geophysical Fluid Dynamics Laboratory Coupled Model (GFDL-CM3),

• Max Planck Institute Coupled Earth System Model (MPI-ESM-LR), and

• Norwegian Earth System Model (NorESM1-M).

Schütte *et al.* (2023) bias corrected the daily rainfall to the spatial resolution of the Quinary catchments, where the bias correction involved matching the GCM output with observations for an identical historical period. To verify whether the GCM output captured the observed record for the SASRI stations, the annual maximum rainfalls derived from the 6 GCMs were plotted against those from the SASRI station AMDRs (Figure 9.41 to Figure 9.79 in Appendix B). Generally, the GCMs' annual maximum rainfalls were found to be greater than the observed values. It is noteworthy that the GCMs' outputs cannot be expected to have the maximum rainfalls at the same time period as the observed values but are rather useful for evaluating future trends. Therefore, the GCMs were used to analyse the projected rainfall for the region.

Using the annual maximum rainfall from the GCMs, design rainfalls were calculated for the 1-day event for the 2-, 10-, 50- and 100-year return periods. The ratios of changes from the GCMs' present (1961-1990) to the near future (2015-2044) and from the present to the distant future (2070-2099) for design rainfalls were calculated. The average projected changes from the 'present to near future' and the 'present to distant future' for the ensemble mean of the 6 GCMs are shown in Figure 3.7and Figure 3.8, respectively. The ratios for each GCM for each return period are presented in Appendix B (Figure 9.80 to Figure 9.87).

The majority of sites along the coastline show no increase in 1-day design rainfall for the near future. Slight increases are notable further inland, with the ratios increasing with an increase in return period. Projected changes into the distant future show a 10-30% increase in 1-day design rainfalls in many locations.

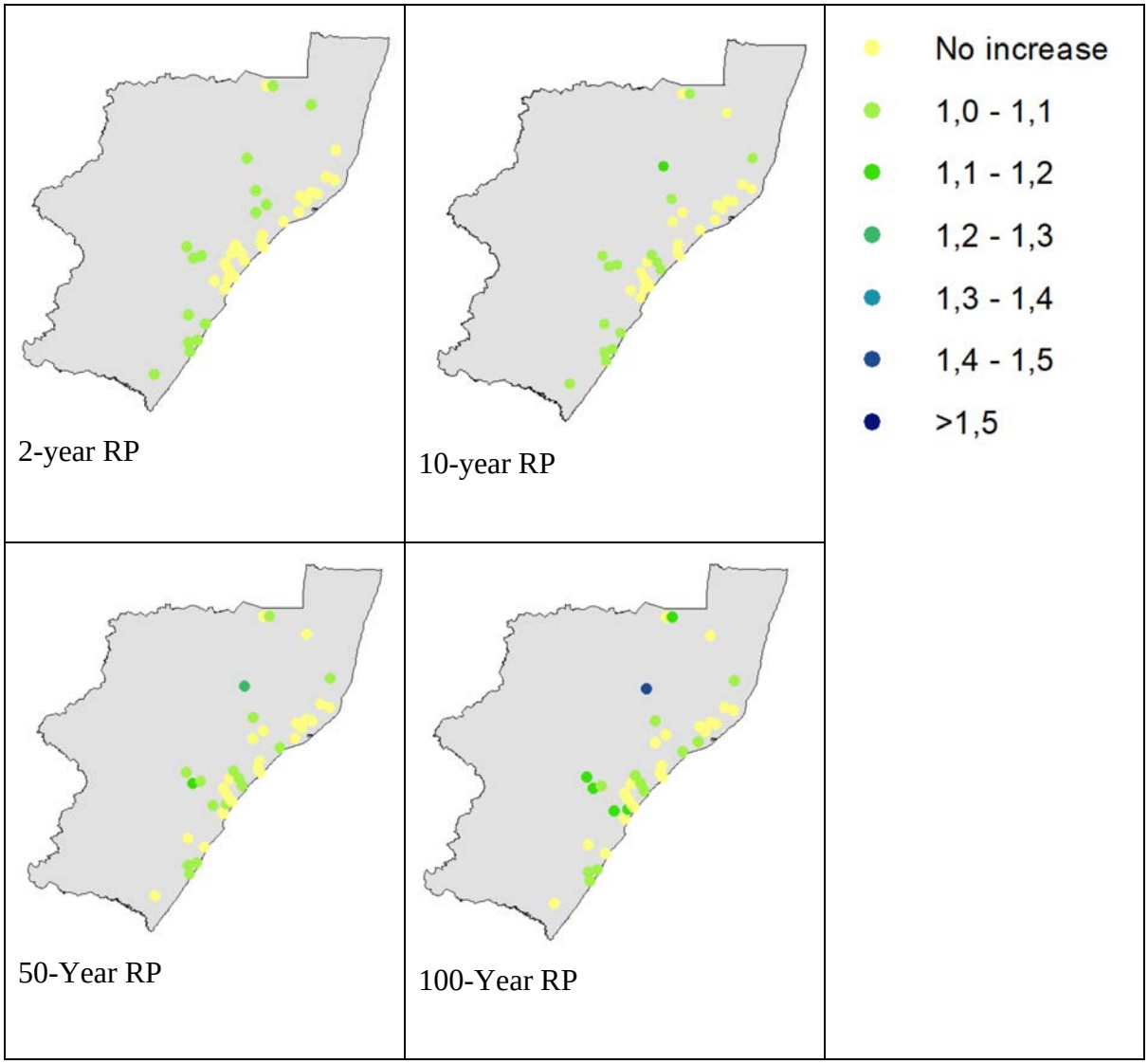

Figure 3.7 Projected changes from the present to the near future in design rainfalls for 1-day design rainfalls for the 2-, 10-, 50-, and 100-year return periods, derived from outputs from multiple GCMs

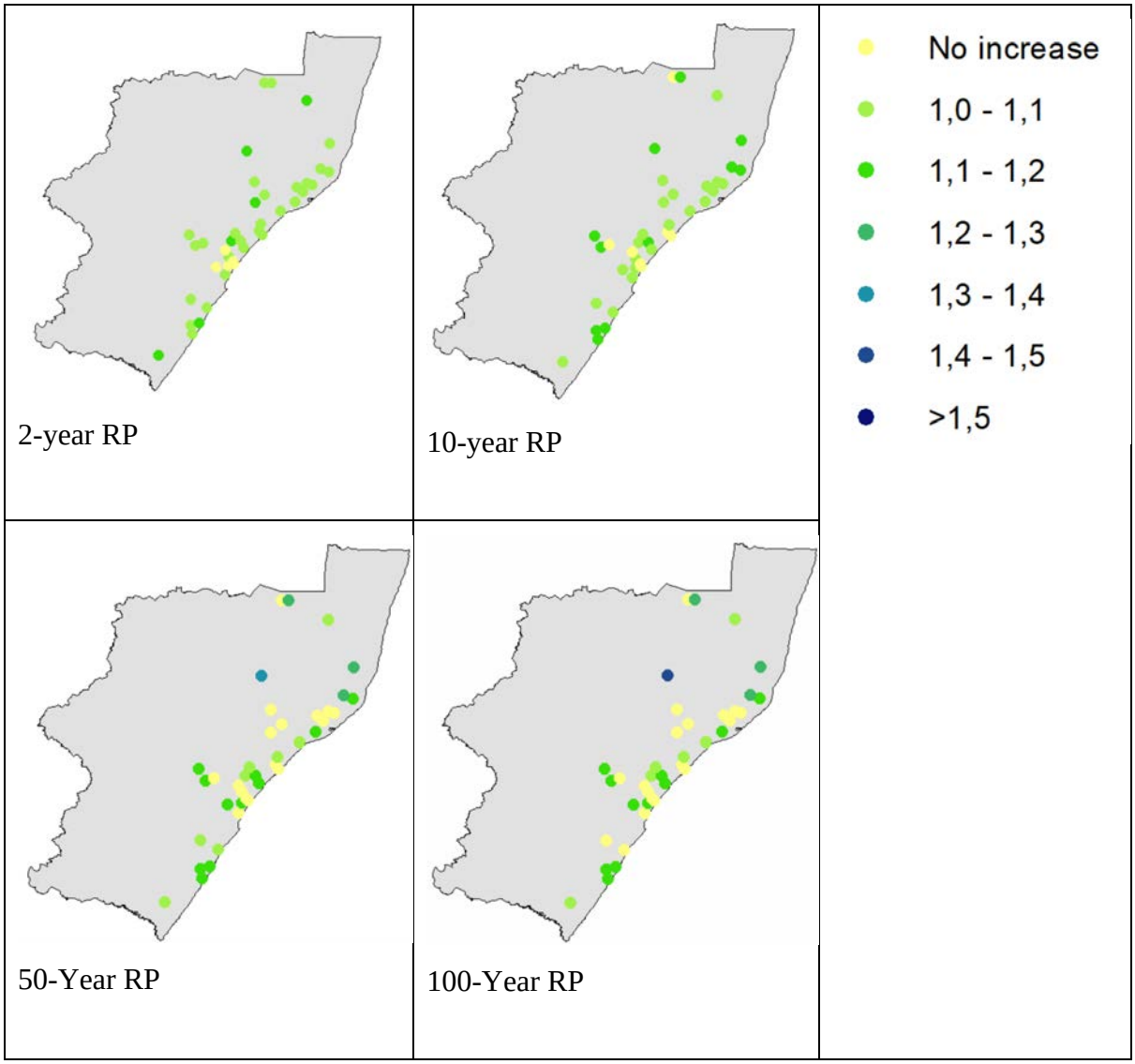

Figure 3.8 Projected changes from the present to the distant future in design rainfalls for 1-day design rainfalls for the 2-, 10-, 50-, and 100-year return period, derived from outputs from multiple GCMs

3.4 Conclusions

The reported increases in extreme rainfall events and their impacts reported from around the world, and particularly the east coast of South Africa in recent years, have motivated a move towards a non-stationary approach to frequency analysis to ensure that the changing properties

of extremes are accounted for in design rainfall estimation, and consequently, in the design and flood risk assessment of hydraulic infrastructure.

This chapter investigated the presence of non-stationarity in the annual maximum values of extreme daily rainfalls in KwaZulu-Natal along the east coast of South Africa. The location of the study was chosen based on data availability from SASRI as no data were accessible through SAWS for use in this study. A total of 39 daily rainfall stations with record lengths of at least 40 years were analysed to investigate trends in the occurrences of extreme rainfalls. The MKT and Sen's slope were used to determine the trends in the AMDR, and results indicate that only one station (No. 38) out of 39 showed a significant increasing trend in annual maximum rainfall occurrences. Frequency analysis was performed using both stationary and non-stationary models using time, SOI, DMI, CO_2 and GMT as covariates and the results show that the stationary models are superior to non-stationary models at most stations when using the model diagnostic and selection methods such as AIC, BIC and RMSE. Only changes in the CO_2 covariate were shown to significantly impact the extreme rainfalls. Investigation of trends at other sites in the country located in various climate zones is recommended.

This non-stationary frequency analysis was done modelling the location and the scale parameters as functions of the covariates. However, modelling a single parameter, e.g. location only, should be investigated as modelling two parameters may result in an overparametrised model.

Endris *et al.* (2019) note that although SOI may not exhibit significant changes, the long-term trend in SST and the corresponding changes in atmospheric circulations may influence SOI related teleconnections. This means that if the conditions associated with SOI change, even if the SOI characteristics do not change, then rainfall characteristics can possibly change in regions that respond to SOI. Therefore, investigating future changes in rainfall associated with SOI and other indices driven by SST changes is crucial in understanding the changing vulnerability to extreme events. Further research into understanding the frequency distributions of the actual covariates, and how they are projected to change, is recommended.

With the increasing availability of projected climate information through GCMs, there is greater opportunity to use such data to determine the potential impacts of future climate scenarios on extreme rainfall and flood events using advanced statistical techniques, and to develop methods/tools to incorporate these trends into design rainfall and flood estimation. This study investigated the projected changes in design rainfalls using data from downscaled GCMs and noted that rainfalls are not projected to change significantly into the near future in the study area. Increases into the distant future along the KZN coastal region are expected to be around 10-30% for many parts. The use of projected rainfalls from GCMs should be well guided by the considerations based on the observed rainfall data trends. However, for other parts of the country, these changes could be greater as was found, for example, by Schütte *et al.*, (2023).

The variability of the results of the non-stationary analysis highlights the importance of understanding the trends and drivers of extreme rainfalls and the impacts on design rainfall and design flood estimation. The results of the non-stationary analysis can be improved by investigating the use of other physical covariates or climate drivers, e.g. large weather systems such as Cut-off Lows, as well as combinations of covariates.

The annual maximum series is widely adopted in rainfall frequency analyses, as the sampling process is straightforward. However, using a peaks-over-threshold (POT) model is an alternative approach used to represent the behaviour of exceedances above a selected threshold, and which offers the opportunity to include more observations in the dataset and hence, more flexibility when compared to the use of annual maxima (Pan *et al.*, 2022). Despite the theoretical advantages, the POT is underutilised internationally due to the complexity in the selection of appropriate thresholds. It is recommended that the POT approach be investigated for detecting non-stationarity in extreme rainfall data in South Africa.

This study analysed the 1-day rainfall event. However, in KZN coastal areas extremes are frequently associated with multi-day events. Therefore, the non-stationary analysis of short duration (< 24h), required for DFE in most urban catchments, and multi-day extreme event data is recommended for future research.

4. DETECTING TRENDS IN HYDROLOGICAL EXTREMES AND NON-STATIONARY EXTREME VALUE ANALYSIS OF FLOOD DATA IN KWAZULU-NATAL

D Mukansi, JC Smithers and KA Johnson

4.1 Introduction

In order to minimise the risk of failure of hydrological structures it is vital to ensure that design floods be adequately estimated. The underestimation of design floods can lead to loss of life and significant economic losses, while overestimation may result in over-design which results in adverse economic impacts. The South African Government has reported that the most common weather-related catastrophe in South African between the period 1900 to 2014 were floods, droughts and large storms (DFFE, 2016). Socio-economic losses due to such disasters can be minimised by adequate Design Flood Estimation (DFE).

As with rainfall analysis, the current methods and models used to determine design flood estimates from flow data assume that hydrological outputs remain stationary (Vogel *et al.*, 2011). However, the magnitude and frequency of extreme flood events is changing in many parts of the world (Vogel *et al.*, 2011; Prosdocimi *et al.*, 2014a; Hesarkazzazi *et al.*, 2021). Therefore, there is a need to investigate, and to incorporate if necessary, non-stationary models in DFE in South Africa.

Where observed data are available, frequency analysis of the data is the recommend approach for design rainfall and flood estimation when there is adequate record length and good quality observed data (Smithers, 2012a). The quality of observed flow data is influenced by hydrometrics such as incorrect manual capturing of data, malfunctioning of measuring instruments, poor maintenance of the gauging site and exceedance of the rating table (Nathanael, 2015). Smithers *et al.* (2015) highlighted that South Africa has relatively few streamflow gauging stations which have more than 50 years of good quality data. However, it is important that data are adequately screened to prevent incorrect estimations of design floods (Calitz, 2020).

This Chapter includes an analysis of trends in extreme floods along the East Coast of KwaZulu-Natal in South Africa. This study site was selected to complement and correspond to the rainfall analyses conducted in Chapter 3. The aims of the study reported in this chapter are to determine if any trends exist in observed extreme flood events along the East Coast of KwaZulu-Natal, and to evaluate the possible non-stationarity in observed flow data. The objectives are to: (i) collect, screen, and analyse the streamflow data for trends, (ii) perform stationary and non-stationary rainfall frequency analyses, (iii) critically evaluate the stationary vs non-stationary models, and (iv) investigate regional magnification factors to detect trends.

4.2 Materials and Methods

4.2.1 Data sources and case study site selection

The Annual Maximum Series (AMS) streamflow data were obtained from the Department of Water and Sanitation (DWS) website, which provides open access of up-to-date flow data for South Africa. Approximately 90 stations with flow data up to the year 2023 were extracted from the DWS database for stations located in the East Coast region of KwaZulu-Natal.

4.2.2 Data screening and assessment

The flow data were then screened according to the criteria and methods described in Sections 3.2.1. In addition to the criteria used in Section 3.2.1, the data were screened based on the recorded depth of flow. If the recorded depth of flow exceeded the maximum rating table depth, the data were extended by a maximum of 20%. However, the percentage of rating table exceedances recorded in the AMS should be less than 20% of the total record length (Nathanael, 2015).

4.2.2.1 Rating table exceedance

Most streamflow gauging stations do not measure the discharge directly; rather, the stations record the stage height which is correlated with discharge (Petersen-Øverleir and Reitan, 2009). Rating table exceedance refers to an occurrence where the maximum stage rating is exceeded. In this case the discharge associated with the maximum stage rating is recorded by DWS for the observations which exceed the maximum rated stage (Nathanael, 2015). The DWS codes this error with "A", which means that some of the potential high flows are not captured and should be extrapolated (Calitz, 2020).

There are various methods used to extrapolate the rating curve, including the extension of the fitted regression line and the hydraulic analysis which requires additional data (Haddad *et al.*, 2010). The various methods contain uncertainty in the estimation of the extrapolated discharge (Petersen-Øverleir and Reitan, 2009). The challenge with extension of the rating curve using a regression approach is that the larger the extension the greater the uncertainty in the estimated flow (Calitz, 2020). Haddad *et al.* (2010) used the rating ratio approach, which is the ratio of estimated flow to the maximum observed flow to determine the maximum allowable extrapolation. Nathanael (2015), Gericke and Smithers (2018), and Calitz (2020) adopted 20% to be the maximum allowable increase in flow discharge. Based on the selection criteria described in Section 3.2.1 and the rating exceedance criteria, 19 sites were selected for this study. Figure 4.1 shows the locations and Table 4.1 contains a summary of the stations selected.

Figure 4.1 Selected DWS streamflow recording stations along the East Coast of KwaZulu-Natal

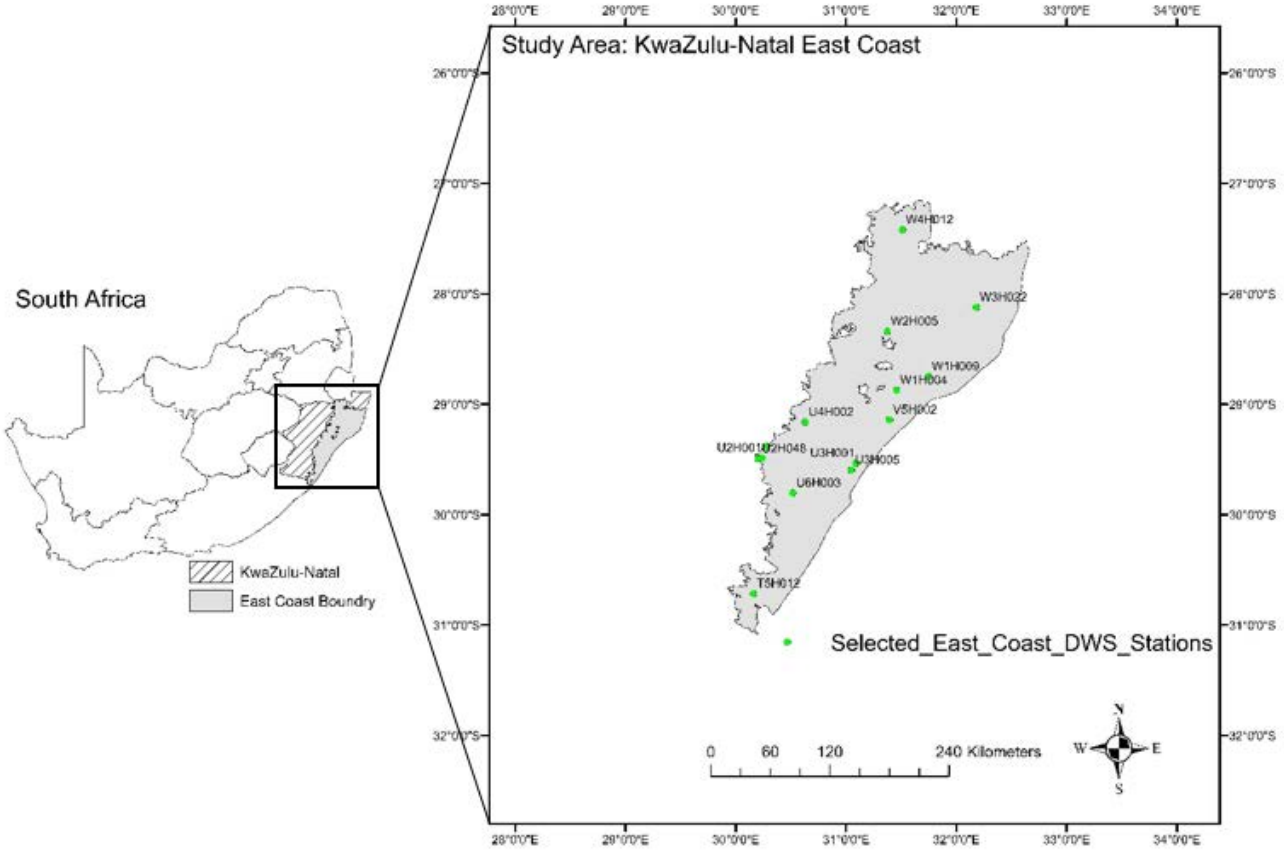

Table 4.1 Station information for case study sites along the East Coast of KwaZulu-Natal

Station Name	DWS Station Number	Start Year	End Year	Record Length (years)
Mzimkhulwana River-Horseshoe	T5H012	1970	2023	53
Mgeni River-Howick	U2H001	1948	1993	45
Mgeni River-Table Mountain	U2H005	1950	2023	73
Karkloof River-Shafton	U2H006	1954	2023	69
Sterk River-Groothoek	U2H012	1960	2023	63
Mgeni River-Albert Falls	U2H014	1964	2023	59
Mgeni River-Midmar	U2H048	1968	2023	55
Mdloti River-Cotton Lands	U3H005	1975	2023	48
Mvoti River-Mistley	U4H002	1949	2023	74
Mlazi River-Umlaas	U6H003	1981	2023	42

Station Name	DWS Station Number	Start Year	End Year	Record Length (years)
Lovu River-Beaulieu Estate	U7H007	1964	2023	59
Tugela River-Mandini	V5H002	1956	2023	67
Mlalazi River-Eshowe	W1H004	1948	2023	75
Mhlatuze-Riverview	W1H009	1960	2023	63
Mhlatuze River-Mhlatuze	W1H028	1979	2023	44
White Mfolozi-Over	W2H005	1960	2020	60
Hluhluwe River-Farm 3/7638	W3H022	1964	2023	59
Right Canal from Phongolo River-The Bokfontein	W4H012	1950	2023	73
Mkuze River @ Rietboklaagte	W3H001	1966	2023	57

4.2.3 Methodology

The basic methodology applied in this study to determine extreme streamflow quantities at a given location, and how they may vary with respect to a selected covariate, are detailed in the following sections. The main steps involved in this approach are summarised in Figure 4.2.

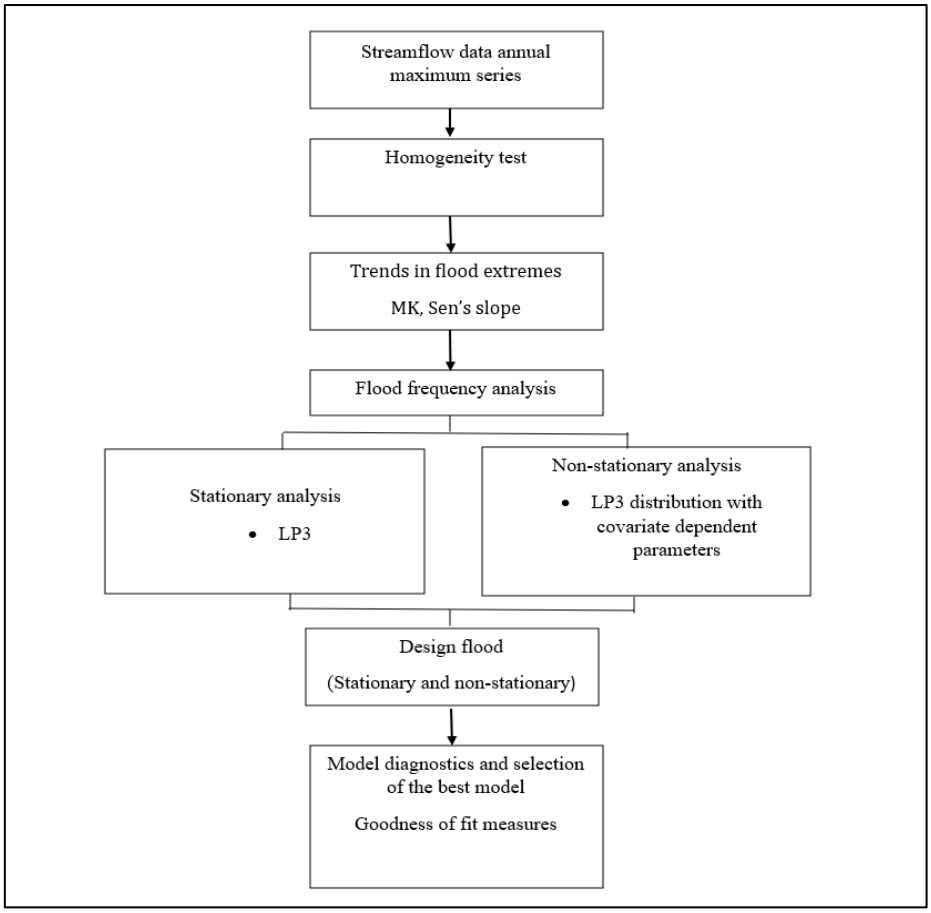

Figure 4.2 Stationary and non-stationary design flood estimation procedures

4.2.3.1 Testing for homogeneity

When performing a trend test it is important that the results reflect only actual changes in the non-stationarity of the hydrological process and not inconsistencies in the measuring system (Xiong and Guo, 2004). There are common measurement errors that occur when data are recorded, such as movement of the gauging station, changes in measurement structures and rating/calibration equations (Mallakpour and Villarini, 2016). A homogeneity test can be used to determine the point/s at which change occur in a data set.

The Pettitt test is a non-parametric method that is used to detect a sudden change in the data set (Conte *et al.*, 2019). A change point is defined as point in the data set where there is a sudden change in the mean, median, and variance. The change may be due to natural or anthropogenic changes in the data set (Scott and Chandler, 2011). The non-parametric method outputs the time of the change and its associated probability (Rougé *et al.*, 2013). The null hypothesis (H_o) of the method is that there is no change in trend, while the alternative hypothesis (H_a) is that there is a trend. The analysis is performed by rejecting the H_o if the probability of the change is greater than the significance level chosen to perform the analysis (Faulkner *et al.*, 2020b). The disadvantage of the method is that it only detects a change at a single point, and that the method categorises gradual trends as sudden changes (Rougé *et al.*, 2013).

4.2.3.2 Trends in flood extremes

The non-parametric Mann-Kendall test and Sen's slope test, as described in Section 3.2.2.1, were used to determine trends in streamflow.

4.2.3.3 Frequency distribution and non-stationary models

Process-informed Nonstationary Extreme Value Analysis (ProNEVA) in MATLAB was used to analyse stationary and non-stationary models. The tool allows the user to incorporate different types of physical drivers and it can be used to model the Log-Pearson Type III (LP3), GEV and Grand Pareto (GPA) distributions. ProNEVA makes use of a newly developed hybrid evolution Markov Chain Monte Carlo approach for uncertainty assessment and numerical

parameters estimation (Ragno *et al.*, 2019a). Details of the LP3 methods were reported by Griffis and Stedinger (2007) and Singo *et al.* (2012). Kjeldsen *et al.* (2002) analysed annual maximum floods in KwaZulu-Natal and concluded that the Log-normal, LP3, and GPA distributions were the most suitable models. Görgens (2007) recommended the use of the LP3 and GEV to model floods in South Africa. The LP3 was chosen in this study as it was found to be suitable for floods analysis in most design flood estimation studies in South Africa.

4.2.3.4 Selection of covariates

Time is often used as a proxy for the identification of physical drivers that vary with time such as land use and land cover changes (Hesarkazzazi *et al.*, 2021). These physical drivers are responsible for the change in the annual flood series. In other studies by Villarini *et al.* (2009) and Prosdocimi *et al.* (2014a), extreme rainfall was used as a covariate. Table 4.2 contains a summary of studies that make use of different covariates such as time, population, and rainfall. In a study by Hesarkazzazi *et al.* (2021), rainfall, time and temperature were used as covariates of annual floods and the study concluded that the best model often includes rainfall as a covariate. Owing to the limitation on the availability of data, only time and rainfall were used as covariates in this study.

Table 4.2 Summary of studies that made use of non-stationary models in design flood estimation (after Prosdocimi and Kjeldsen (2021)

Distribution	Variable	Model	Covariate	Reference
Log-Normal LN(μ,σ)	River discharge	Location: $\mu = \mu_0 + \mu_1 x$ scale: $\sigma = \sigma_0$ (constant)	Time	(Vogel *et al.*, 2011)
Gumbel(μ,σ)	River discharge	Location: $\mu = g(x)$ (non-parametric) scale: $\sigma = g(x)$ (non-parametric)	Time, population, and rainfall	(Villarini *et al.*, 2009)
Log-Normal LN(μ,σ)	River discharge	Location: $\mu = \mu_0 + \mu_1 x + \mu_{12} r$ scale: $\sigma = \sigma_0$ (constant)	Time and 99th rainfall	(Prosdocimi *et al.*, 2014a)
Log-Normal LN(μ,σ)	River discharge	Location: $\mu = \mu_0 + \mu_1 x$ scale: $\sigma = \sigma_0$ (constant)	Time	(Zhang *et al.*, 2015)
GEV(μ,σ,ξ)	River discharge	Location: $\mu = \mu_0 + \mu_1 x$ scale: $\exp(\sigma = \sigma_0 + \sigma_1 x)$ (constant) shape: $\xi = \xi_0$ (constant)	Time and rainfall	(Šraj *et al.*, 2016)
Log-Normal LN(μ,σ) and GEV(μ,σ,ξ)	Rainfall or River discharge	Location: $\mu = \mu_0 + \mu_1 x$ scale: $\sigma = \sigma_0$ (constant) shape: $\xi = \xi_0$ (constant)	Time	(Salas *et al.*, 2018)
Log-Normal LN(μ,σ)	River discharge	Location: $\mu = \mu_0 + \mu_1 x$ scale: $\sigma = \sigma_0$ (constant)	Time	(Kjeldsen and Prosdocimi, 2021b)

4.2.3.5 Linking streamflow to rainfall

In order to investigate the relationship between flow and rainfall, flow stations were linked to rainfall stations that fall within the same Quinary catchment. These stations were then used to perform stationary and non-stationary flood frequency analysis with time and rainfall as covariates.

4.2.3.6 Model diagnostics and selection of the best model

The AIC, BIC, and RMSE that as described in detail in Section 3.2.2.4 were used to select the best model.

4.3 Results and Discussion

4.3.1 Homogeneity test

Table 4.3 contains a summary of results of the AMS for 19 stations subjected to the Petit homogeneity test to detect a split in the data, which refers to a point at which there is change in the data set. The results show that six stations (T5H012, U2H005, U2H012, U2H014, U7H007 and W1H028) have a split and are therefore not homogenous. However, Station T5H012 was included in further analysis because the period of data after the split was more than 40 years. Thus 14 stations were retained for further analyses.

Table 4.3 Homogenity test of DWS stations in the East Coast of KwaZulu-Natal

Station Number	Pettit test p value	Interpretation
T5H012	< 0.0001	Not homogenous
U2H001	0.931	Homogenous
U2H005	0.003	Not homogenous
U2H006	0.937	Homogenous
U2H012	0.008	Not homogenous
U2H014	0.046	Not homogenous
U2H048	0.194	Homogenous
U3H005	0.069	Homogenous
U4H002	0.145	Homogenous
U6H003	0.739	Homogenous
U7H007	<0.0001	Not homogenous
V5H002	0.008	Homogenous
W1H004	0.722	Homogenous
W1H009	0.261	Homogenous
W1H028	0.015	Not homogenous
W2H005	0.399	Homogenous
W3H022	0.274	Homogenous
W4H012	0.101	Homogenous
W3H001	0.166	Homogenous

4.3.2 Trend detection

Table 4.4 contains a summary of results of the trend analyses in the AMS for the 14 stations subjected to the MKT and Sen's slope test. The test was performed using the 5% significance level. Based on the tests, the results indicate that majority of the stations along the East Coast

of KwaZulu-Natal experienced an insignificant trend, with approximately 21% of stations showing a positive trend and only one station (W4H012), showing a significant positive trend. The Sen's slopes for 79% of the stations are negative, which indicates that even though the trend is not significant at the majority of the stations, the direction of the trend is negative. Figure 10.1 (a-n) in Appendix C contains graphs depicting the time series plot for each station assessed. The linear trend lines in most of the time series graphs are negative, which is consistent with the result of the Mann-Kendall test which resulted in a negative trend for 79% of the stations analysed.

Table 4.4 Trends in annaul maximum streamflows at stations along the East Coast of KwaZulu-Natal using the Mann-Kendall test

Station Number	p-value	Sen's slope	Interpretation of Test
T5H012	0.831	0.182	insignificant positive trend
U2H001	0.688	0.056	insignificant positive trend
U2H006	0.239	-0.099	insignificant negative trend
U2H048	0.099	-0.306	insignificant negative trend
U3H005	**0.012***	**-1.069***	**significant negative trend***
U4H002	0.086	-0.004	insignificant negative trend
U6H003	0.0452	-0.146	insignificant negative trend
V5H002	**0.00001***	**-25.847***	**significant negative trend***
W1H004	0.819	-0.003	insignificant negative trend
W1H009	0.086	-1.148	insignificant negative trend
W2H005	0.599	-0.033	insignificant negative trend
W3H022	0.306	-0.077	insignificant negative trend
W4H012	**<0.0001***	**0.102***	**significant positive trend***
W3H001	0.078	-0.236	insignificant negative trend

***Significant trends at 5% level identified**

4.3.3 Analysis of stationary and non-stationary models

Both stationary and non-stationary frequency analyses were undertaken using the LP3 distribution for the 14 stations in the study area. For the non-stationary frequency analysis, the location parameter of the LP3 distribution were modelled as linear functions of the selected covariate. The scale and shape parameters were kept constant. The plots, as shown in Figure

10.2 to Figure 10.15 in Appendix C, show no significant differences between the stationary and non-stationary models as both models are under-simulating the high flows.

Table 4.5 contains a summary of results for the AIC, BIC and RMSE tests considering time as a covariate at the 14 stations used in the study. In the majority of the stations AIC and BIC and RMSE values of the stationary model are lower than those of the non-stationary model. The non-stationary models provide a better fit than the corresponding stationary model at only five stations (U3H001, U3H005, V5H002, W1H009 and W4H012). Based on the AIC, the results indicate that 6 out of 14 stations (43%) along the East Coast are better modelled through the stationary model, as low values of AIC and BIC from the same data indicate a better performing model (Faulkner *et al.*, 2020a). Using the BIC measure, the non-stationary models for only one station (U3H005) was found to give a better fit of the data.

Table 4.5 The LP3 statistical model selection criteria of selected sites in the East Coast of KwaZulu-Natal AMS for time as a covariate

Station Number	**Stationary**			**Non-Stationary**		
	AIC	**BIC**	**RMSE**	**AIC**	**BIC**	**RMSE**
T5H012	168.38	174.24	21.94	170.24	178.04	**19.25***
U2H001	138.91	144.19	38.25	140.85	147.89	**29.08***
U2H006	185.00	191.75	12.10	186.16	195.15	13.24
U2H048	207.09	213.16	34.94	**206.50***	214.57	40.36
U3H001	107.06	112.16	19.71	**106.37***	113.12	**15.17***
U3H005	176.15	181.37	9782.30	**168.51***	**175.45***	**404.24***
U4H002	167.92	174.15	14.02	168.48	176.79	**13.75***
U6H003	167.27	172.48	24.84	169.36	176.31	31.58
V5H002	122.90	128.58	29.43	**108.19***	**115.76***	**11.72***
W1H004	299.17	305.95	25.47	301.55	310.60	66.88
W1H009	168.59	174.44	32.37	**164.98***	**172.80***	**25.28***
W2H005	123.26	129.28	32.81	123.91	131.94	**32.22***
W3H022	249.08	254.94	64.95	251.06	258.86	**47.91***
W4H012	19.89	26.28	22.27	**-78.60***	**-70.09***	32.32

*** Non-stationary model performs better than stationary model**

Station W4H012 was the only station to show a significant increase in streamflow. This station also showed an increase in the effective return period of streamflow. Figure 4.3 depicts the LP3 for the: (a) stationary model, (b) non-stationary model, and (c) effective return period as a function of time for Station W4H012. The effective return period for Station W4H012 is shown to increase as a function of time for all return periods. Appendix C (Figure 10.2 to Figure 10.15) contains the plots for the stationary and non-stationary frequency analyses for all covariates and effective return periods for all stations.

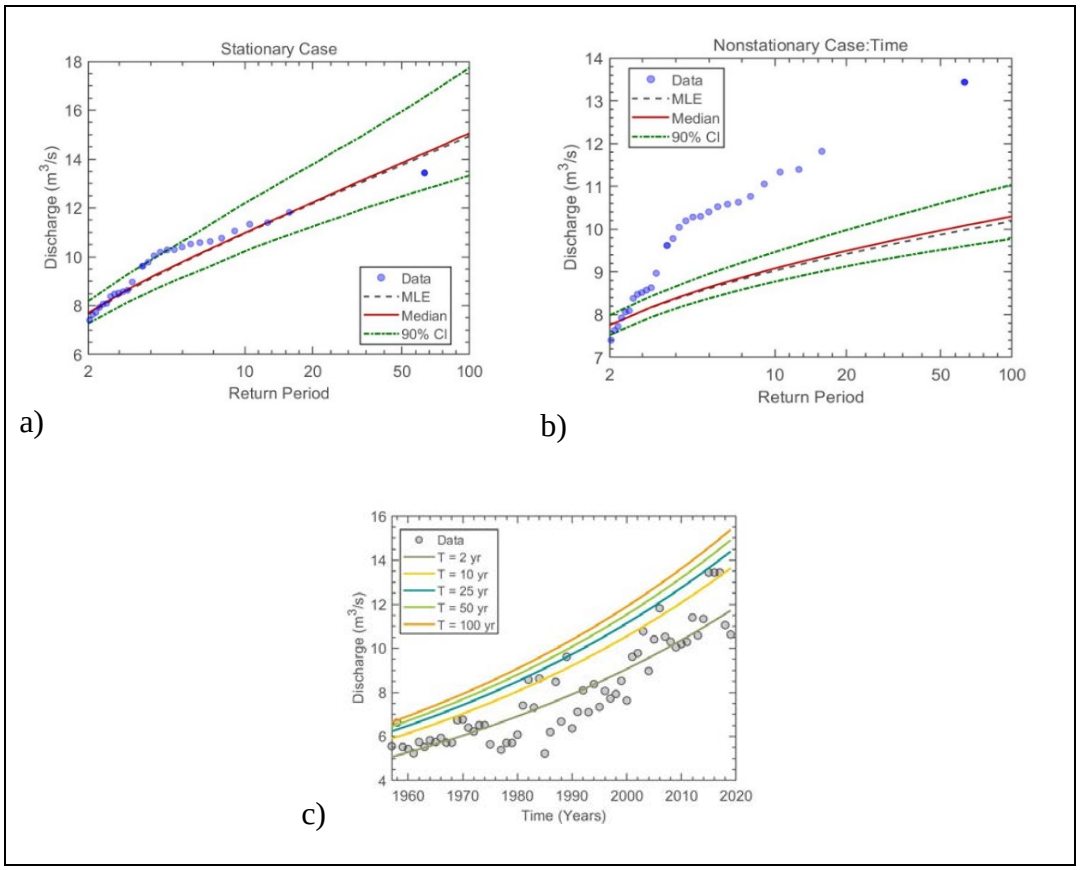

Figure 4.3 The LP3 (a) stationary model, (b) non-stationary model considering time as a covariate, and (c) effective return period as a function of time for Station W4H012

Figure 4.4 and Figure 4.5 show the locations of which models best fit the data based on AIC and BIC, respectively. No spatial patterns are evident based on the location of the best-fit stationary models.

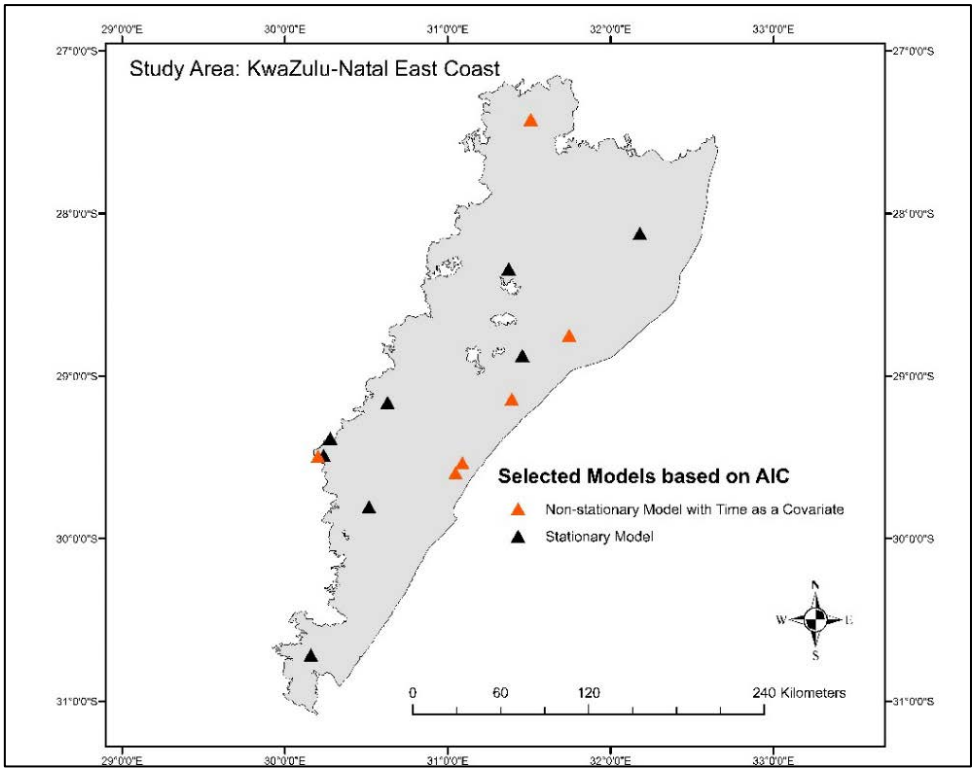

Figure 4.4 Best-fit distribution model, based on the AIC measure

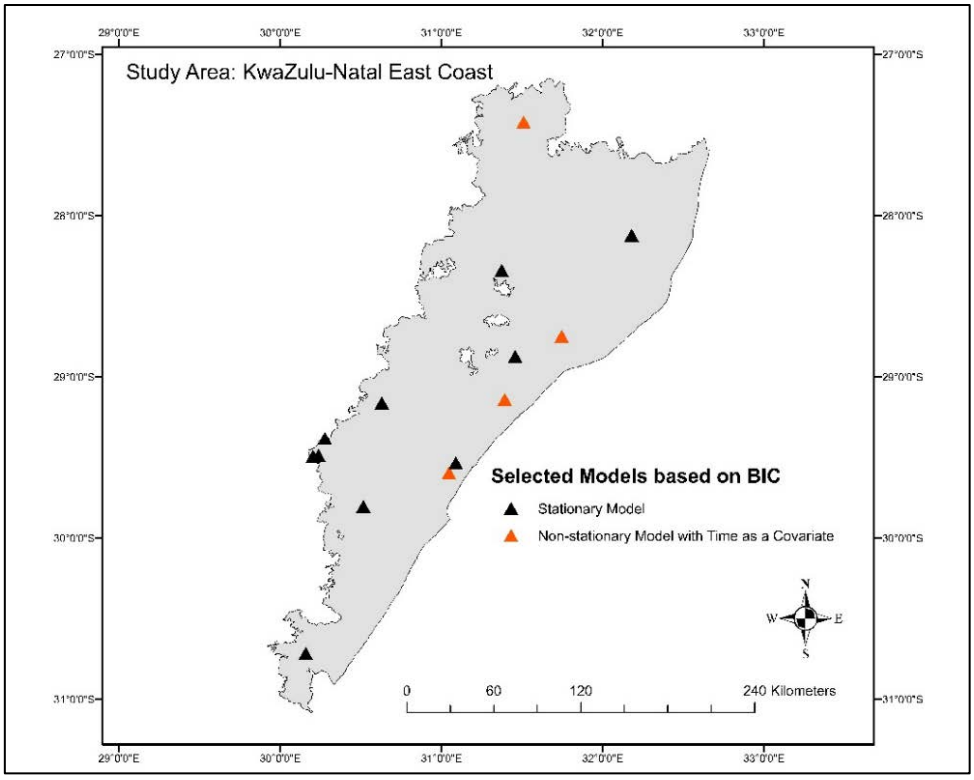

Figure 4.5 Best-fit distribution model, based on the BIC measure

4.3.4 Linking rainfall to flow

Figure 4.6 depicts the time series for annual maximum streamflow and annual maximum rainfall for stations along the East Coast of KwaZulu-Natal. Figure 4.6(b, c, d, e, and h) show the stations that have a relation between streamflow and rainfall. However, Figure 4.6 (a, f, g, and h) depict the stations (U2H003, W3H008,W4H003, and W3H015) that could not be used for further analysis as there was no correlation between streamflow and rainfall. This could be for several reasons, not limited to the location of the raingauges within the catchments, antecedent soil water conditions, and land use change. These stations had more than 20% of the AMS data exceeding the rating table and therefore, did not meet the screening requirements and were discarded from further analyses.

Table 4.6 contains a summary of the best-fit models for the stationary and non-stationary cases based on AIC and BIC measures. The non-stationary models considering time and rainfall as covariates were compared to the stationary models for each station. The detailed results are presented in Table 10.1 in Appendix C. The non-stationary models perform better than the stationary models at 100% and 80% of stations based on the AIC and BIC measures, respectively. Non-stationary model with rainfall as covariate performed better than time as a covariate at 60% of the stations based on AIC but performed similarly at 40% of the stations with respect to BIC.

The results of this study indicate that the best model of non-stationarity includes rainfall as a covariate. The same conclusion was established by Hesarkazzazi *et al.* (2021) for floods in the northwest of England.

Figure 4.7 and Figure 4.8 show the locations of which models best fit the data based on AIC and BIC, respectively, for those flow stations that are linked to a rainfall station. No spatial patterns are evident based on the location of the best-fit models.

Table 4.6 Summary of best-fit models for all stationary and non-stationary cases

AIC		BIC	
Model	**Number of best-fit models**	**Model**	**Number of best-fit models**
Stationary	0 (0%)	Stationary	1(20%)
Non-stationary – Time	2(40%)	Non-stationary – Time	2 (40%)
Non-stationary – Rainfall	3 (60%)	Non-stationary – Rainfall	2 (40%)

a)

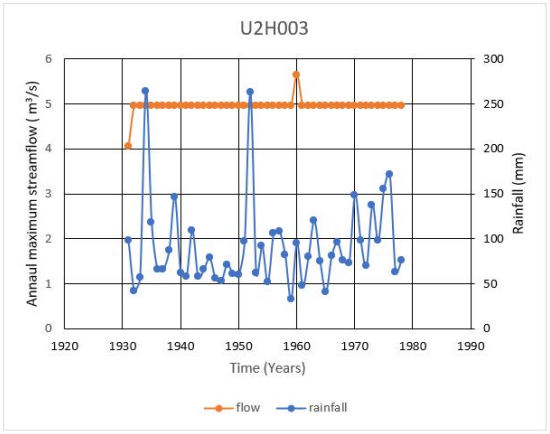
U2H003
Annaul maximum streamflow (m³/s)
Rainfall (mm)
Time (Years)
flow
rainfall

b)

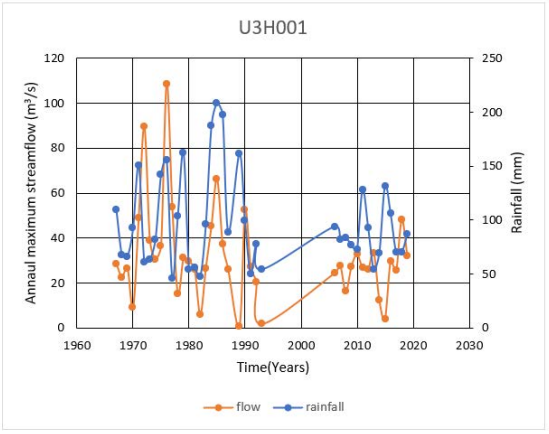
U3H001
Annaul maximum streamflow (m³/s)
Rainfall (mm)
Time(Years)
flow
rainfall

c)

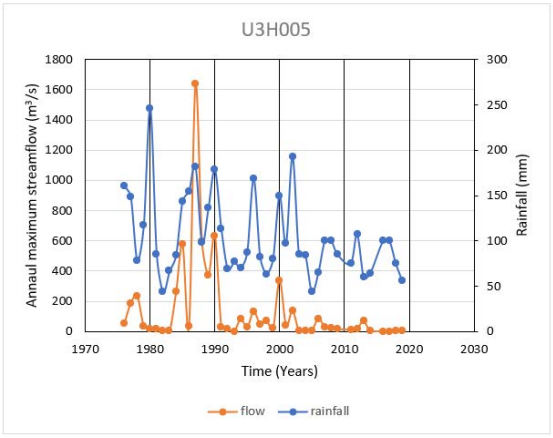
U3H005
Annaul maximum streamflow (m³/s)
Rainfall (mm)
Time (Years)
flow
rainfall

d)

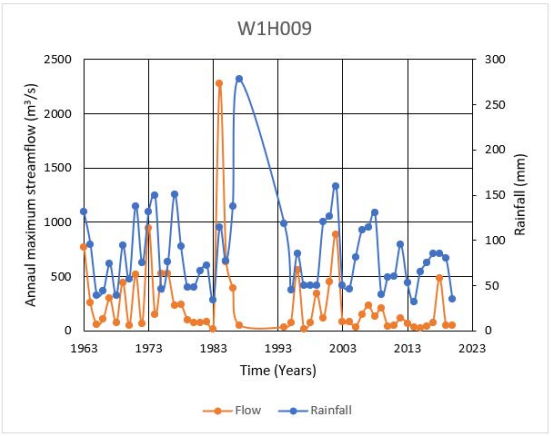
W1H009
Annaul maximum streamflow (m³/s)
Rainfall (mm)
Time (Years)
Flow
Rainfall

e)

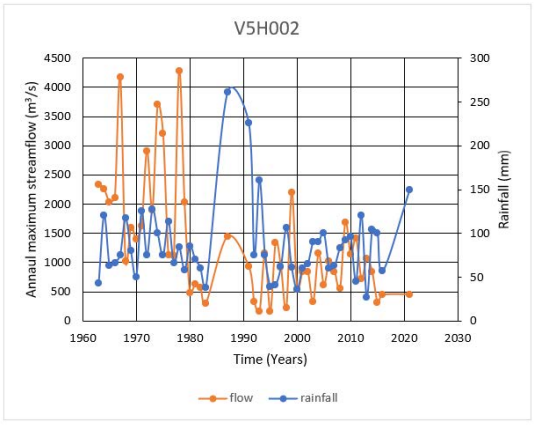
V5H002
Annaul maximum streamflow (m³/s)
Rainfall (mm)
Time (Years)
flow
rainfall

f)

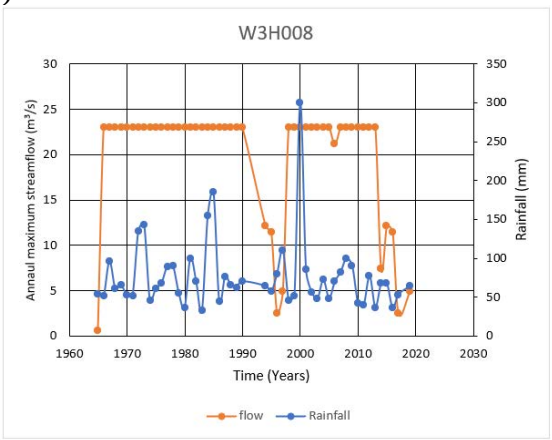
W3H008
Annaul maximum streamflow (m³/s)
Rainfall (mm)
Time (Years)
flow
Rainfall

g)

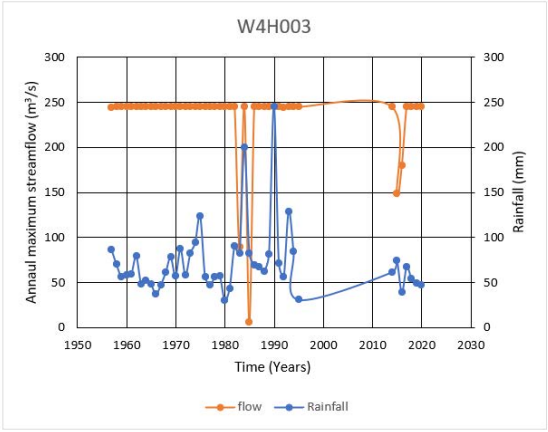

h)

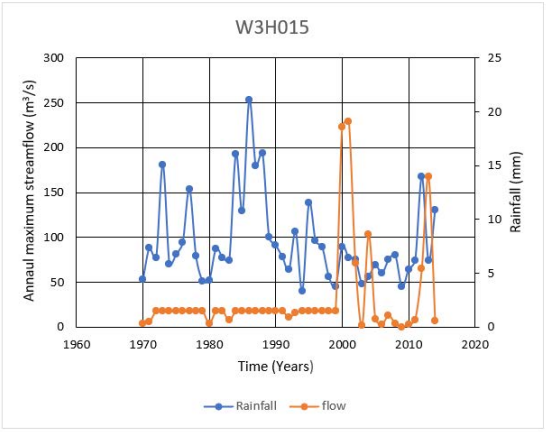

i)

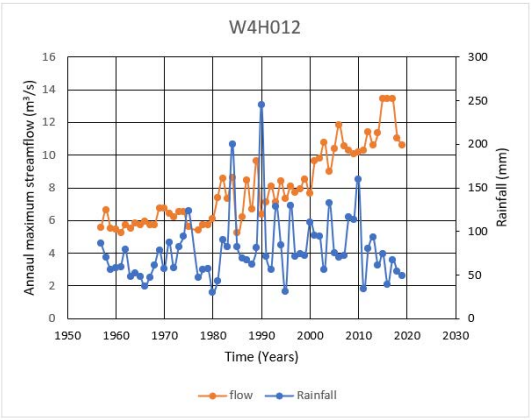

Figure 4.6 Time series for annual maximum streamflow and rainfall stations in the East Coast of KwaZulu-Natal

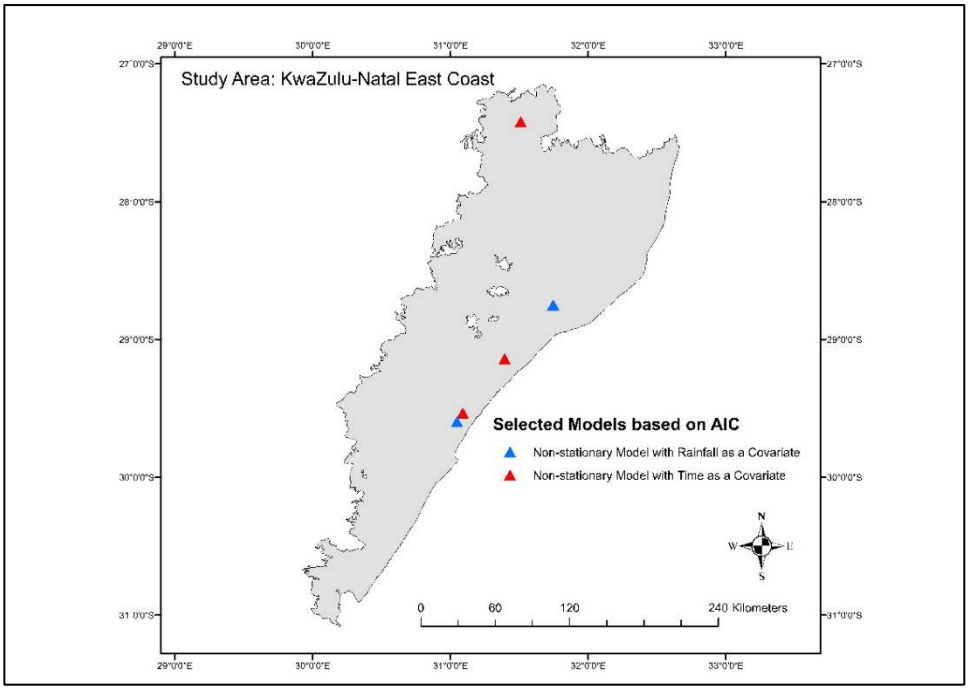

Figure 4.7 Best-fit distribution model, based on the AIC measure for flow stations linked with a rainfall station

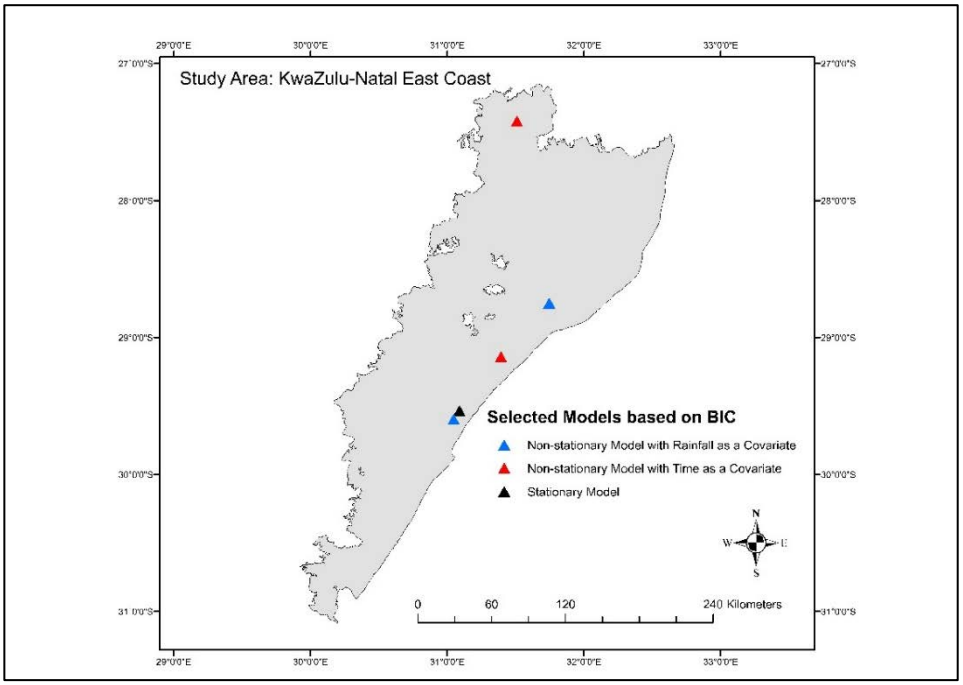

Figure 4.8 Best-fit distribution model, based on the BIC measure for flow stations linked with a rainfall station

4.4 Conclusions

DFE is vital to ensure adequate design and flood risk assessment of hydraulic structures and to minimise failure due to floods. However, as with rainfall, the current methods used to estimate design floods using streamflow data assume that hydrological conditions remain stationary over time. Studies reported in the literature are challenging this assumption as the frequency and magnitude of extremes are reported to be increasing as consequence of anthropogenic factors such as land use and climate change. Despite advances reported in the international literature, no studies from South Africa have reported the use of non-stationary models in DFE.

The accuracy of the DFE is based on the quality of data used. This chapter details the criteria used to screen and select stations for use in this study and the methodology adopted to determine trends in hydrological extremes of streamflow data. The study area had a total of approximately 90 stations with flow data up to the year 2023 which are available from the DWS website. After screening the data and performing a homogeneity test using the Pettit test, 14 stations were found suitable for further analysis.

The 14 streamflow stations with record lengths of at least 40 years were analysed to detect trends in the occurrences of extreme floods. Trends in annual maximum streamflow data were analysed using the non-parametric Man-Kendall Test. The results showed that approximately 79% of the analysed stations in the East Coast of KwaZulu-Natal had negative trends with approximately 18% of the negative trends being significant ($p < 0.05$). Only one station (W4H012) out of the 14 showed a significant increase in the trend of annual maximum streamflow.

Flood frequency analysis was performed using both stationary and non-stationary models using time and rainfall as covariates. The graphical approach between the different models was similar because the models could not accurately model the high flows for all return periods. This may be attributed to the model failing to model potential outlier events. For non-stationary analysis, the skewness can be varied as a function of a covariate which may be used to improve the simulation in future studies.

The non-stationary analysis was also able to determine the changes in magnitude of floods associated with a particular return period. The results also show that the stationary models are superior to non-stationary models at most stations with time as a covariate when using the model

diagnostic and selection methods such as AIC, BIC and RMSE. At selected stations where flow was linked with rainfall, the non-stationary model with rainfall as a covariate performed better than both the stationary model and non-stationary model with time as a covariate. Therefore, further research of trends at other sites in the country located in various climate zones is recommended with rainfall being used as a covariate. Other recommendations include varying the other parameters of the probability distribution as a function of rainfall, especially the skewness as the LP3 distribution.

Regional magnification factors both at site and at regional level were not pursued further in this study as regional magnification factors are dependent on the general direction of the trend of the observed data. Since approximately 79% of the stations analysed in this study showed a negative trend, the magnification factors that would be calculated would results in a decrease in the DFE as these factors would be lower than one. It is recommended that future research investigate the causes of the negative trends in the annual maximum flow data, and more in-depth investigation into trends in the flow which may not be evident in the annual maximum flow data.

5. DISCUSSIONS, CONCLUSIONS AND RECOMMENDATIONS

The ability to reliably estimate the expected magnitude and frequency of extreme rainfall and flood events is fundamental for improving design concepts and risk assessment methods. This is particularly important for extreme events that have significant impacts on society, infrastructure, and human lives, such as extreme precipitation events causing flooding and landslides.

The 1-day PMP estimates have been updated for South Africa using an updated climate database and methodology compared to the currently used guidelines. The definition of the PMP implies a zero probability of exceedance. However, many studies, including this one, have shown that previously derived PMP estimates have been exceeded by new events which are not typical or characteristic of the region. The PMP is based on extreme rainfalls which have been documented up to a certain point and should be updated periodically to include new extreme rainfalls. This study presents 1-day PMPs for South Africa; however, sub-daily and multi-day PMPs are also needed for engineering design. The limited availability of sub-daily rainfall data in South Africa prevents the estimation of reliable and accurate sub-daily PMPs. Methods to estimate the sub-daily and multi-day PMP should be investigated. The possible exceedance probabilities of the PMP should be investigated as well.

An updated hydro-meteorological database is critical to the success of estimating accurate PMPs. Such a database should be continually updated and used to revise the PMP and design rainfalls following the occurrence of new extreme rainfall events. This study has been impacted by the lack of freely available rainfall data and climate data in South Africa.

A Workshop was held to inform practitioners and the scientific community of the updated 1-day PMP estimates, to make the dataset available for use in industry, and to facilitate discussions around the new estimates. The Workshop was attended by several academics, researchers, practitioners, and stakeholders. The materials of the Workshop have been provided on the online WRO platform, where they are openly available. The contact details of the authors were provided to encourage further engagement and feedback from practitioners.

The assumption that hydrological processes remain stationary is still applied for DFE in South Africa. However, several studies have challenged this assumption as the hydrological conditions

change due to anthropogenic factors such as climate change, land cover changes, and land use changes. This project aimed to contribute new knowledge on a method to account for non-stationary data, which incorporates the impacts of a changing climate in extreme design rainfall and flood estimates in South Africa. Therefore, the pilot undertaken in this study focussed on investigating trends in extreme rainfall and floods, incorporating non-stationarity in frequency analysis on annual maximum rainfall and streamflow data, and investigating the use of magnification factors to account for trends in varying hydrological conditions.

The results of the trend analysis of rainfall data show weak evidence that the annual maximum daily rainfalls in the study region have been increasing in magnitude over time. In addition, non-stationary analysis of rainfall considering various climate drivers as covariates show that most rainfall records exhibit a stationary behaviour. Results of the analysis of annual maximum streamflow show decreasing trends in magnitude and frequency at the majority of stations. As with rainfall, at most streamflow stations, the stationary models are superior to the non-stationary models when considering changes over time. However, non-stationary models considering rainfall as a covariate were found to often be superior to the corresponding stationary models. Despite the majority of the stations showing an insignificant negative trend, the presence of the trend can be used to challenge the assumption of stationarity.

The outcomes presented in this report are sometimes contrary to the outputs from GCMs reported in international studies, and to reported increases in extreme events in South Africa. This may be due to the limited study area, the limited spatial density and record length of stations, the selected duration of events, and high upstream abstraction of streamflow that cannot be accounted for when performing extreme value analysis. The results may differ in other parts of the country and further analysis on a national scale covering different climatic zones is recommended. Furthermore, the sampling uncertainty of projections from GCMs used to investigate potential future changes in extreme events should be investigated.

The annual maximum series approach, which is widely adopted in rainfall frequency analyses, was used in this study. This approach has the limitation that only the highest event is used per year and thus, other large events within the same year are not captured in the analyses. However, using a peaks-over-threshold (POT) approach is an alternative to the annual maxima approach, which can

be used to represent the behaviour of exceedances above a selected threshold. A POT approach offers the opportunity to include more observations in the dataset and hence, more flexibility when compared to the use of only annual maxima (Pan *et al.*, 2022). It is recommended that the POT approach be investigated for detecting non-stationarity in extreme rainfall data in South Africa in future studies.

The identification and analysis of climate drivers of extreme events is vital to understanding the trends of the driving mechanisms of extreme rainfalls and floods. The results of the non-stationary analysis can be improved by investigating the use of other physical covariates or climate drivers, e.g. large weather systems such as Cut-off Lows, as well as combinations of covariates. Rainfall was incorporated in the non-stationary streamflow models as a covariate. However, to link specific rainfall and flood events, rainfall and streamflow should be linked through a hydrological model, e.g. rainfall-runoff model, in future research. Furthermore, catchment rainfall, time of concentration, and flood peaks should be considered in non-stationary rainfall-runoff relationships in future research.

This study analysed the 1-day rainfall and flood events to evaluate potential non-stationarity in the data. However, in KZN coastal areas extremes are often associated with multi-day events. Furthermore, extreme events in other parts of the country may be driven by shorter, more intense events occurring within a single day. Therefore, the non-stationary analysis of short duration (< 24h) and multi-day extreme event data is recommended for future research. Given the generally negative trends in annual maximum flood data, it is recommended that future research investigate the causes of the negative trends in the annual maximum flow data, and more in-depth investigation into trends in the flow which may not be evident in the annual maximum flow data.

Regional magnification factors were not investigated further in this study as the majority of the stations within the study area showed a negative trend, which would mean the application of a regional magnification factor would result in a reduction of the design floods estimated using non-stationary-based methods. However, it is recommended that further investigation into the use of regional magnification factors in other parts of South Africa should be undertaken.

6. CAPACITY BUILDING

The students involved in the project and their roles are summarised in Table 6.1.

Table 6.1: List of students involved in the project

Name	Degree	Role	Comment
Ms KA Johnson	PhD Engineering	Project leader, PhD Candidate	Completed research towards doctoral degree with PhD. Graduated May 2024.
Mr DV Mukansi	PhD Engineering	PhD Candidate	Continuing with doctoral degree with intention to submit in 2025.
Mr MS Nyathi	BSc Engineering (Civil)	Undergraduate student	Completed degree and final year research dissertation project in 2022.
Mr N Singh	BSc Engineering (Civil)	Undergraduate student	Completed final year research dissertation project in 2022.

This research has been shared at the South African Hydrological Society Conference in October 2022 and at the International Association of Hydrological Sciences Assembly in Germany in July 2023, and presented at the annual NFSP workshop in May 2024 at Stellenbosch University. These events were attended by practitioners, stakeholders, and academic researchers.

7. REFERENCES

Abbs, DJ. 1999. A numerical modeling study to investigate the assumptions used in the calculation of probable maximum precipitation. *Water Resources Research* 35 (3): 785-796.

Afzali-Gorouh, Z, Bakhtiari, B and Qaderi, K. 2018. Probable maximum precipitation estimation in a humid climate. *Natural Hazards and Earth System Sciences* 18 3109-3119.

Agilan, V and Umamahesh, NV. 2017. Modelling nonlinear trend for developing non-stationaryrainfall intensity-duration-frequency curve. *International Journal of Climatology* 37 (2017): 1265-1281.

Agilan, V and Umamahesh, NV. 2018. Covariate and parameter uncertainty in non-stationary rainfall IDF curve. *International Journal of Climatology* 38 365-383.

Akaike, H. 1974. A new look at the statistical model identification. *IEEE Transactions on Automatic Control* 19 (6): 716-723.

Bates, B, Kundzewicz, ZW, Wu, S and Palutikof, J. 2008. *Climate Change and Water. Technical Paper of the Intergovernmental Panel on Climate Change*. IPCC Secretariat, Geneva, Switzerland.

Boota, M, Nabi, G, Abbas, T, Jin, H, Yousaf, A and Boota, M. 2018. Comparative study of probable maximum precipitation and isohyetal maps for mountainous regions, Pakistan. *Sciences in Cold and Arid Regions* 10 (1): 55-68.

Botes, ZA. 2014. Flooding in KwaZulu-Natal: Modelling, history and future aspects. Unpublished thesis, School of Agricultural, Earth and Environmental Sciences, University of KwaZulu-Natal, Durban, South Africa.

Braun, K, Bar-Matthews, M, Ayalon, A, Zilberman, T and Matthews, A. 2017. Rainfall isotopic variability at the intersection between winter and summer rainfall regimes in coastal South Africa (Mossel Bay, Western Cape Province). *South African Journal of Geology* 120 (3): 323-340.

Bronowicka-Mielniczuk, U, Mielniczuk, J, Obroślak, R and Przystupa, W. 2019. A comparison of some interpolation techniques for determining spatial distribution of nitrogen compounds in groundwater. *International Journal of Environmental Research* 13 (2019): 679-687.

Bureau of Meteorology. 2003. *The Estimation of Probable Maximum Precipitation in Australia: Generalised Short-Duration Method*. Hydrometeorological Advisory Service, HAS, Canberra, Australia.

Bureau of Meteorology. 2023. Forcast & Drivers: Climate Driver Update – Climate drivers in the Pacific, Indian and Southern oceans and the Tropics. [Internet]. Available from: http://www.bom.gov.au/climate/enso/. [Accessed: 18 April].

Calitz, JP. 2020. Development and assessment of regionalised approaches to design flood estimation in South Africa. Unpublished PhDEng thesis, School of Engineering, University of KwaZulu-Natal, Pietermaritzburg, South Africa

Chavan, RS and Srinivas, VV. 2015. Probable Maximum Precipitation Estimation for Catchments in Mahanadi River Basin. *Aquatic Procedia* 4 892-899.

Cheng, L, AghaKouchak, A, Gilleland, E and Katz, RW. 2014. Non-stationary extreme value analysis in a changing climate. *Climatic Change* 127 (2): 353-369.

Clark, RA.1987. Hydrologic design criteria and climate variability. *Tlie Influence of Climate Change and Climatic Variability on the Hydrologic Regime and Water Resources*, IAHS, Vancouver Symposium.

Coles, S. 2001. *An Introduction to Modelling of Extreme Values*. Springer, London, UK.

Conte, LC, Bayer, DM and Bayer, FM. 2019. Bootstrap Pettitt test for detecting change points in hydroclimatological data: case study of Itaipu Hydroelectric Plant, Brazil. *Hydrological Sciences Journal* 64 (11): 1312-1326.

Cullis, J, Alton, T, Arndt, C, Cartwright, A, Chang, A, Gabriel, S, Gebretsadik, Y, Hartley, F, de Jager, G, Makrelov, K, Robertson, G, Schlosser, CA, Strzepek, K and Thurlow, J. 2015. *An Uncertainty Approach to Modelling Climate Change Risk in South Africa.* WIDER Working Paper 2015/045. World Institute for Development Economics Research, Finland.

Cullis, J, Görgens, AHM and Lyons, S. 2007. *Review of the Selection of Acceptable Flood Capacity for Dams in South Africa in the Context of Dam Safety*. WRC Report No. 1420/1/07. Water Research Commission, Pretoria, RSA.

de Gaetano, AT and Belcher, BN. 2007. Spatial interpolation of daily maximum and minimum air temperature based on meteorological model analyses and independent observations. *Journal of Applied Meteorology and Climatology* 46 1981-1992.

de Silva, MT and Hornberger, GM. 2019. Identifying El Niño-Southern Oscillation influences on rainfall with classification models: implications for water resource management of Sri Lanka. *Hydrology and Earth System Sciences* 23 (4): 1905-1929.

Demaria, EMC, Goodrich, D and Keefer, T. 2017. Frequency Analysis of Extreme Sub-Daily Precipitation under Stationary and Non-Stationary Conditions across Two Contrasting Hydroclimatic Environments. *Hydrology and Earth System Sciences*

Department of Environmental Affairs. 2014a. *Climate change adaptation: Perspectives for disaster risk reduction and management in South Africa*. Provisional modelling of drought, flood and sea level rise impacts and a description of adaptation responses, Report no 3 for the Long Term Adaptation Scenarios Research Flagship Program (LTAS) (Draft). Department of Environmental Affairs, Pretoria.

Department of Environmental Affairs. 2014b. *National climate change repsonse: White paper*. Department of Environmental Affairs Pretoria.

Department of Environmental Affairs. 2017. *South Africa's 2nd Annual Climate Change Report 2016*. Department of Environmental Affairs, Pretoria.

DFFE. 2016. Climate information and early warning systems for supporting the Disaster Risk Reduction and Management Sector in South Africa. [Internet]. Department of Environmental Affiars South Africa, Pretoria, South Africa. Available from: https://www.dffe.gov.za/sites/default/files/reports/ltasbook2of7_climateinformationandearlywarningsystemsforsupportingtheDRR.pdf. [Accessed: 09 Novemeber 2022].

Ehsani, N, Vörösmarty, CJ, Fekete, BM and Stakhiv, EZ. 2017. Reservoir operations under climate change: Storage capacity options to mitigate risk. *Journal of Hydrology* 555 (2017): 435-446.

Endris, HS, Lennard, C, Hewitson, BC, Dosio, A, Nikulin, G and Artan, GA. 2019. Future changes in rainfall associated with ENSO, IOD and changes in the mean state over Eastern Africa. *Climate Dynamics* 52 2029-2053.

Fattahi, E, Noorian, AM and Noohi, K. 2011. Comparison of Physical and Statistical Methods for Estimating Probable Maximum Precipitation in Southwestern Basins of Iran. *Desert* 15 (2010): 127-132.

Faulkner, D, Griffin, A, Hannaford, J, Sharkey, P, Warren, S and Shelton, K. 2020a. b Development of Interim National Guidance on Non-stationary Fluvial Flood Frequency Estimation. *Science Report FRS18087/IG* 1

Faulkner, D, Griffin, A, Hannaford, J, Sharkey, P, Warren, S and Shelton, K. 2020b. b Development of Interim National Guidance on Non-stationary Fluvial Flood Frequency Estimation. *Science Report FRS18087/IG* 1 (1): 1-232.

Fluixá-Sanmartín, J, Morales-Torres, A, Escuder-Bueno, I and Paredes-Arquiola, J. 2019. Quantification of climate change impact on dam failure risk under hydrological scenarios: a case study from a Spanish dam. *Natural Hazards and Earth System Sciences* 19 (2019): 2117-2139.

Gao, M and Zheng, H. 2018. Nonstationary extreme value analysis of temperature extremes in China. *Stochastic Environmental Research and Risk Assessment* 32 1299-1315.

Gaughan, AE, Staub, CG, Hoell, A, Weaver, A and Waylen, PR. 2016. Inter- and Intra-annual precipitation variability and associated relationships to ENSO and the IOD in southern Africa. *International Journal of Climatology* 36 1643-1656.

Gericke, O and Smithers, J. 2018. An improved and consistent approach to estimate catchment response time parameters: Case study in the C5 drainage region, South Africa. *Journal of Flood Risk Management* 11 S284-S301.

Global Carbon Atlas. 2023. Global carbon Atlas – Emissions. [Internet]. Available from: https://globalcarbonatlas.org/emissions/carbon-emissions/. [Accessed: 23 June].

Görgens, A. 2007. *Joint peak-volume (JPV) design flood hydrographs for South Africa*. Water Research Commission Pretoria, South Africa.

Görgens, A, Lyons, S, Hayes, L, Makhabane, M and Maluleke, D. 2007. *Modernised South African design flood practice in the context of dam safety*. WRC Report No. 1420/2/07. Water Research Commission, RSA.

Gregersen, IB, Madsen, H, Rosbjerg, D and Arnbjerg-Nielsen, K. 2017. A regional and nonstationary model for partial duration series of extreme rainfall. *Water Resources Research* 53 2659-2678.

Griffis, V and Stedinger, J. 2007. Log-Pearson type 3 distribution and its application in flood frequency analysis. I: Distribution characteristics. *Journal of Hydrologic Engineering* 12 (5): 482-491.

Grobler, RR. 2003. A framework for modelling losses arising from natural catastprophes in South Africa. Unpublished Masters thesis, Univeristy of Pretoria, Pretoria, RSA.

Haddad, K, Rahman, A, Weinmann, PE, Kuczera, G and Ball, J. 2010. Streamflow data preparation for regional flood frequency analysis: Lessons from southeast Australia. *Australasian Journal of Water Resources* 14 (1): 17-32.

Hansen, EM, Fenn, DD, Schreiner, LC, Stodt, RW and Miller, JF. 1988. *Probable maximum precipitation estimates, United States between the Continental Divide and the 103rd meridian*. Hydrometeorological Report No. 55a. National Oceanic and Atmospheric Administration, Silver Spring, Md, USA.

Hattingh, L.2021. Surveillance and climate change. In: ed. WRC, *Roadshow: Advancing Dam Safety in The Context of Climate Change in South Africa*, Water Research Commission, RSA

Hesarkazzazi, S, Arabzadeh, R, Hajibabaei, M, Rauch, W, Kjeldsen, TR, Prosdocimi, I, Castellarin, A and Sitzenfrei, R. 2021. Stationary vs non-stationary modelling of flood frequency distribution across northwest England. *Hydrological Sciences Journal* 66 (4): 729-744.

Hoell, A, Gaughan, AE, Magadzire, T and Harrison, L. 2021. The Modulation of Daily Southern Africa Precipitation by El Niño-Southern Oscillation across the Summertime Wet Season. *Journal of Climate* 34 (3): 1115-1134.

Hosking, JRM and Wallis, JR. 1997. *Regional Frequency Analysis: An Approach Based on L-Moments*. Cambridge University Press, Cambridge, UK.

HRU. 1972. *Design flood determination in South Africa*. 1/72. Hydrological Research Institute, University of the Witwatersrand, Johannesburg, RSA.

IPCC. 2017a. *Climate updates.* The Royal Society, London, United Kingdoms.

IPCC. 2017b. *Climate updates. What have we learnt since the IPCC 5th Assessment Report*. The Royal Society, London.

IPCC. 2018. Summary for Policymakers. In: eds. Masson-Delmotte, V, Pörtner, H-O, Skea, J, Zhai, P, Roberts, D, Shukla, PR, A. Pirani, W. Moufouma-Okia, C. Péan, R. Pidcock, S. Connors, J. B. R. Matthews, Y. Chen, X. Zhou, M. I. Gomis, E. Lonnoy, T. Maycock, M. Tignor and Waterfield, T, *Global warming of 1.5°C. An IPCC Special Report on the impacts of global warming of 1.5°C above pre-industrial levels and related global greenhouse gas emission pathways, in the context of strengthening the global response to the threat of climate change, sustainable development, and efforts to eradicate poverty*. World Meteorological Organization, Geneva, Switzerland.

Johnson, K, Smithers, J and Schulze, R. 2021. A review of methods to account for impacts of non-stationary climate data on extreme rainfalls for design rainfall estimation in South Africa. *Journal of the South African Institution of Civil Engineering* 63 (3): 55-61.

Johnson, KA and Smithers, JC. 2019. Methods for the estimation of extreme rainfall events. *Water SA* 45 (3): 501-512.

Johnson, KA and Smithers, JC. 2020. Updating the estimation of 1-day probable maximum precipitation in South Africa. *Journal of Hydrology: Regional Studies* 32 (2020): 1-15.

Kappel, B.2019. Hurricane Harvey rainfall, did it exceed PMP and what are the implications. In: eds. Tournier, J-P, Bennett, T and Bibeau, J, *ICOLD 2019 Symposium*, 3167-3179. CRC Press, Taylor and Francis Group, Ottawa, Canada.

Kendall, M. 1962. *Rank CorrelationMethods*. Hafner Publishing Company, New York, NY. USA.

Kjeldsen, T and Prosdocimi, I. 2021a. Assessment of trends in hydrological extremes using regional magnification factors. *Advances in Water Resources* 149 (2021): 103852.

Kjeldsen, TR and Prosdocimi, I. 2021b. Assessment of trends in hydrological extremes using regional magnification factors. *Advances in Water Resources* 149 103852.

Kjeldsen, TR, Smithers, J and Schulze, R. 2002. Regional flood frequency analysis in the KwaZulu-Natal province, South Africa, using the index-flood method. *Journal of hydrology* 255 (1-4): 194-211.

Kundzewicz, ZW. 2019. *Changes in flood risk in Europe*. CRC Press, Postdam, Germany.

Landman, WA, Kgatuke, M, Mbedzi, M, Beraki, A, Bartman, A and Du Piesanne, A. 2006. *Skill comparison of dynamical and empirical downscaling methods for southern Africa from a seasonal climate modelling perspective*. 1335/1/06. South African Weather Service, Pretoria, RSA.

Lee, O, Park, Y, Kim, ES and Kim, S. 2016. Projection of Korean Probable Maximum Precipitation under Future Climate Change Scenarios. *Advances in Meteorology* 2016 1-17.

Lüdecke, H-J, Müller-Plath, G, Wallace, MG and Lüning, S. 2021. Decadal and multidecadal natural variability of African rainfall. *Journal of Hydrology: Regional Studies* 34 (2021): 100795.

Luxford, F and Faulkner, D. 2020. *Recommendations for future research and practice on non-stationarity in UK flooding*. Report FRS18087/REA/R2. Bristol, UK.

Mallakpour, I and Villarini, G. 2016. A simulation study to examine the sensitivity of the Pettitt test to detect abrupt changes in mean. *Hydrological Sciences Journal* 61 (2): 245-254.

Mangini, W, Viglione, A, Hall, J, Hundecha, Y, Ceola, S, Montanari, A, Rogger, M, Salinas, JL, Borzì, I and Parajka, J. 2018. Detection of trends in magnitude and frequency of flood peaks across Europe. *Hydrological Sciences Journal* 63 (4): 493-512.

Mann, HB. 1945. Nonparametric tests against trend. *Econometrica* 13 (3): 245-259.

Mathivha, F, Nkosi, M and Mutoti, M. 2021. Evaluating the relationship between hydrological extremes and groundwater in Luvuvhu River Catchment, South Africa. *Journal of Hydrology: Regional Studies* 37 100897.

McBride, C, Kruger, AC and L.Dyson. 2022. Changes in extreme daily rainfall characteristics in South Africa: 1921-2020. *Weather and Climate Extremes* 38 100517.

Micovic, Z, Schaefer, MG and Taylor, GA. 2014. Uncertainty analysis for Probable Maximum Precipitation estimates. *Journal of Hydrology* 521 360-373.

Minty, LJ, Meighen, J and Kennedy, MR. 1996. *Development of the Generalised Southeast Australia Method for Estimating Probable Maximum Precipitation*. Report No. 4. Hydrology Report Series, Bureau of Meteorology, Melbourne, Australia.

Moyo, P and Nyoni, B.2021. Impact of Climate on the Safety of Concrete Arch Dams. In: ed. WRC, *Roadshow: Advancing Dam Safety in The Context of Climate Change in South Africa*,

Nathanael, J, Jonathan. 2015. Assessing the performance of regional flood frequency analysis methods in South Africa. Unpublished MSc thesis, School of Hydrology University of KwaZulu-Natal, Pietermaritzburg, South Africa

National Aeronautics and Space Administration. 2023. Global Climate Change: Vital Signs – Global Temperature. [Internet]. Available from: https://climate.nasa.gov/vital-signs/global-temperature/. [Accessed: 23 July].

NWS. 1980. *Probable Maximum Precipitation Estimates – United States east of the 105th meridian*. 51. National Oceanic and Atmospheric Administration, Washington, DC, USA.

Ouarda, TBMJ, Charron, C and St-Hilaire, A. 2020. Uncertainty of stationary and nonstationary models for rainfall frequency analysis. *International Journal of Climatology* 40 2373-2392.

Pan, X, Rahman, A, Haddad, K and Ouarda, TBMJ. 2022. Peaks-over-threshold model in flood frequency analysis: a scoping review. *Stochastic Environmental Research and Risk Assessment* 36 (2022): 2419-2435.

Papalexiou, SM and Koutsoyiannis, D. 2006. A probabilistic approach to the concept of Probable Maximum Precipitation. *Advances in Geosciences* 7 (2006): 51-54.

Pedretti, D and Irannezhad, M. 2019. Non-stationary peaks-over-threshold analysis of extreme precipitation events in Finland, 1961-2016. *International Journal of Climatology* 39 1128-1143.

Petersen-Øverleir, A and Reitan, T. 2009. Accounting for rating curve imprecision in flood frequency analysis using likelihood-based methods. *Journal of Hydrology* 366 (1-4): 89-100.

Pfahl, S, O'Gorman, PA and Fischer, EM. 2017. Understanding the regional pattern of projected future changes in extreme precipitation. *Nature Climate Change*

Pinto, I, Zachariah, M, Wolski, P, Landman, S, Phakula, V, Maluleka, W, Bopape, M, Engelbrecht, C, Jack, C, McClure, A, Bonnet, R, Vautard, R, Philip, S, Kew, S, Heinrich, D, Vahlberg, M, Singh, R, Arrighi, J, Thalheimer, L, Van Aalst, M, Li, S, Sun, J, Vecchi, G, Yang, W, Tradowsky, J, Otto, F and Dipura, R. 2022. Climate change exacerbated rainfall causing devastating flooding in Eastern South Africa. *World weather attribution intiative* 1 (1): 1-31.

Prosdocimi, I, Kjeldsen, T and Svensson, C. 2014a. Non-stationarity in annual and seasonal series of peak flow and precipitation in the UK. *Natural Hazards and Earth System Sciences* 14 (5): 1125-1144.

Prosdocimi, I, Kjeldsen, TR and Svensson, C. 2014b. Non-stationarity in annual and seasonal series of peak flow and precipitation in the UK. *Natural Hazards and Earth Systems Sciences* 14 1125-1144.

Ragno, E, AghaKouchak, A, Cheng, L and Sadegh, M. 2019a. A generalized framework for process-informed nonstationary extreme value analysis. *Advances in Water Resources* 130 270-282.

Ragno, E, AghaKouchak, A, Cheng, L and Sadegh, M. 2019b. A generalized framework for process-informed nonstationary extreme value analysis. *Advances in Water Resources* 130 (2019): 270-282.

Ragno, E, AghaKouchak, A, Cheng, L and Sadegh, M. 2019c. Process-informed Nonstationary Extreme Value Analysis (ProNEVA) User Manual.

Rastogi, D, Kao, S-C, Ashfaq, M, Mei, R, Kabela, ED, Gangrade, S, Naz, BS, Preston, BL, Singh, N and Anantharaj, VG. 2017. Effects of climate change on probable maximum precipitation: A sensitivity study over the Alabama-Coosa-Tallapoosa River Basin. *Journal of geophysical research: atmospheres* 122 4808-4828.

Roffe, SJ, Fitchett, JM and Curtis, CJ. 2019. Classifying and mapping rainfall seasonality in South Africa: a review. *South African Geographical Journal* 101 (2): 158-174.

Rougé, C, Ge, Y and Cai, X. 2013. Detecting gradual and abrupt changes in hydrological records. *Advances in Water Resources* 53 33-44.

Rouhani, H. 2016. Climate change impact on probable maximum precipitation and probable maximum flood in Québec. Unpublished thesis, Department of Civil Engineering, University of Sherbrooke, Québec, Canada.

Rouhani, H and Leconte, R. 2016. A novel method to estimate the maximization ratio of the Probable Maximum Precipitation (PMP) using regional climate model output. *Water Resources Research* 52 7347-7365.

Rousseau, AN, Klei, IM, Freudiger, D, Gagnon, P, Frigon, A and Ratté-Fortin, C. 2014. Development of a methodology to evaluate probable maximum precipitation (PMP) under changing climate conditions: Application to southern Quebec, Canada. *Journal of Hydrology* 519 (2014): 3094-3109.

Rusu, C and Rusu, V. 2006. Radial basis functions versus geostatistics in spatial interpolations. In: ed. Bramer, M, *Artificial Intelligence in Theory and Practice*. Springer, Boston.

Sadegh, M, Vrugt, JA, Xu, C and Volpi, E. 2015. The stationarity paradigm revisited: hypothesis testing using diagnostics, summary metrics, and DREAM(ABC). *Water Resources Research* 51 (11): 9207-9231.

Salas, J, Obeysekera, J and Vogel, R. 2018. Techniques for assessing water infrastructure for nonstationary extreme events: a review. *Hydrological Sciences Journal* 63 (3): 325-352.

Salas, JD, Gavilan, G, Salas, FR, Julien, PY and Abdullah, J. 2014. Uncertainty of the PMP and PMF. In: ed. Eslamian, S, *Handbook of Engineering Hydrology*. Taylor & Francis Group, LLC, USA.

SANCOLD. 1991. *Guidelines on Safety in Relation to Floods: Safety evaluation of dams*. South African National Committee on Large Dams, Pretoria, RSA.

Sarhadi, A and Soulis, ED. 2017. Time-varying extreme rainfall intensity-duration-frequency curves in a changing climate,. *Geophysical Research Letters* 44 2454-2463.

Schulze, RE. 2011. South Africa: A Brief Overview. In: ed. Schulze, R, *A 2011 Perspective on Climate Change and the South African Water Sector, Ch. 1.2, WRC Report TT 518/12*. Water Research Commission, Pretoria, RSA.

Schulze, RE and Maharaj, M. 2004. *Development of a Database of Gridded Daily Temperatures for Southern Africa*. WRC Report No. 1156/2/04. Water Research Commission, Pretoria, RSA.

Schumann, TEW and Hofmeyer, WL. 1938. The partition of a region into rainfall districts with special reference to South Africa. *Quarterly Journal of the Royal Meteorological Society* 64 (276): 482-488.

Schütte, S, Schulze, RE, Clark, DJ, Kunz, RP, Wolski, P, Lumsden, T, Smithers, JC, Stuart-Hill, SI, Thornton-Dibb, SLC, Horan, MJC, Toucher, ML and Jele, Z. 2023. *A National Assessment of Potential Climate Change Impacts on the Hydrological Yield of Different Hydro-Climatic Zones of South Africa: Report 1 Methodology and Results*. WRC Report No. 2833/1/22. Water Research Commission, Pretoria, RSA.

Schwarz, G. 1978. Estimating the dimension of a model. *The Annals of Statistics* 6 (2): 461-464.

Scott, M and Chandler, R. 2011. *Statistical methods for trend detection and analysis in the environmental sciences*. John Wiley & Sons, London, United Kingdom.

Sen, PK. 1968. Estimates of the Regression Coefficient based on Kendall's Tau. *Journal of the American Statistical Association* 63 (324): 1379-1389.

Serinaldi, F and Kilsby, CG. 2015. Stationarity is undead: Uncertainty dominates the distribution of extremes. *Advances in Water Resources* 77 (2015): 17-36.

Silva, DF, Simonovic, SP, Schardong, A and Goldenfum, AV. 2021. Assessment of non-stationary IDF curves under a changing climate: Case study of different climatic zones in Canada. *Journal of Hydrology: Regional Studies* 36 (2021): 100870.

Singh, K. 2019. Durban floods damage estimated at over R650m. [Internet]. News24, Durban, South Africa. Available from: https://www.news24.com/News24/durban-floods-damage-estimated-at-over-r650m-20190426. [Accessed: 09 November 2022].

Singo, L, Kundu, P, Odiyo, J, Mathivha, F and Nkuna, T. 2012. Flood frequency analysis of annual maximum stream flows for Luvuvhu river catchment, Limpopo province, South Africa.

Smithers, J. 2012a. Methods for design flood estimation in South Africa. *Water SA* 38 (4): 633-646.

Smithers, J, Streatfield, J, Gray, R and Oakes, E. 2015. Performance of regional flood frequency analysis methods in KwaZulu-Natal, South Africa. *Water SA* 41 (3): 390-397.

Smithers, JC. 1996. Short-duration rainfall frequency model selection in Southern Africa. *Water SA* 22 (3): 211-217.

Smithers, JC. 2012b. Review of methods for design flood estimation in South Africa. *Water SA* 38 (4): 633-646.

Smithers, JC, Görgens, A, Gericke, J, Jonker, V and Roberts, CPR. 2014. *The initiation of a national flood studies programme for South Africa*. RSA.

Smithers, JC, Görgens, A, Gericke, J, Jonker, V and Roberts, CPR. 2016. *The Initiation of a National Flood Studies Programme for South Africa*. South African National Committee on Large Dams (SANCOLD), Pretoria, South Africa.

Smithers, JC and Schulze, RE. 2000a. *Development and evaluation of techniques for estimating short duration design rainfall in South Africa*. 681/1/00. Water Research Commission, Pretoria, RSA.

Smithers, JC and Schulze, RE. 2000b. *Long duration design rainfall estimates for South Africa*. 811/1/00. Water Research Commission, Pretoria, RSA.

Song, X, Zou, X, Mo, Y, Zhang, J, Zhang, C and Tian, Y. 2020. Nonstationary bayesian modeling of precipitation extremes in the Beijing-Tianjin-Hebei Region, China. *Atmospheric Research* 242

South African Weather Bureau. 1960. *Climate of South Africa. Part 5, District rainfall*. (W.B. 23). South African Weather Bureau, Research Branch, Pretoria, RSA.

South African Weather Bureau. 1972. *Climate of South Africa. Part 10, District rainfall for South Africa and the annual March of rainfall over southern Africa*. (W.B. 35). South African Weather Bureau, Research Branch, Pretoria, RSA.

Šraj, M, Viglione, A, Parajka, J and Blöschl, G. 2016. The influence of non-stationarity in extreme hydrological events on flood frequency estimation. *J. Hydrol. Hydromech* 64 (4): 426-437.

Tan, X and Gan, TY. 2017. Non-stationary analysis of the frequency and intensity of heavy precipitation over Canada and their relations to large-scale climate patterns. *Climate Dynamics* 48 2983-3001.

Thoithi, W, Blamey, RC and Reason, CJC. 2023. April 2022 Floods over East Coast South Africa: Interactions between a Mesoscale Convective System and a Coastal Meso-Low. *Atmosphere* 14 (78): 1-23.

Thuy, LTT, Kawagoe, S and Sarukkalige, R. 2019. Estimation of probable maximum precipitation at three provinces in Northeast Vietnam using historical data and future climate change scenarios. *Journal of Hydrology: Regional Studies* 23 (2019):

Vasiliades, L, Galiatsatou, P and Loukas, A. 2015. Nonstationary frequency analysis of annual maximum rainfall using climate covariates. *Water Resource Management* 29 339-358.

Villarini, G, Smith, JA, Serinaldi, F, Bales, J, Bates, PD and Krajewski, WF. 2009. Flood frequency analysis for nonstationary annual peak records in an urban drainage basin. *Advances in water resources* 32 (8): 1255-1266.

Vogel, RM, Yaindl, C and Walter, M. 2011. Nonstationarity: flood magnification and recurrence reduction factors in the United States 1. *JAWRA Journal of the American Water Resources Association* 47 (3): 464-474.

Walland, DJ, Meighen, J, Xuereb, KC, Beesley, CA and T, HTM. 2003. *Revision of the Generalised Tropical Storm Method for Estimating Probable Maximum Precipitation*. 8. Hydrology Report Series, Bureau of Meteorology, Melbourne, Australia.

Wang, B-H. 1984. Estimation of probable maximum precipitation: case studies. *Journal of Hydraulic Engineering* 110 (10): 1457-1472.

Wanielista, M, Kersten, R and Eaglin, R. 1997. *Hydrology: Water Quantity and Quality Control, second edition*. John Wiley & Sons, Inc,

WMO. 1994. *Guide to Hydrological Practises*. WMO Report No. 168.

WMO. 2009. *A manual on estimation of probable maximum precipitation (PMP).* World Meterological Organisation – No. 1045. Geneva, Switzerland.

WRC. 2021. Roadshow: Advancing Dam Safety in The Context of Climate Change in South Africa. [Internet]. Available from: https://wrc.org.za/?mdocs-file=61565. [Accessed: 12 May].

Xiong, L and Guo, S. 2004. Trend test and change-point detection for the annual discharge series of the Yangtze River at the Yichang hydrological station/Test de tendance et détection de rupture appliqués aux séries de débit annuel du fleuve Yangtze à la station hydrologique de Yichang. *Hydrological sciences journal* 49 (1): 99-112.

Yilmaz, AG, Hossain, I and Perera, BJC. 2014. Effect of climate change and variability on extreme rainfall intensity-frequency-duration relationships: A case study of Melbourne. *Hydrology and Earth System Sciences* 18 4065-4076.

Yilmaz, AG and Perera, BJC. 2015. Spatiotemporal Trend Analysis of Extreme Rainfall Events in Victoria, Australia. *water Resource Management* 29 (2015): 4465-4480.

Zhang, Q, Gu, X, Singh, VP, Xiao, M and Xu, CY. 2015. Flood frequency under the influence of trends in the Pearl River basin, China: changing patterns, causes and implications. *Hydrological Processes* 29 (6): 1406-1417.

Zhou, C, R, Chen, Y, F, Gu, S, H, Huang, Q, Yuan, J, C and Yu, S, N. 2016. A new threshold selection method for peak over for non-stationary time series. *IOP Conference Series: Earth and Environmental Science* 39

Ziervogel, G, New, M, Archer van Garderen, E, Midgley, G, Taylor, A, Hamann, R, Stuart-Hill, S, Myers, J and Warburton, M. 2014. Climate change impacts and adaptation in South Africa. *WIREs Climate Change* 5 605-620.

8. APPENDIX A: Updating the 1-day PMP Estimates

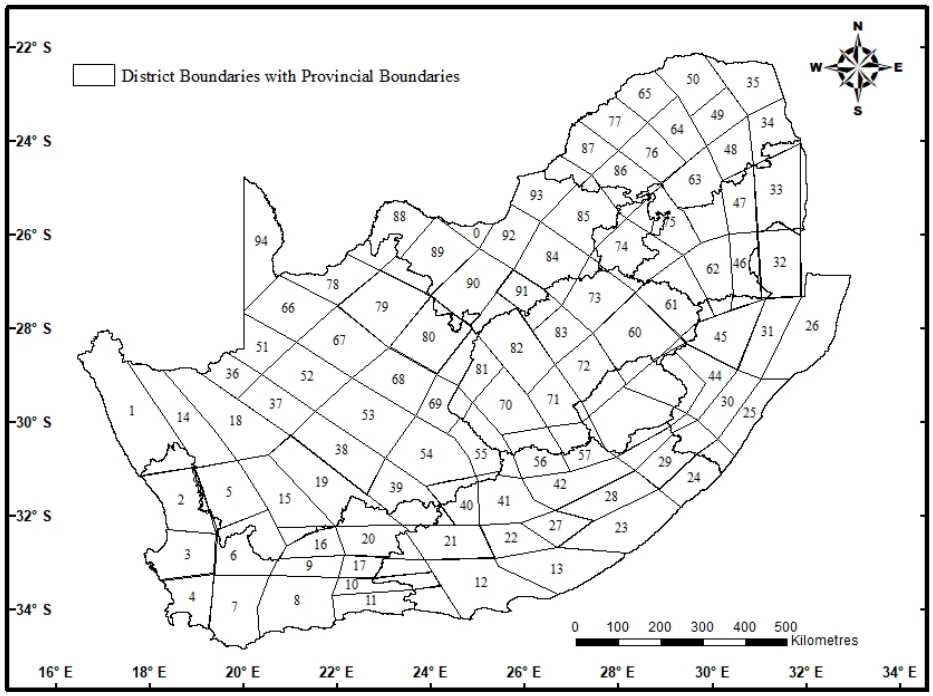

Figure 8.1 Homogeneous rainfall districts for South Africa

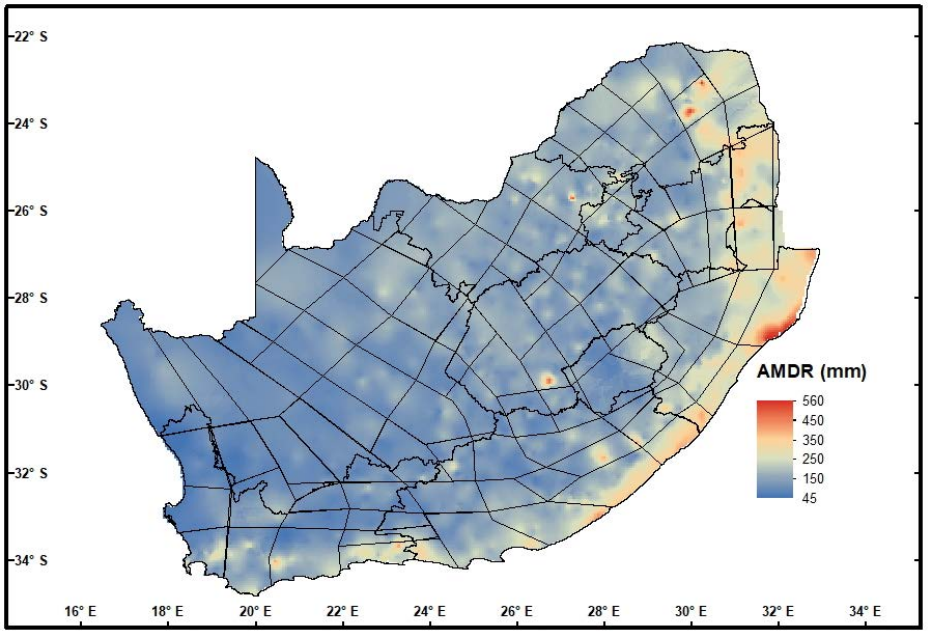

Figure 8.2 Map of Annual Maximum Daily Rainfalls for South Africa

Table 8.1 Critical analysis of selected stations with large moisture maximisation ratios

Station ID	**Date of Maximum 1-day Rainfall Event**	**Observed Maximum 1-day Rainfall (mm)**	**Moisture Maximisation Ratio (R_m)**	**Calculated PMP (mm)**	**Comment**
0094730_W	26/08/1970	146	6,35	927,1	Correlates to location of flooding in Eastern Cape dated 24-28/08/1970 (Grobler, 2003).
0095395_W	26/08/1970	152.5	4,39	669,5	
0302699_W	04/07/1963	248	4,56	1130,1	Correlates to location of flooding in Northern KwaZulu-Natal on 05/07/1963 (Botes, 2014).
0372496_W	04/07/1963	170	5,28	896,8	
0336283_W	30/03/1984	157	3,19	498,6	Correlates to location of flooding in Northern KwaZulu-Natal 01/02/ 1984 (Botes, 2014).
0302628_W	28/09/1987	254	3,83	973	Correlates to location of flooding in KwaZulu-Natal dated 30/09/ 1987 (Botes, 2014).
0302687_W	28/09/1987	292	3,85	1102	
0270722_W	27/09/1987	273	3,77	1030	
0238022_A	17/05/1959	225	4,11	676	Correlates to location of flooding in Southern KwaZulu-Natal dated 16-18/05/1987(Botes, 2014).
0238132_W	17/05/1959	189	4,40	830	
0208635_W	17/05/1959	190	5,17	982,3	
0208107_A	17/05/1959	129,5	4,77	618,3	
0176372_W	20/02/1988	115	4,14	476,9	Correlates to location of flooding in the Central
0204640_W	21/02/1988	145	3,08	448,4	

Station ID	Date of Maximum 1-day Rainfall Event	Observed Maximum 1-day Rainfall (mm)	Moisture Maximisation Ratio (R_m)	Calculated PMP (mm)	Comment
					Interior dated 29/02/ 1988 (Grobler, 2003).
0066027_W	24/01/1984	191	5,46	1042	Correlates to location of flooding in Laingsburg (Western Cape) on 25/01/1984 (Grobler, 2003).
0198524_W	01/03/1974	166,5	3,63	604,9	Correlates to location of flooding in the Central Interior dated 04/03/ 1974 (Grobler, 2003).
0256638_W	01/03/1974	108,2	4,25	459,4	

9. APPENDIX B: Non-stationary Frequency Analysis of Extreme Rainfalls in KwaZulu-Natal

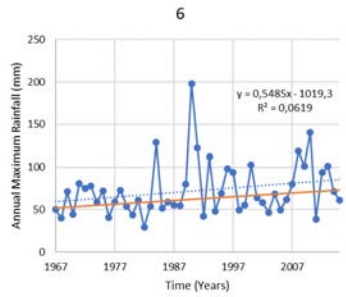

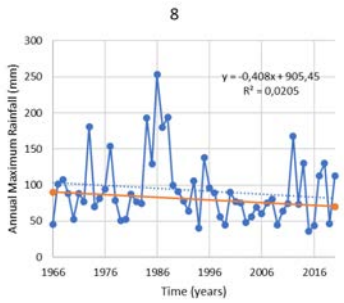

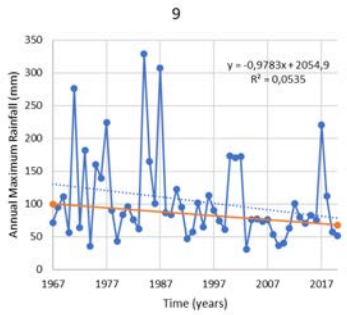

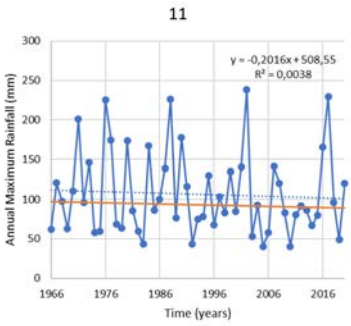

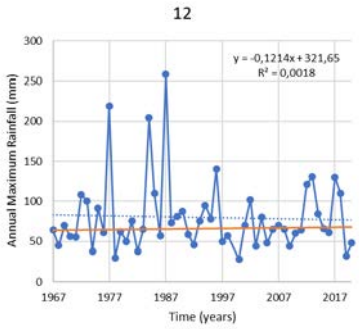

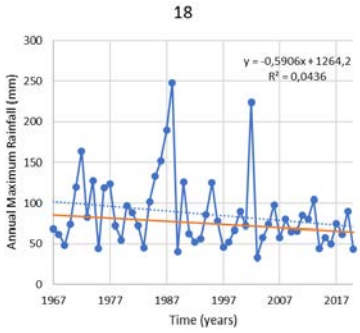

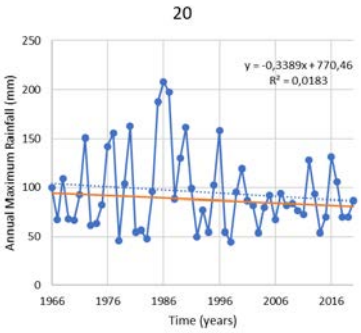

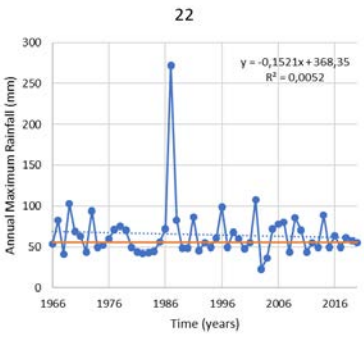

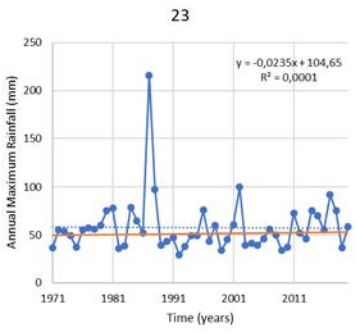

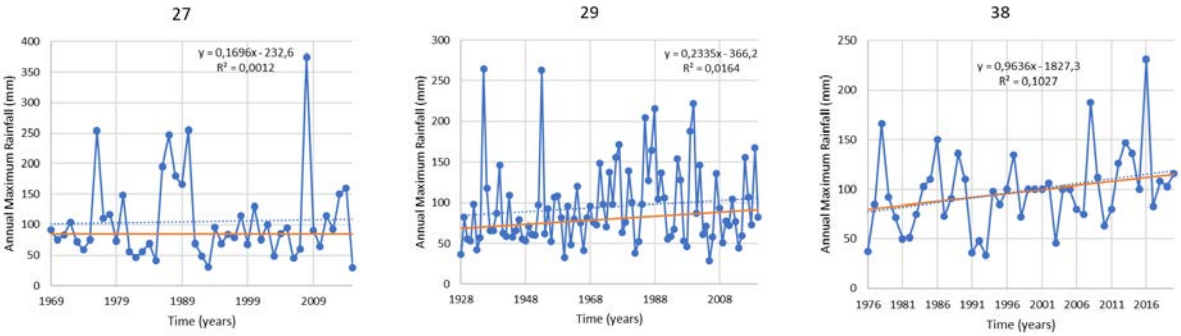
27
y = 0,1696x - 232,6
R² = 0,0012
Annual Maximum Rainfall (mm)
Time (years)

29
y = 0,2335x - 366,2
R² = 0,0164
Annual Maximum Rainfall (mm)
Time (years)

38
y = 0,9636x - 1827,3
R² = 0,1027
Annual Maximum Rainfall (mm)
Time (years)

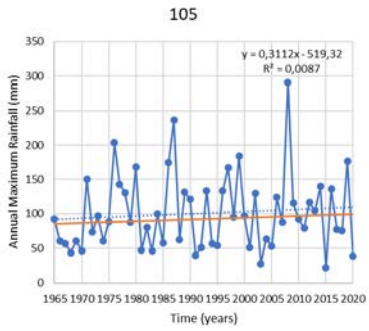
105
y = 0,3112x - 519,32
R² = 0,0087
Annual Maximum Rainfall (mm)
Time (years)

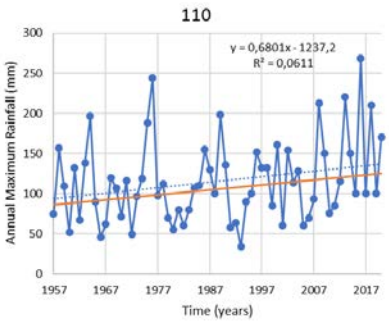
110
y = 0,6801x - 1237,2
R² = 0,0611
Annual Maximum Rainfall (mm)
Time (years)

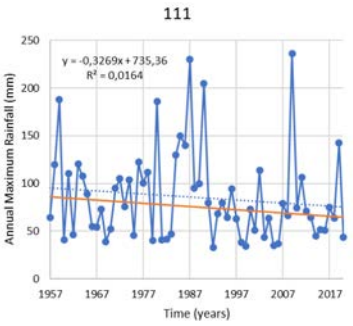
111
y = -0,3269x + 735,36
R² = 0,0164
Annual Maximum Rainfall (mm)
Time (years)

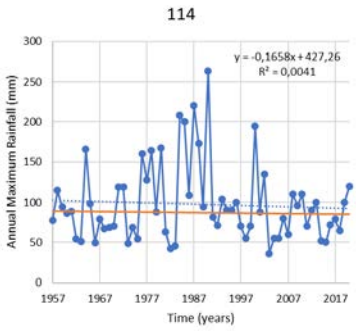
114
y = -0,1658x + 427,26
R² = 0,0041
Annual Maximum Rainfall (mm)
Time (years)

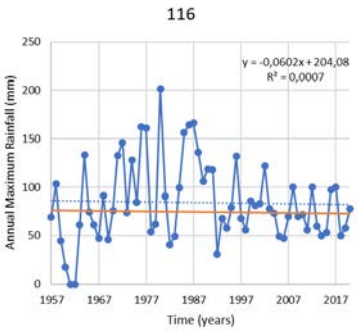
116
y = -0,0602x + 204,08
R² = 0,0007
Annual Maximum Rainfall (mm)
Time (years)

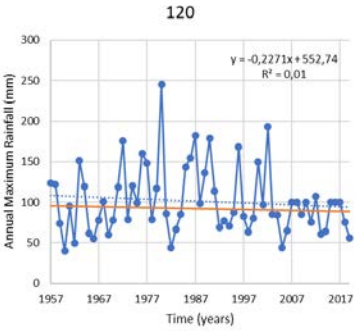
120
y = -0,2271x + 552,74
R² = 0,01
Annual Maximum Rainfall (mm)
Time (years)

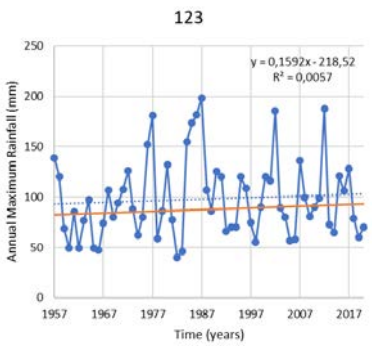
123
y = 0,1592x - 218,52
R² = 0,0057
Annual Maximum Rainfall (mm)
Time (years)

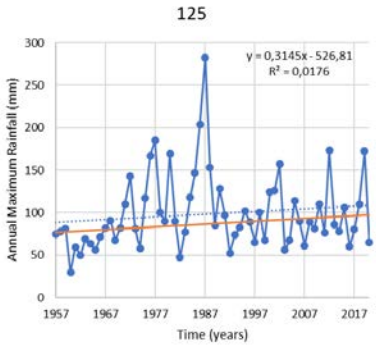
125
y = 0,3145x - 526,81
R² = 0,0176
Annual Maximum Rainfall (mm)
Time (years)

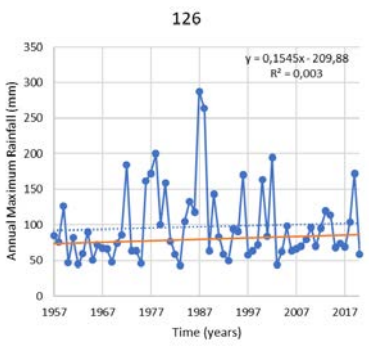
126
y = 0,1545x - 209,88
R² = 0,003
Annual Maximum Rainfall (mm)
Time (years)

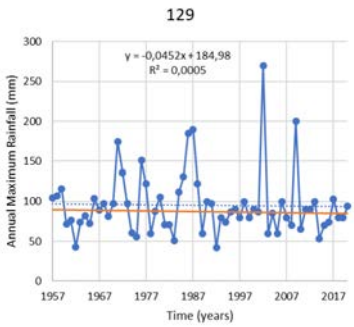
129
y = -0,0452x + 184,98
R² = 0,0005
Annual Maximum Rainfall (mm)
Time (years)

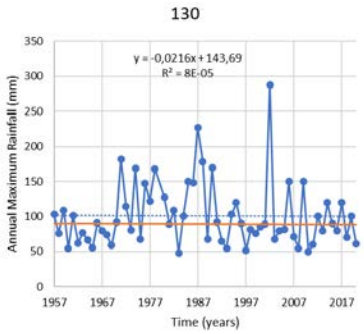
130
y = -0,0216x + 143,69
R² = 8E-05
Annual Maximum Rainfall (mm)
Time (years)

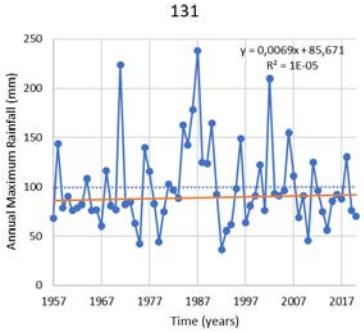
131
y = 0,0069x + 85,671
R² = 1E-05
Annual Maximum Rainfall (mm)
Time (years)

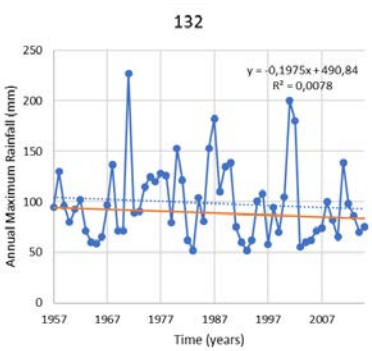
132
y = -0,1975x + 490,84
R² = 0,0078
Annual Maximum Rainfall (mm)
Time (years)

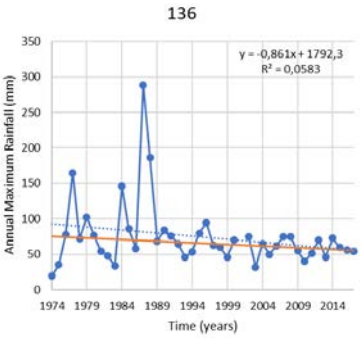
136
y = -0,861x + 1792,3
R² = 0,0583
Annual Maximum Rainfall (mm)
Time (years)

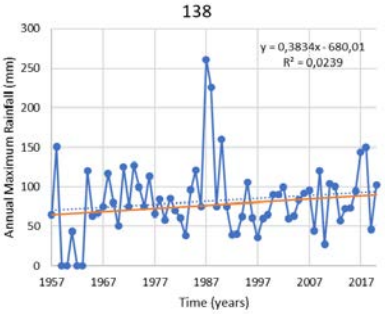
138
y = 0,3834x - 680,01
R² = 0,0239
Annual Maximum Rainfall (mm)
Time (years)

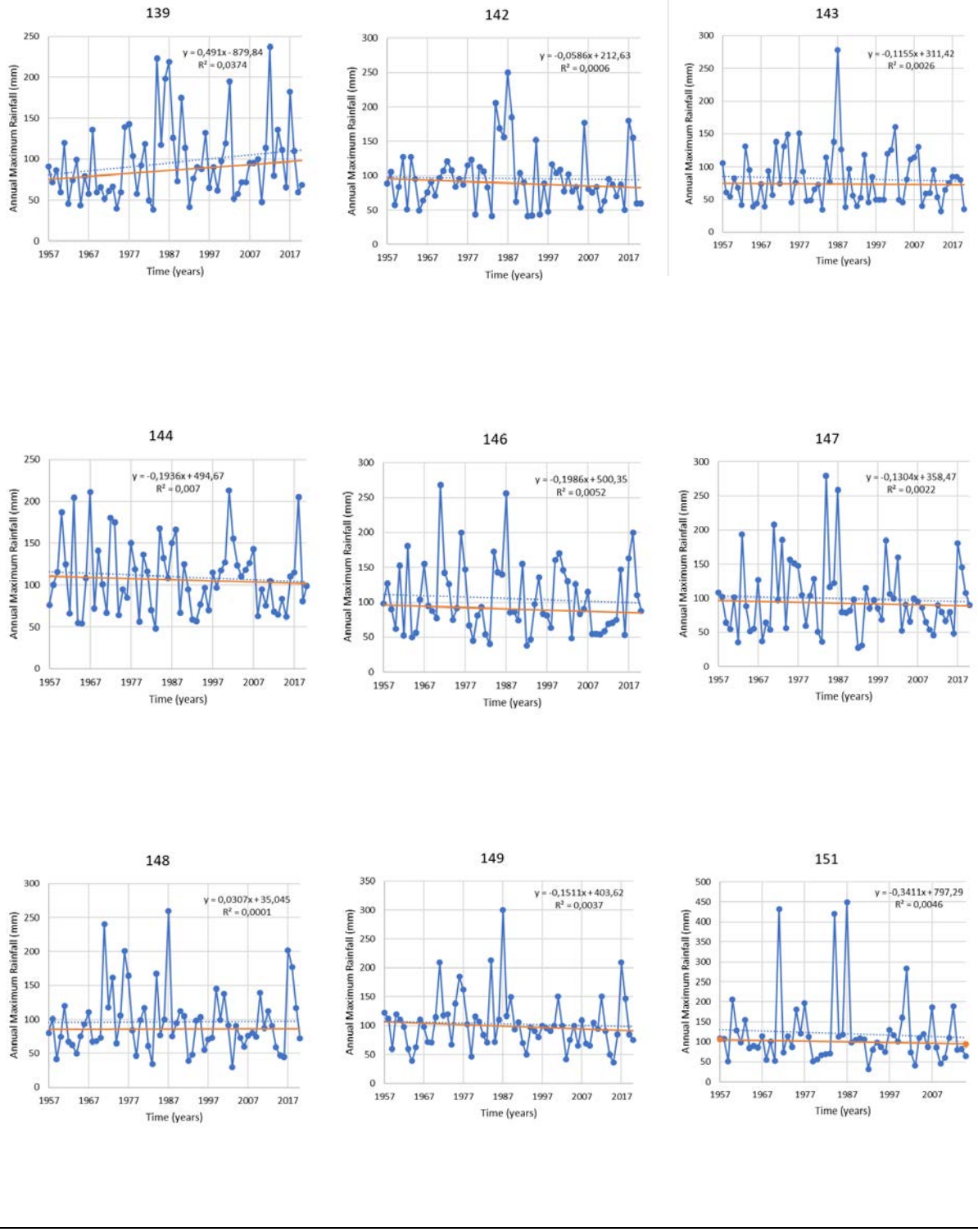
139
y = 0,491x - 879,84
R² = 0,0374
142
y = -0,0586x + 212,63
R² = 0,0006
143
y = -0,1155x + 311,42
R² = 0,0026
144
y = -0,1936x + 494,67
R² = 0,007
146
y = -0,1986x + 500,35
R² = 0,0052
147
y = -0,1304x + 358,47
R² = 0,0022
148
y = 0,0307x + 35,045
R² = 0,0001
149
y = -0,1511x + 403,62
R² = 0,0037
151
y = -0,3411x + 797,29
R² = 0,0046
Annual Maximum Rainfall (mm)
Time (years)

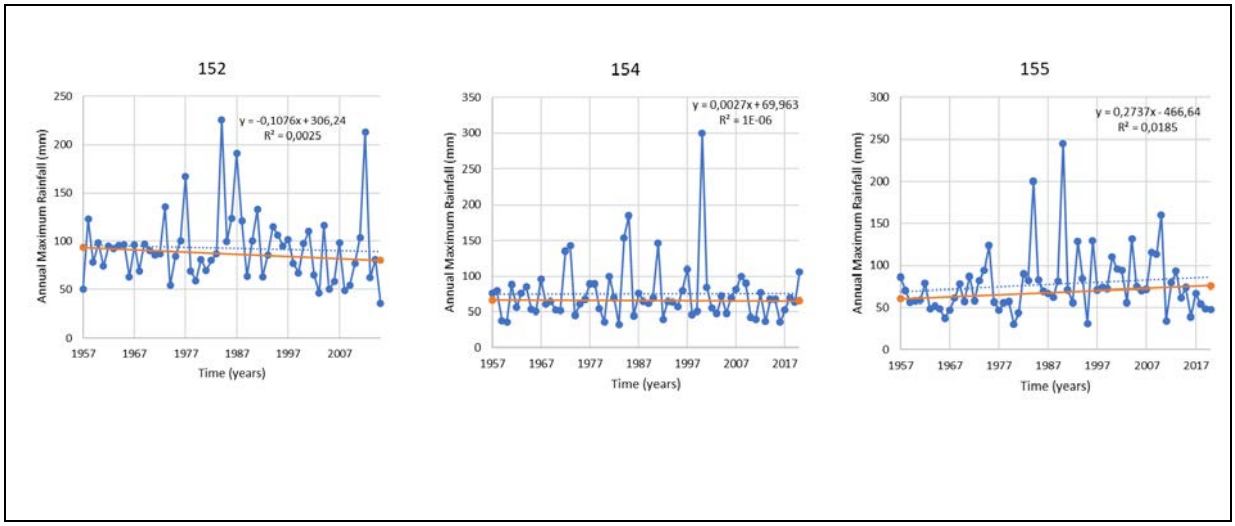

Figure 9.1 Time series of all annual maximum rainfalls at all SASRI stations used in this research

Table 9.1 The GEV statistical model performance criteria of KwaZulu-Natal AMDR for all covariates

Station	Stationary			Time			SOI			DMI			CO_2			GMT		
	AIC	BIC	RMSE	AIC	BIC	RMSE	AIC	BIC	RMSE	AIC	BIC	RMSE	AIC	BIC	RMSE	AIC	BIC	RMSE
6	**460.81***	**466.49***	1.62	462.90	474.25	1.29	466.03	477.38	1.99	467.20	478.55	1.29	462.24	473.59	1.80	464.75	476.10	2.19
8	**558.34***	**564.36***	1.55	562.22	574.27	1.27	564.37	576.41	1.72	565.59	577.63	1.95	563.35	575.40	1.48	568.60	580.65	2.76
9	**575.74***	**581.70***	1.82	579.30	591.24	1.60	581.04	592.97	2.18	578.66	590.59	2.87	578.19	590.13	1.55	582.89	594.83	2.07
11	**580.81***	**586.83***	1.32	587.07	599.11	1.41	588.62	600.67	0.81	588.92	600.96	2.03	587.58	599.63	1.31	591.74	603.79	2.19
12	**524.07***	**529.98***	2.01	530.18	542.00	2.18	528.74	540.56	2.26	531.72	543.54	2.54	530.49	542.31	1.99	532.85	544.67	3.09
18	**538.31***	**544.27***	1.24	542.06	553.99	1.63	543.78	555.71	1.70	545.74	557.68	1.39	543.40	555.34	0.69	543.70	555.64	1.32
20	**549.95***	**555.97***	1.24	553.22	565.27	1.66	552.50	564.55	1.35	557.23	569.28	2.11	555.74	567.79	1.25	557.10	569.14	1.33
22	**493.72***	**499.74***	4.30	495.97	508.02	3.57	493.85	505.89	3.47	498.92	510.96	4.52	498.78	510.82	5.28	503.65	515.69	3.39
23	**433.83***	**439.57***	2.60	440.31	451.78	2.73	440.62	452.09	2.55	441.10	452.57	3.89	439.35	450.83	1.89	440.19	451.66	3.48
26	**531.30***	**537.10***	1.76	536.26	547.85	1.35	534.84	546.43	1.96	537.86	549.45	1.85	535.87	547.47	1.45	538.18	549.77	1.61
27	**504.05***	**509.60***	1.88	508.19	519.30	1.58	508.46	519.56	2.44	512.28	523.38	2.82	508.10	519.20	1.89	511.83	522.93	1.81
29	954.38	961.98	1.45	956.19	971.39	1.16	958.87	974.07	1.60	959.00	974.19	1.42	**643.43***	**656.10***	1.50	961.56	976.75	1.38
38	449.01	**454.36***	1.79	**447.38***	456.30	1.71	461.64	472.48	1.85	463.70	474.54	1.66	458.18	469.02	1.85	459.78	470.62	1.32
105	**597.12***	**603.20***	1.22	600.91	613.06	0.99	604.05	616.20	1.61	603.70	615.86	0.91	600.57	612.72	1.21	605.83	617.98	0.91
110	678.80	685.27	1.18	681.18	694.14	0.97	683.75	696.70	1.71	683.33	696.28	1.14	**650.71***	**663.37***	1.08	683.65	696.60	1.10
111	**650.68***	**657.16***	1.71	654.17	667.12	1.47	655.94	668.89	1.49	657.11	670.06	2.04	650.80	663.46	1.29	656.77	669.73	2.39
114	**654.36***	660.84	1.68	660.62	673.57	1.49	658.41	669.20	1.75	662.80	675.75	2.06	**633.35***	**646.01***	1.70	662.84	675.80	1.99
120	**638.31***	644.73	1.12	641.61	654.47	0.97	640.56	653.42	1.97	644.34	657.20	1.54	**612.32***	**624.89***	1.25	644.00	656.86	1.82
123	644.55	651.02	1.53	649.04	662.00	1.39	**642.21***	655.17	1.41	651.48	664.43	1.58	**618.31***	**630.98***	1.32	650.09	663.05	1.57
125	646.42	652.90	1.87	647.89	660.84	2.15	647.01	659.96	1.66	650.52	663.48	1.87	**620.45***	**633.11***	1.49	649.62	662.57	1.53
126	650.56	657.04	1.75	655.20	668.15	1.57	656.14	669.09	1.93	657.72	670.67	2.10	**626.12***	**638.78***	2.00	658.26	671.21	2.70
129	624.55	631.03	2.60	627.67	640.62	2.11	**622.30***	635.25	1.66	631.82	644.77	2.37	**600.28***	**612.94***	2.06	630.02	642.97	2.21
130	633.31	639.74	1.45	639.00	651.86	1.15	**628.60***	641.46	1.39	641.77	654.62	2.33	**611.81***	**624.38***	0.97	641.73	654.59	1.63

Station	Stationary			Time			SOI			DMI			CO_2			GMT		
	AIC	**BIC**	**RMSE**	**AIC**	**BIC**	**RMSE**	**AIC**	**BIC**	**RMSE**	**AIC**	**BIC**	**RMSE**	**AIC**	**BIC**	**RMSE**	**AIC**	**BIC**	**RMSE**
131	644.40	650.87	1.62	650.88	663.84	1.88	650.17	663.12	1.75	**642.24***	655.19	2.44	**621.77***	**634.43***	1.92	653.09	666.04	2.61
132	**582.99***	589.23	1.38	**587.49***	599.96	0.96	589.90	602.36	1.06	592.20	604.67	0.83	**559.93***	**572.08***	0.99	588.75	601.21	1.46
136	449.30	454.65	5.50	**441.49***	**450.41***	4.77	451.62	462.33	4.52	457.21	467.91	6.41	**445.74***	456.45	4.92	449.28	459.98	6.54
138	669.56	676.04	3.14	**663.81**	**674.60**	2.37	677.33	690.28	3.75	679.25	692.20	2.71	633.86	**646.53***	2.44	669.05	682.00	2.74
139	**655.28***	661.76	1.53	658.52	671.47	1.26	659.45	672.41	1.19	663.34	676.29	1.30	629.94	**642.60***	1.54	661.57	674.52	1.22
142	**649.98***	656.46	1.43	653.17	666.12	1.03	655.72	668.68	1.65	656.72	669.67	1.73	626.53	**639.19***	1.14	654.73	667.69	2.10
143	**639.43***	645.91	1.86	644.96	657.91	1.61	645.66	658.62	2.57	646.46	659.41	2.48	617.40	**630.07***	1.64	649.00	661.96	1.43
144	658.45	664.92	1.53	662.85	675.80	1.41	665.18	678.13	1.15	664.23	677.19	1.39	**633.52***	**646.18***	1.67	666.58	679.54	1.29
146	674.01	680.48	1.63	679.81	692.77	1.53	674.94	687.90	1.56	679.88	692.83	1.71	**650.45***	**663.11***	1.54	681.38	694.34	1.73
147	672.21	678.69	1.42	677.51	690.46	2.02	676.90	689.86	2.11	679.51	692.47	1.83	**647.37***	**660.03***	0.97	678.23	691.18	1.52
148	**658.21***	664.68	1.61	664.53	677.49	1.64	665.19	678.15	1.37	665.33	678.29	1.87	635.96	**648.63***	1.15	668.46	681.41	2.32
149	**656.35***	662.82	2.01	664.71	677.66	2.00	661.89	674.84	2.43	663.86	676.81	1.94	632.88	**645.55***	1.88	666.08	679.03	1.90
151	**639.67***	645.90	3.13	645.48	657.94	2.83	646.86	659.32	3.32	641.45	653.91	3.53	616.16	**628.31***	2.22	648.76	661.23	4.23
152	578.80	585.03	2.13	578.77	591.24	1.31	583.30	595.76	2.11	588.86	601.33	3.06	546.38	**558.53***	1.62	578.97	591.44	3.86
154	612.12	618.59	2.37	617.67	630.62	1.14	615.03	627.98	2.03	618.64	631.59	2.38	**590.86***	**603.53***	2.42	621.78	634.73	3.37
155	615.82	622.30	2.09	618.61	631.57	2.37	**615.63***	628.58	2.16	617.83	630.79	2.07	**591.24***	**603.90***	1.38	621.73	634.68	3.17

***Best-fit model based on AIC and BIC**

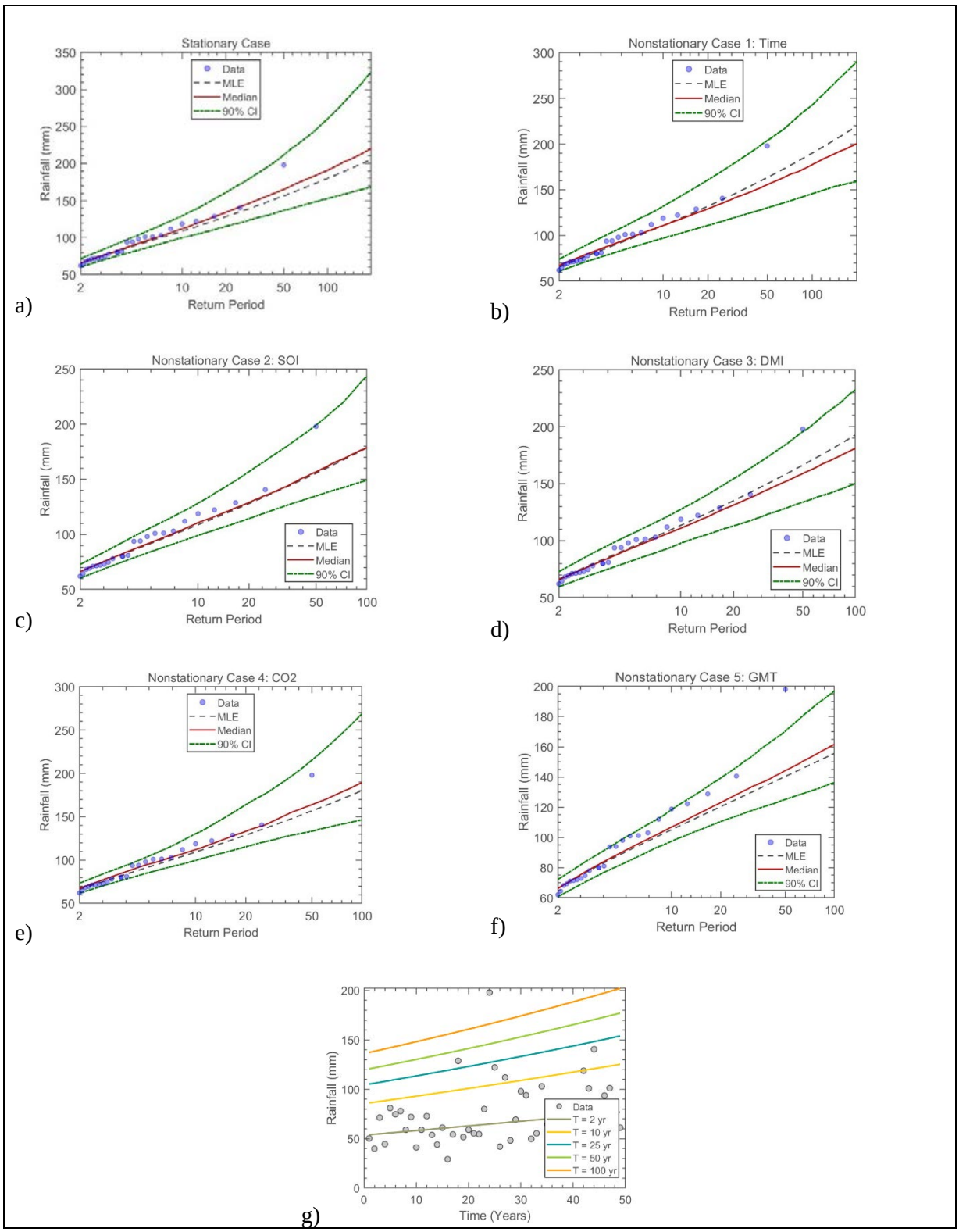

Figure 9.2 The GEV (a) stationary model, (b) non-stationary model considering time as a covariate, (c) non-stationary model considering SOI as a covariate, (d) non-stationary model considering DMI as a covariate, (e) non-stationary model considering CO_2 as a covariate, (f) non-stationary model considering GMT as a covariate and (g) effective return period as a function of time for Station 6: Pongola – SASRI

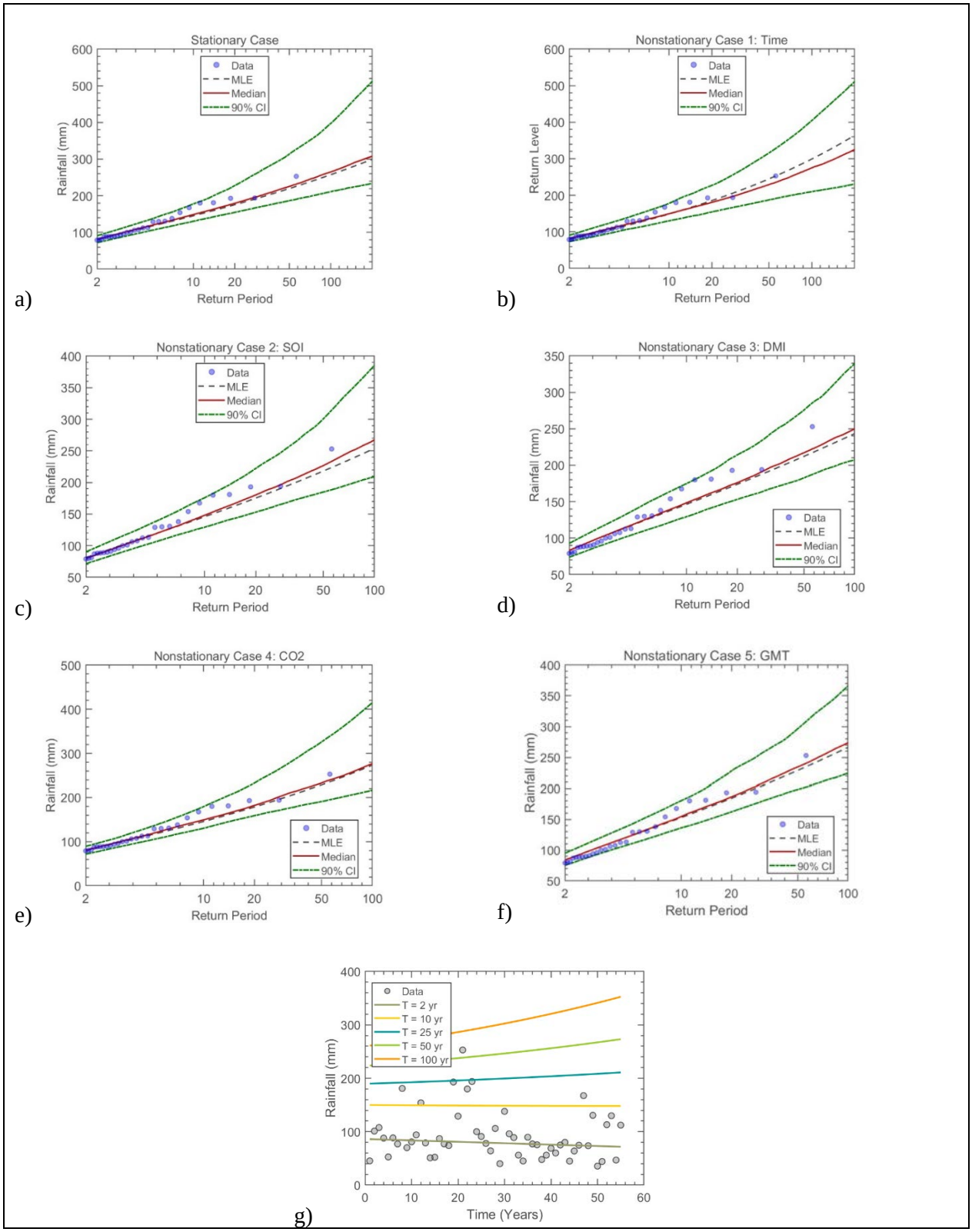

Figure 9.3 The GEV (a) stationary model, (b) non-stationary model considering time as a covariate, (c) non-stationary model considering SOI as a covariate, (d) non-stationary model considering DMI as a covariate, (e) non-stationary model considering CO_2 as a covariate, (f) non-stationary model considering GMT as a covariate and (g) effective return period as a function of time for Station 8: Glen Park – St Lucia Farms

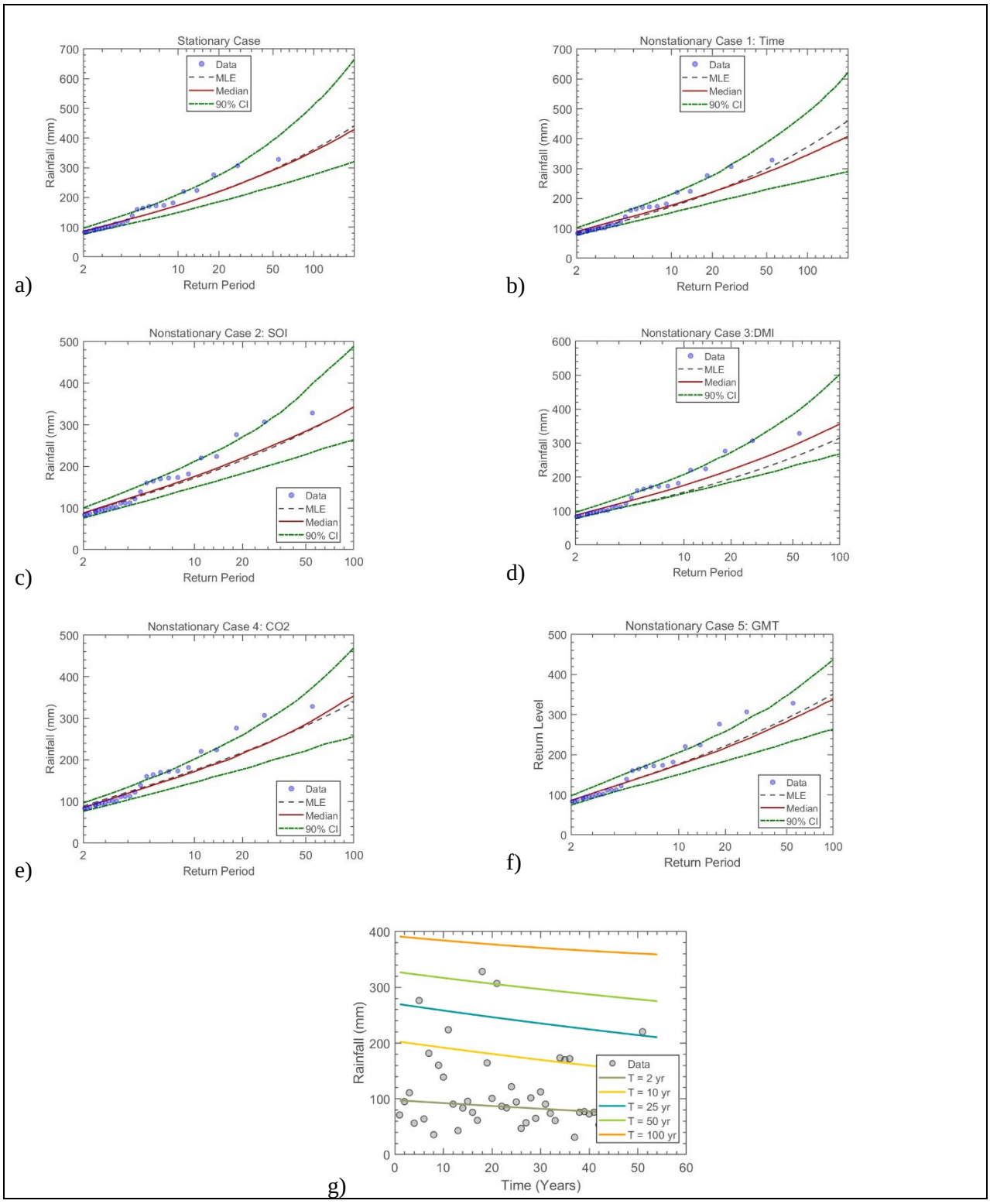

Figure 9.4 The GEV (a) stationary model, (b) non-stationary model considering time as a covariate, (c) non-stationary model considering SOI as a covariate, (d) non-stationary model considering DMI as a covariate, (e) non-stationary model considering CO_2 as a covariate, (f) non-stationary model considering GMT as a covariate and (g) effective return period as a function of time for Station 9: Mtubatuba – Riverview Sugar Mill

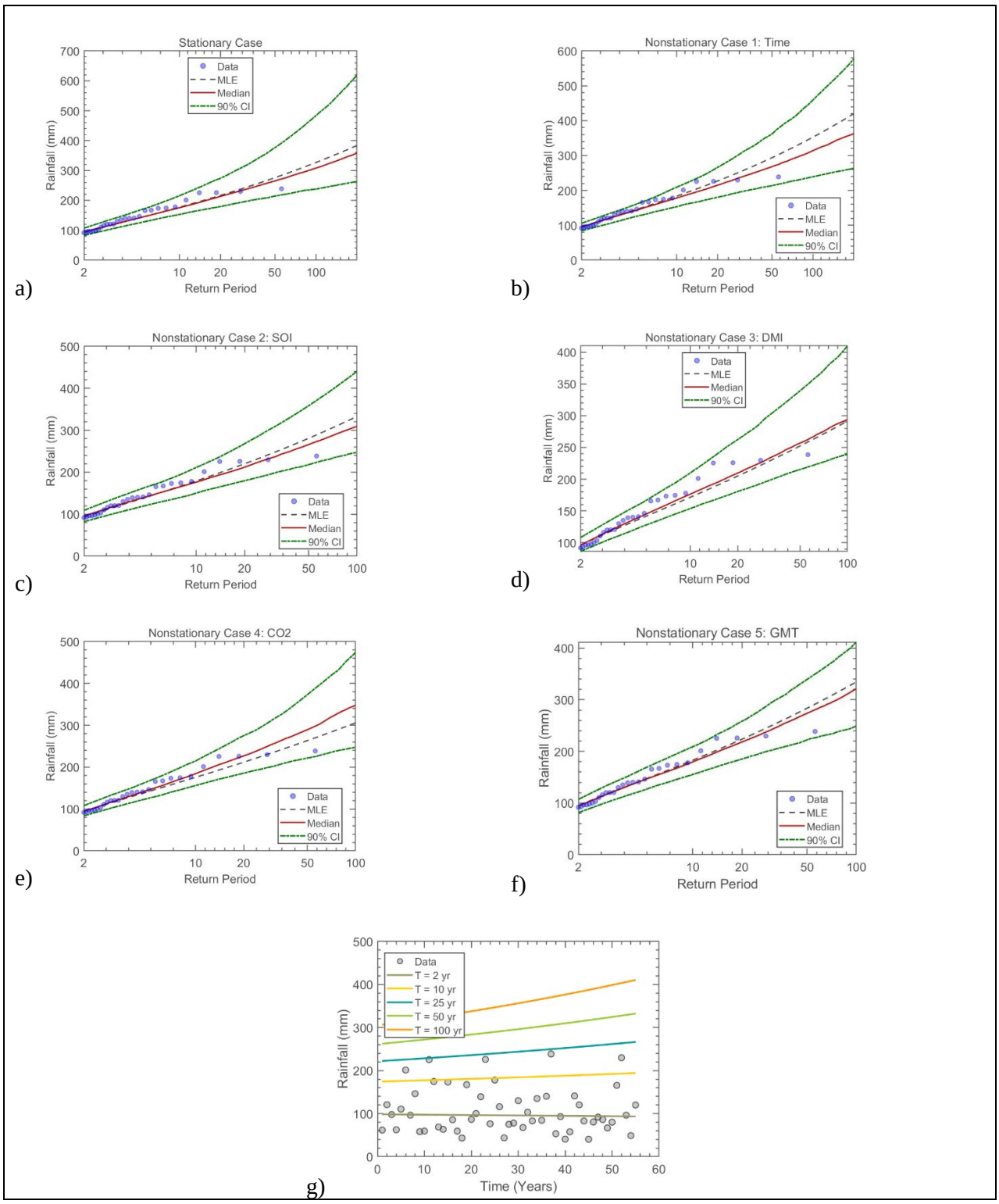

Figure 9.5 The GEV (a) stationary model, (b) non-stationary model considering time as a covariate, (c) non-stationary model considering SOI as a covariate, (d) non-stationary model considering DMI as a covariate, (e) non-stationary model considering CO_2 as a covariate, (f) non-stationary model considering GMT as a covariate and (g) effective return period as a function of time for Station 11: Mtunzini – ex SASRI

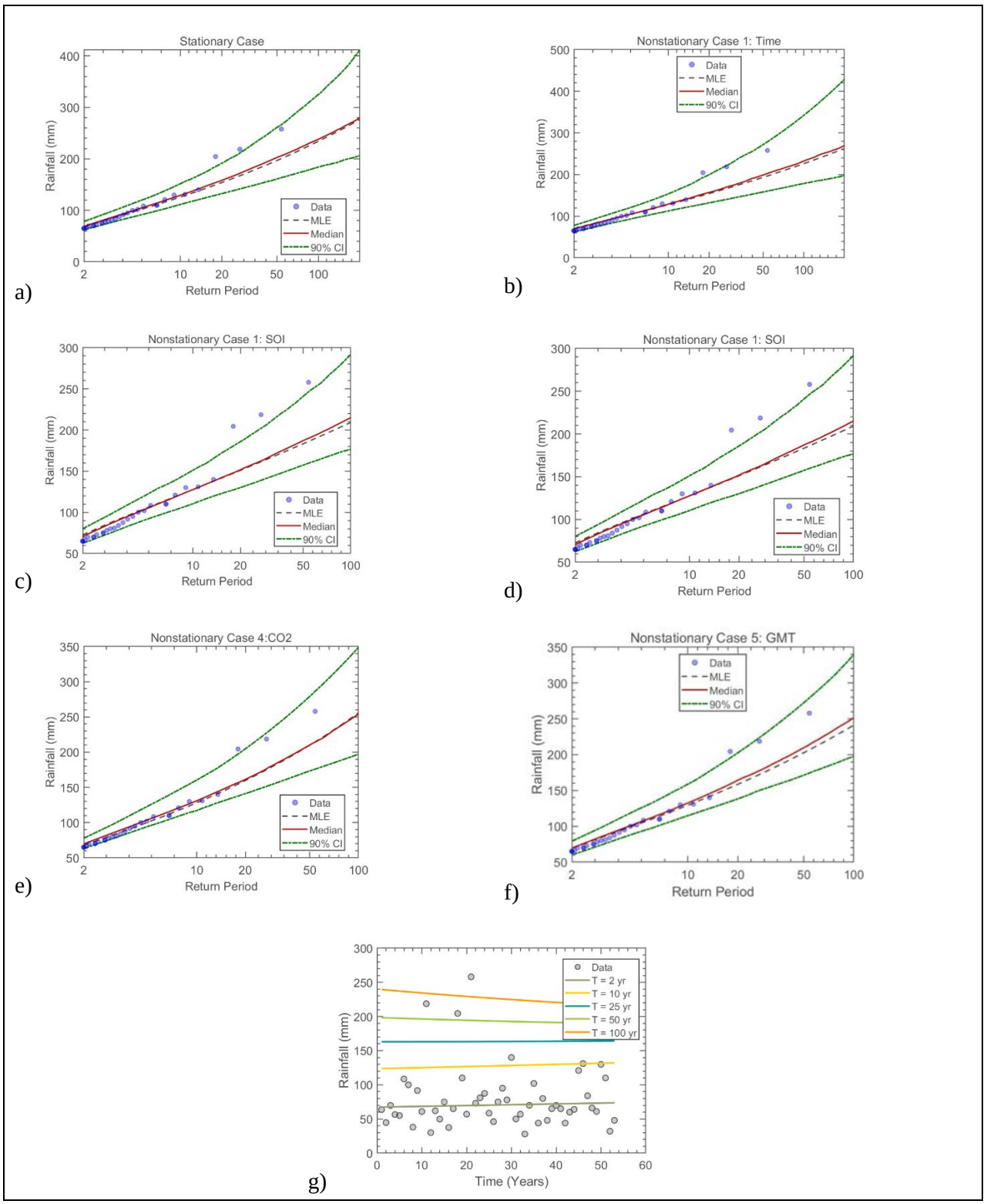

Figure 9.6 The GEV (a) stationary model, (b) non-stationary model considering time as a covariate, (c) non-stationary model considering SOI as a covariate, (d) non-stationary model considering DMI as a covariate, (e) non-stationary model considering CO_2 as a covariate, (f) non-stationary model considering GMT as a covariate and (g) effective return period as a function of time for Station 12: Melmoth – CA Leith & Sons

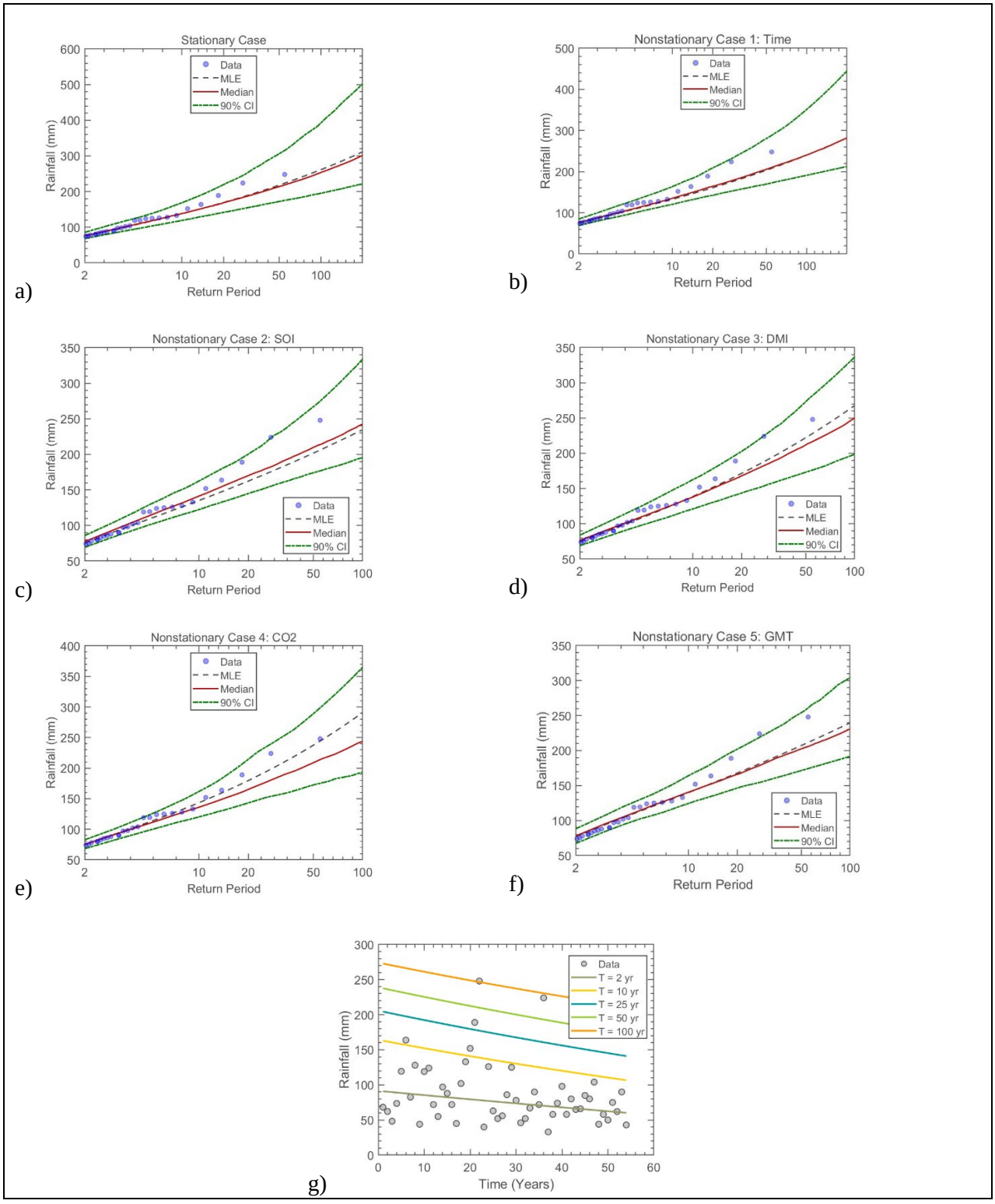

Figure 9.7 The GEV (a) stationary model, (b) non-stationary model considering time as a covariate, (c) non-stationary model considering SOI as a covariate, (d) non-stationary model considering DMI as a covariate, (e) non-stationary model considering CO_2 as a covariate, (f) non-stationary model considering GMT as a covariate and (g) effective return period as a function of time for Station 18: Glendale – Tenrith Farm

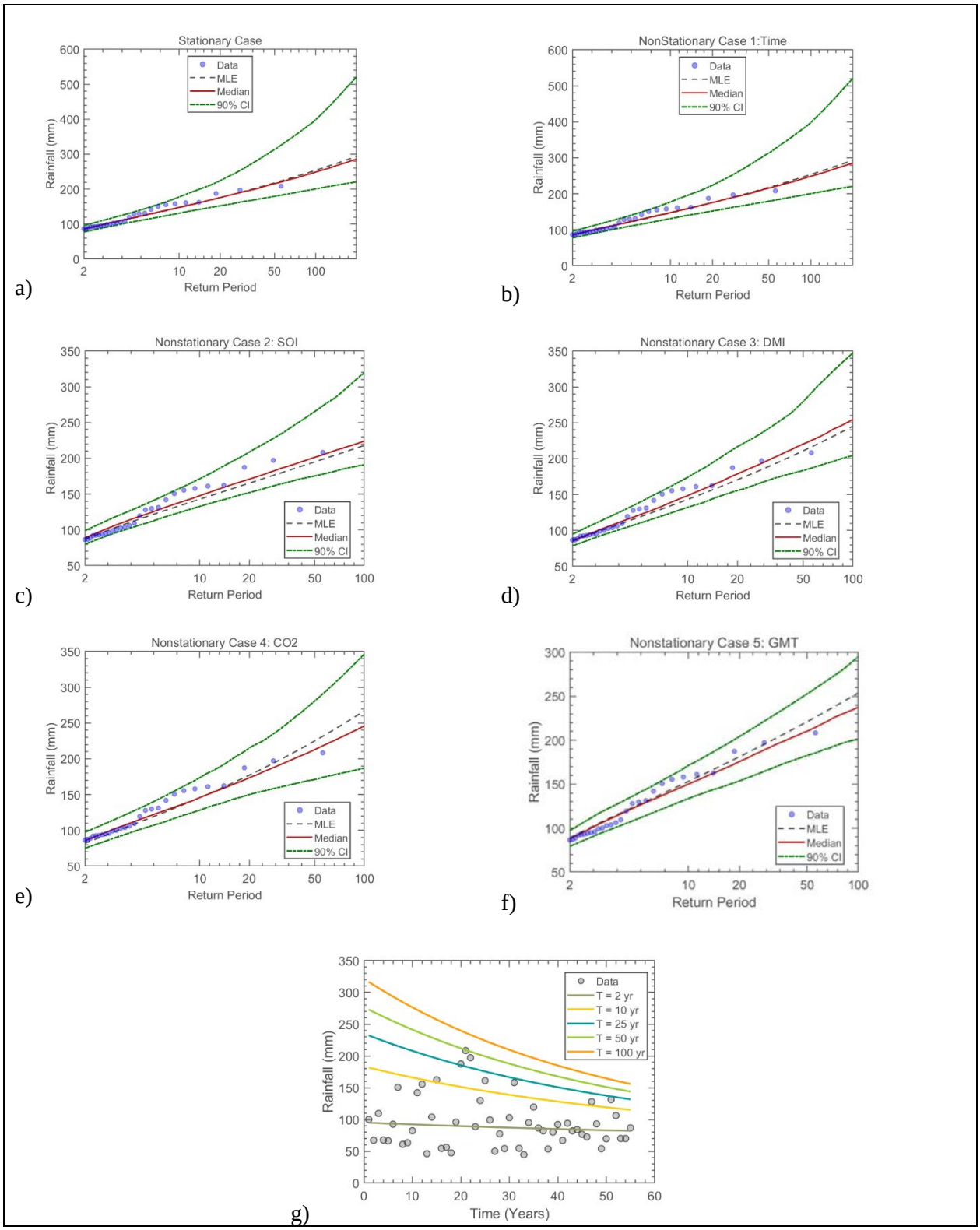

Figure 9.8 The GEV (a) stationary model, (b) non-stationary model considering time as a covariate, (c) non-stationary model considering SOI as a covariate, (d) non-stationary model considering DMI as a covariate, (e) non-stationary model considering CO_2 as a covariate, (f) non-stationary model considering GMT as a covariate and (g) effective return period as a function of time for Station 20: Tongaat – Klipfontein (THS)

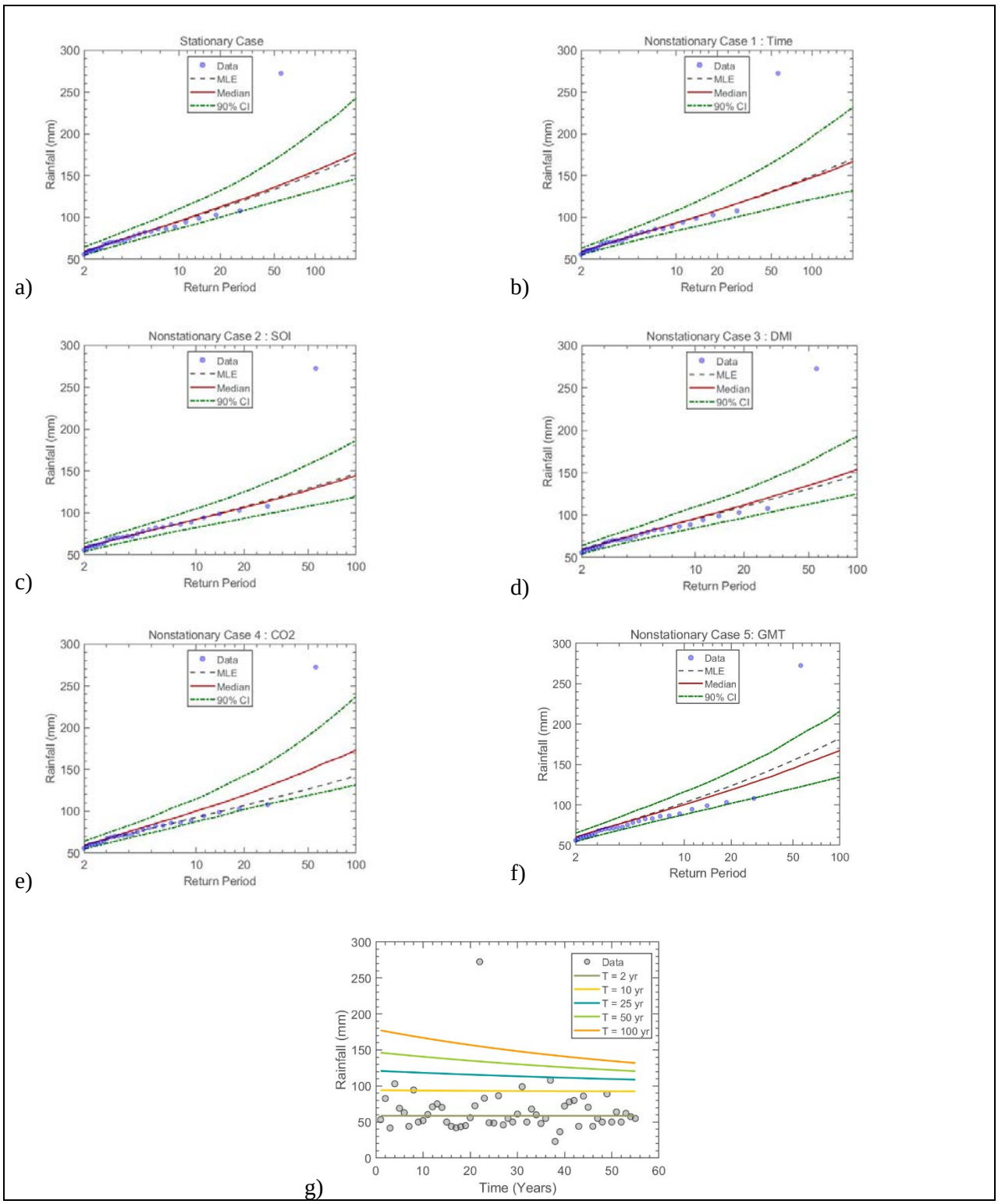

Figure 9.9 The GEV (a) stationary model, (b) non-stationary model considering time as a covariate, (c) non-stationary model considering SOI as a covariate, (d) non-stationary model considering DMI as a covariate, (e) non-stationary model considering CO_2 as a covariate, (f) non-stationary model considering GMT as a covariate and (g) effective return period as a function of time for Station 22: Seven Oaks – Saw Mill

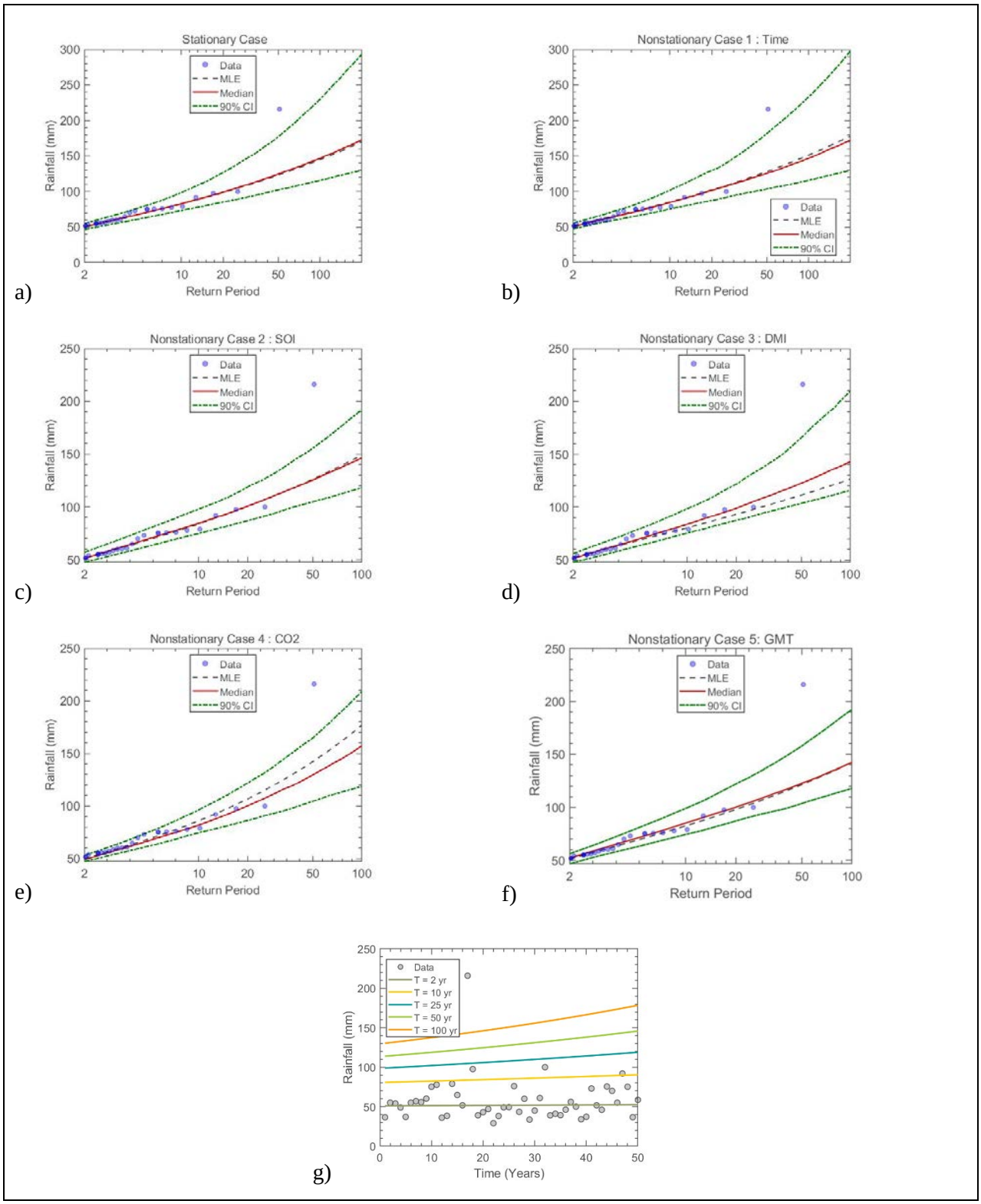

Figure 9.10 The GEV (a) stationary model, (b) non-stationary model considering time as a covariate, (c) non-stationary model considering SOI as a covariate, (d) non-stationary model considering DMI as a covariate, (e) non-stationary model considering CO_2 as a covariate, (f) non-stationary model considering GMT as a covariate and (g) effective return period as a function of time for Station 23: Noodsberg – Illovo Sugar Mill

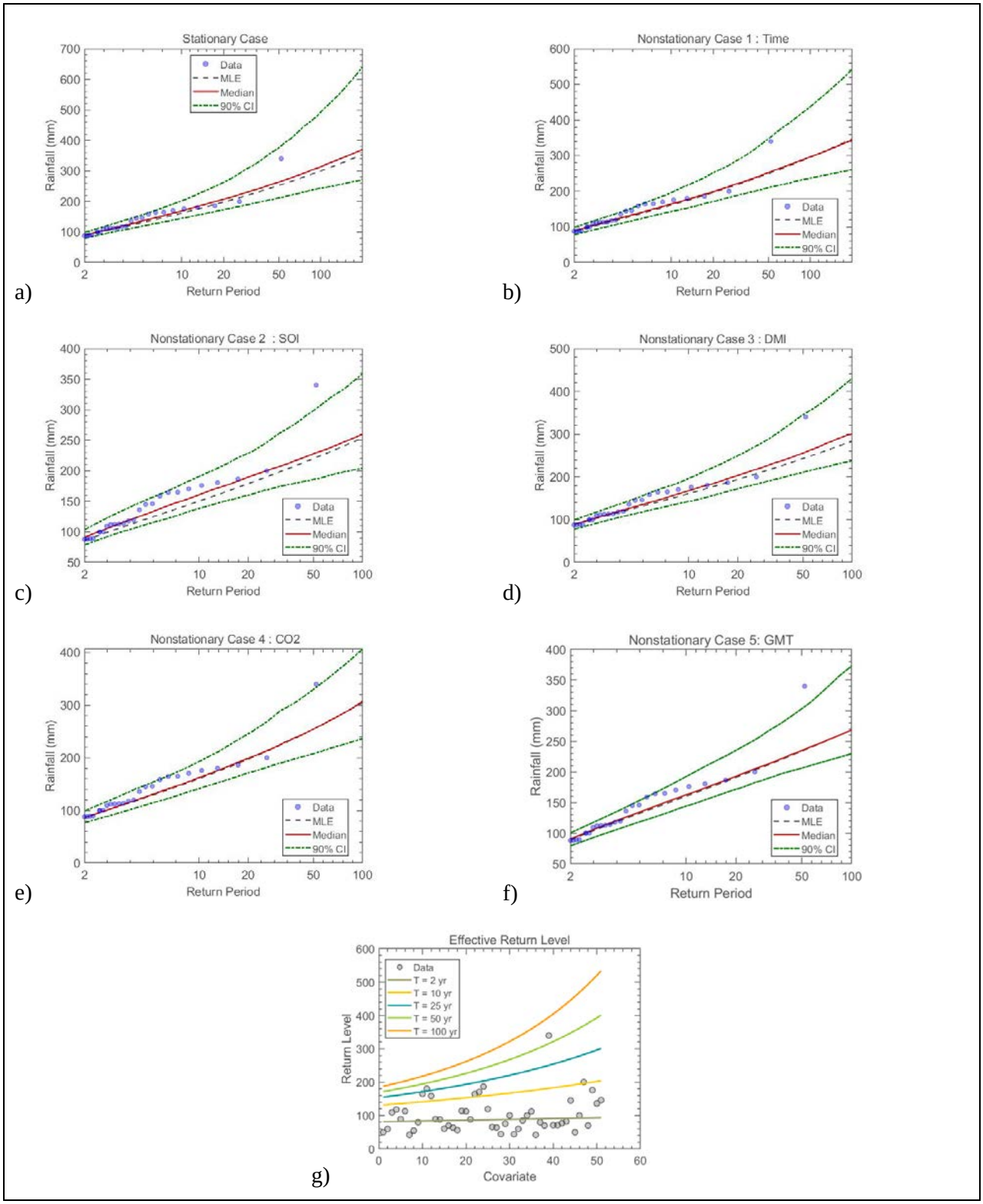

Figure 9.11 The GEV (a) stationary model, (b) non-stationary model considering time as a covariate, (c) non-stationary model considering SOI as a covariate, (d) non-stationary model considering DMI as a covariate, (e) non-stationary model considering CO_2 as a covariate, (f) non-stationary model considering GMT as a covariate and (g) effective return period as a function of time for Station 26: Illovo – Sugar Estate

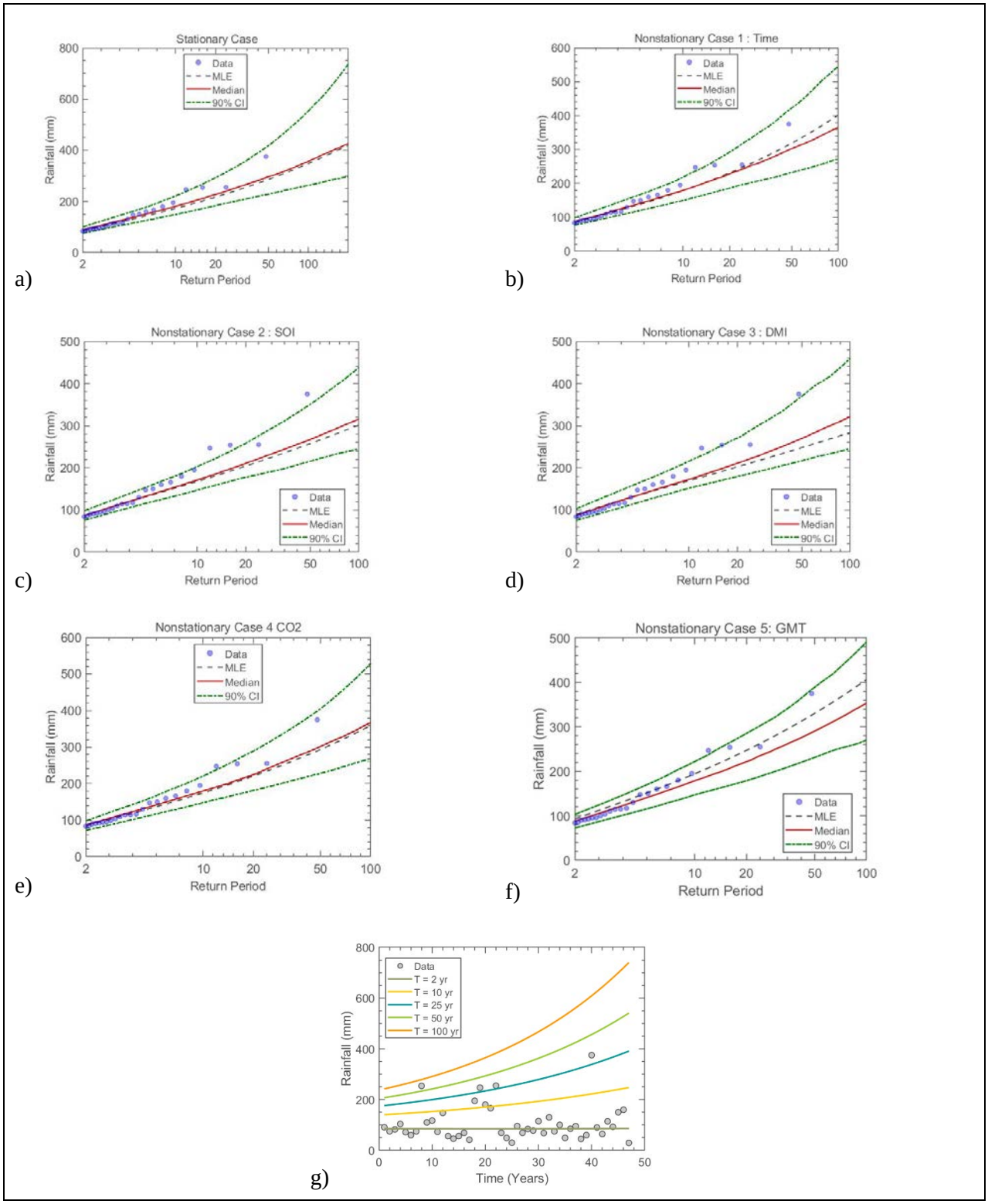

Figure 9.12 The GEV (a) stationary model, (b) non-stationary model considering time as a covariate, (c) non-stationary model considering SOI as a covariate, (d) non-stationary model considering DMI as a covariate, (e) non-stationary model considering CO_2 as a covariate, (f) non-stationary model considering GMT as a covariate and (g) effective return period as a function of time for Station 27: Vulamehlo – Esperanza

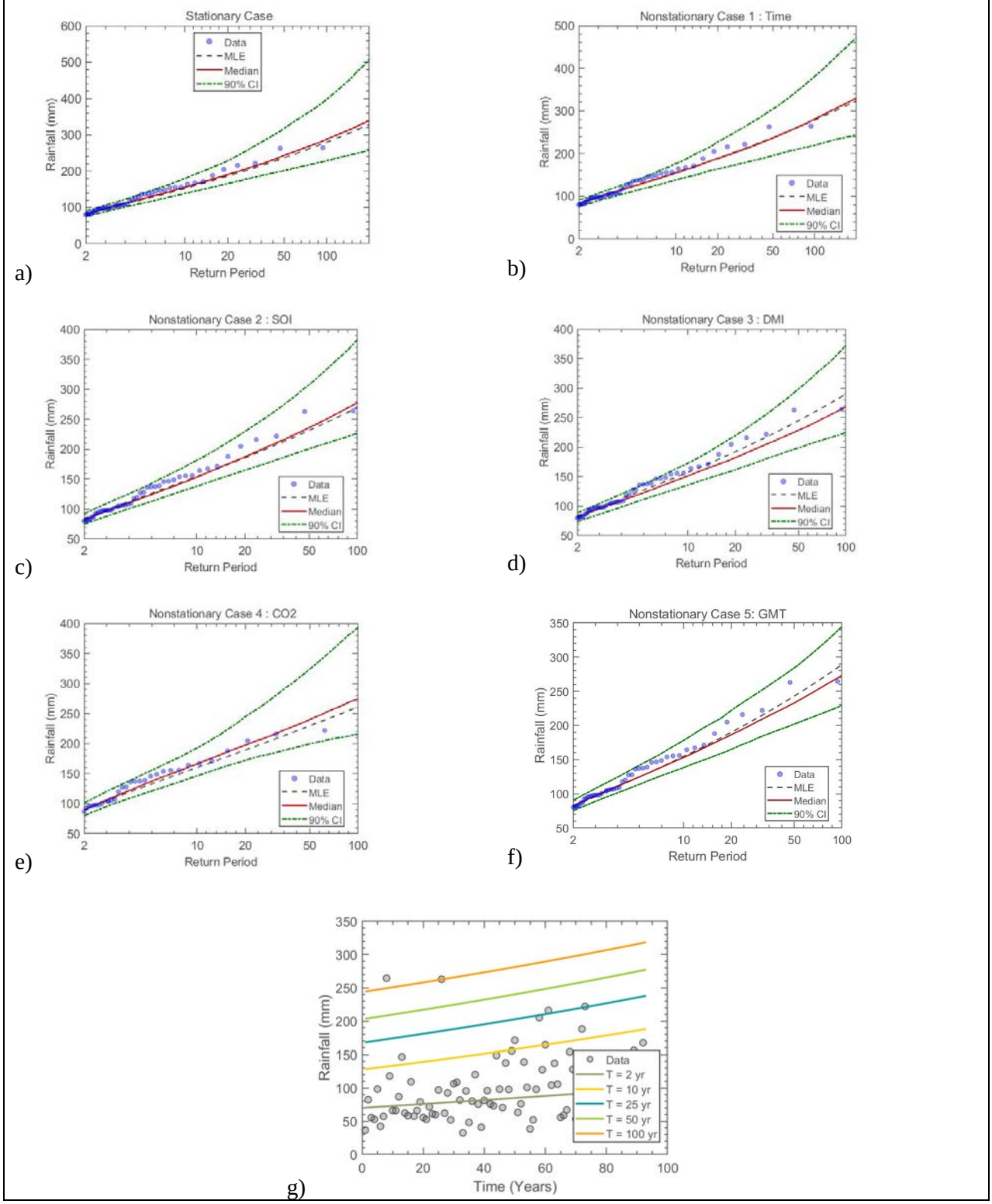

Figure 9.13 The GEV (a) stationary model, (b) non-stationary model considering time as a covariate, (c) non-stationary model considering SOI as a covariate, (d) non-stationary model considering DMI as a covariate, (e) non-stationary model considering CO_2 as a covariate, (f) non-stationary model considering GMT as a covariate and (g) effective return period as a function of time for Station 29: Mt Edgecombe – SASRI

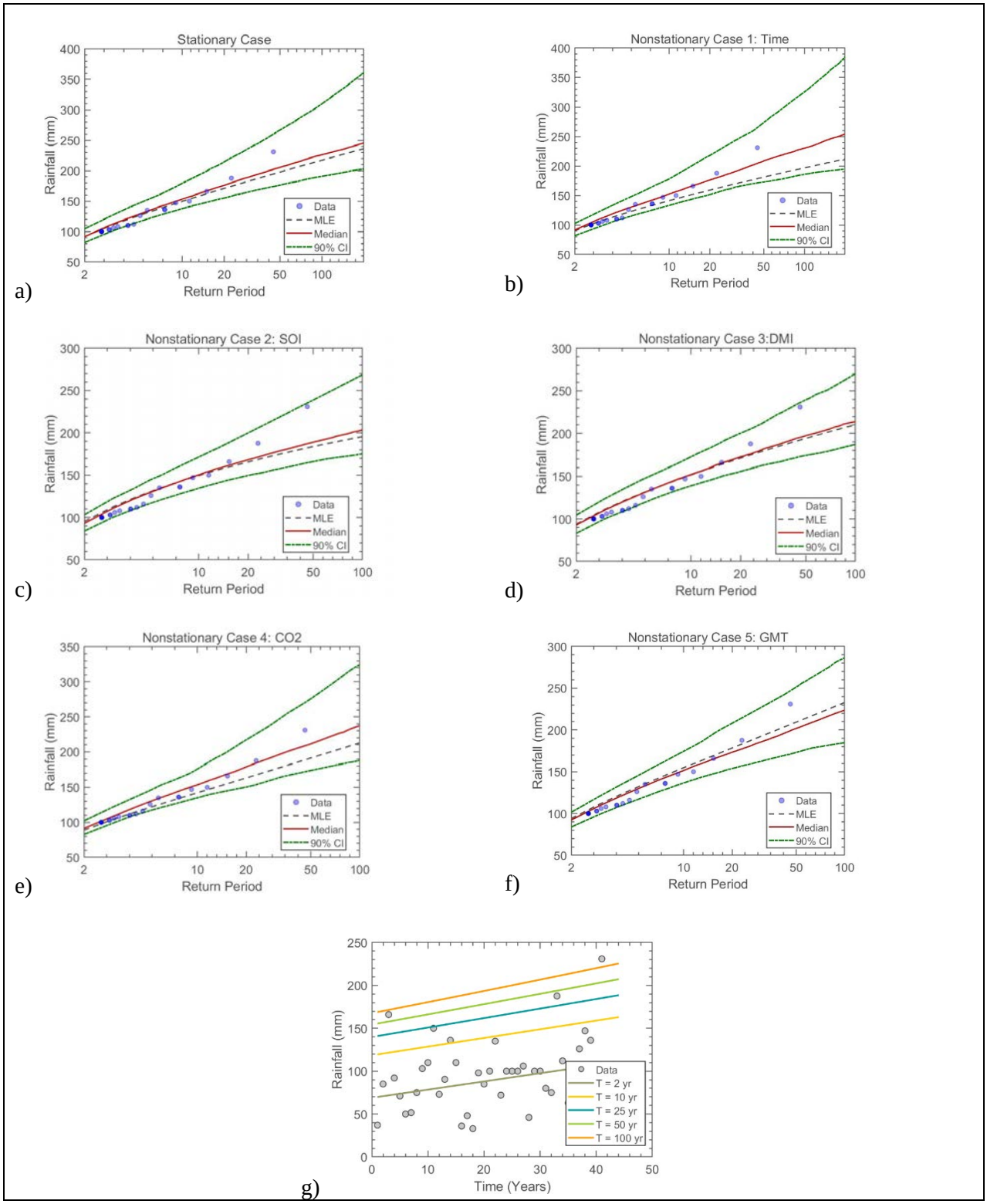

Figure 9.14 The GEV (a) stationary model, (b) non-stationary model considering time as a covariate, (c) non-stationary model considering SOI as a covariate, (d) non-stationary model considering DMI as a covariate, (e) non-stationary model considering CO_2 as a covariate, (f) non-stationary model considering GMT as a covariate and (g) effective return period as a function of time for Station 38: Sezela – Illovo Sugar Estate

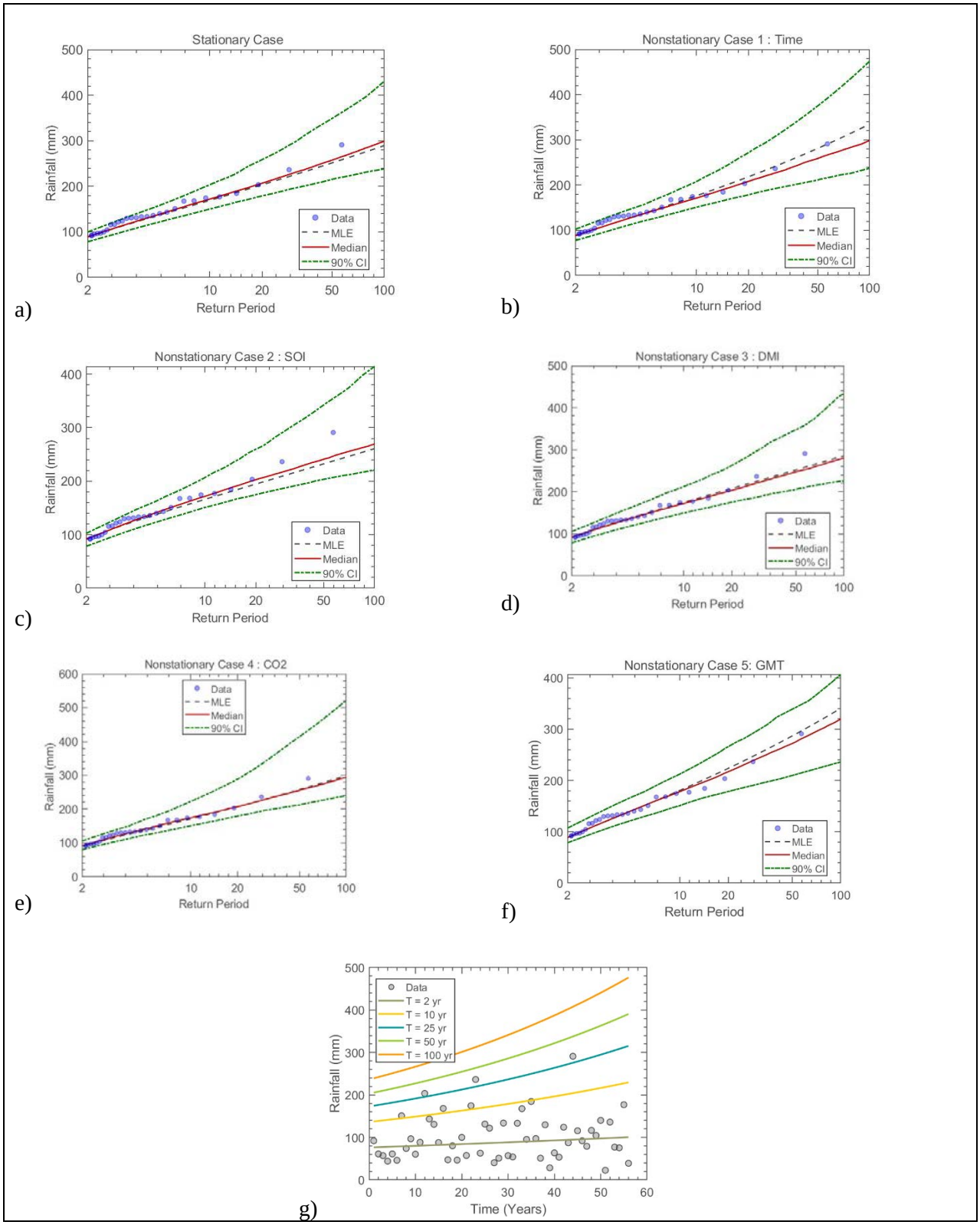

Figure 9.15 The GEV (a) stationary model, (b) non-stationary model considering time as a covariate, (c) non-stationary model considering SOI as a covariate, (d) non-stationary model considering DMI as a covariate, (e) non-stationary model considering CO_2 as a covariate, (f) non-stationary model considering GMT as a covariate and (g) effective return period as a function of time for Station 105: Oribi Flats – Minnehaha Farm

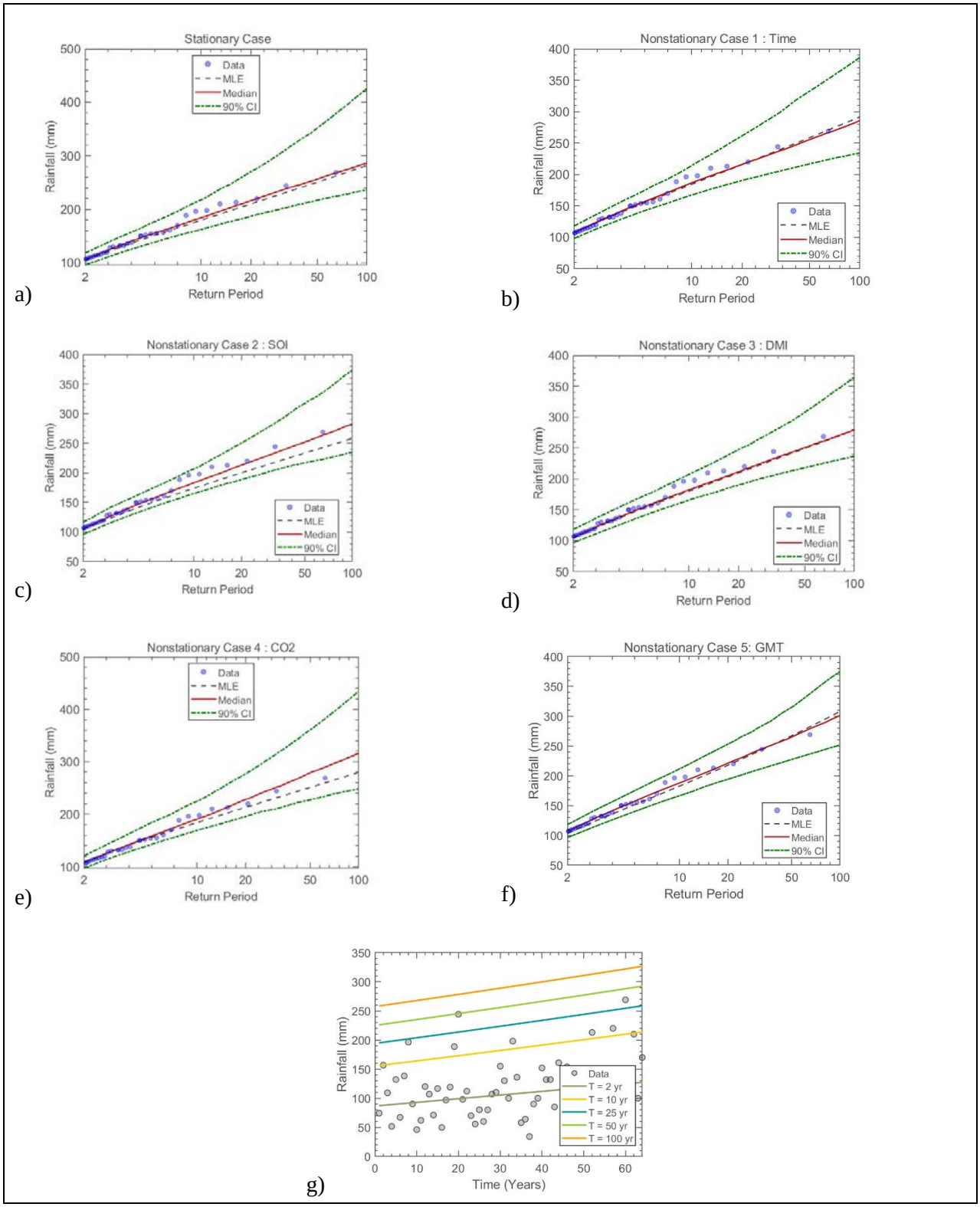

Figure 9.16 The GEV (a) stationary model, (b) non-stationary model considering time as a covariate, (c) non-stationary model considering SOI as a covariate, (d) non-stationary model considering DMI as a covariate, (e) non-stationary model considering CO_2 as a covariate, (f) non-stationary model considering GMT as a covariate and (g) effective return period as a function of time for Station 110: Renishaw – Crooks Bros Estate

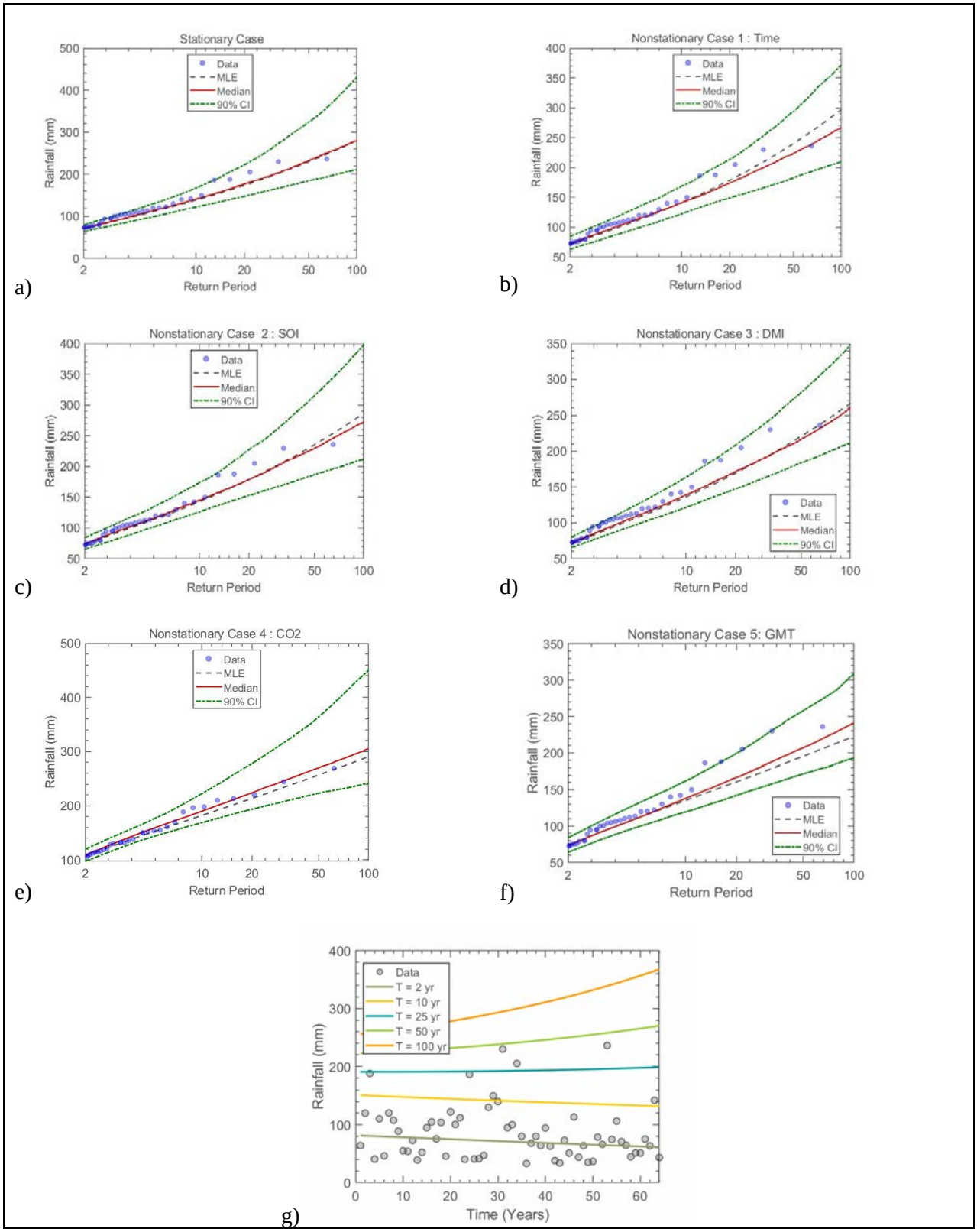

Figure 9.17 The GEV (a) stationary model, (b) non-stationary model considering time as a covariate, (c) non-stationary model considering SOI as a covariate, (d) non-stationary model considering DMI as a covariate, (e) non-stationary model considering CO_2 as a covariate, (f) non-stationary model considering GMT as a covariate and (g) effective return period as a function of time for Station 111: Powerscourt – Roseleigh Estate

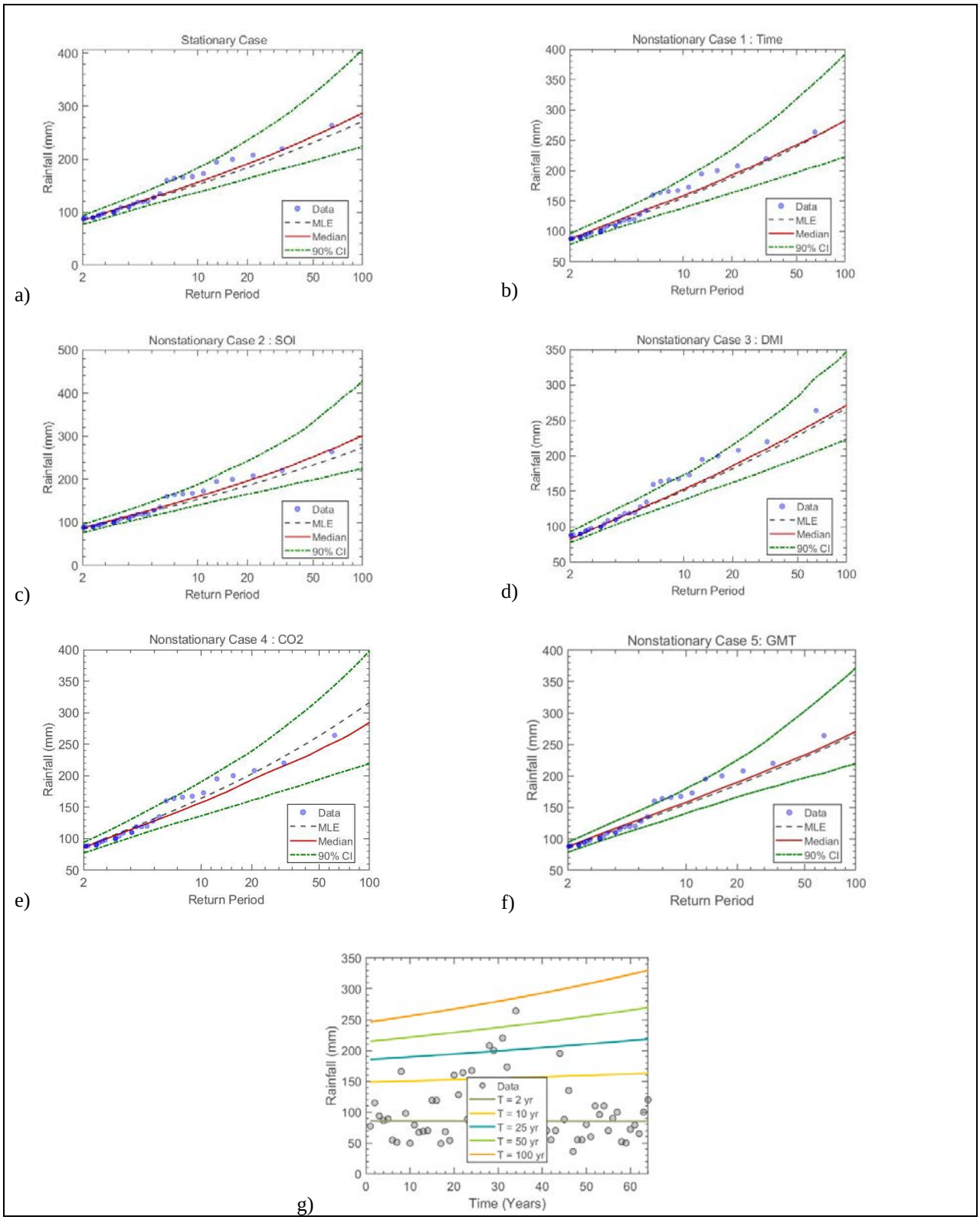

Figure 9.18 The GEV (a) stationary model, (b) non-stationary model considering time as a covariate, (c) non-stationary model considering SOI as a covariate, (d) non-stationary model considering DMI as a covariate, (e) non-stationary model considering CO_2 as a covariate, (f) non-stationary model considering GMT as a covariate and (g) effective return period as a function of time for Station 114: Inanda – Farm

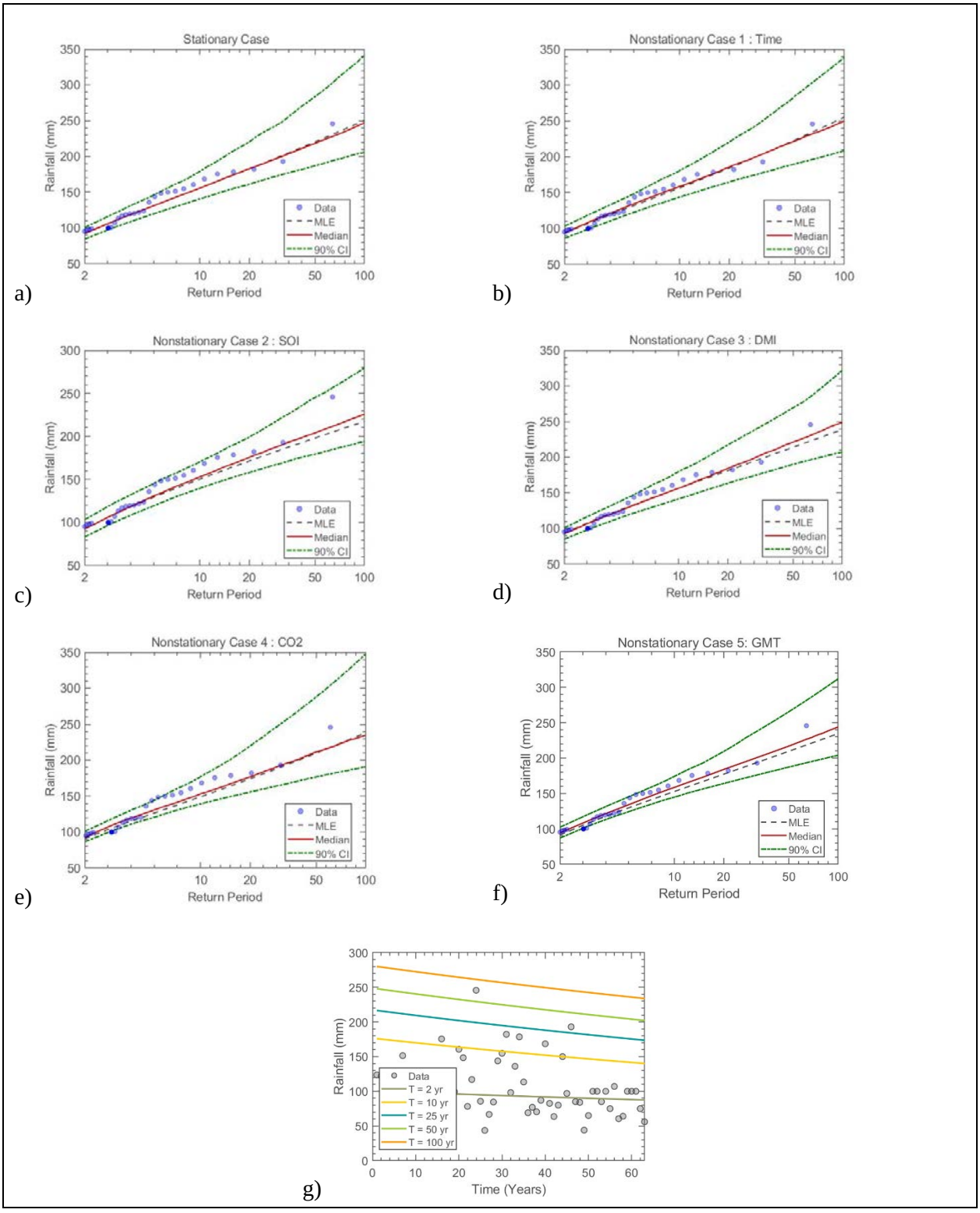

Figure 9.19 The GEV (a) stationary model, (b) non-stationary model considering time as a covariate, (c) non-stationary model considering SOI as a covariate, (d) non-stationary model considering DMI as a covariate, (e) non-stationary model considering CO_2 as a covariate, (f) non-stationary model considering GMT as a covariate and (g) effective return period as a function of time for Station 120: Inyaninga – THS

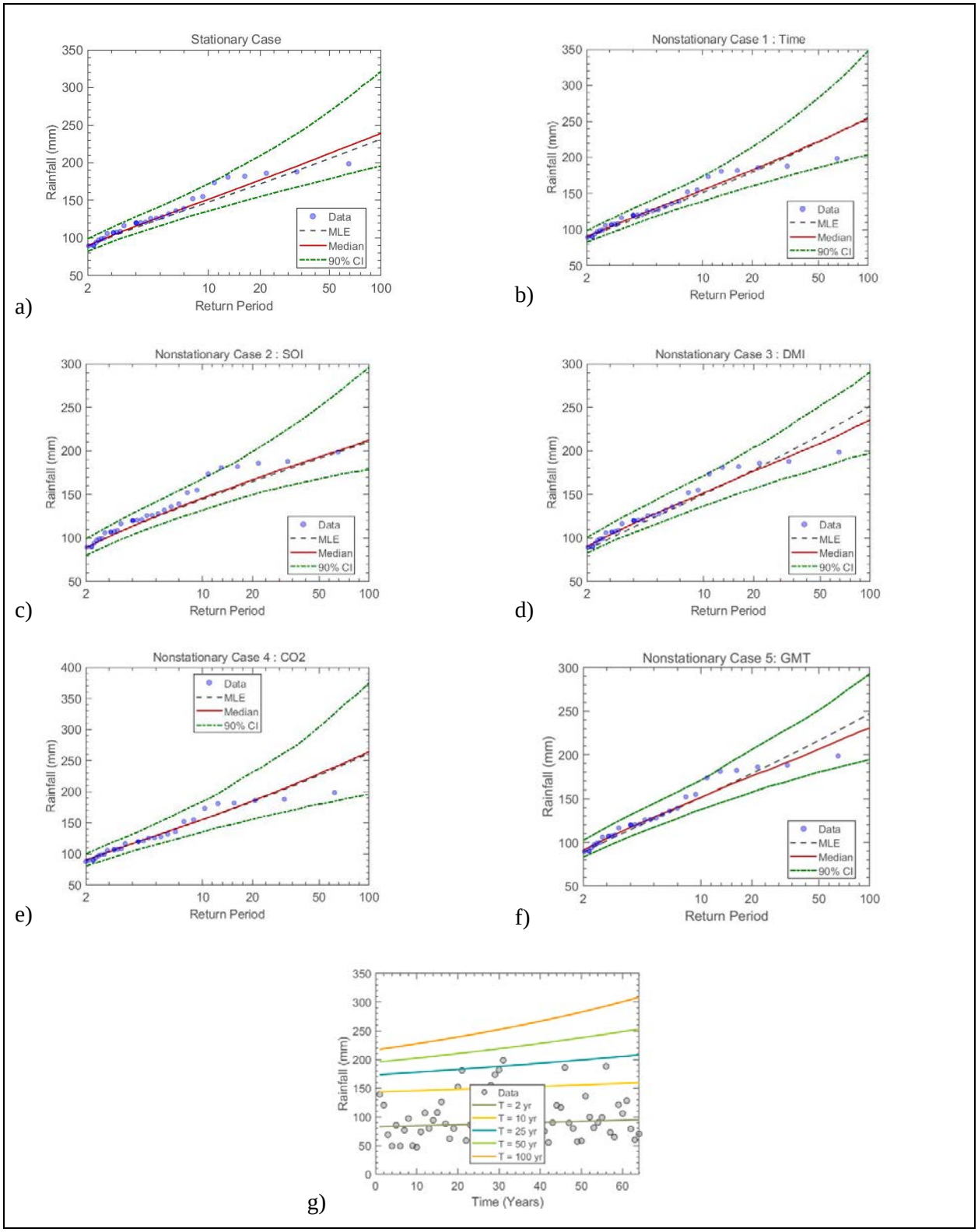

Figure 9.20 The GEV (a) stationary model, (b) non-stationary model considering time as a covariate, (c) non-stationary model considering SOI as a covariate, (d) non-stationary model considering DMI as a covariate, (e) non-stationary model considering CO_2 as a covariate, (f) non-stationary model considering GMT as a covariate and (g) effective return period as a function of time for Station 123: Maidstone – Sugar Mill (THS)

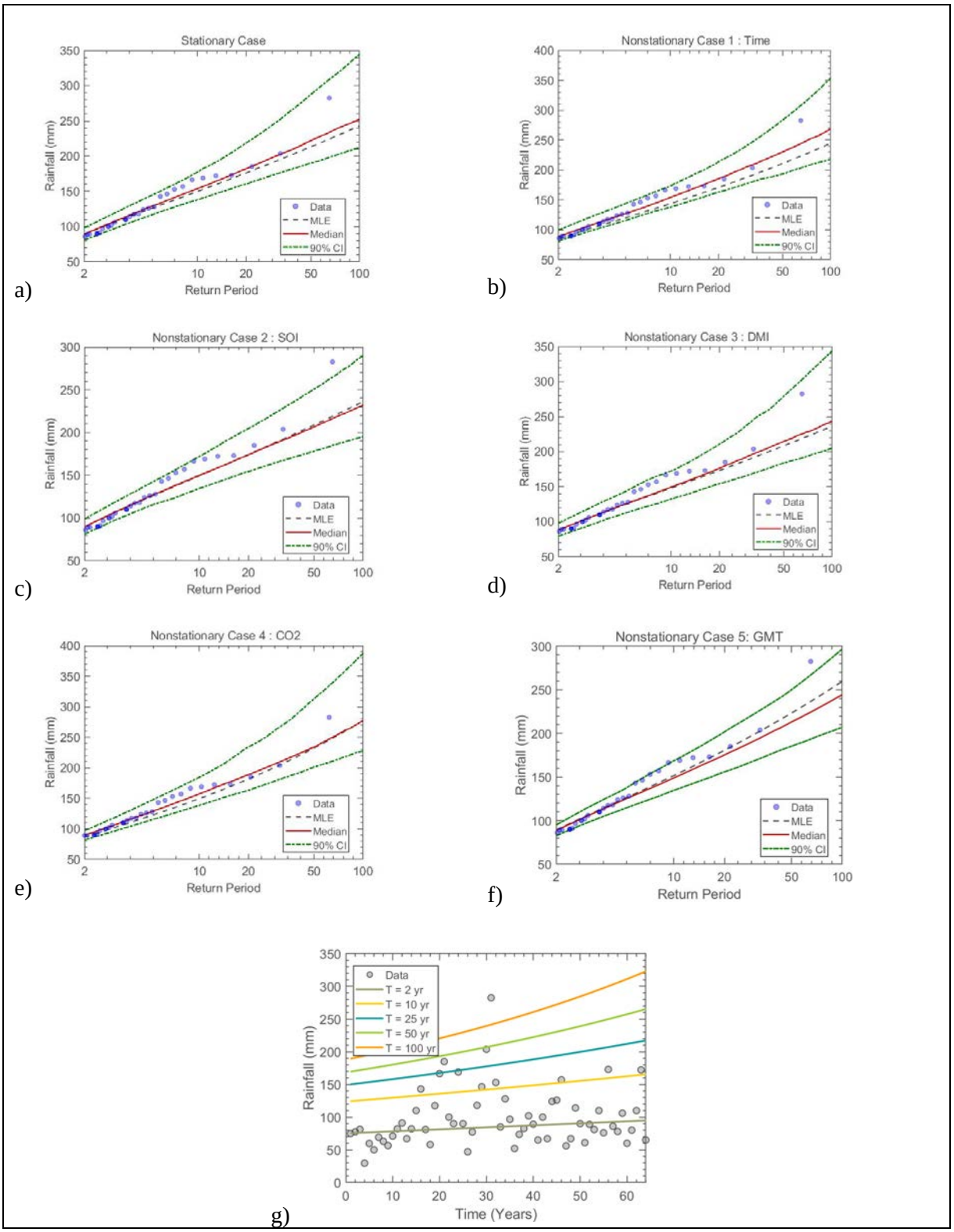

Figure 9.21 The GEV (a) stationary model, (b) non-stationary model considering time as a covariate, (c) non-stationary model considering SOI as a covariate, (d) non-stationary model considering DMI as a covariate, (e) non-stationary model considering CO_2 as a covariate, (f) non-stationary model considering GMT as a covariate and (g) effective return period as a function of time for Station 125: Sinembe – Spreyton Farm

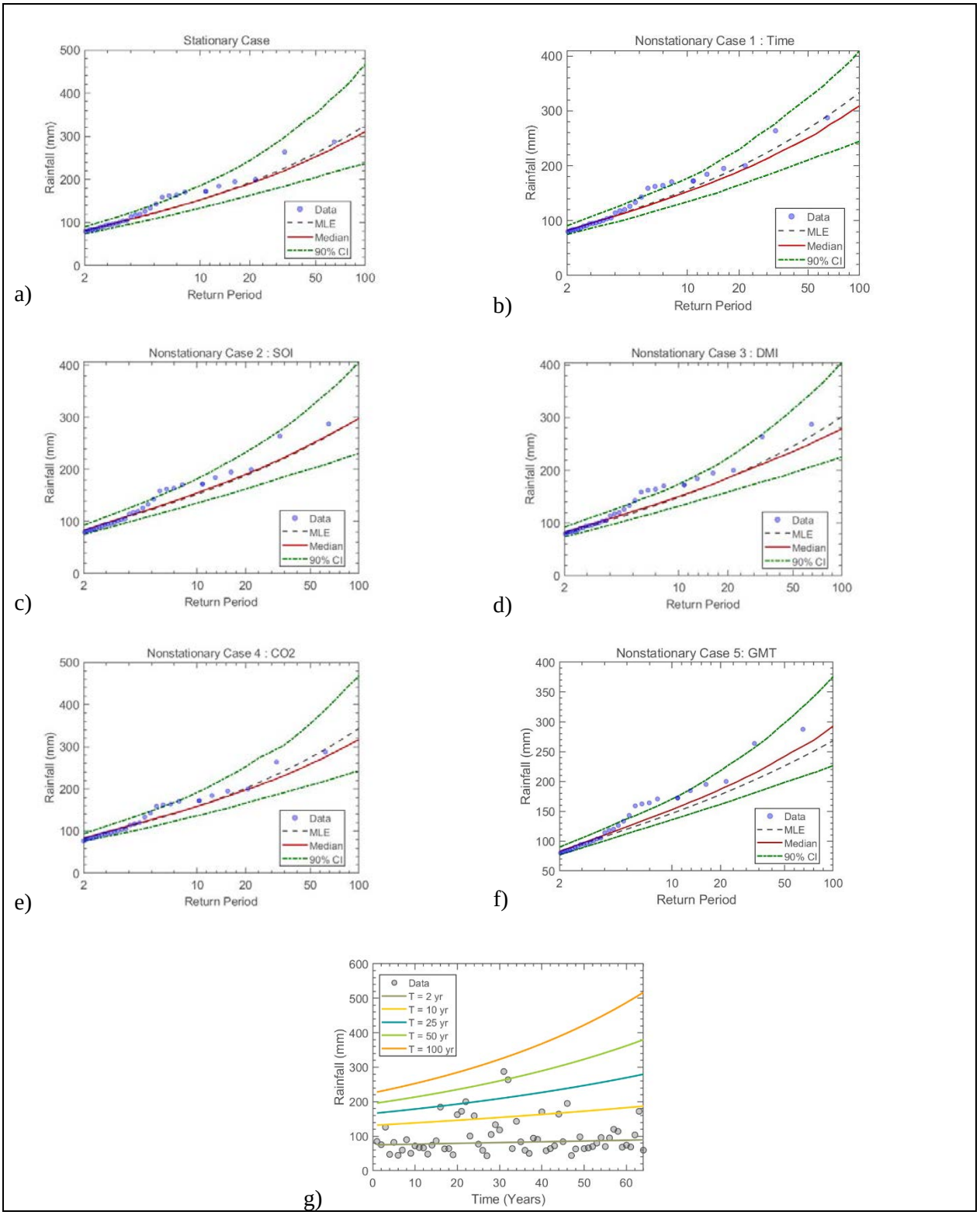

Figure 9.22 The GEV (a) stationary model, (b) non-stationary model considering time as a covariate, (c) non-stationary model considering SOI as a covariate, (d) non-stationary model considering DMI as a covariate, (e) non-stationary model considering CO_2 as a covariate, (f) non-stationary model considering GMT as a covariate and (g) effective return period as a function of time for Station 126: Upper Tongaat – Barwon Farm

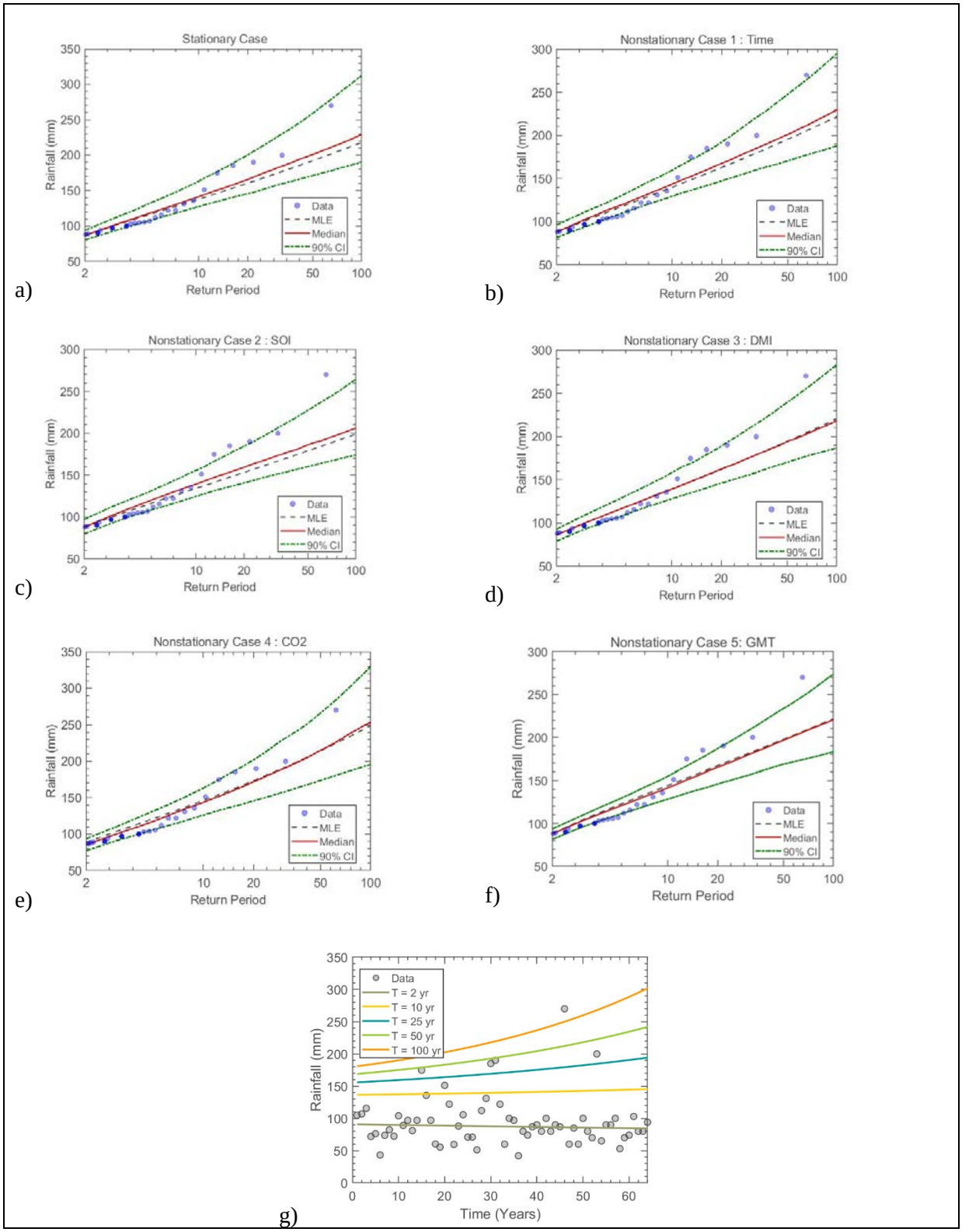

Figure 9.23 The GEV (a) stationary model, (b) non-stationary model considering time as a covariate, (c) non-stationary model considering SOI as a covariate, (d) non-stationary model considering DMI as a covariate, (e) non-stationary model considering CO_2 as a covariate, (f) non-stationary model considering GMT as a covariate and (g) effective return period as a function of time for Station 129: Kearsney – Ocean Lodge

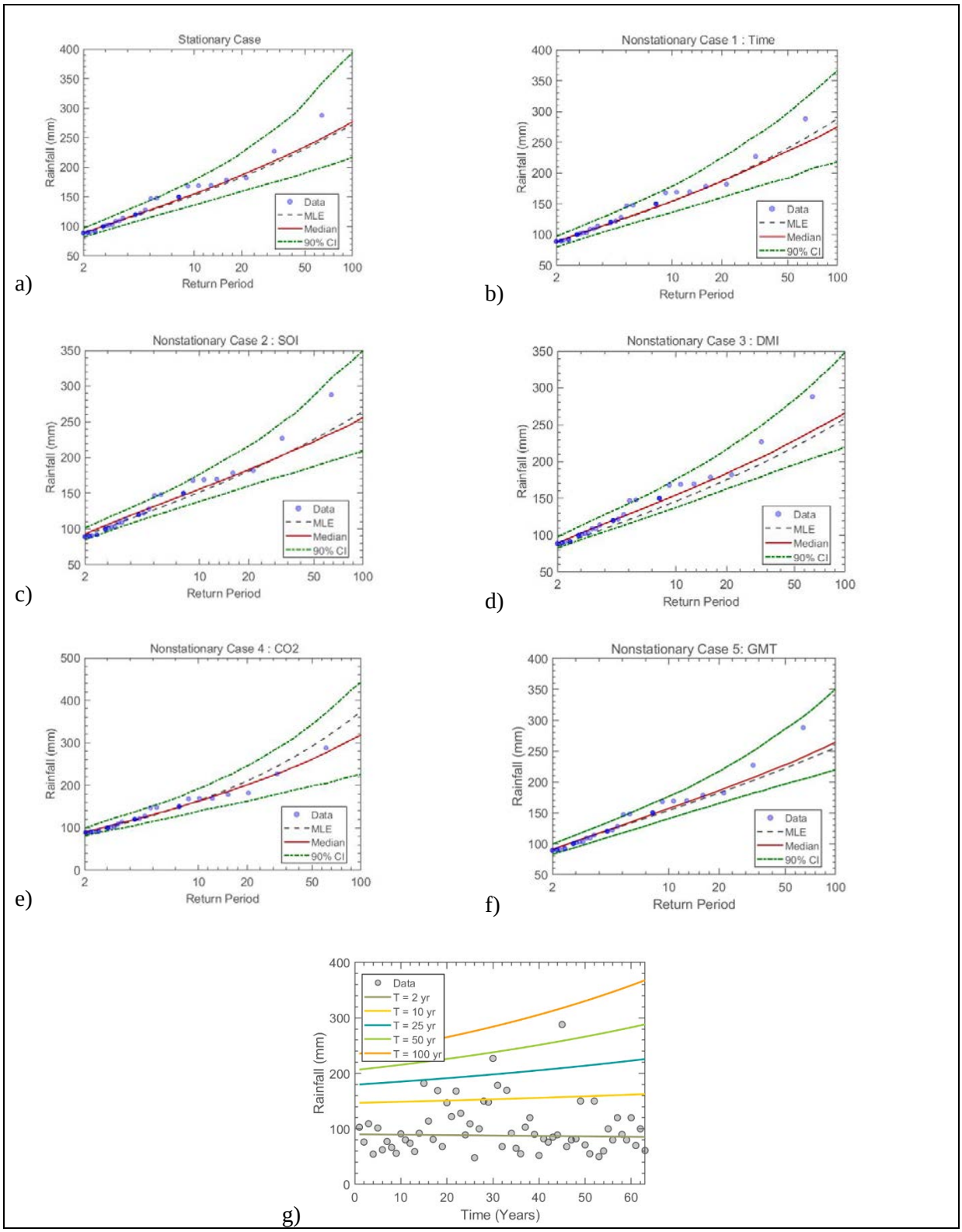

Figure 9.24 The GEV (a) stationary model, (b) non-stationary model considering time as a covariate, (c) non-stationary model considering SOI as a covariate, (d) non-stationary model considering DMI as a covariate, (e) non-stationary model considering CO_2 as a covariate, (f) non-stationary model considering GMT as a covariate and (g) effective return period as a function of time for Station 130: Doornkop – Langespruit Farm

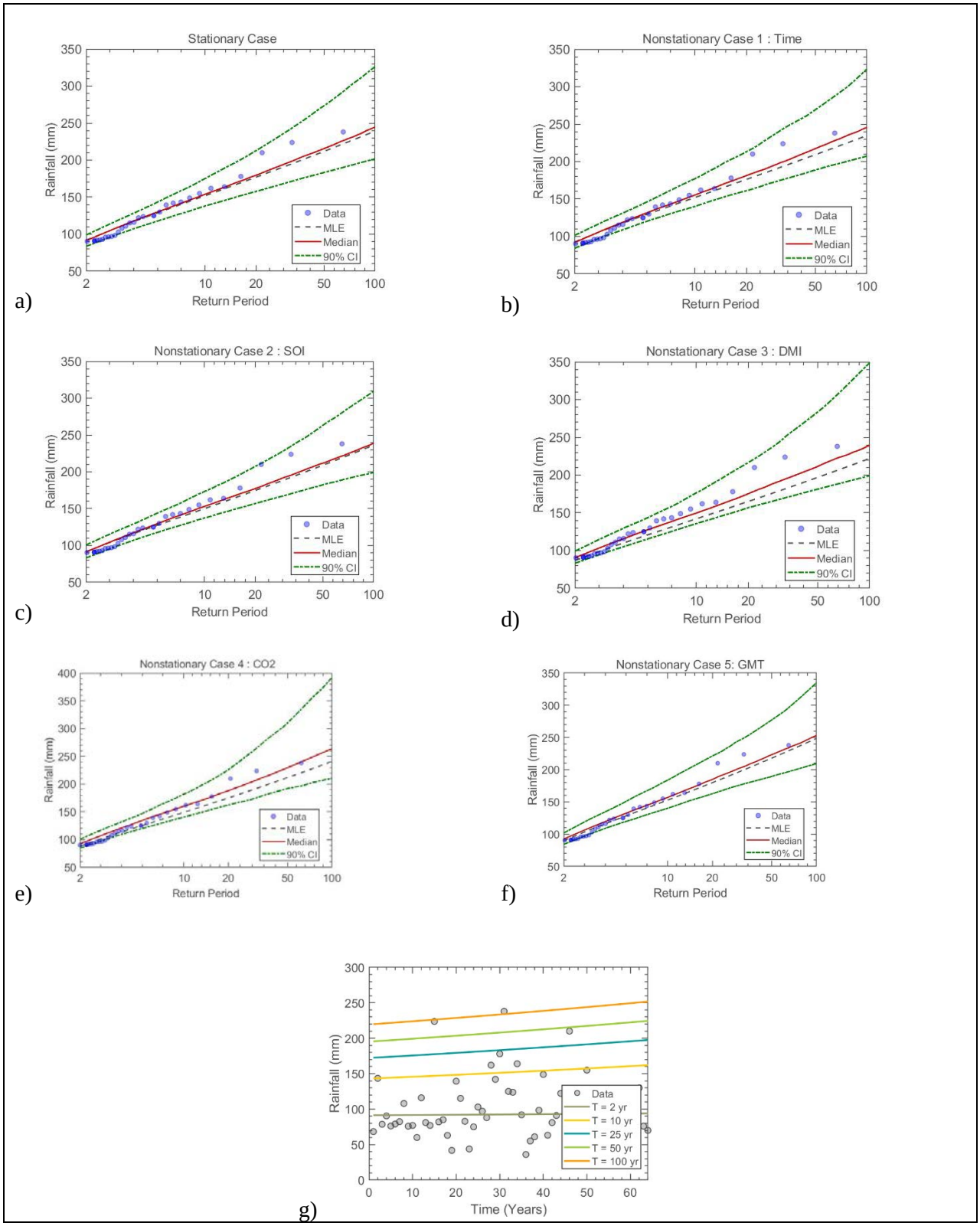

Figure 9.25 The GEV (a) stationary model, (b) non-stationary model considering time as a covariate, (c) non-stationary model considering SOI as a covariate, (d) non-stationary model considering DMI as a covariate, (e) non-stationary model considering CO_2 as a covariate, (f) non-stationary model considering GMT as a covariate and (g) effective return period as a function of time for Station 131: Darnall – Sugar Mill (THS)

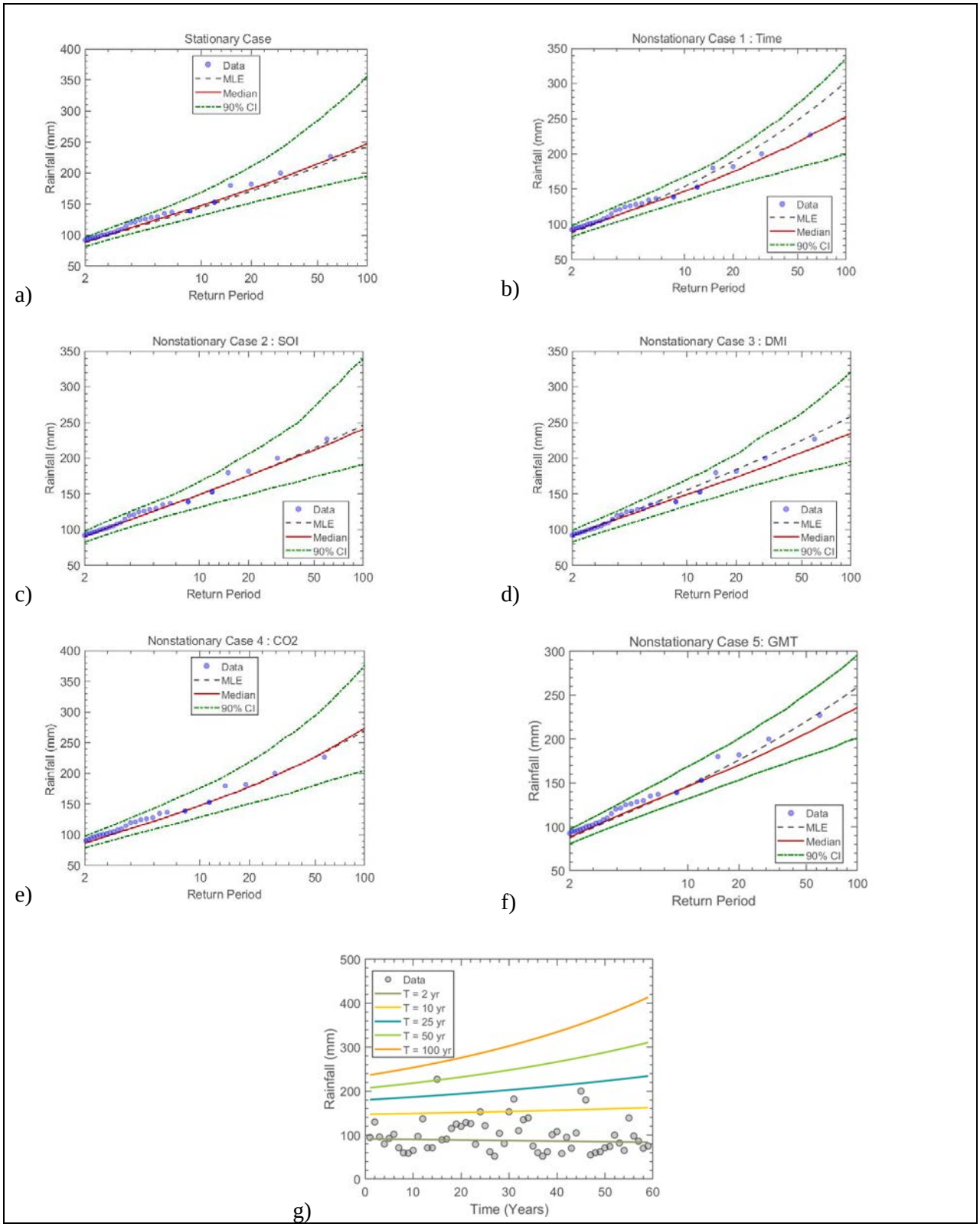

Figure 9.26 The GEV (a) stationary model, (b) non-stationary model considering time as a covariate, (c) non-stationary model considering SOI as a covariate, (d) non-stationary model considering DMI as a covariate, (e) non-stationary model considering CO_2 as a covariate, (f) non-stationary model considering GMT as a covariate and (g) effective return period as a function of time for Station 132: Tugela Mouth – Wetherly Estate

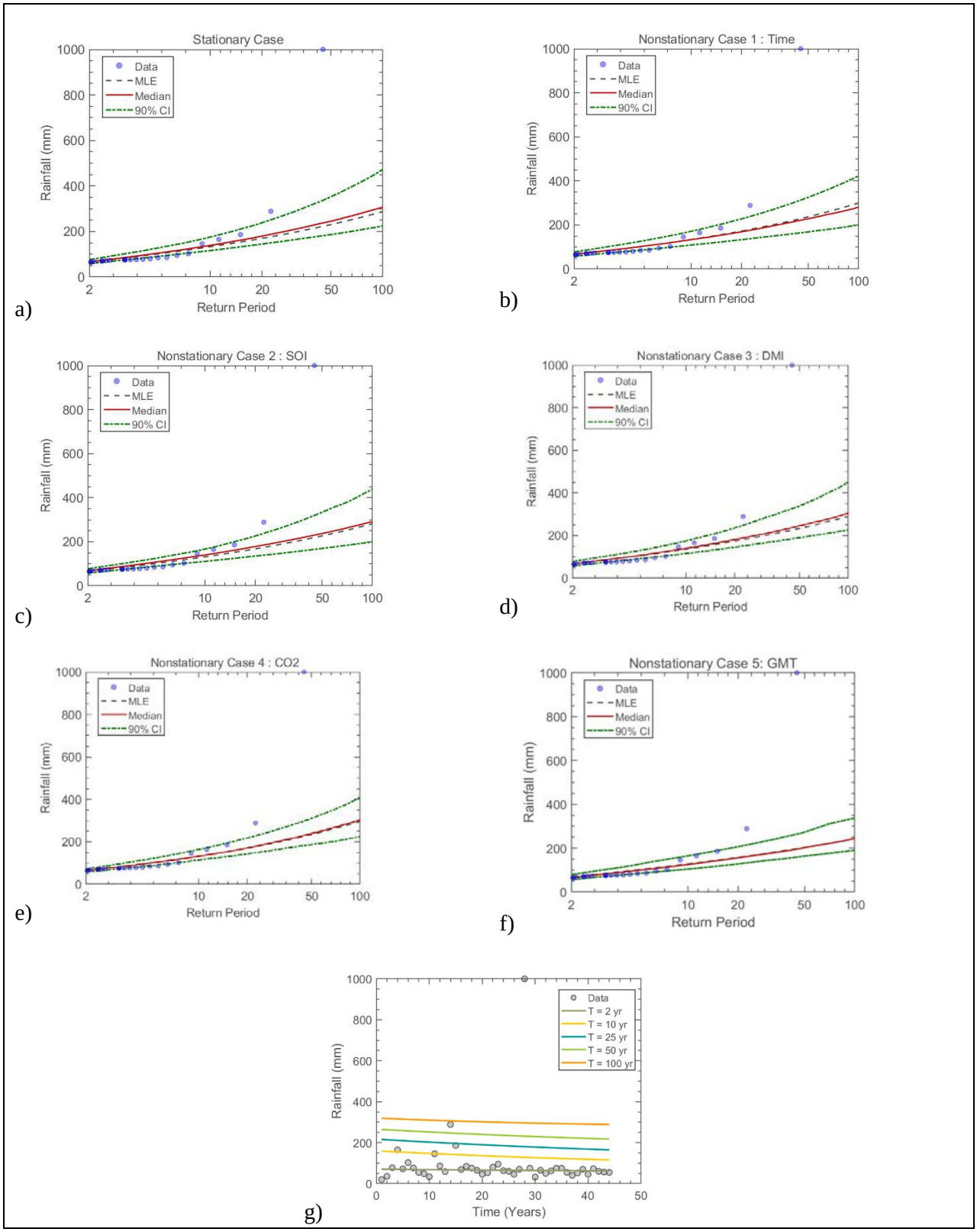

Figure 9.27 The GEV (a) stationary model, (b) non-stationary model considering time as a covariate, (c) non-stationary model considering SOI as a covariate, (d) non-stationary model considering DMI as a covariate, (e) non-stationary model considering CO_2 as a covariate, (f) non-stationary model considering GMT as a covariate and (g) effective return period as a function of time for Station 136: Glenside – Misty Krantz Estate

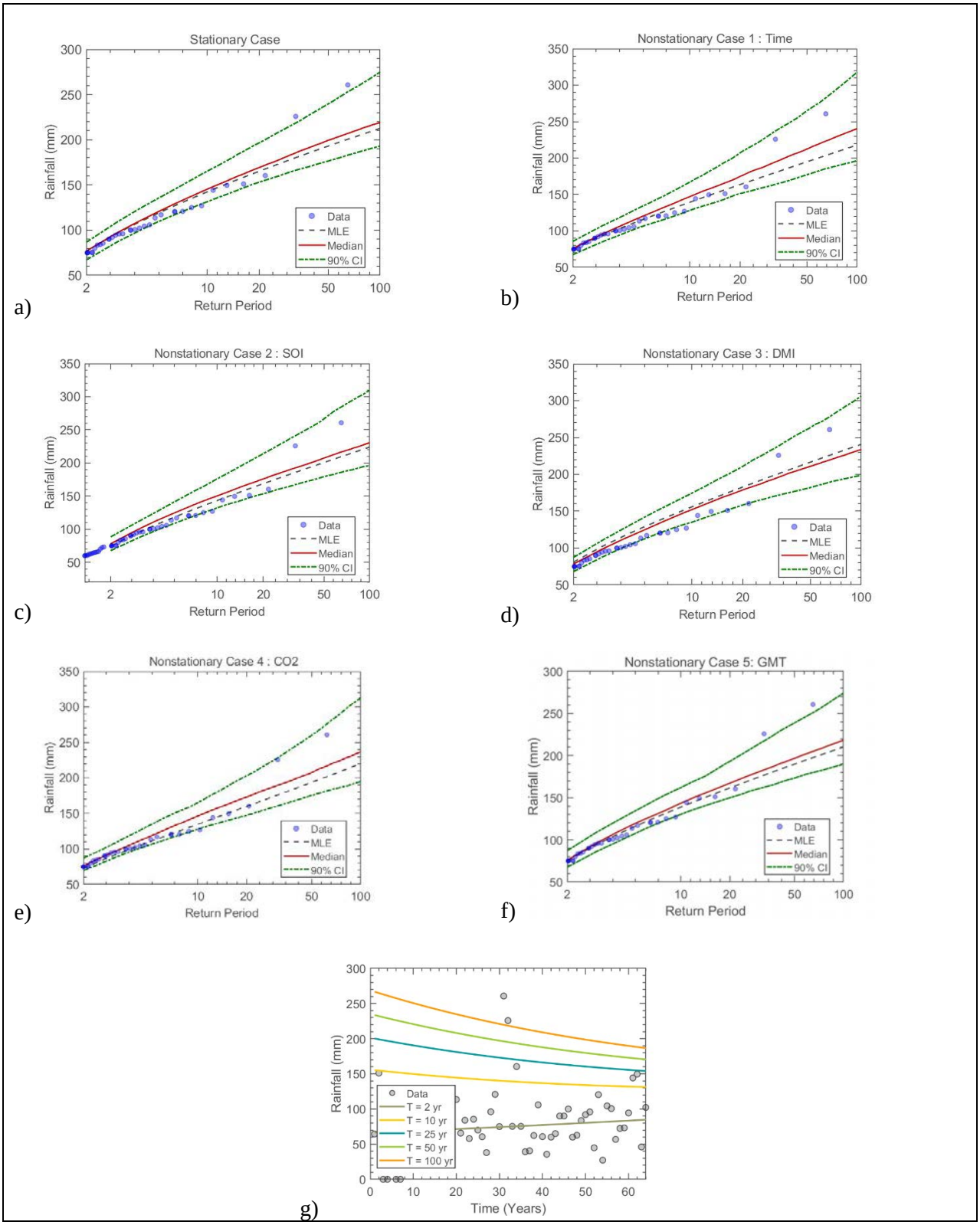

Figure 9.28 The GEV (a) stationary model, (b) non-stationary model considering time as a covariate, (c) non-stationary model considering SOI as a covariate, (d) non-stationary model considering DMI as a covariate, (e) non-stationary model considering CO_2 as a covariate, (f) non-stationary model considering GMT as a covariate and (g) effective return period as a function of time for Station 138: Mandini – SAWS

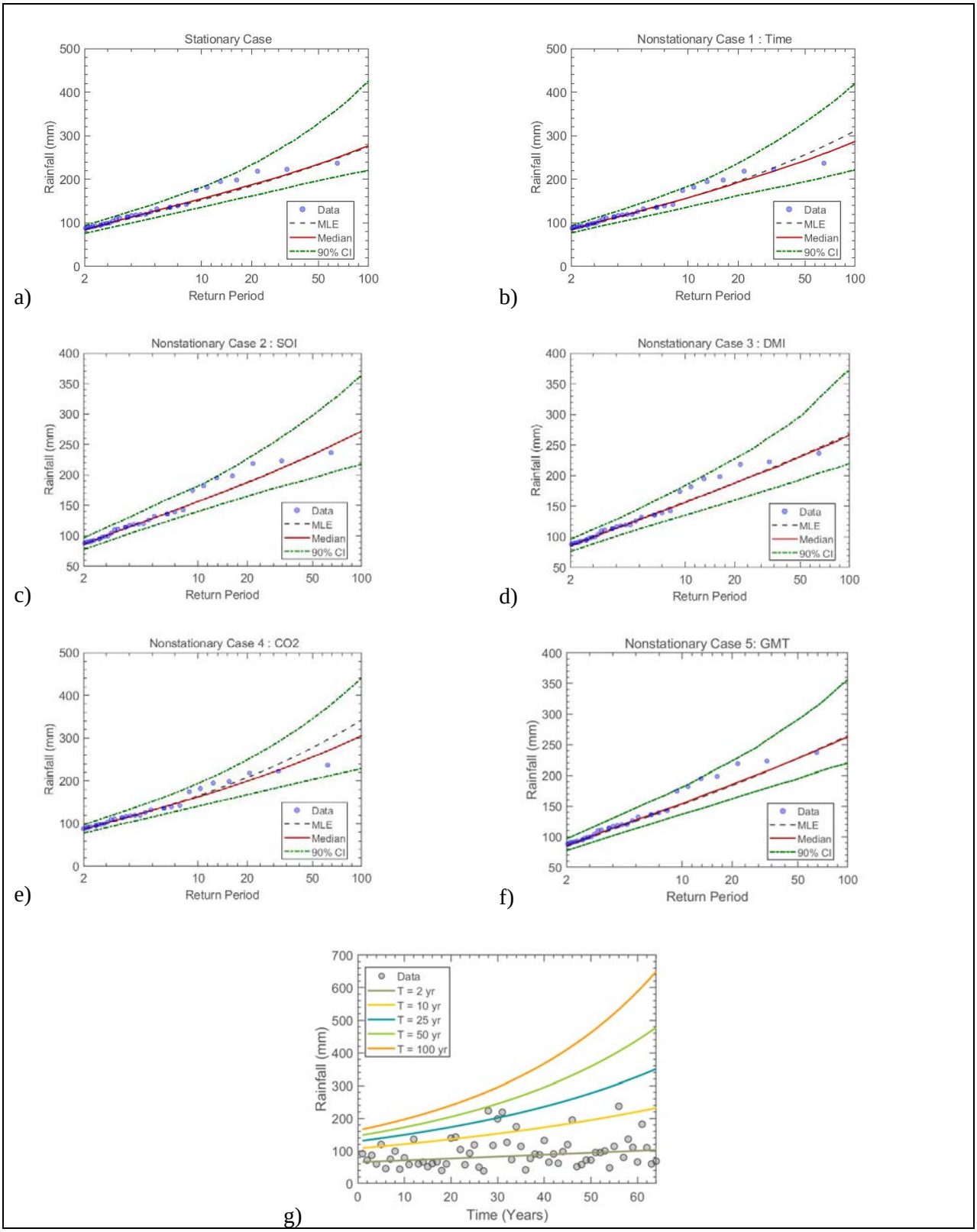

Figure 9.29 The GEV (a) stationary model, (b) non-stationary model considering time as a covariate, (c) non-stationary model considering SOI as a covariate, (d) non-stationary model considering DMI as a covariate, (e) non-stationary model considering CO_2 as a covariate, (f) non-stationary model considering GMT as a covariate and (g) effective return period as a function of time for Station 139: Inyoni – Myrln Estate

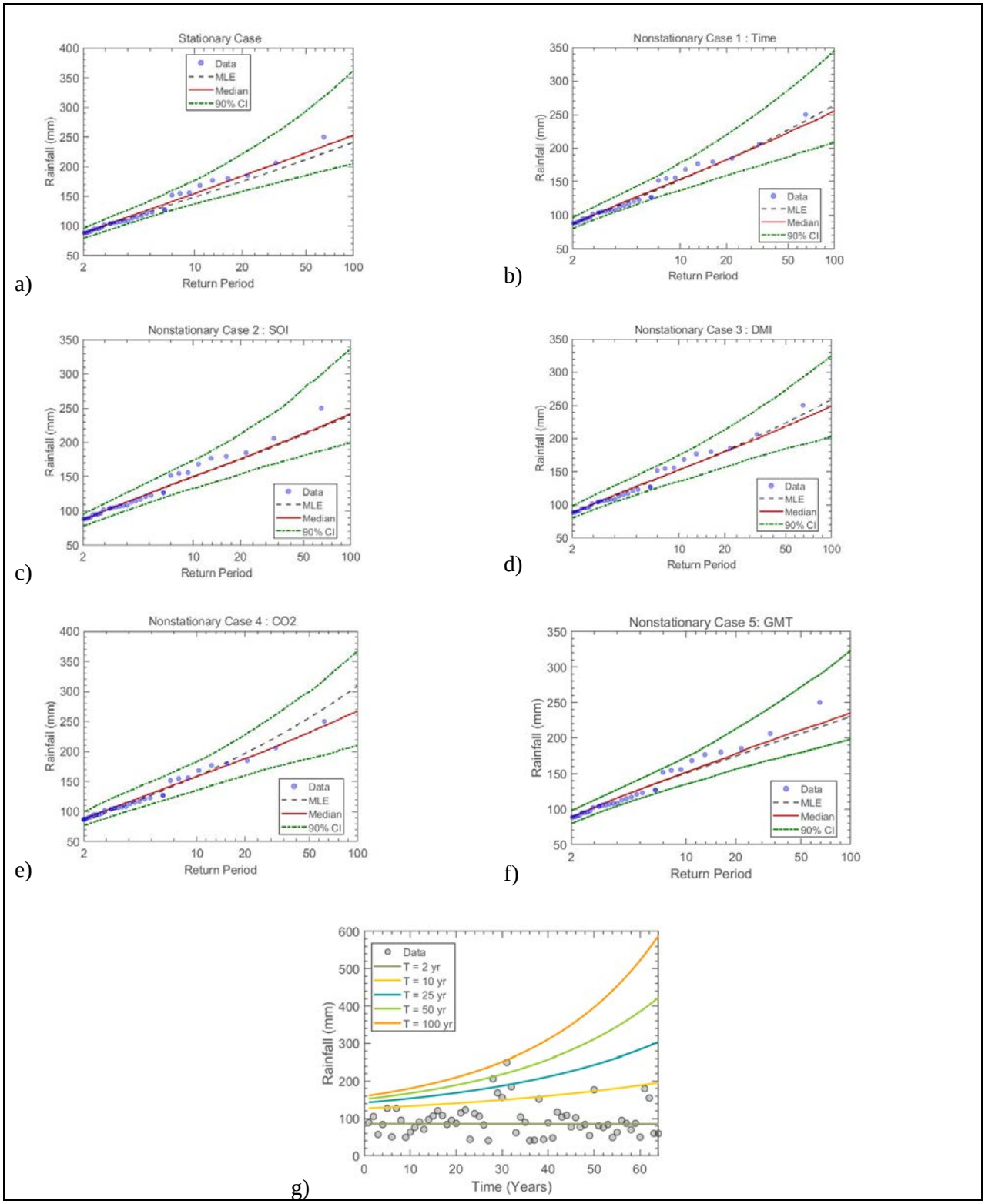

Figure 9.30 The GEV (a) stationary model, (b) non-stationary model considering time as a covariate, (c) non-stationary model considering SOI as a covariate, (d) non-stationary model considering DMI as a covariate, (e) non-stationary model considering CO_2 as a covariate, (f) non-stationary model considering GMT as a covariate and (g) effective return period as a function of time for Station 142: Eshowe – Brocklee Farm

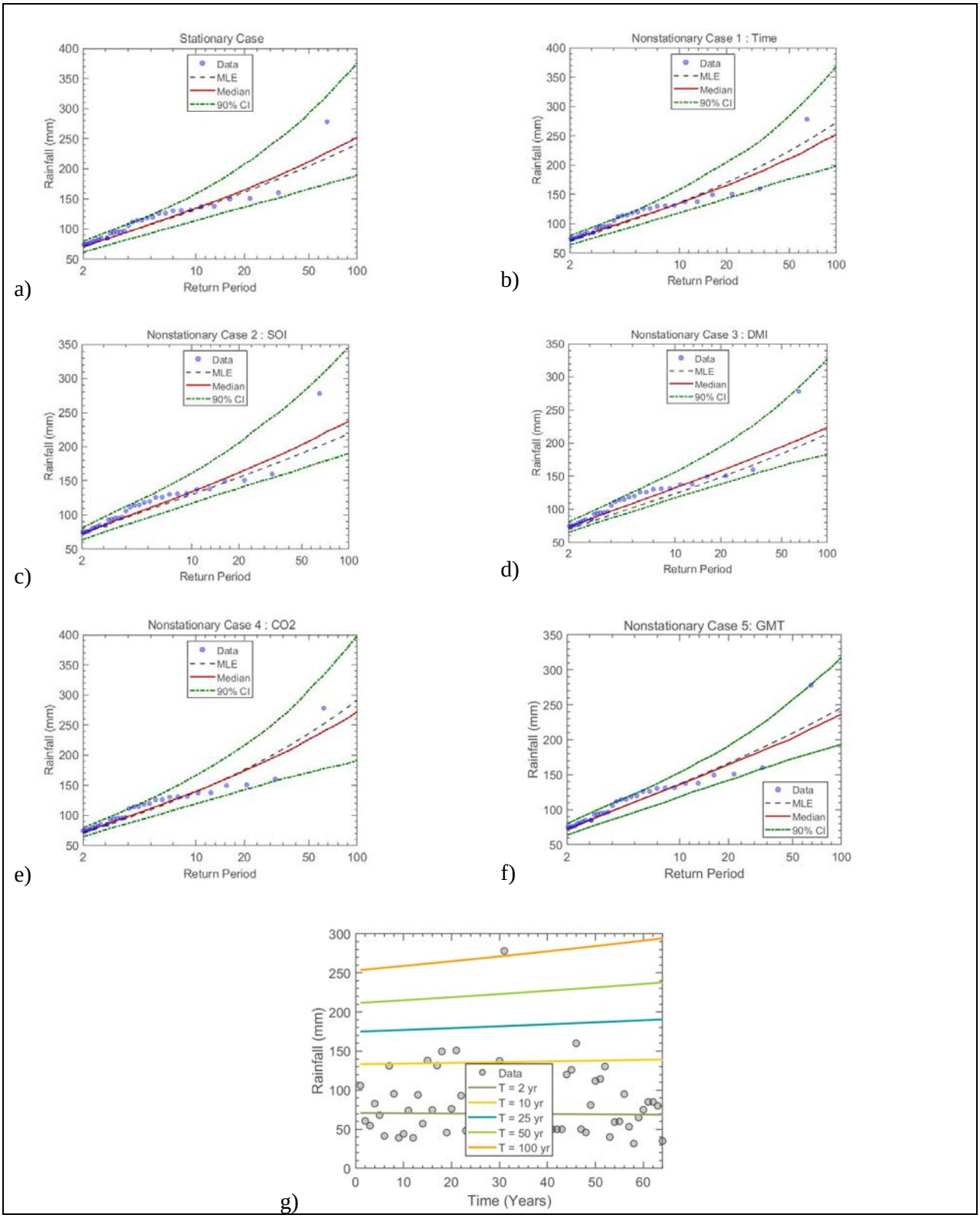

Figure 9.31 The GEV (a) stationary model, (b) non-stationary model considering time as a covariate, (c) non-stationary model considering SOI as a covariate, (d) non-stationary model considering DMI as a covariate, (e) non-stationary model considering CO_2 as a covariate, (f) non-stationary model considering GMT as a covariate and (g) effective return period as a function of time for Station 143: Nkwaleni – Zigagazi

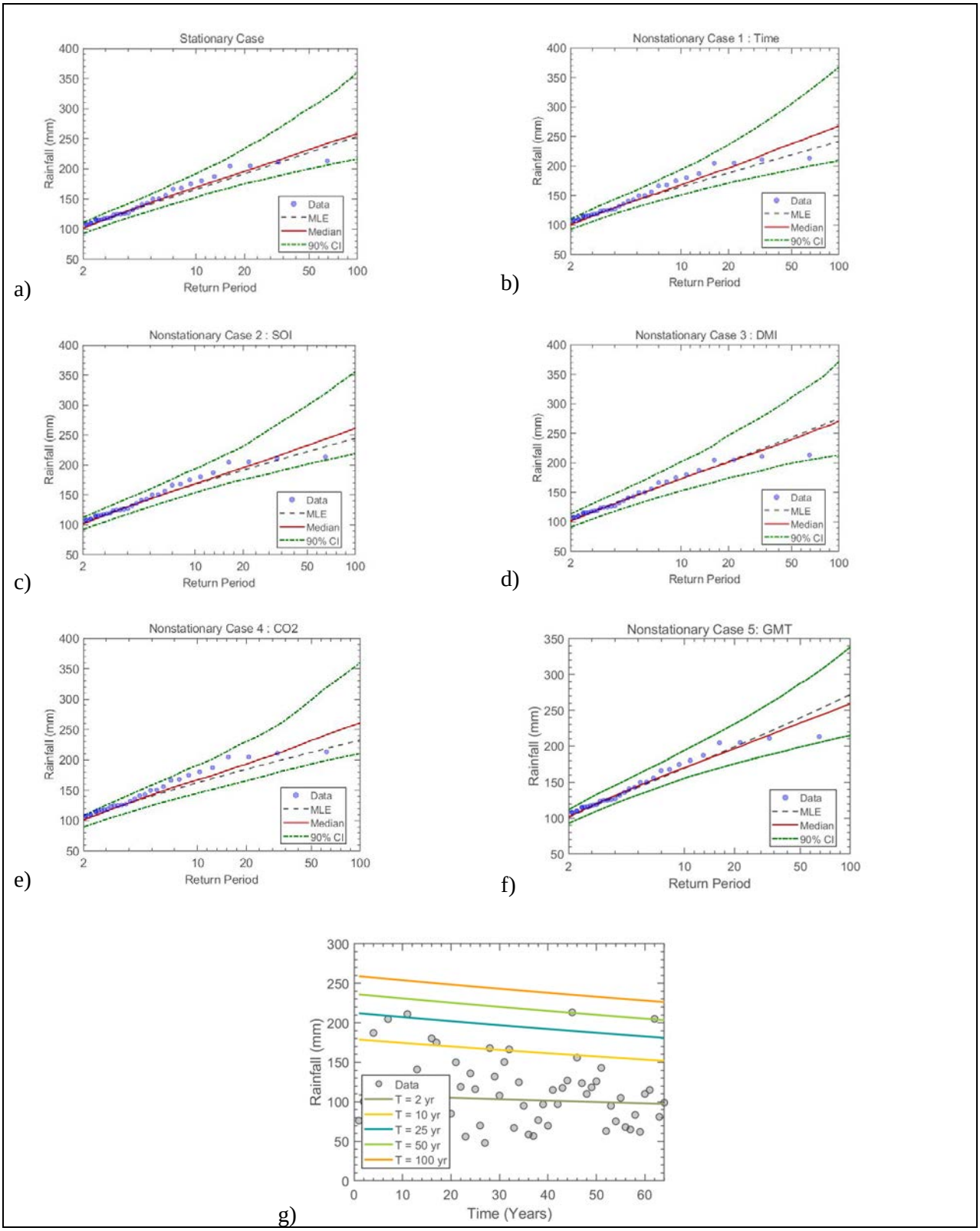

Figure 9.32 The GEV (a) stationary model, (b) non-stationary model considering time as a covariate, (c) non-stationary model considering SOI as a covariate, (d) non-stationary model considering DMI as a covariate, (e) non-stationary model considering CO_2 as a covariate, (f) non-stationary model considering GMT as a covariate and (g) effective return period as a function of time for Station 144: Felixton – Sugar Mill (THS)

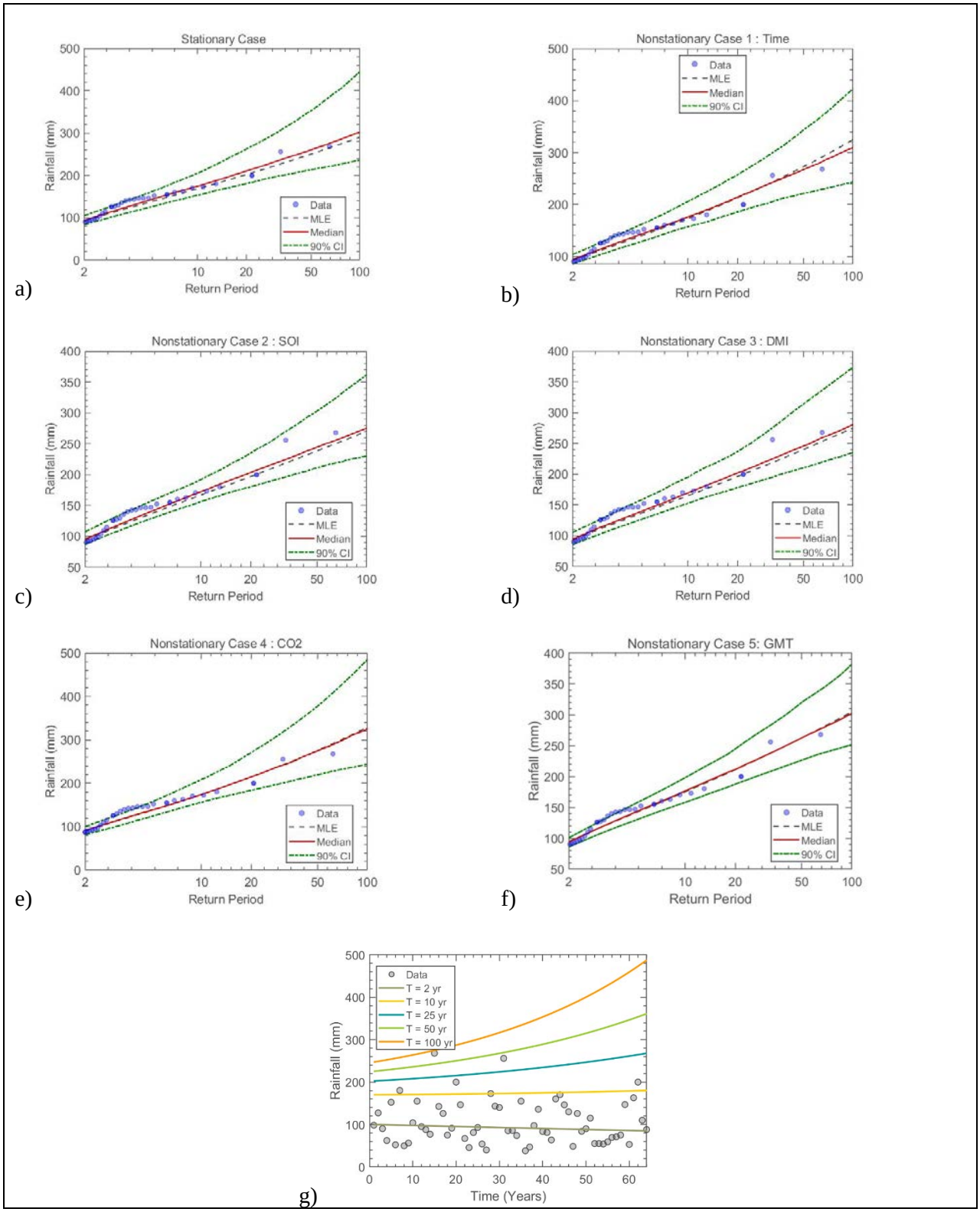

Figure 9.33 The GEV (a) stationary model, (b) non-stationary model considering time as a covariate, (c) non-stationary model considering SOI as a covariate, (d) non-stationary model considering DMI as a covariate, (e) non-stationary model considering CO_2 as a covariate, (f) non-stationary model considering GMT as a covariate and (g) effective return period as a function of time for Station 146: Kulu Halt – Honey Farm

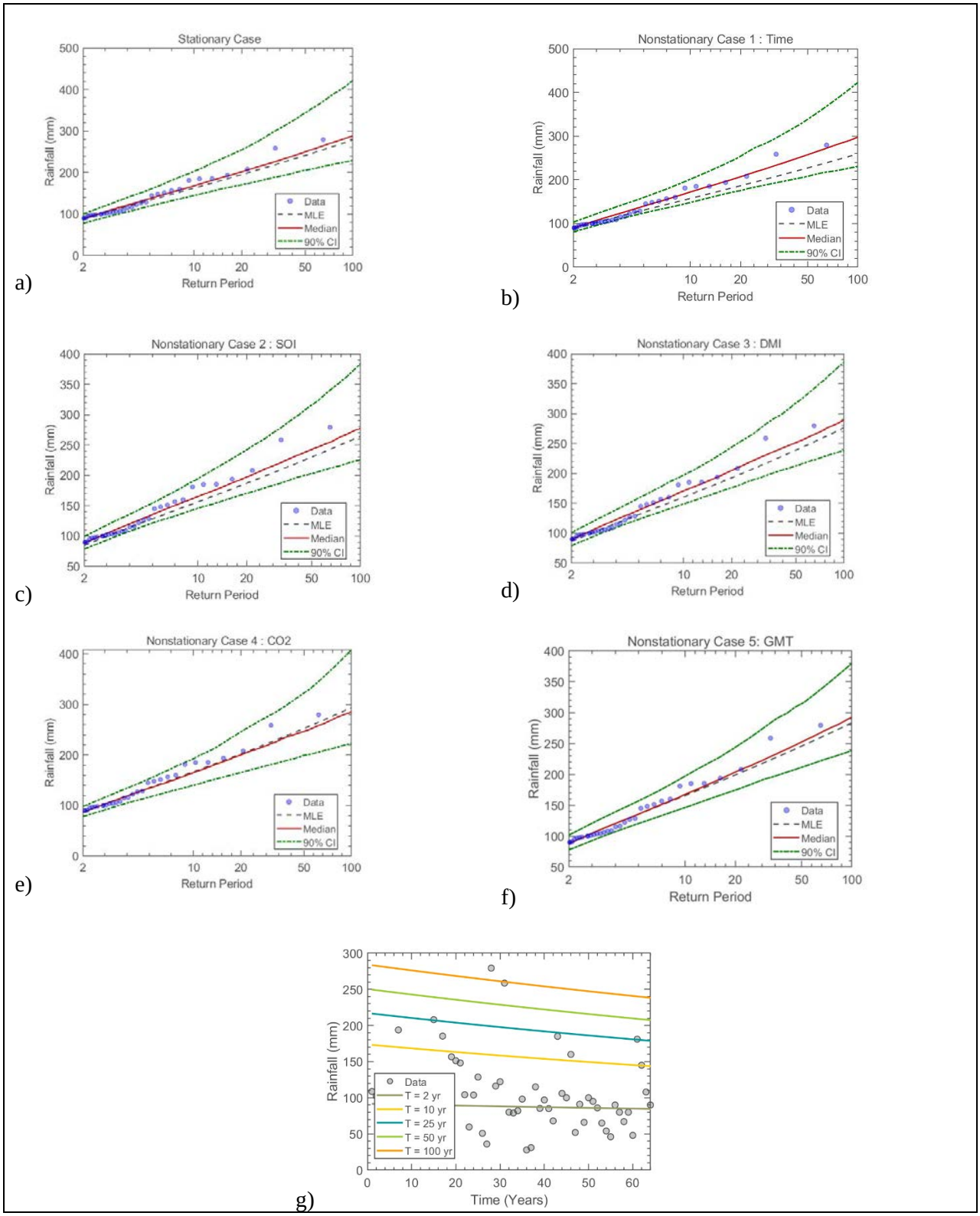

Figure 9.34 The GEV (a) stationary model, (b) non-stationary model considering time as a covariate, (c) non-stationary model considering SOI as a covariate, (d) non-stationary model considering DMI as a covariate, (e) non-stationary model considering CO_2 as a covariate, (f) non-stationary model considering GMT as a covariate and (g) effective return period as a function of time for Station 147: Ukulu Properties – Crystal Holdings

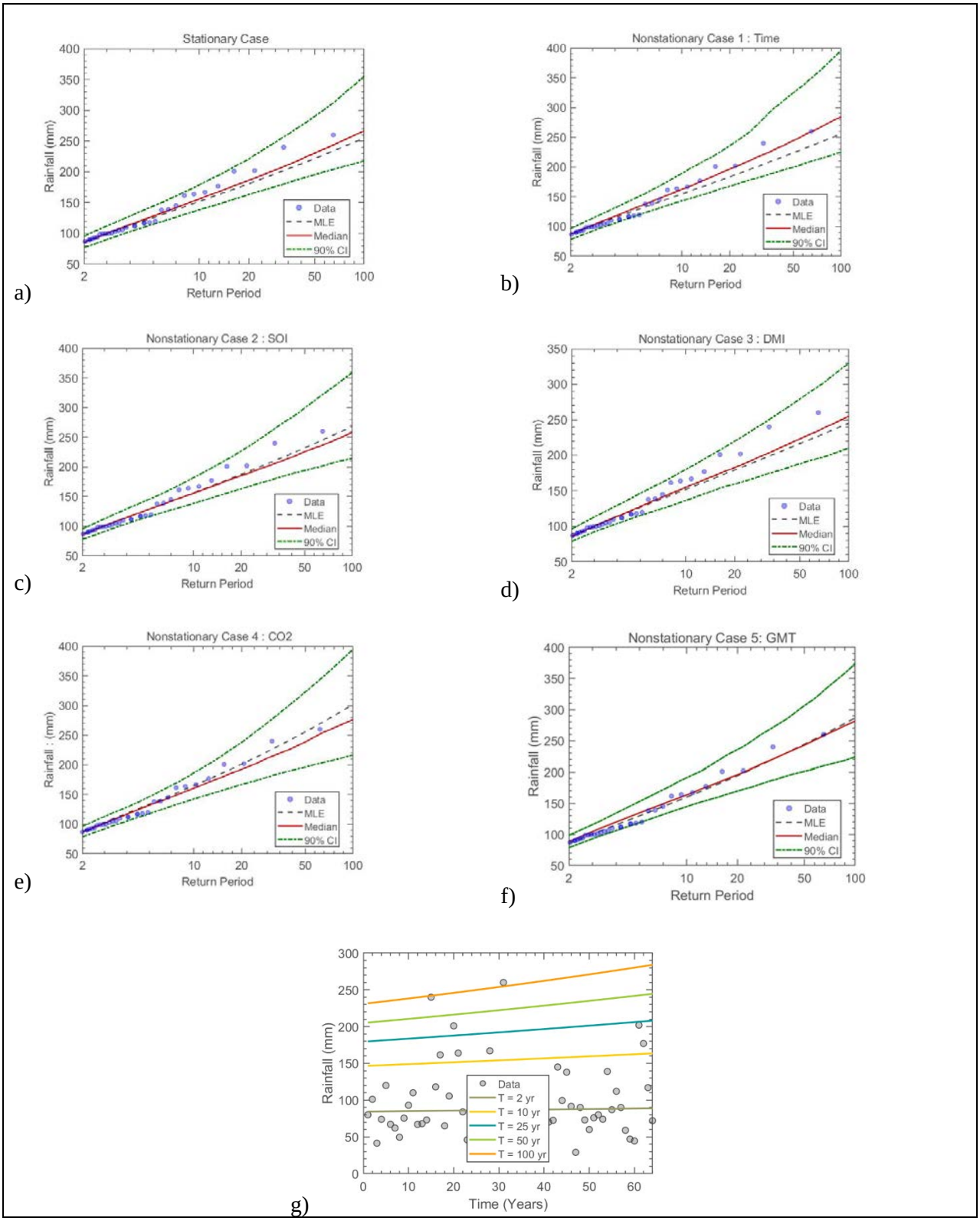

Figure 9.35 The GEV (a) stationary model, (b) non-stationary model considering time as a covariate, (c) non-stationary model considering SOI as a covariate, (d) non-stationary model considering DMI as a covariate, (e) non-stationary model considering CO_2 as a covariate, (f) non-stationary model considering GMT as a covariate and (g) effective return period as a function of time for Station 148: Mposa – Redcroft Farm

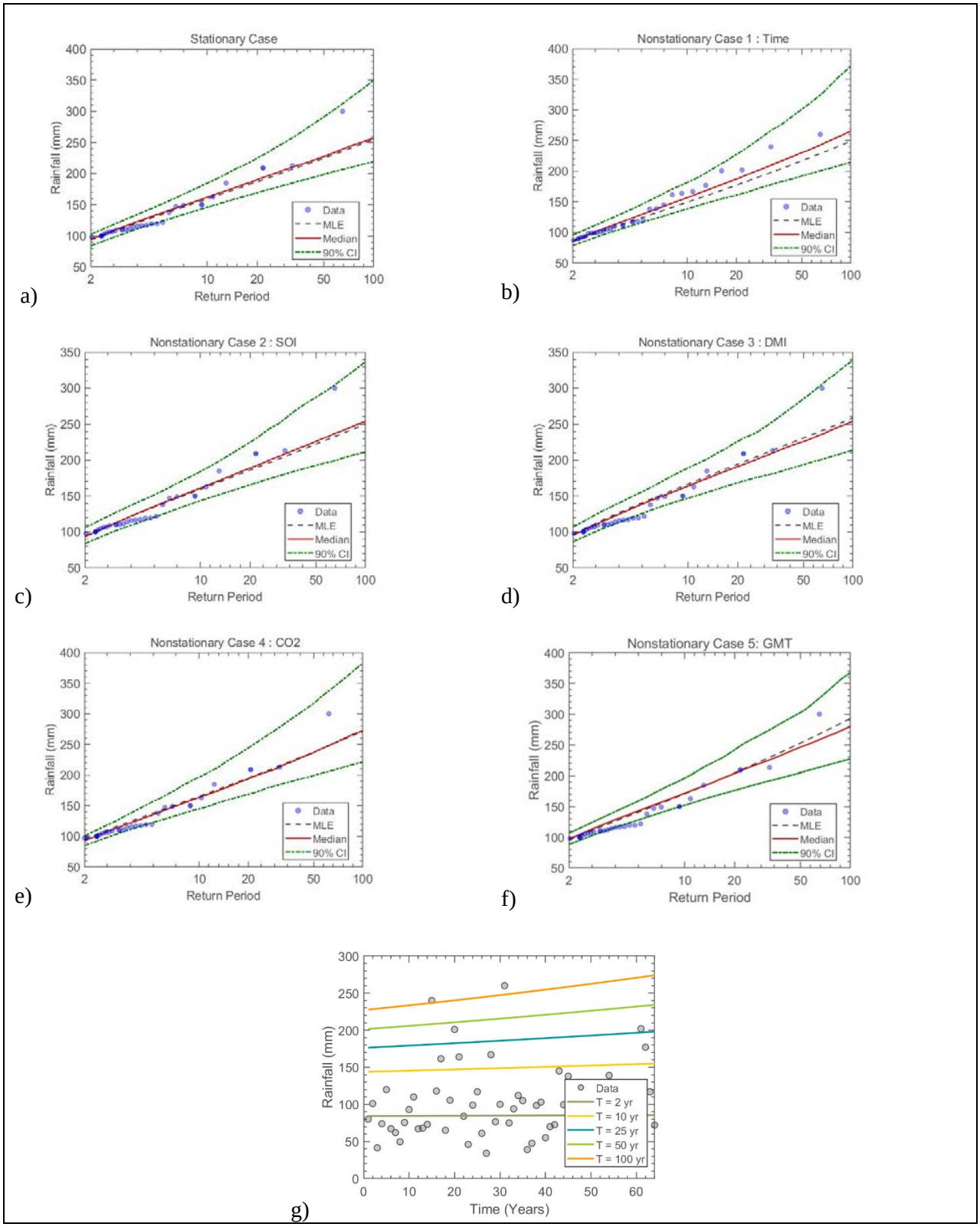

Figure 9.36 The GEV (a) stationary model, (b) non-stationary model considering time as a covariate, (c) non-stationary model considering SOI as a covariate, (d) non-stationary model considering DMI as a covariate, (e) non-stationary model considering CO_2 as a covariate, (f) non-stationary model considering GMT as a covariate and (g) effective return period as a function of time for Station 149: Kwambonambi – Mondi Forestry

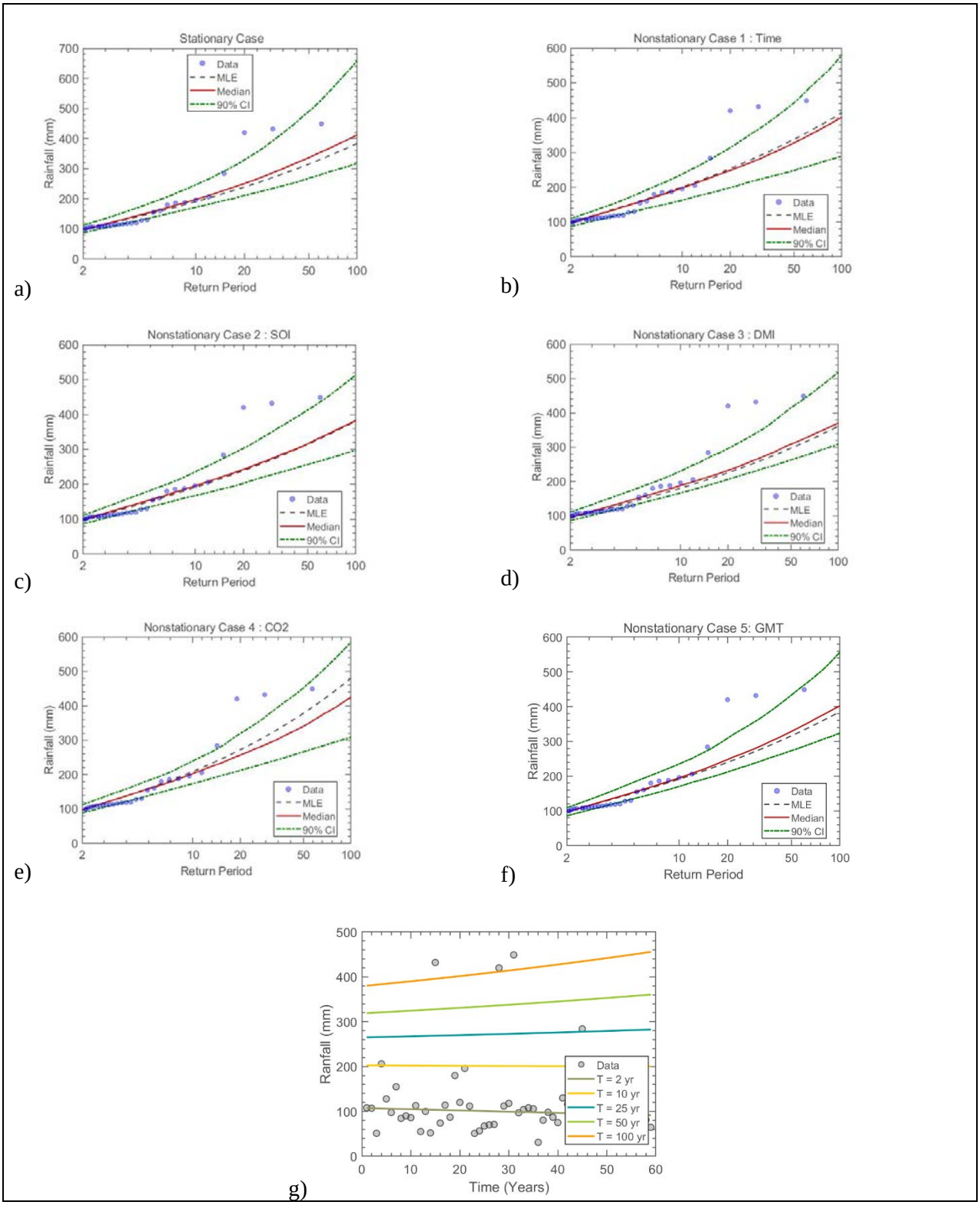

Figure 9.37 The GEV (a) stationary model, (b) non-stationary model considering time as a covariate, (c) non-stationary model considering SOI as a covariate, (d) non-stationary model considering DMI as a covariate, (e) non-stationary model considering CO_2 as a covariate, (f) non-stationary model considering GMT as a covariate and (g) effective return period as a function of time for Station 151: ULOA – Mark & Ross Sugar Estate

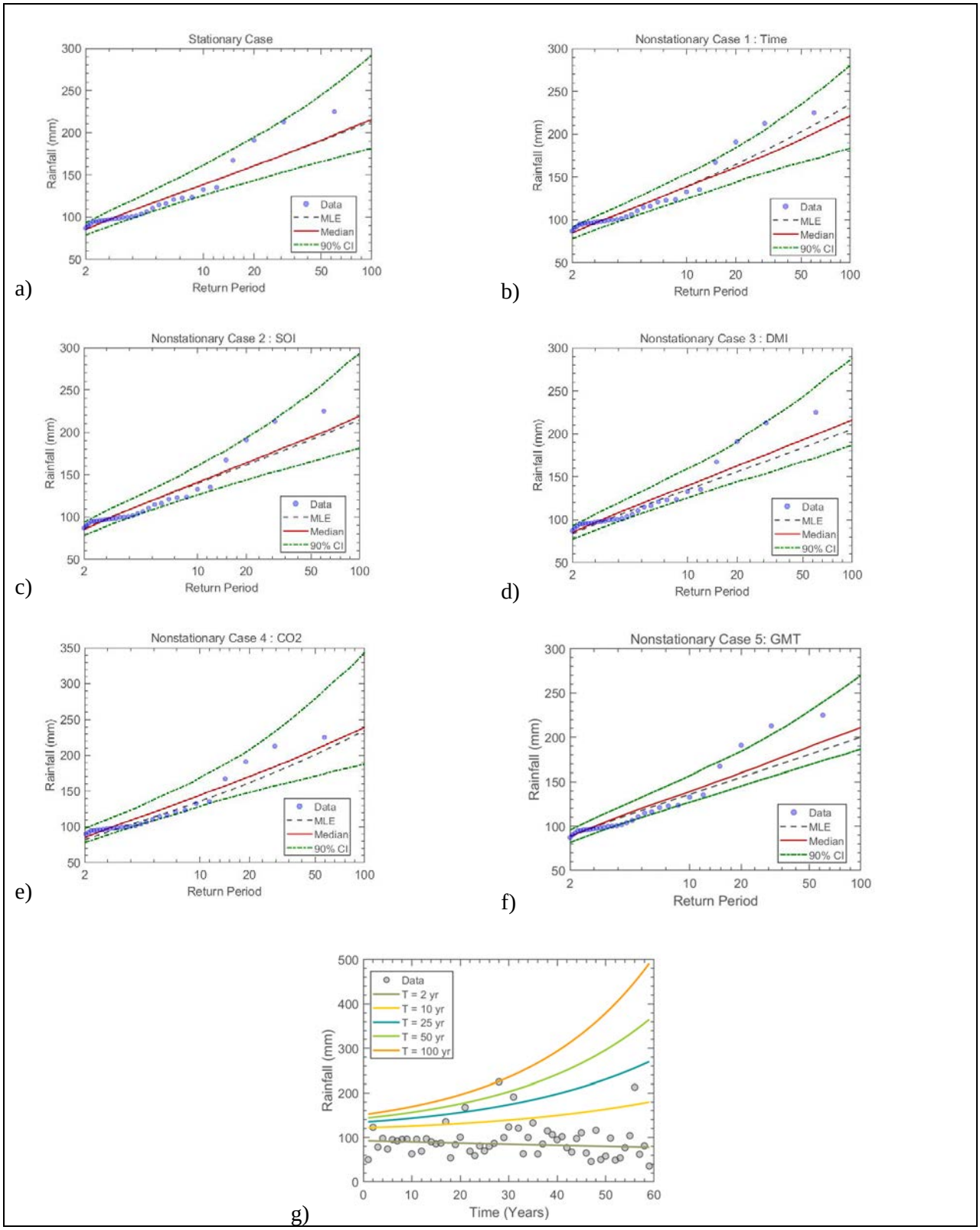

Figure 9.38 The GEV (a) stationary model, (b) non-stationary model considering time as a covariate, (c) non-stationary model considering SOI as a covariate, (d) non-stationary model considering DMI as a covariate, (e) non-stationary model considering CO_2 as a covariate, (f) non-stationary model considering GMT as a covariate and (g) effective return period as a function of time for Station 152: Mtubatuba – Nyalazi River

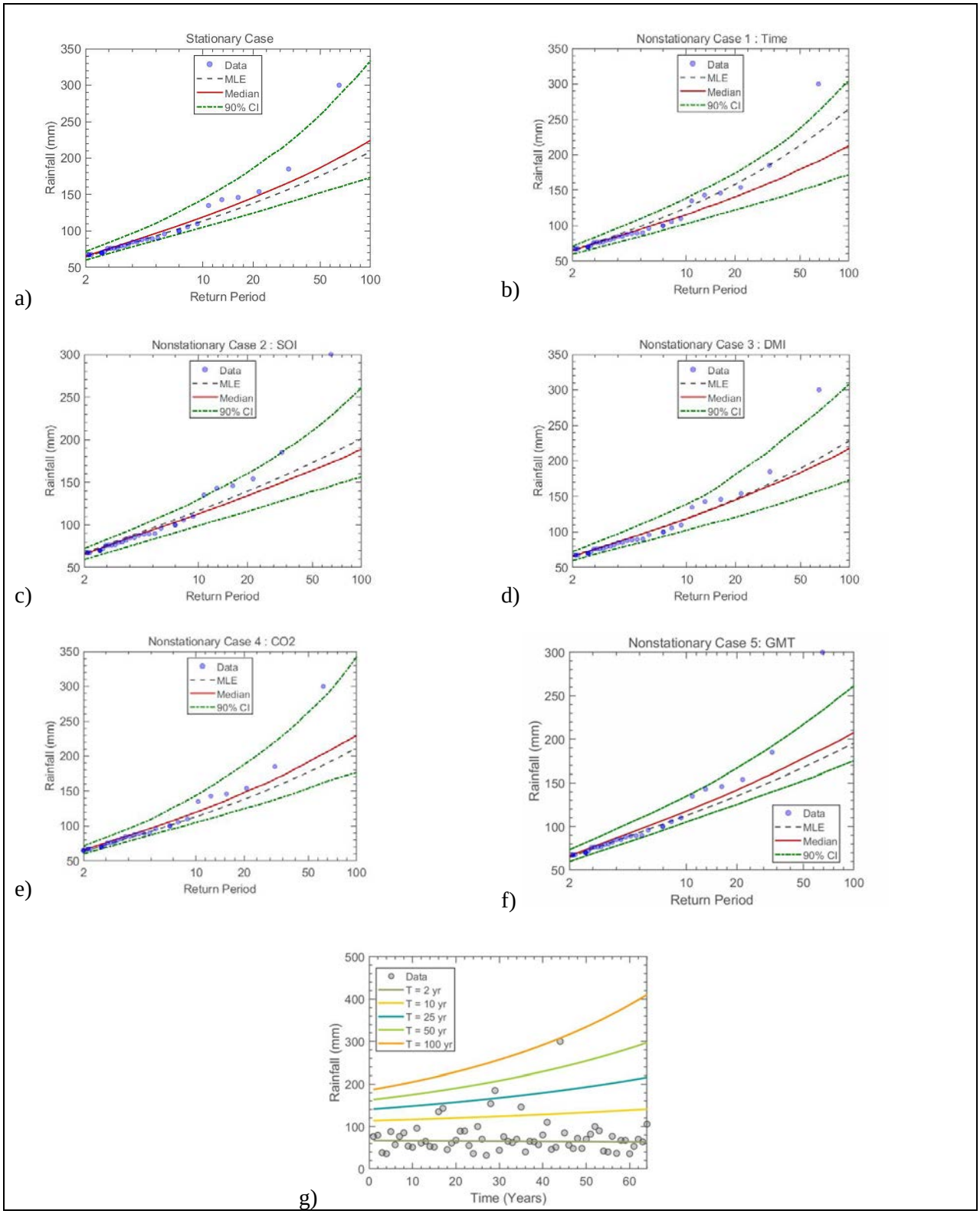

Figure 9.39 The GEV (a) stationary model, (b) non-stationary model considering time as a covariate, (c) non-stationary model considering SOI as a covariate, (d) non-stationary model considering DMI as a covariate, (e) non-stationary model considering CO_2 as a covariate, (f) non-stationary model considering GMT as a covariate and (g) effective return period as a function of time for Station 154: Mkuze – Mkuze Estate

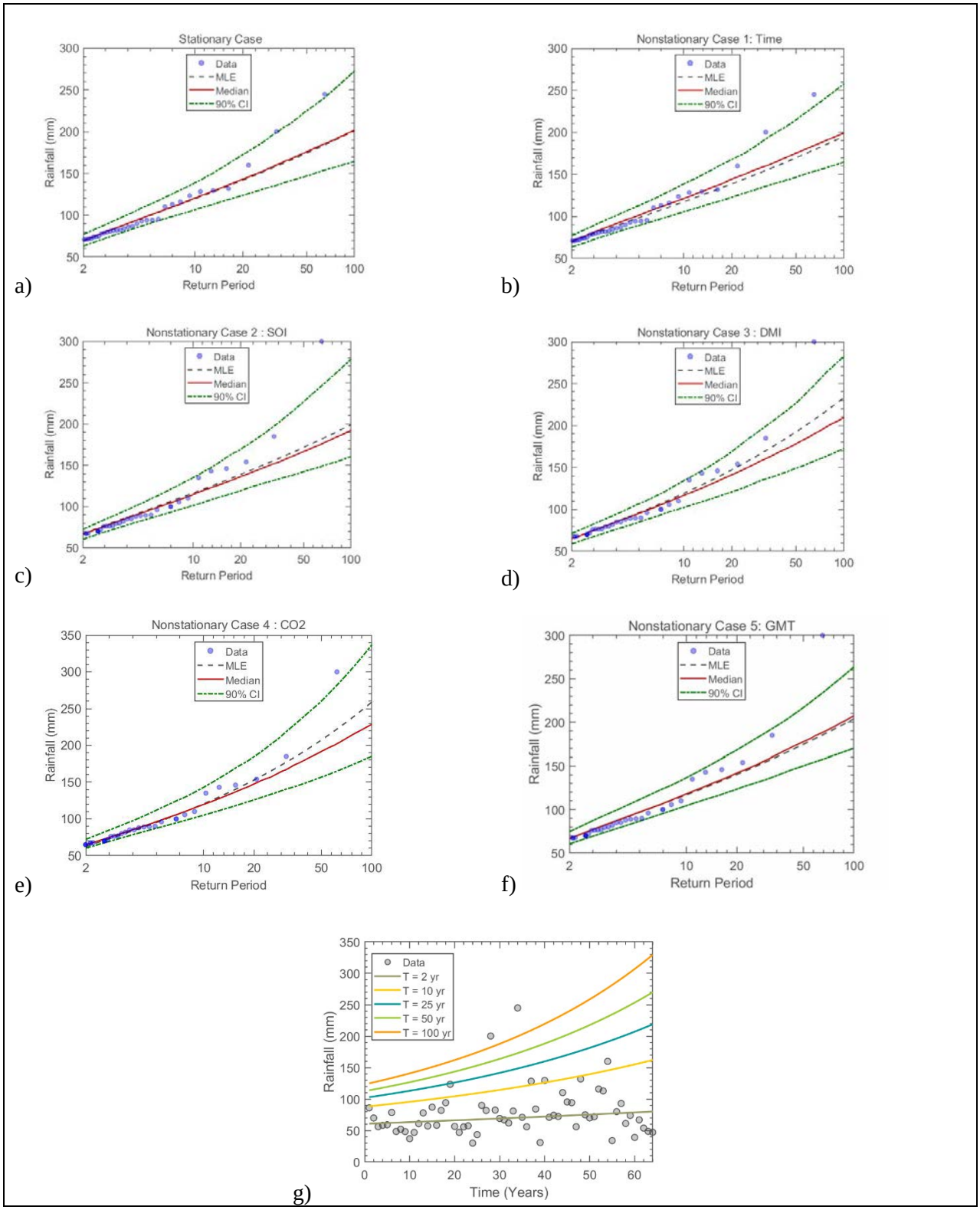

Figure 9.40 The GEV (a) stationary model, (b) non-stationary model considering time as a covariate, (c) non-stationary model considering SOI as a covariate, (d) non-stationary model considering DMI as a covariate, (e) non-stationary model considering CO_2 as a covariate, (f) non-stationary model considering GMT as a covariate and (g) effective return period as a function of time for Station 155: Pongola – Impala Irrigation Board

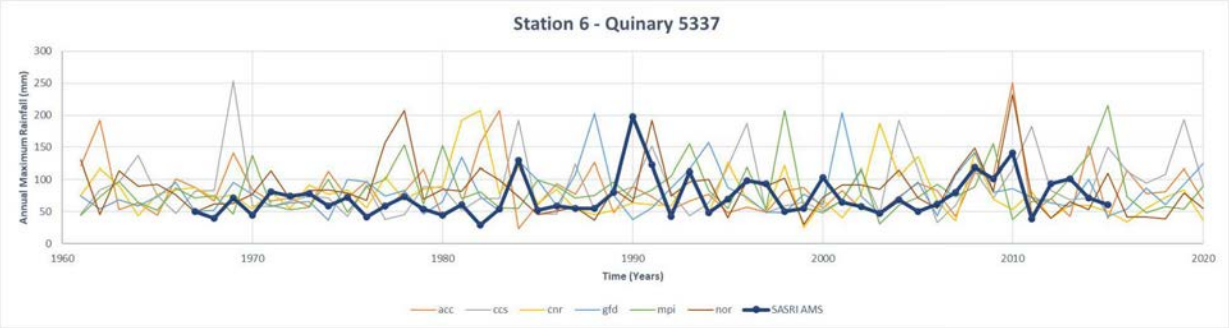

Figure 9.41 Time series of annual maximum rainfall for SASRI station 6 and 6 GCMs for corresponding years

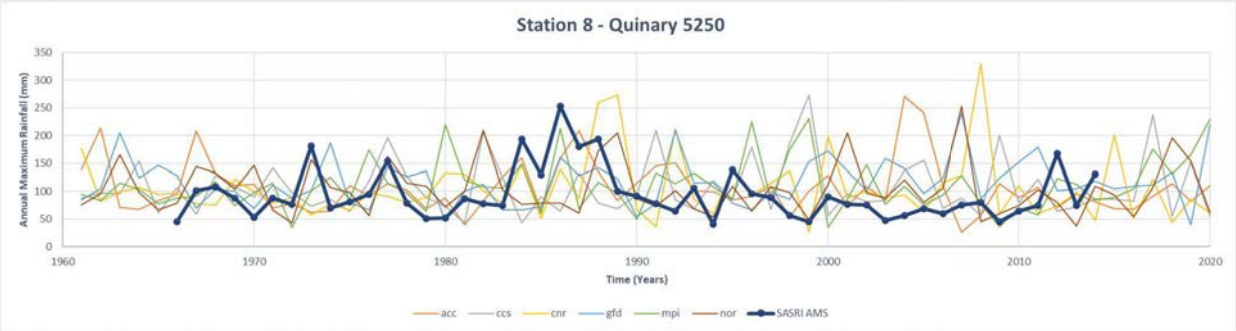

Figure 9.42 Time series of annual maximum rainfall for SASRI station 8 and 6 GCMs for corresponding years

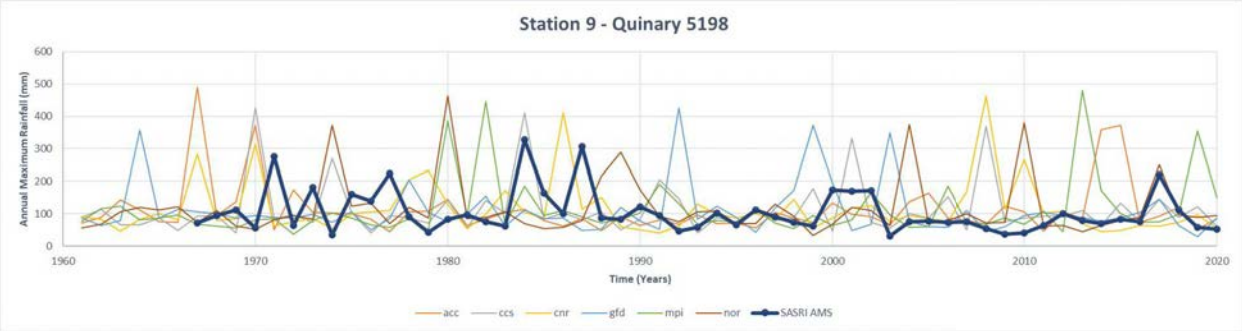

Figure 9.43 Time series of annual maximum rainfall for SASRI station 9 and 6 GCMs for corresponding years

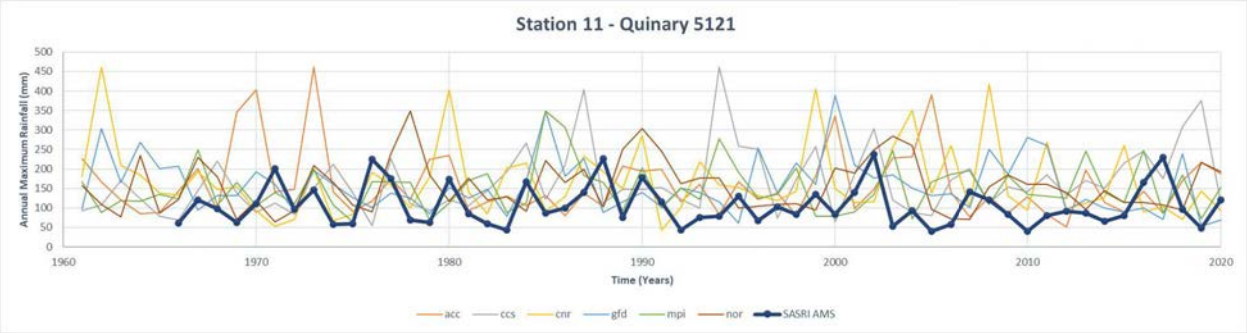

Figure 9.44 Time series of annual maximum rainfall for SASRI station 11 and 6 GCMs for corresponding years

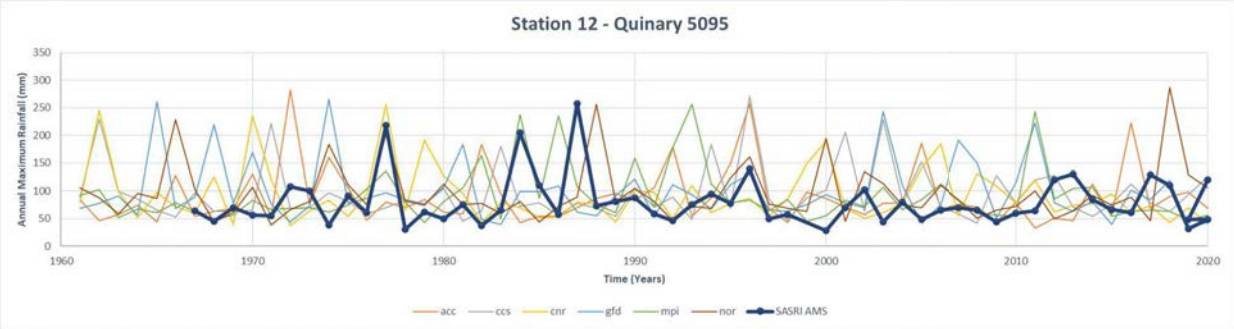

Figure 9.45 Time series of annual maximum rainfall for SASRI station 12 and 6 GCMs for corresponding years

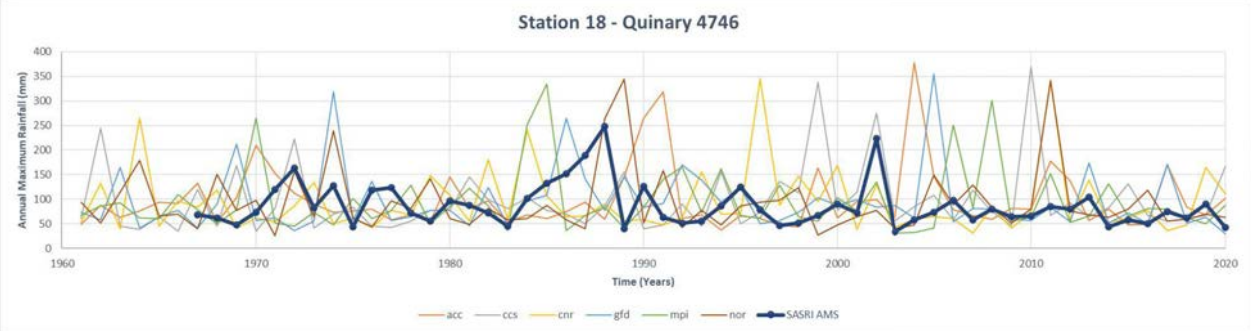

Figure 9.46 Time series of annual maximum rainfall for SASRI station 18 and 6 GCMs for corresponding years

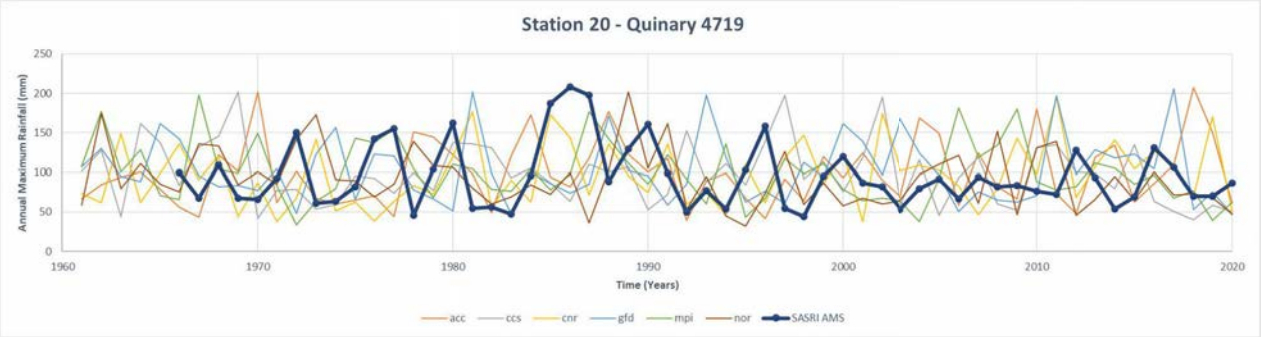

Figure 9.47 Time series of annual maximum rainfall for SASRI station 20 and 6 GCMs for corresponding years

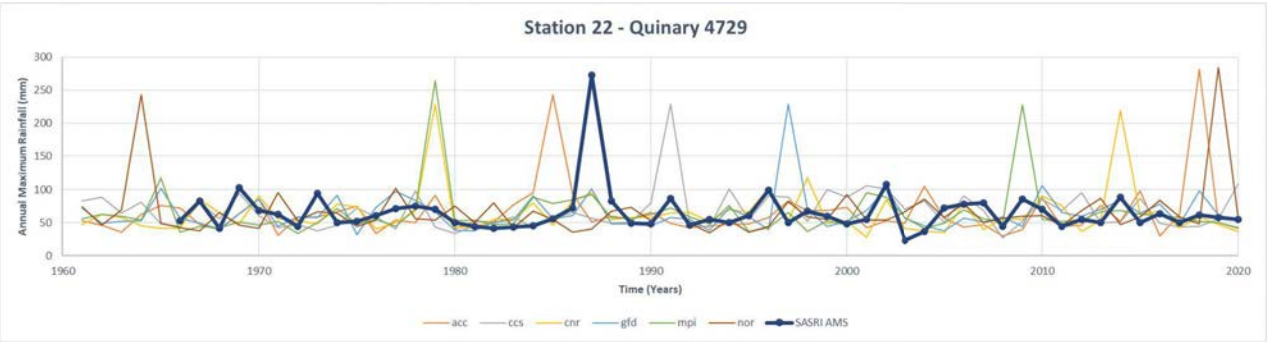

Figure 9.48 Time series of annual maximum rainfall for SASRI station 22 and 6 GCMs for corresponding years

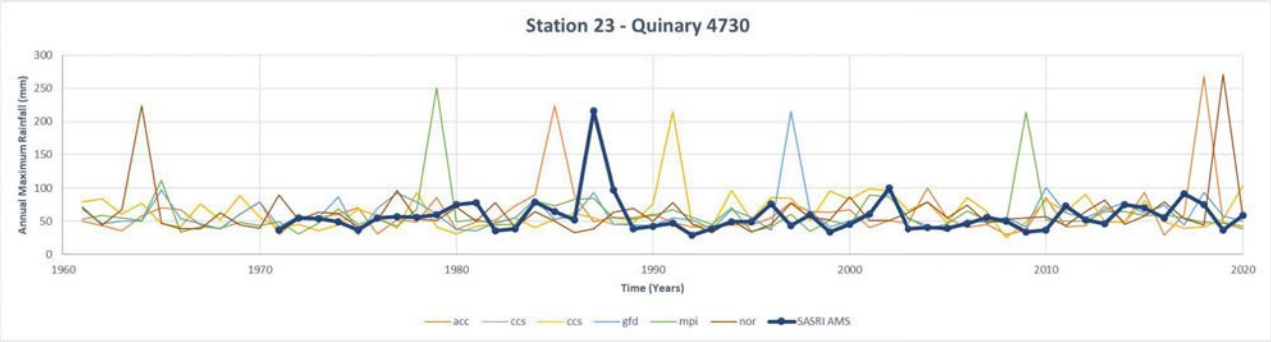

Figure 9.49 Time series of annual maximum rainfall for SASRI station 23 and 6 GCMs for corresponding years

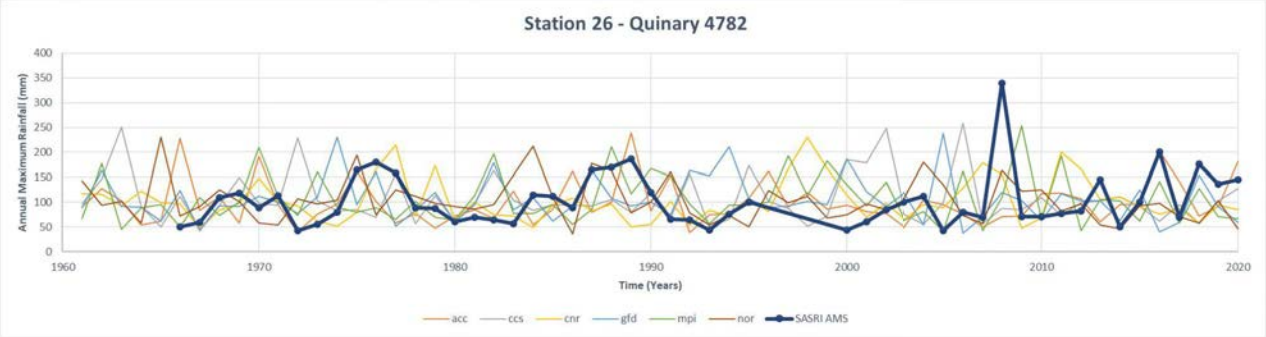

Figure 9.50 Time series of annual maximum rainfall for SASRI station 26 and 6 GCMs for corresponding years

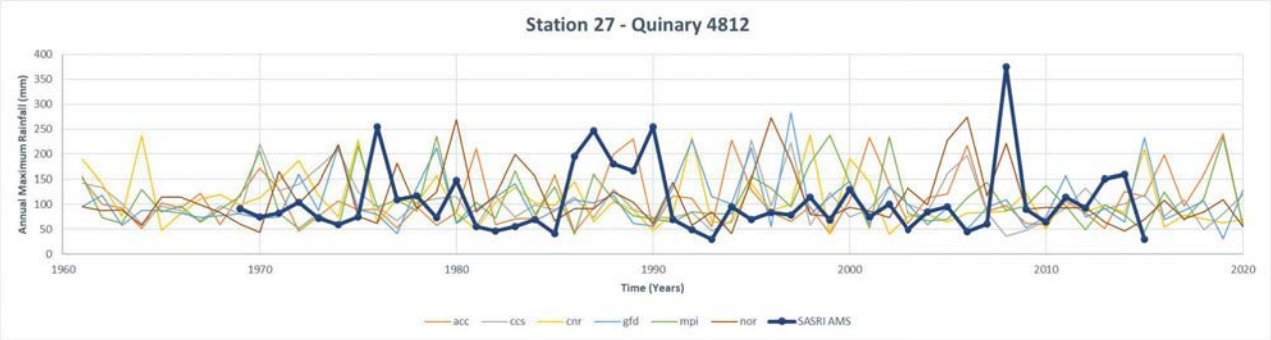

Figure 9.51 Time series of annual maximum rainfall for SASRI station 27 and 6 GCMs for corresponding years

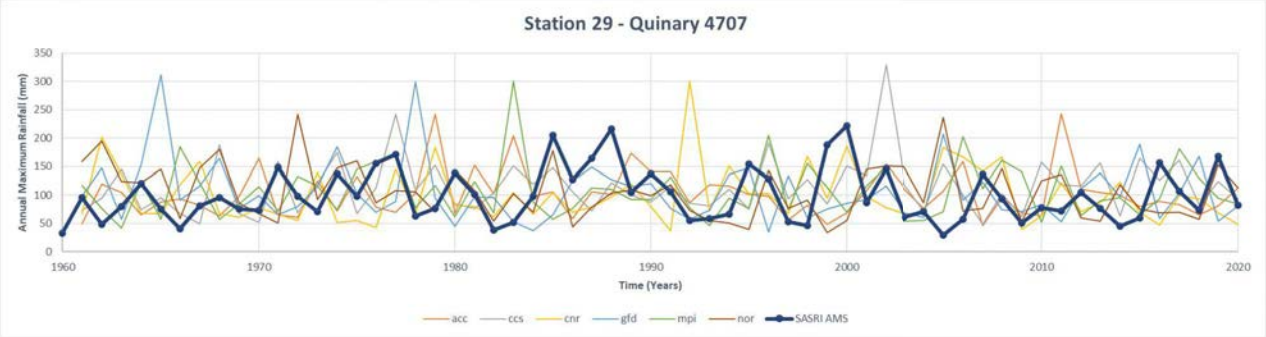

Figure 9.52 Time series of annual maximum rainfall for SASRI station 29 and 6 GCMs for corresponding years

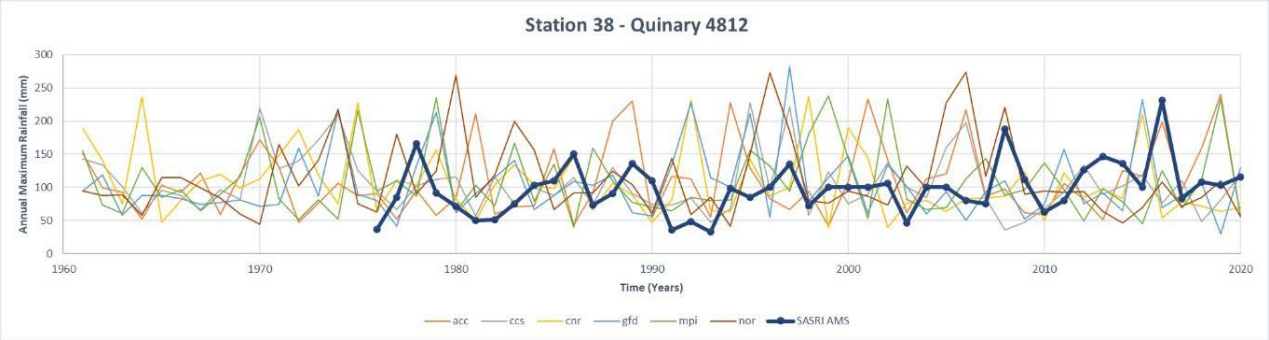

Figure 9.53 Time series of annual maximum rainfall for SASRI station 38 and 6 GCMs for corresponding years

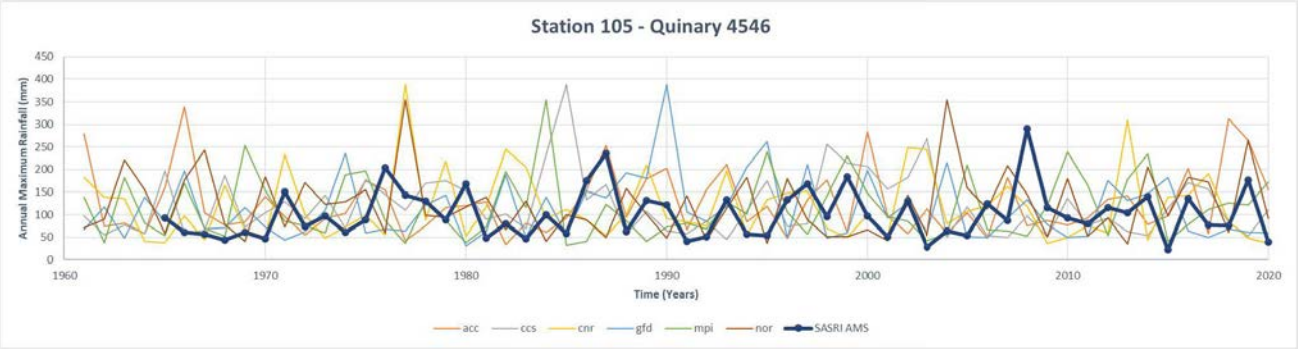

Figure 9.54 Time series of annual maximum rainfall for SASRI station 105 and 6 GCMs for corresponding years

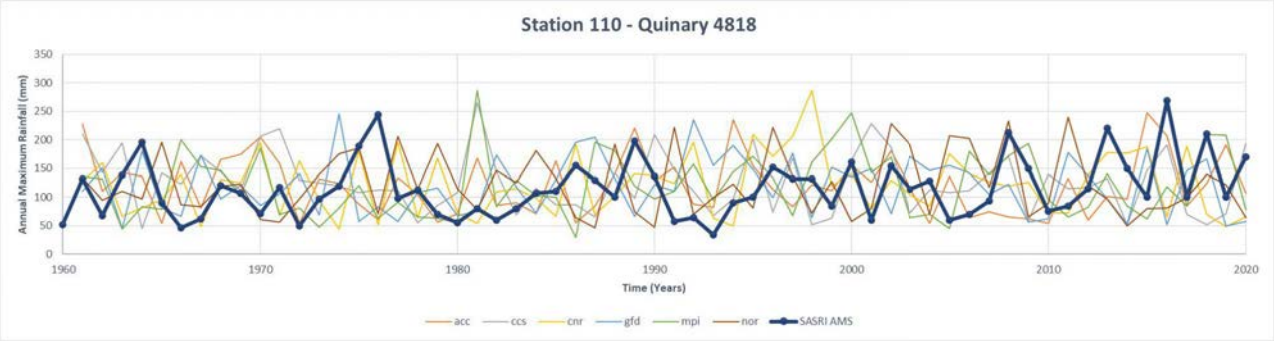

Figure 9.55 Time series of annual maximum rainfall for SASRI station 110 and 6 GCMs for corresponding years

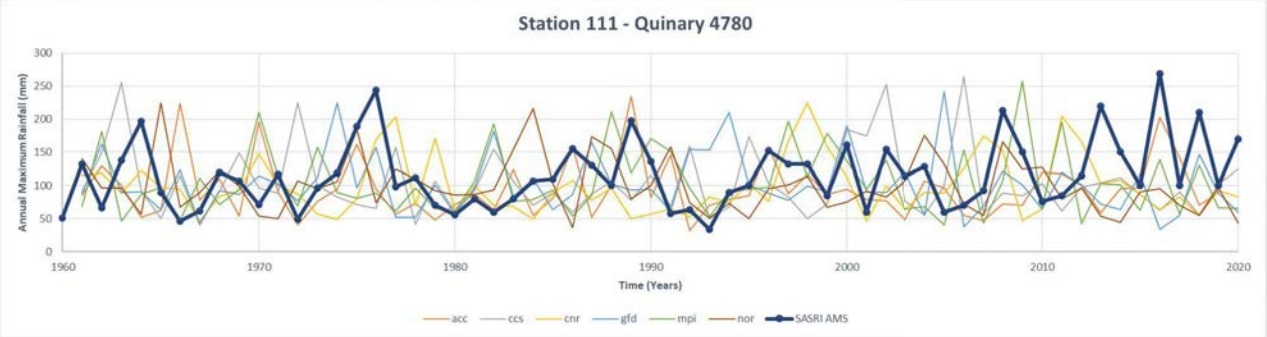

Figure 9.56 Time series of annual maximum rainfall for SASRI station 111 and 6 GCMs for corresponding years

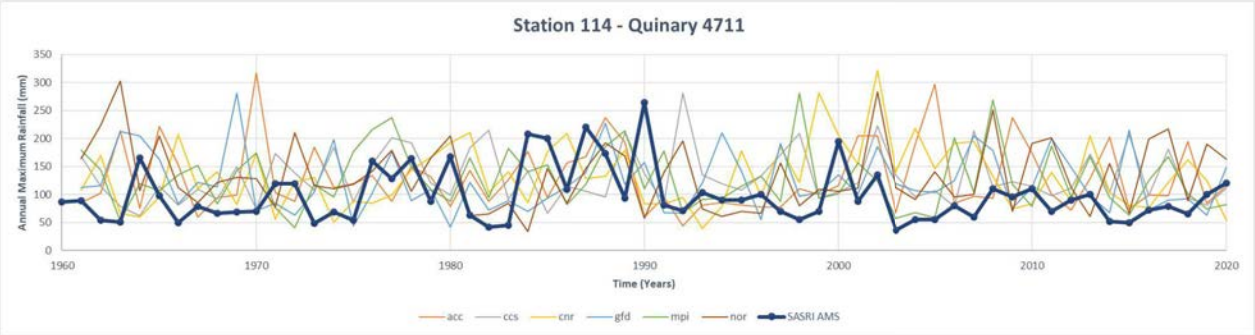

Figure 9.57 Time series of annual maximum rainfall for SASRI station 114 and 6 GCMs for corresponding years

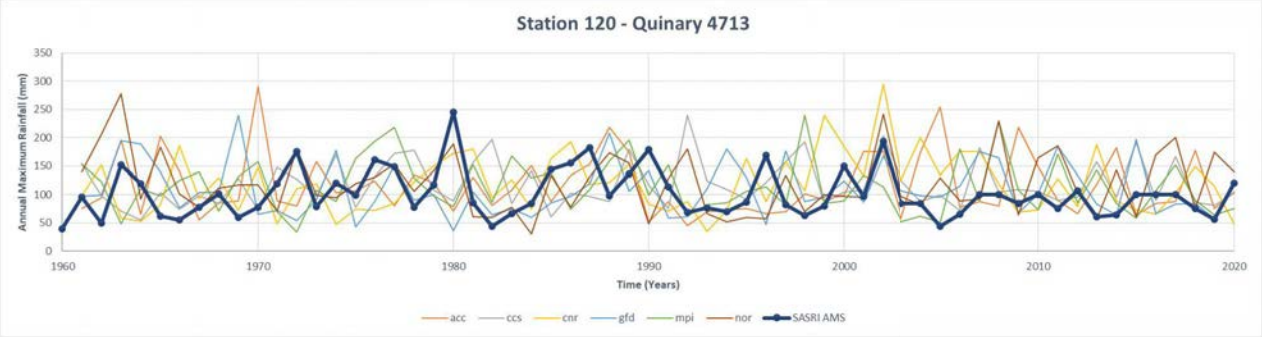

Figure 9.58 Time series of annual maximum rainfall for SASRI station 120 and 6 GCMs for corresponding years

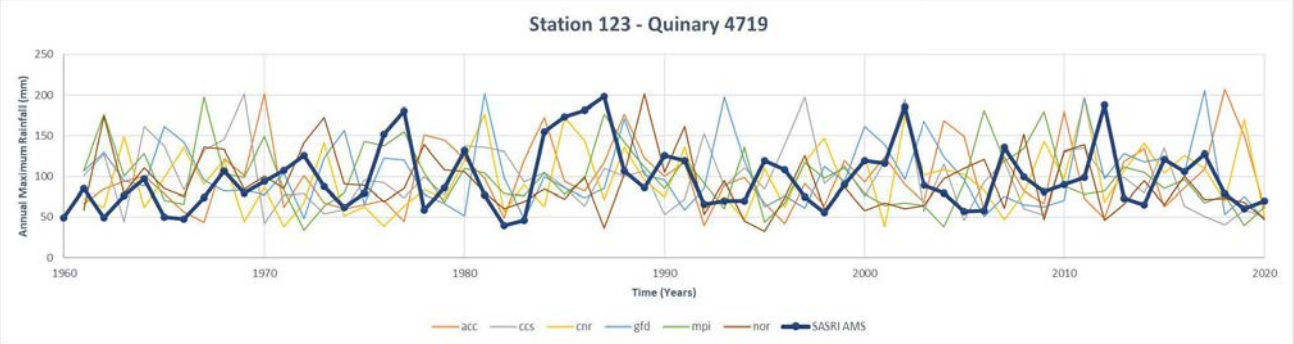

Figure 9.59 Time series of annual maximum rainfall for SASRI station 123 and 6 GCMs for corresponding years

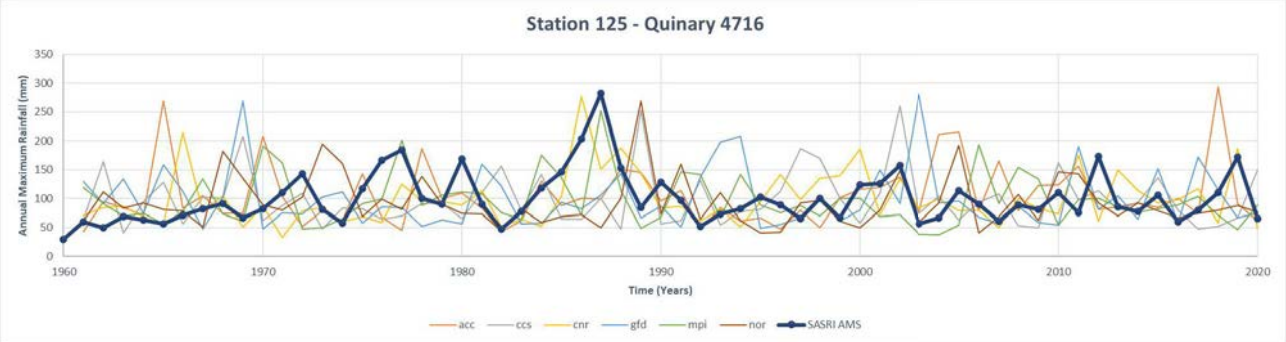

Figure 9.60 Time series of annual maximum rainfall for SASRI station 125 and 6 GCMs for corresponding years

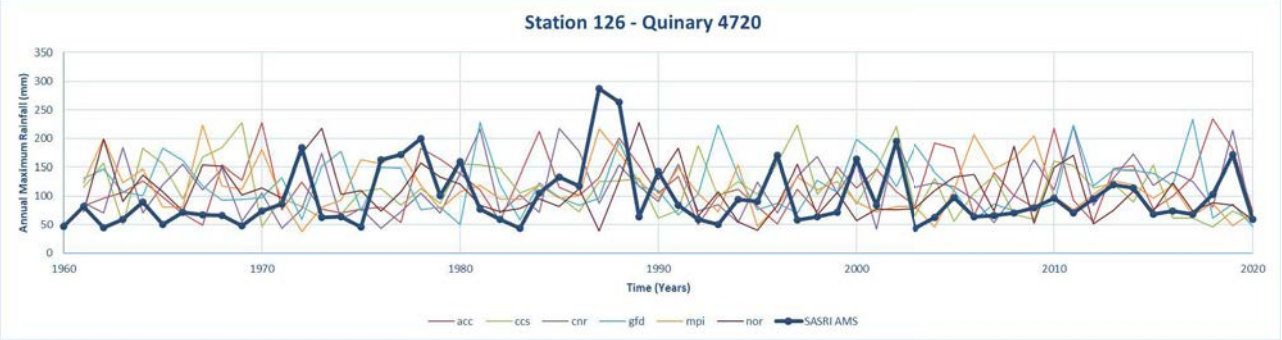

Figure 9.61 Time series of annual maximum rainfall for SASRI station 126 and 6 GCMs for corresponding years

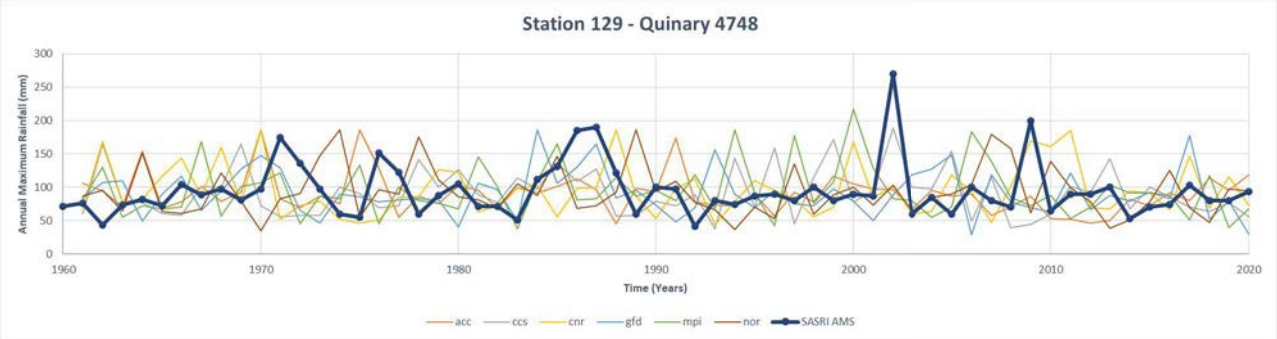

Figure 9.62 Time series of annual maximum rainfall for SASRI station 129 and 6 GCMs for corresponding years

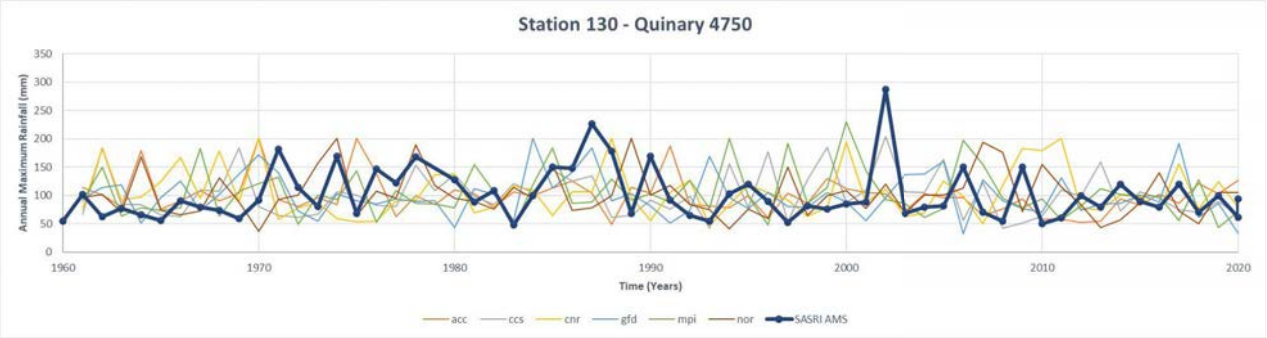

Figure 9.63 Time series of annual maximum rainfall for SASRI station 130 and 6 GCMs for corresponding years

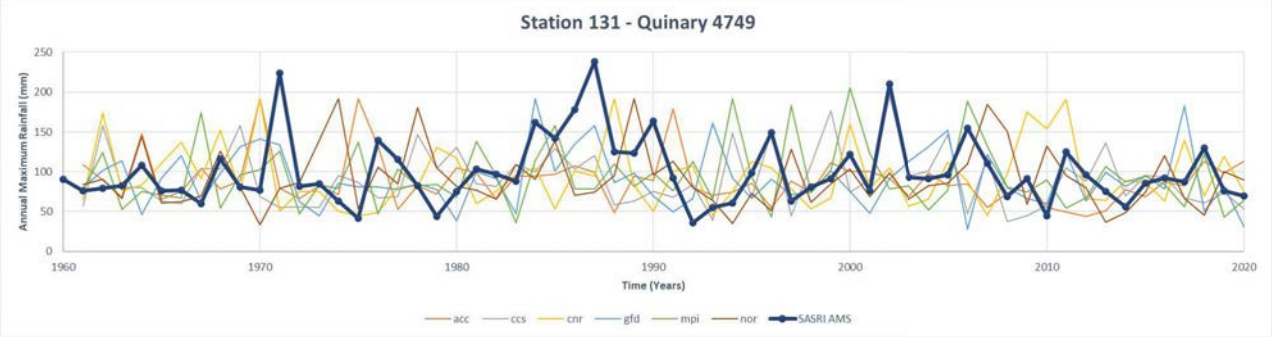

Figure 9.64 Time series of annual maximum rainfall for SASRI station 131 and 6 GCMs for corresponding years

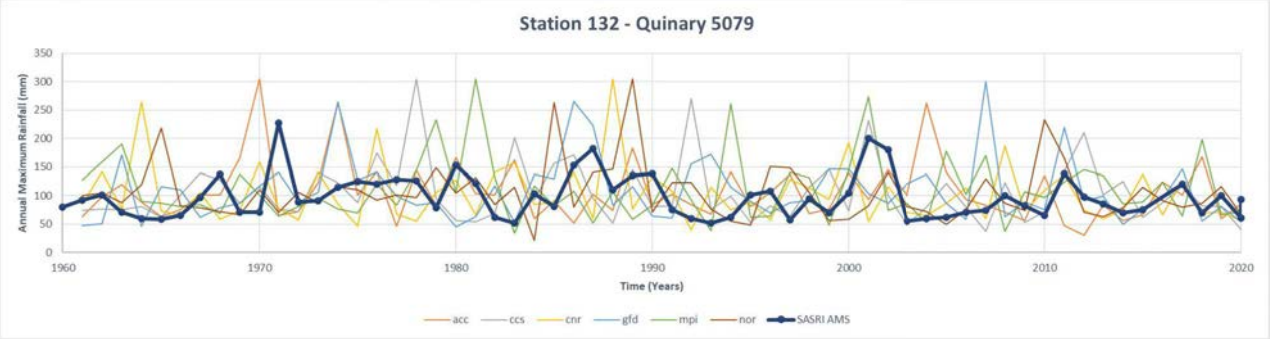

Figure 9.65 Time series of annual maximum rainfall for SASRI station 132 and 6 GCMs for corresponding years

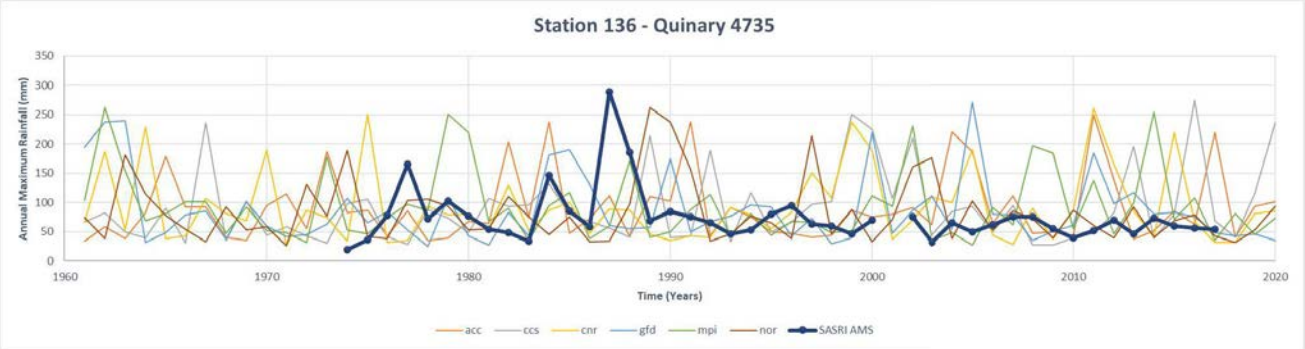

Figure 9.66 Time series of annual maximum rainfall for SASRI station 136 and 6 GCMs for corresponding years

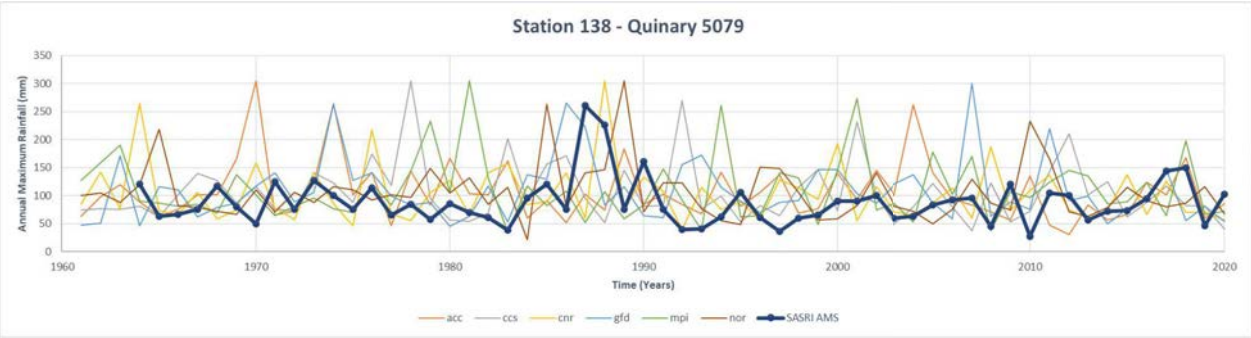

Figure 9.67 Time series of annual maximum rainfall for SASRI station 138 and 6 GCMs for corresponding years

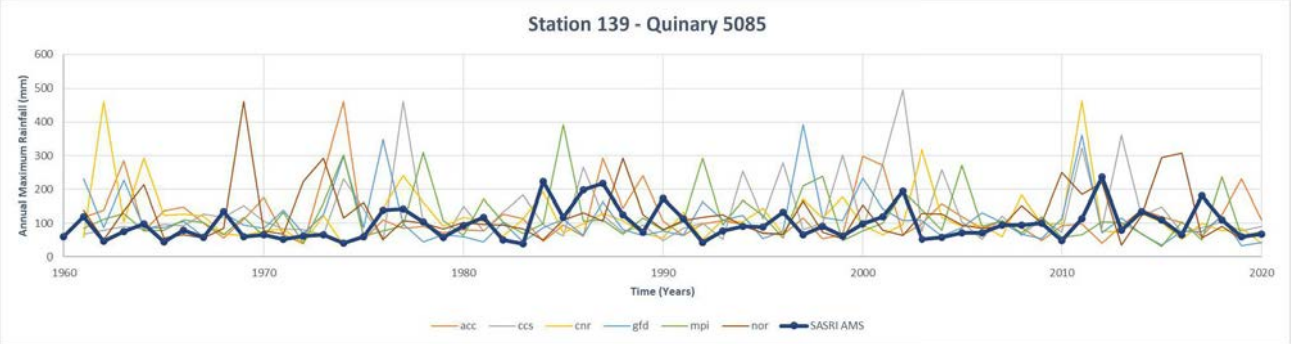

Figure 9.68 Time series of annual maximum rainfall for SASRI station 139 and 6 GCMs for corresponding years

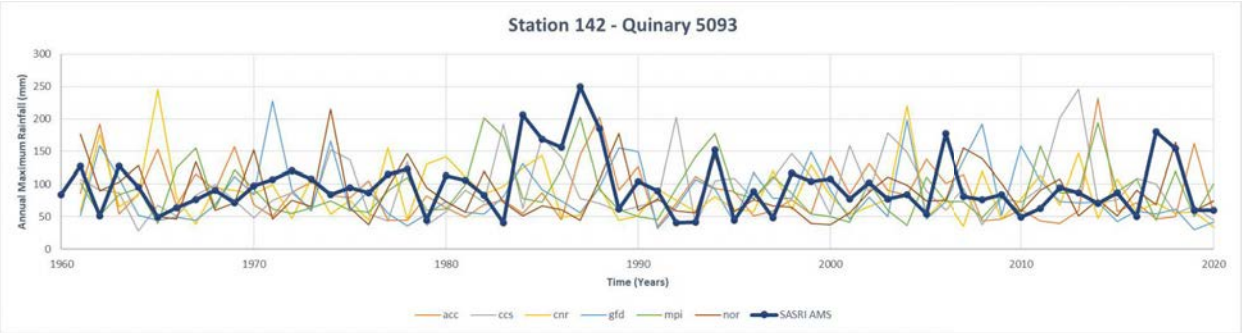

Figure 9.69 Time series of annual maximum rainfall for SASRI station 142 and 6 GCMs for corresponding years

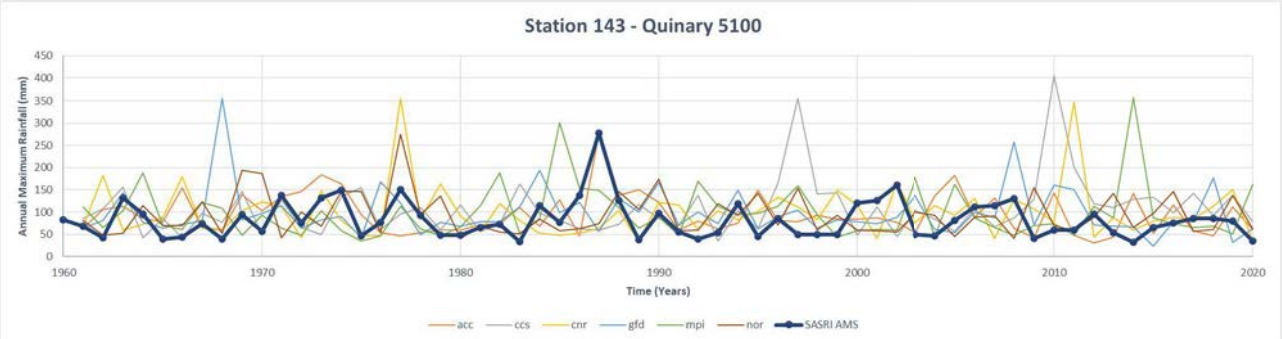

Figure 9.70 Time series of annual maximum rainfall for SASRI station 143 and 6 GCMs for corresponding years

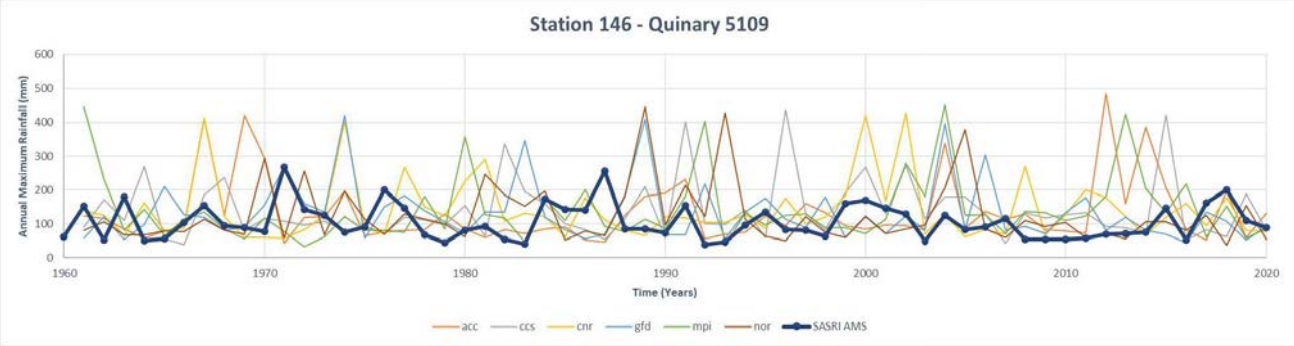

Figure 9.71 Time series of annual maximum rainfall for SASRI station 146 and 6 GCMs for corresponding years

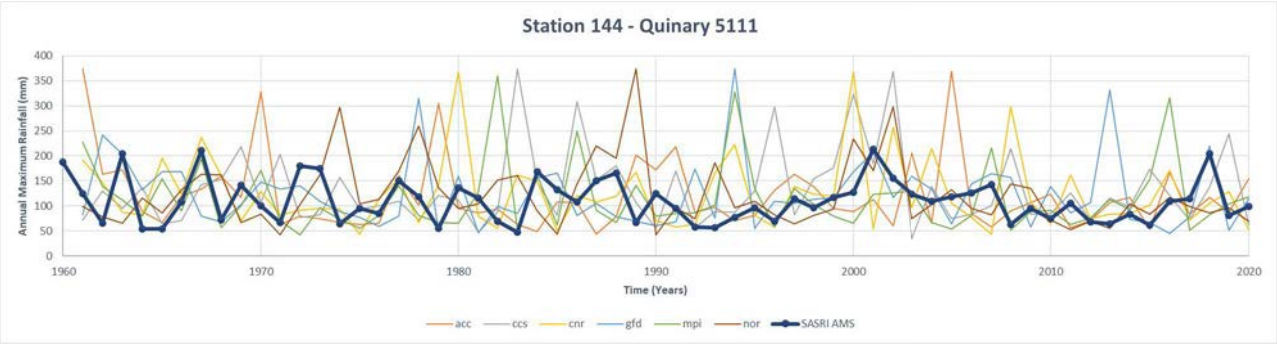

Figure 9.72 Time series of annual maximum rainfall for SASRI station 144 and 6 GCMs for corresponding years

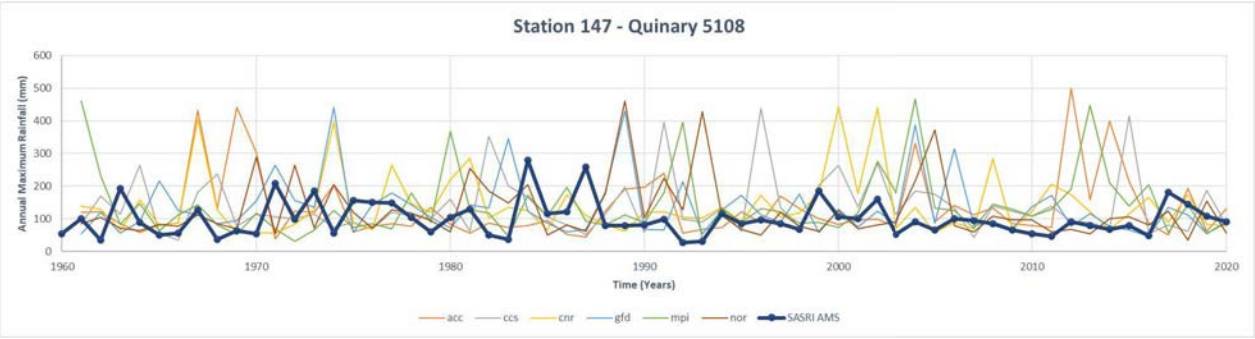

Figure 9.73 Time series of annual maximum rainfall for SASRI station 147 and 6 GCMs for corresponding years

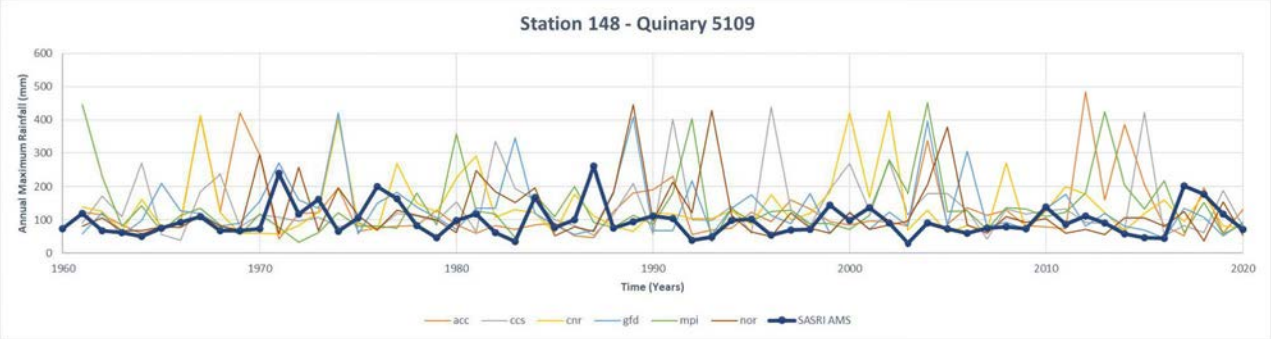

Figure 9.74 Time series of annual maximum rainfall for SASRI station 148 and 6 GCMs for corresponding years

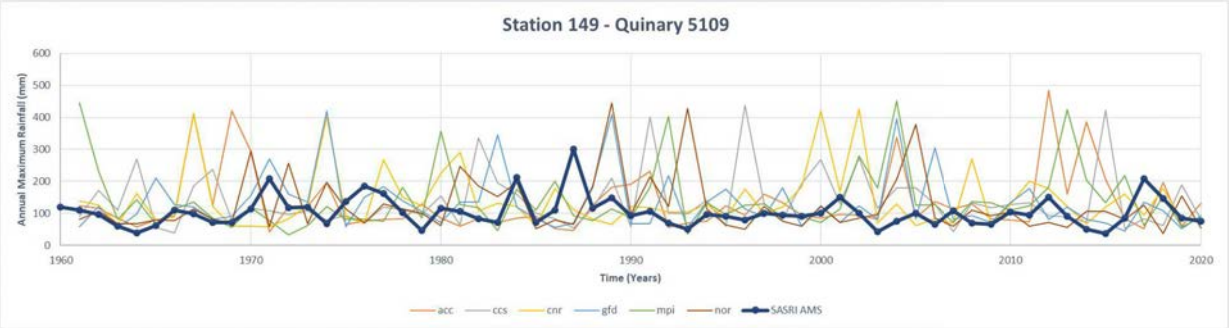

Figure 9.75 Time series of annual maximum rainfall for SASRI station 149 and 6 GCMs for corresponding years

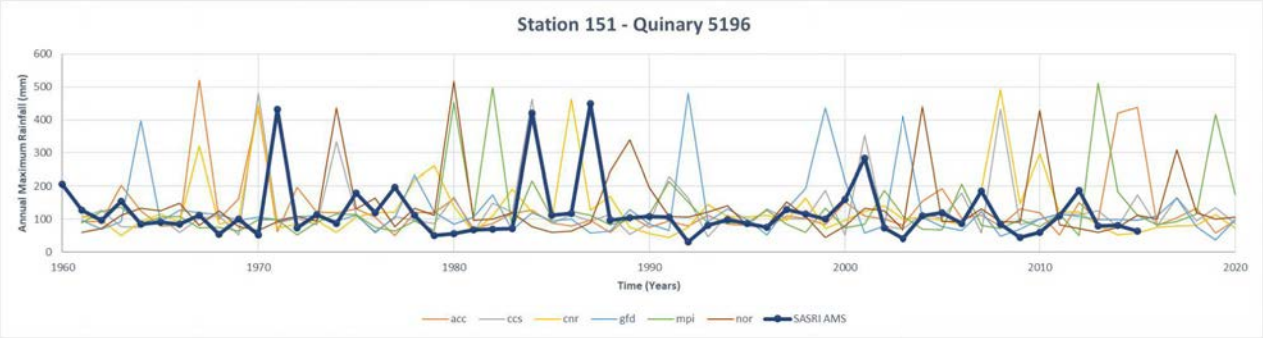

Figure 9.76 Time series of annual maximum rainfall for SASRI station 151 and 6 GCMs for corresponding years

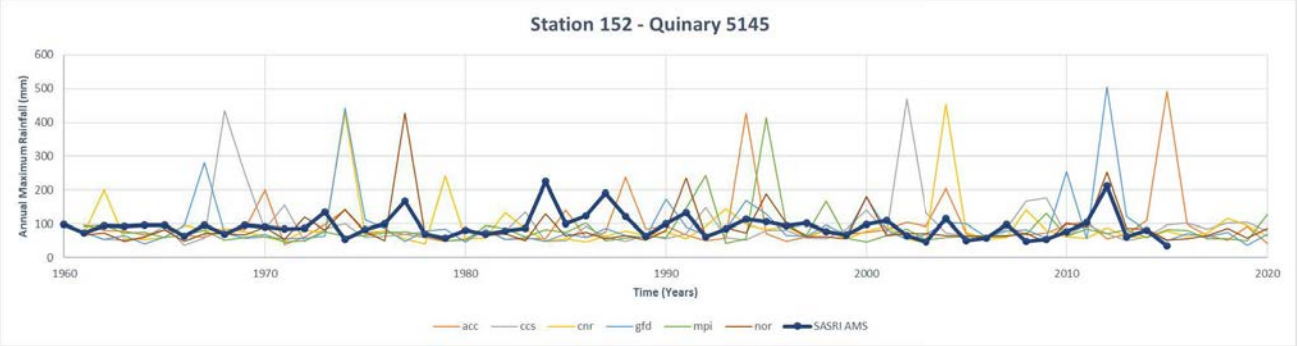

Figure 9.77 Time series of annual maximum rainfall for SASRI station 152 and 6 GCMs for corresponding years

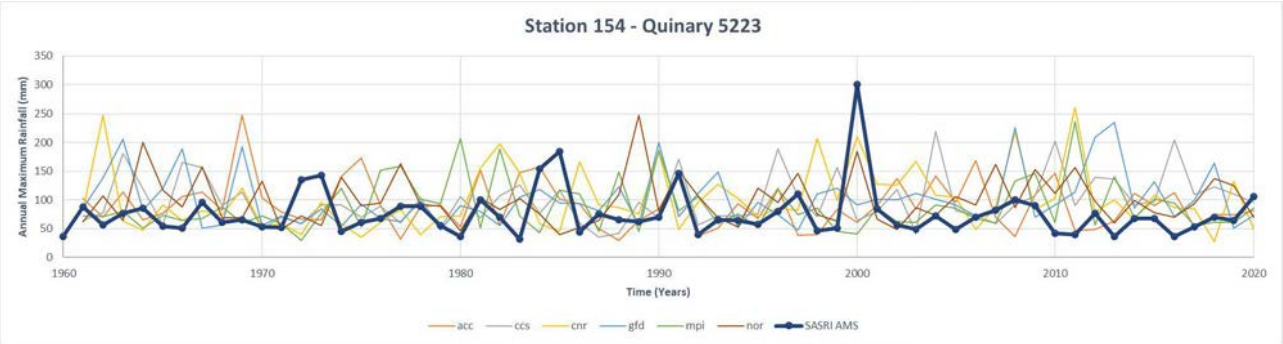

Figure 9.78 Time series of annual maximum rainfall for SASRI station 154 and 6 GCMs for corresponding years

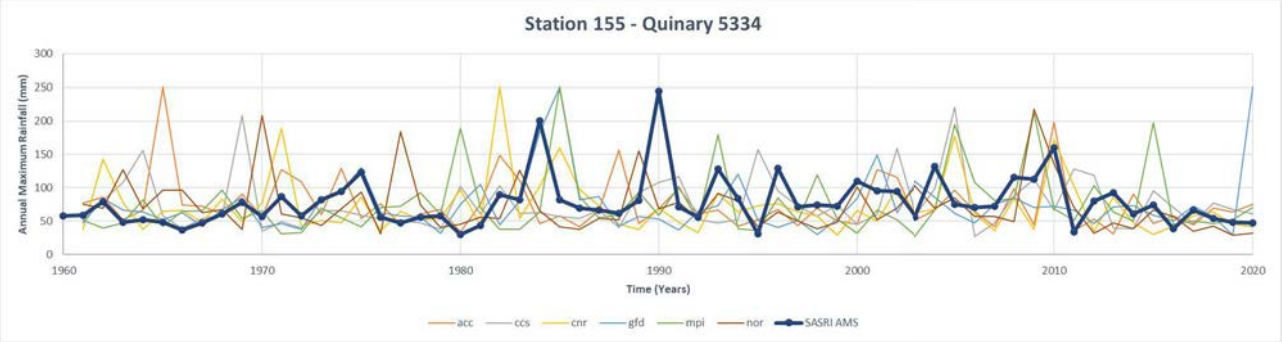

Figure 9.79 Time series of annual maximum rainfall for SASRI station 155 and 6 GCMs for corresponding years

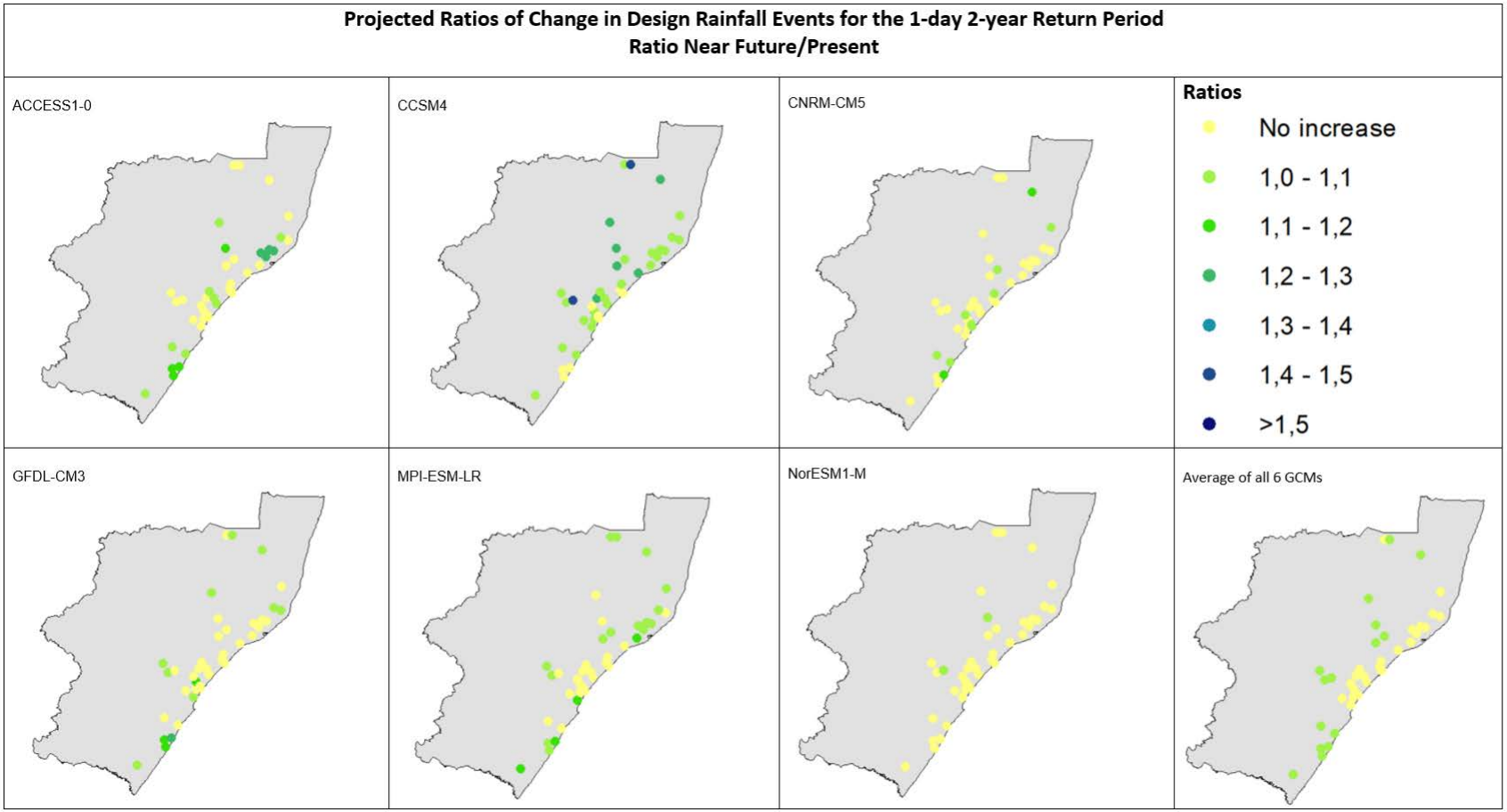

Figure 9.80 Projected changes from the present to the near future in design rainfalls for the 1-day 2-year Return Period derived from outputs from multiple GCMs

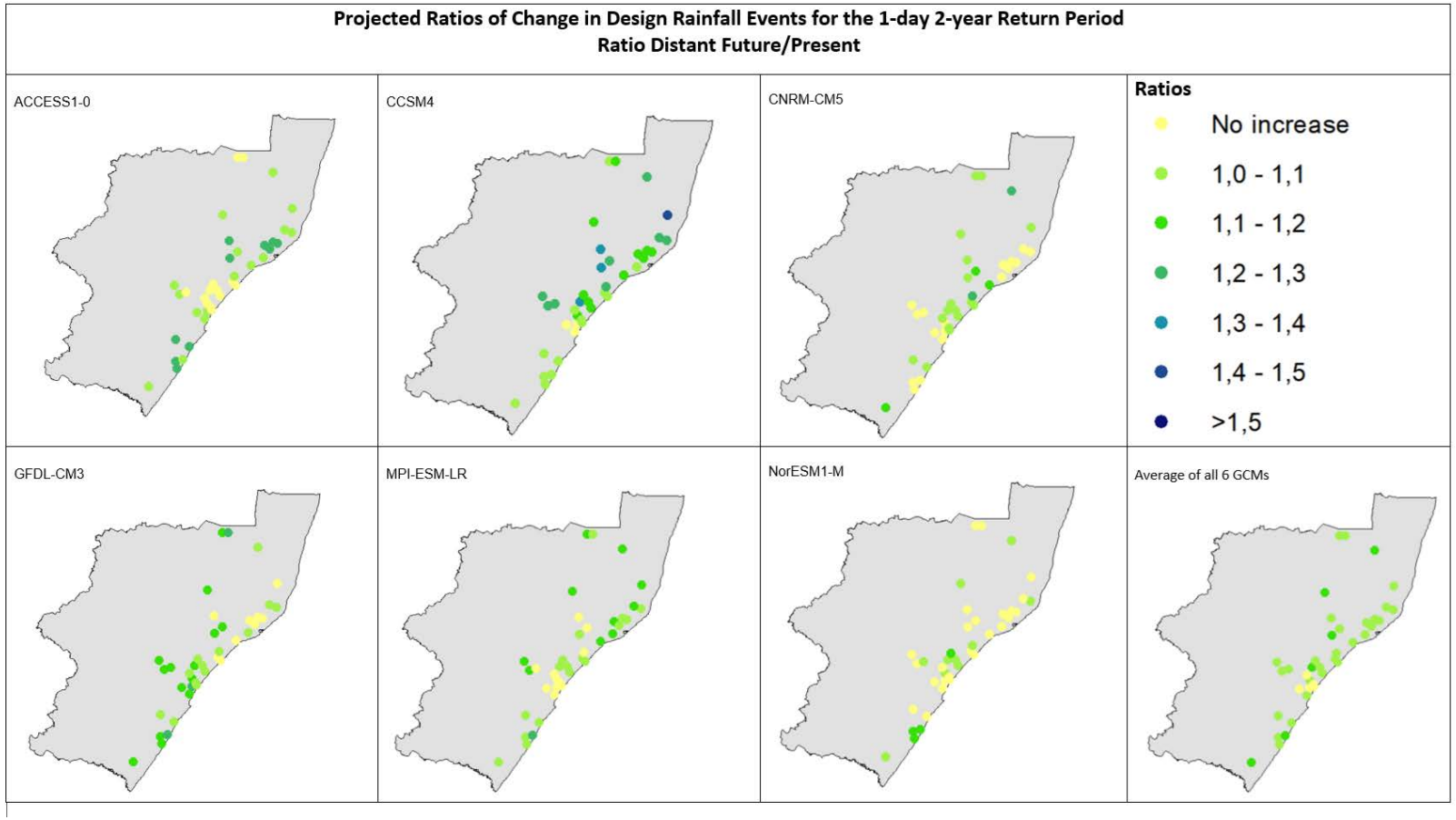

Figure 9.81 Projected changes from the present to the distant future in design rainfalls for the 1-day 2-year Return Period derived from outputs from multiple GCMs

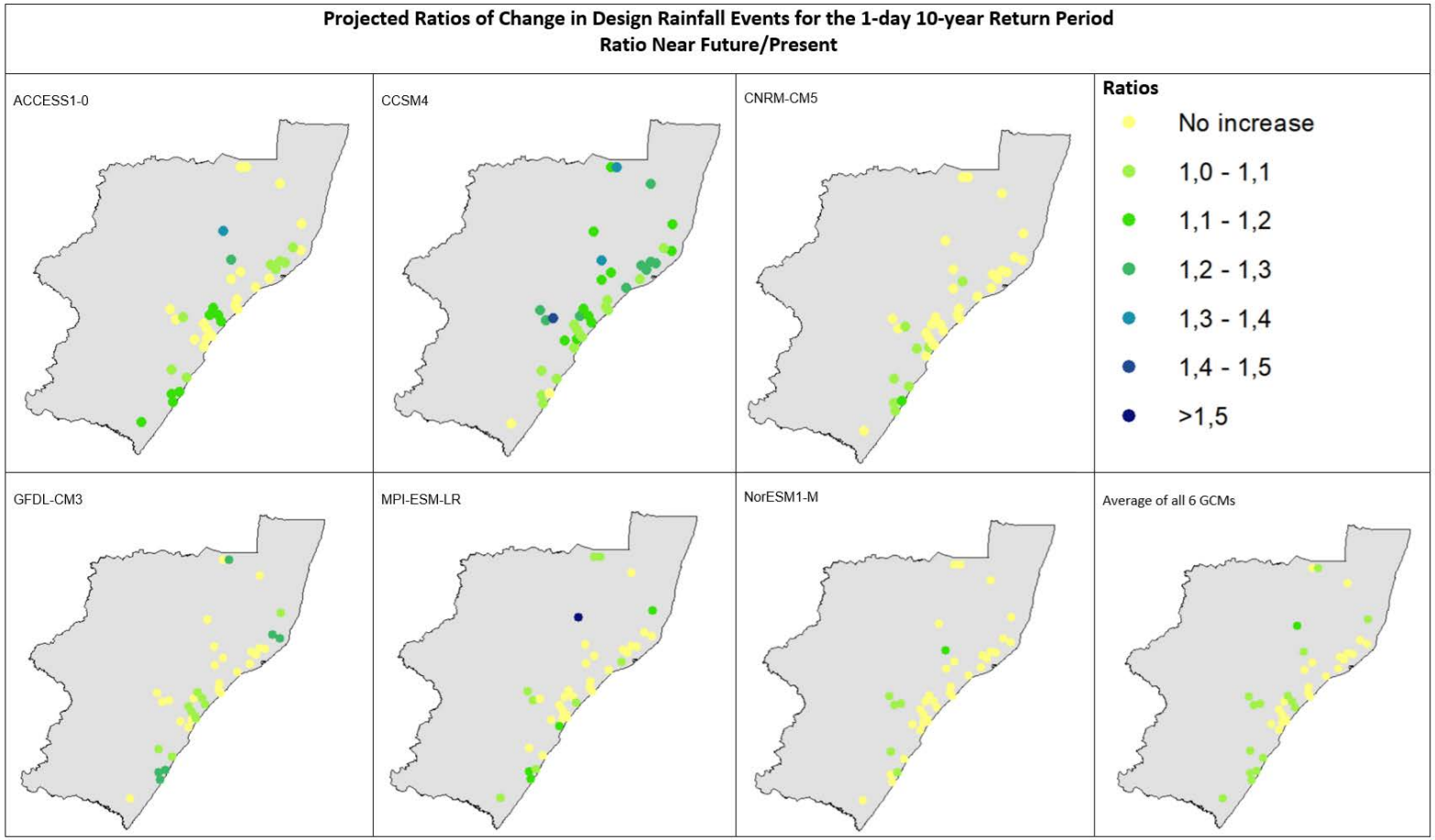

Figure 9.82 Projected changes from the present to the near future in design rainfalls for the 1-day 10-year Return Period derived from outputs from multiple GCMs

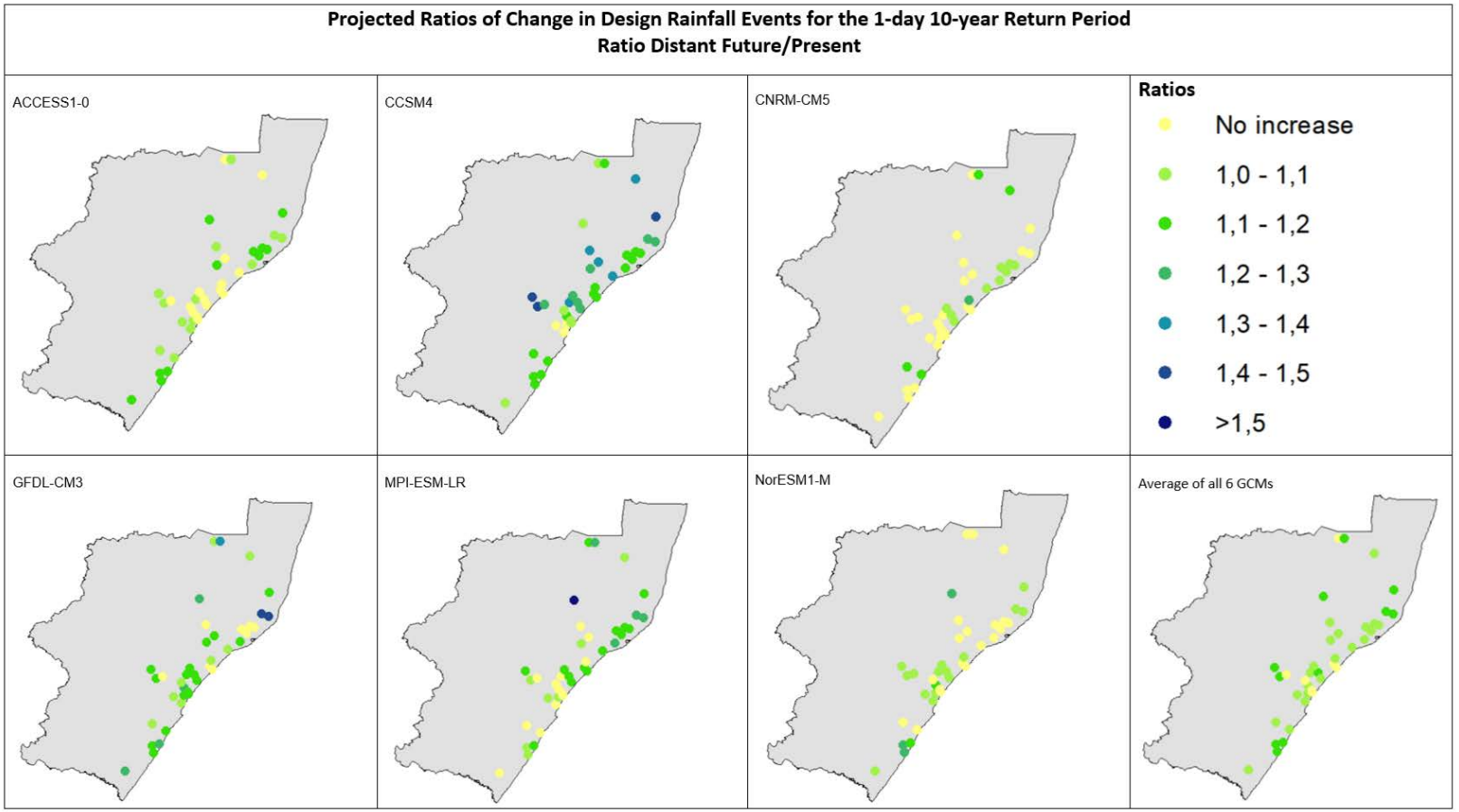

Figure 9.83 Projected changes from the present to the distant future in design rainfalls for the 1-day 10-year Return Period derived from outputs from multiple GCMs

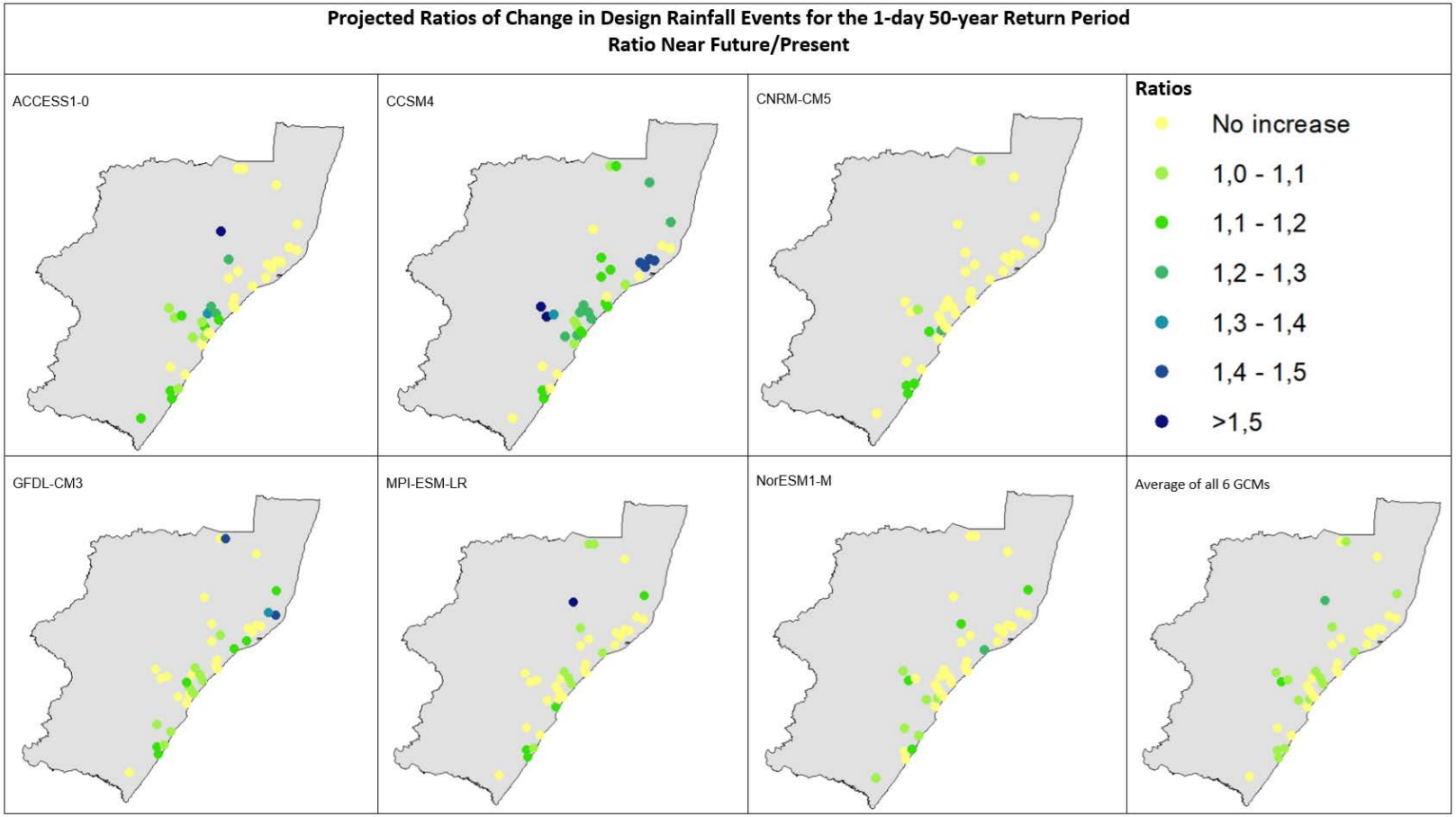

Figure 9.84 Projected changes from the present to the near future in design rainfalls for the 1-day 50-year Return Period derived from outputs from multiple GCMs

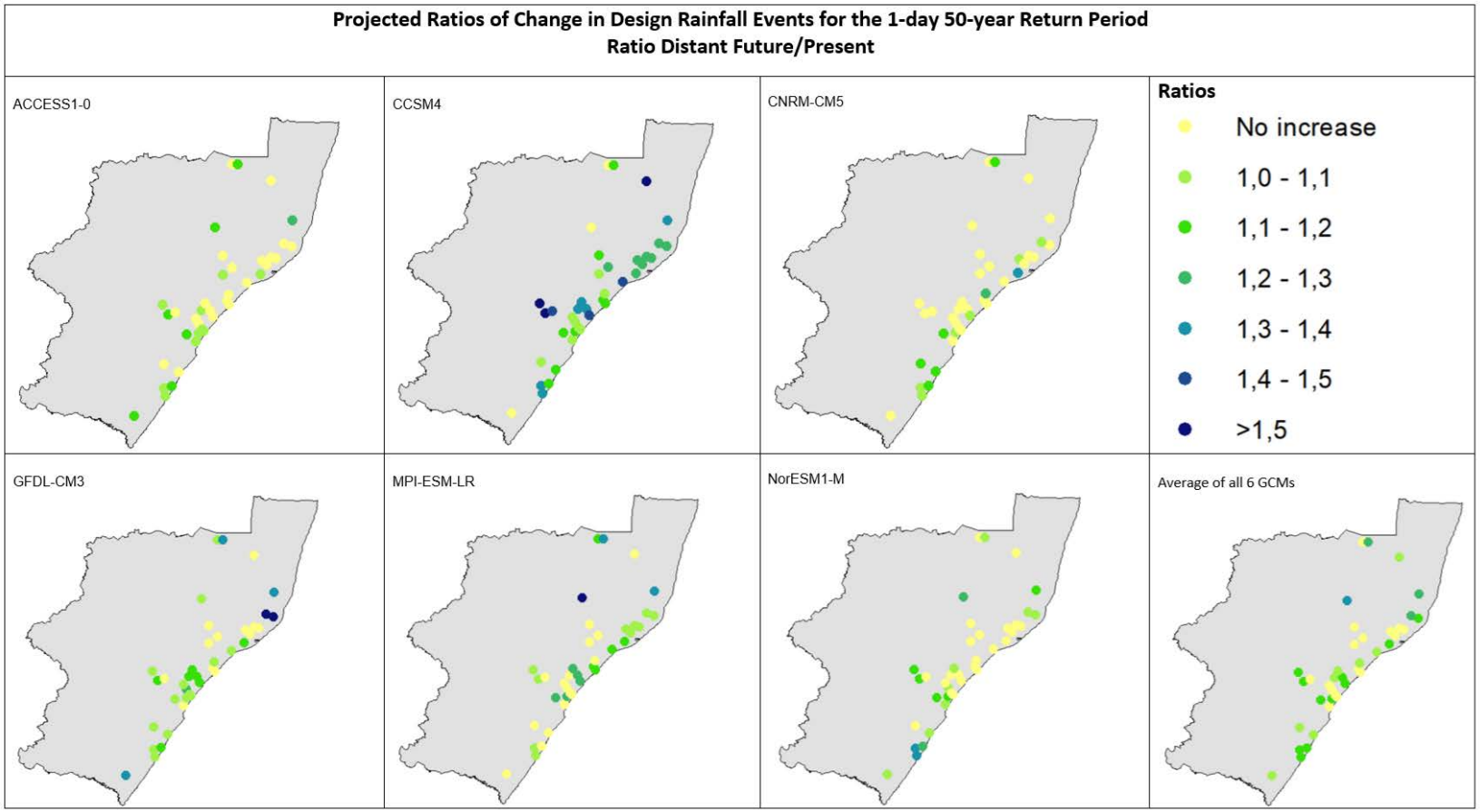

Figure 9.85 Projected changes from the present to the distant future in design rainfalls for the 1-day 50-year Return Period derived from outputs from multiple GCMs

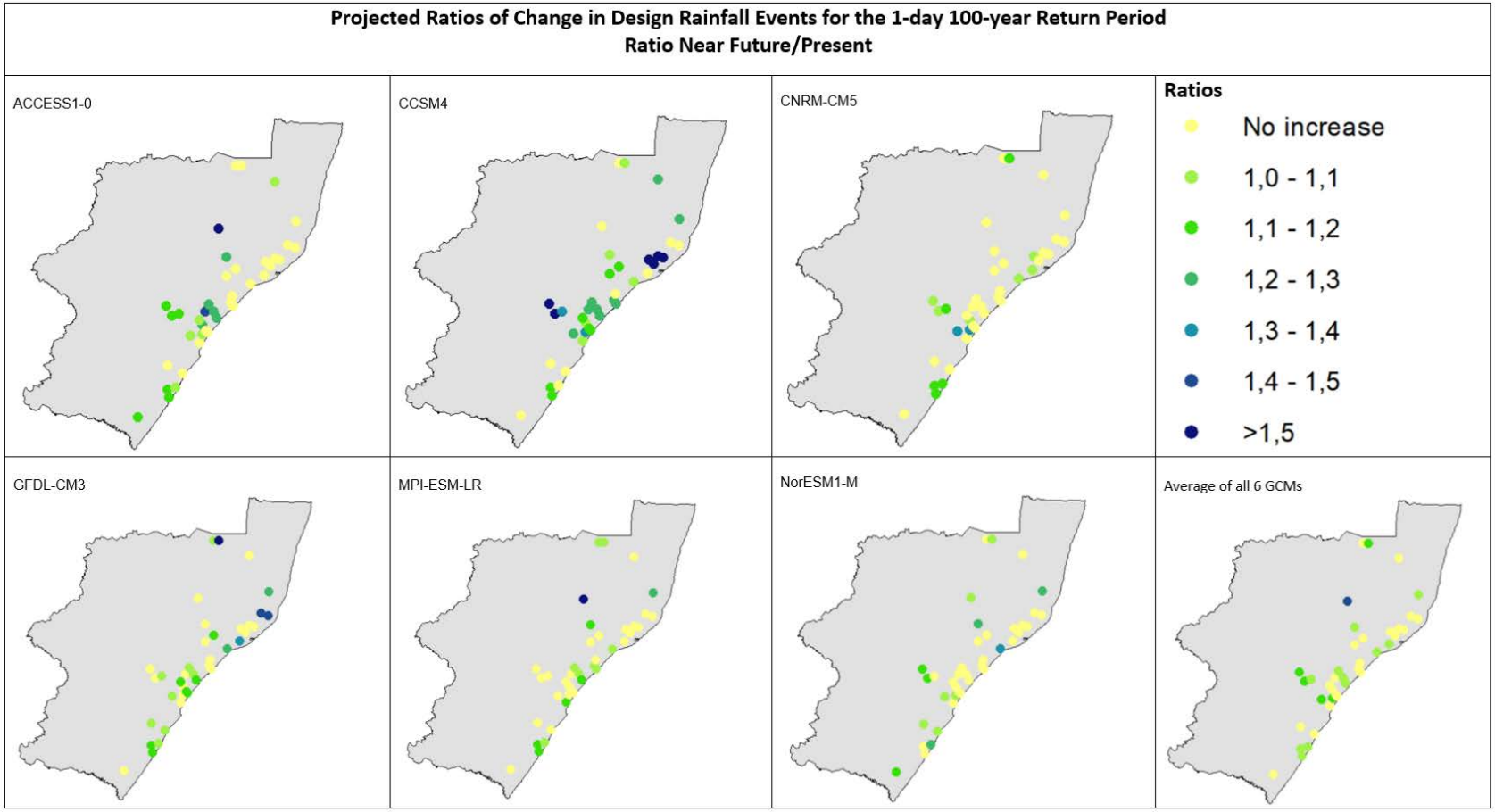

Figure 9.86 Projected changes from the present to the near future in design rainfalls for the 1-day 100-year Return Period derived from outputs from multiple GCMs

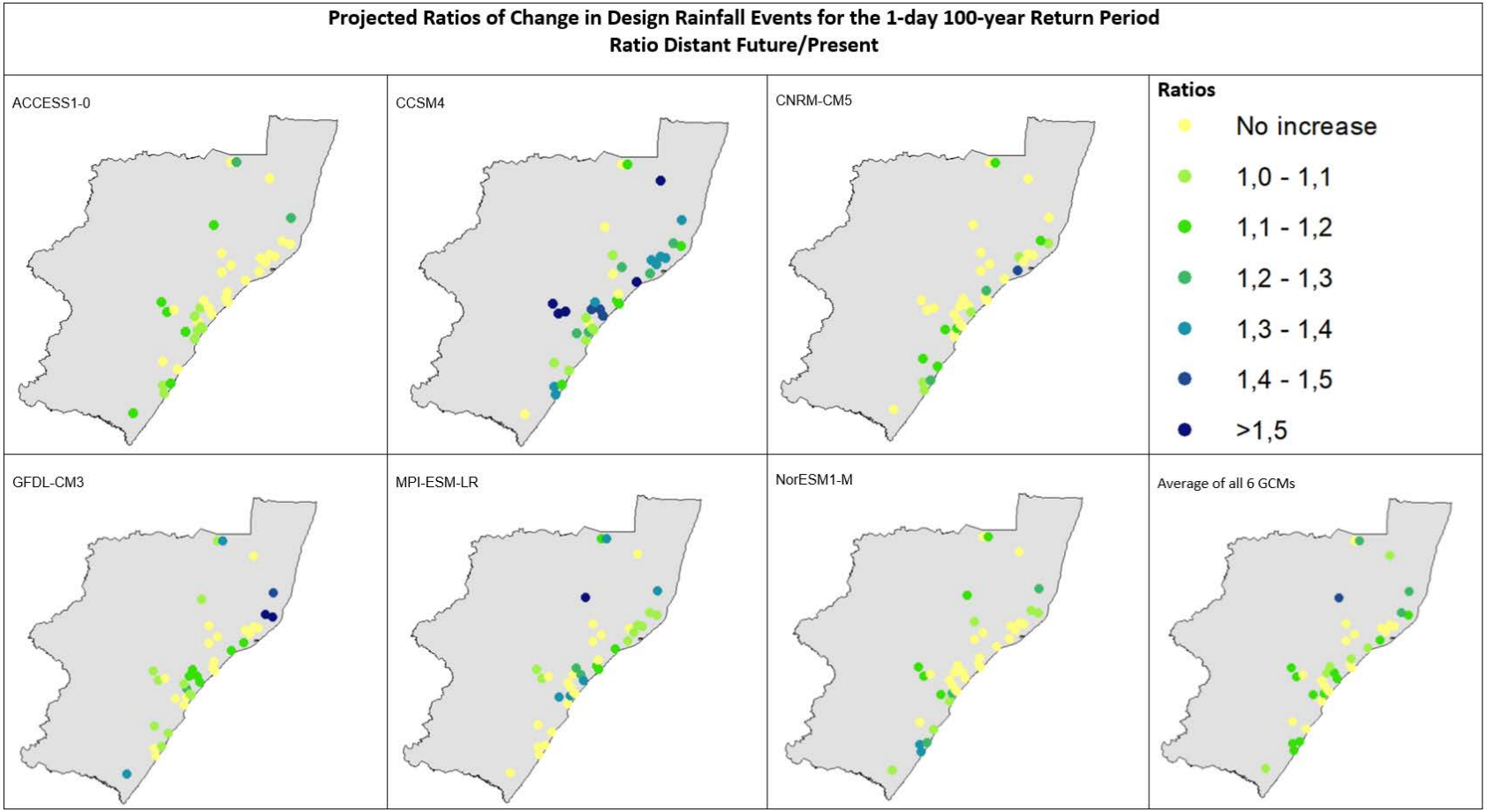

Figure 9.87 Projected changes from the present to the distant future in design rainfalls for the 1-day 100-year Return Period derived from outputs from multiple GCMs

10. APPENDIX C: Non-stationary Frequency Analysis of Extreme Floods in KwaZulu-Natal

a)

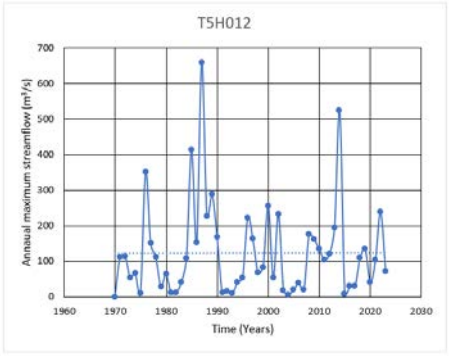
T5H012
Annaul maximum streamflow (m³/s)
Time (Years)

b)

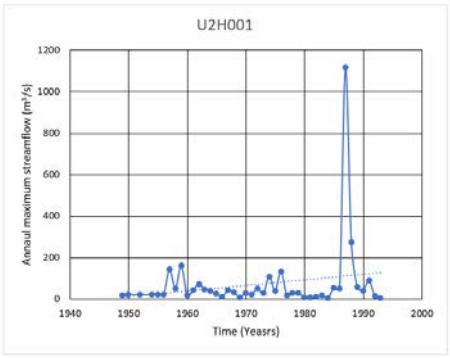
U2H001
Annaul maximum streamflow (m³/s)
Time (Yeasrs)

c)

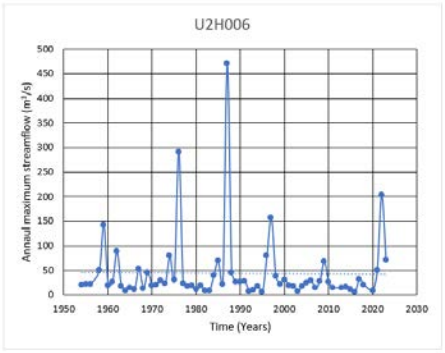
U2H006
Annaul maximum streamflow (m³/s)
Time (Years)

d)

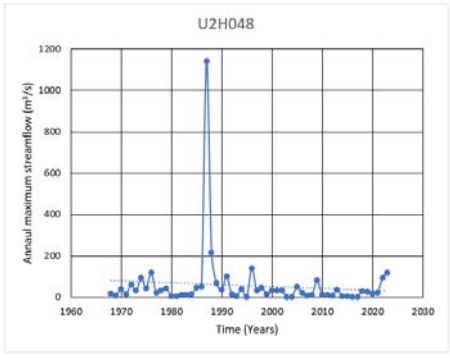
U2H048
Annaul maximum streamflow (m³/s)
Time (Years)

e)

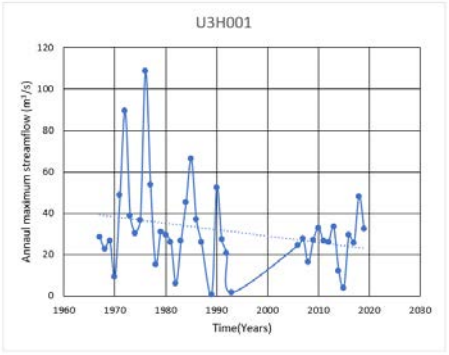
U3H001
Annaul maximum streamflow (m³/s)
Time(Years)

f)

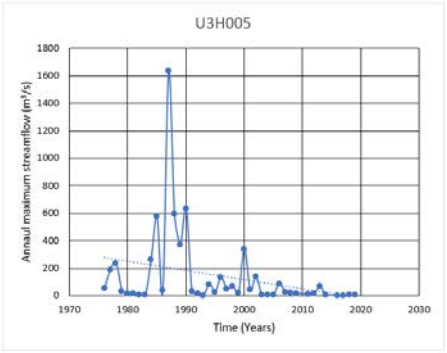
U3H005
Annaul maximum streamflow (m³/s)
Time (Years)

g)

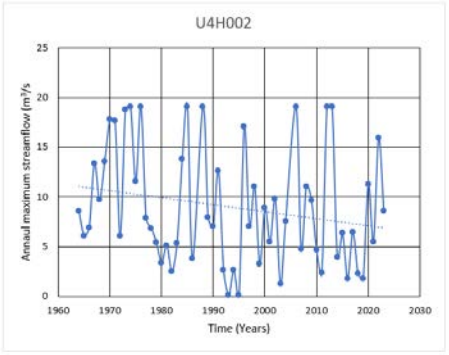
U4H002
Annaul maximum streamflow (m³/s
Time (Years)

h)

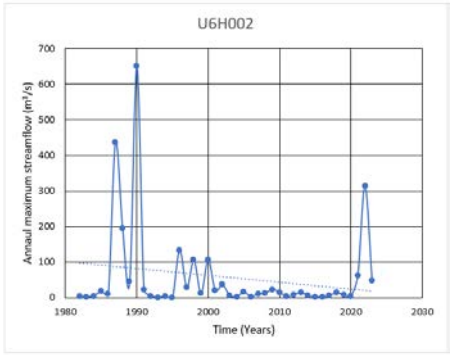
U6H002
Annaul maximum streamflow (m³/s)
Time (Years)

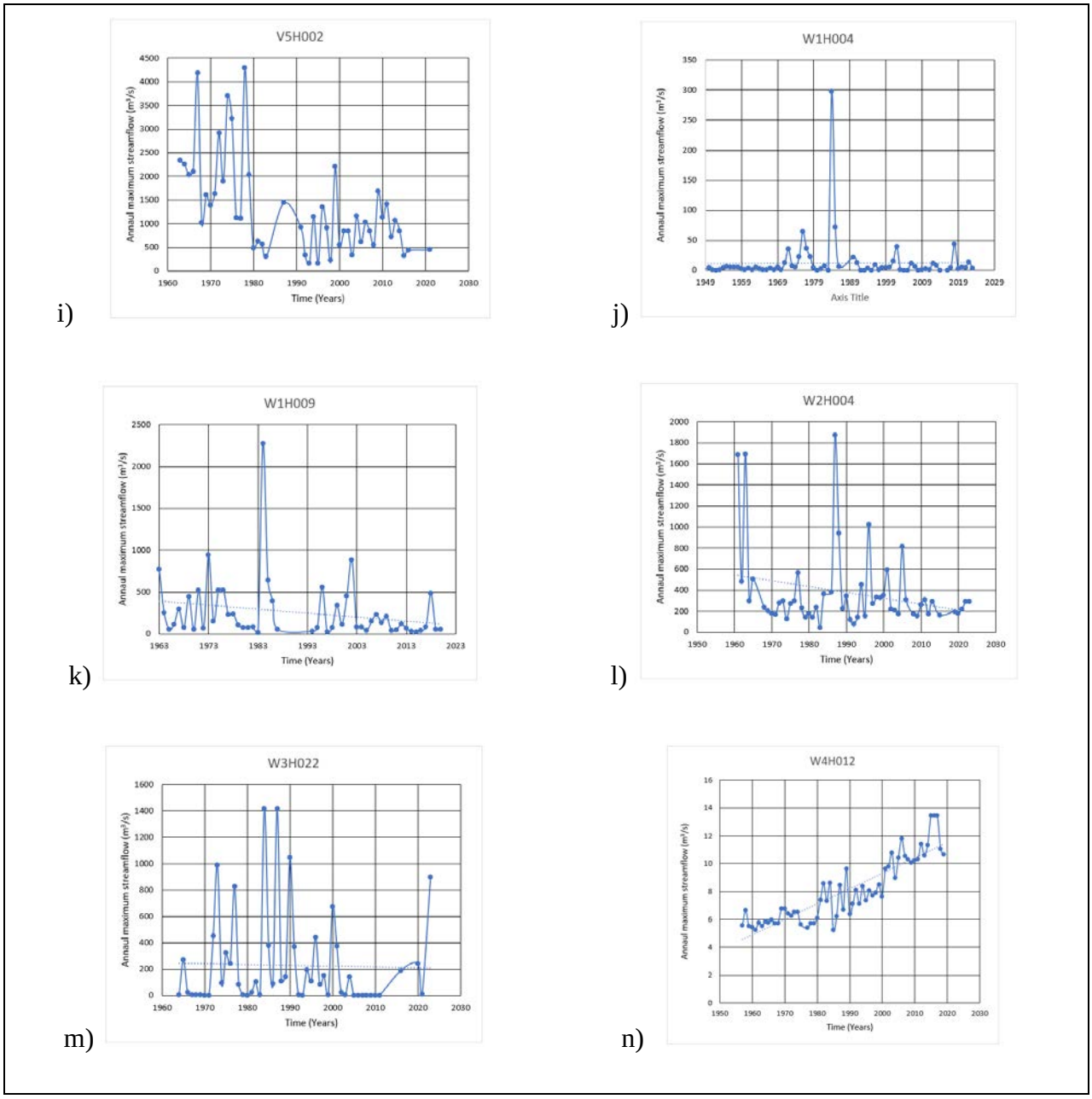

Figure 10.1 Time series of annual streamflows at stations along the East Coast of KwaZulu-Natal

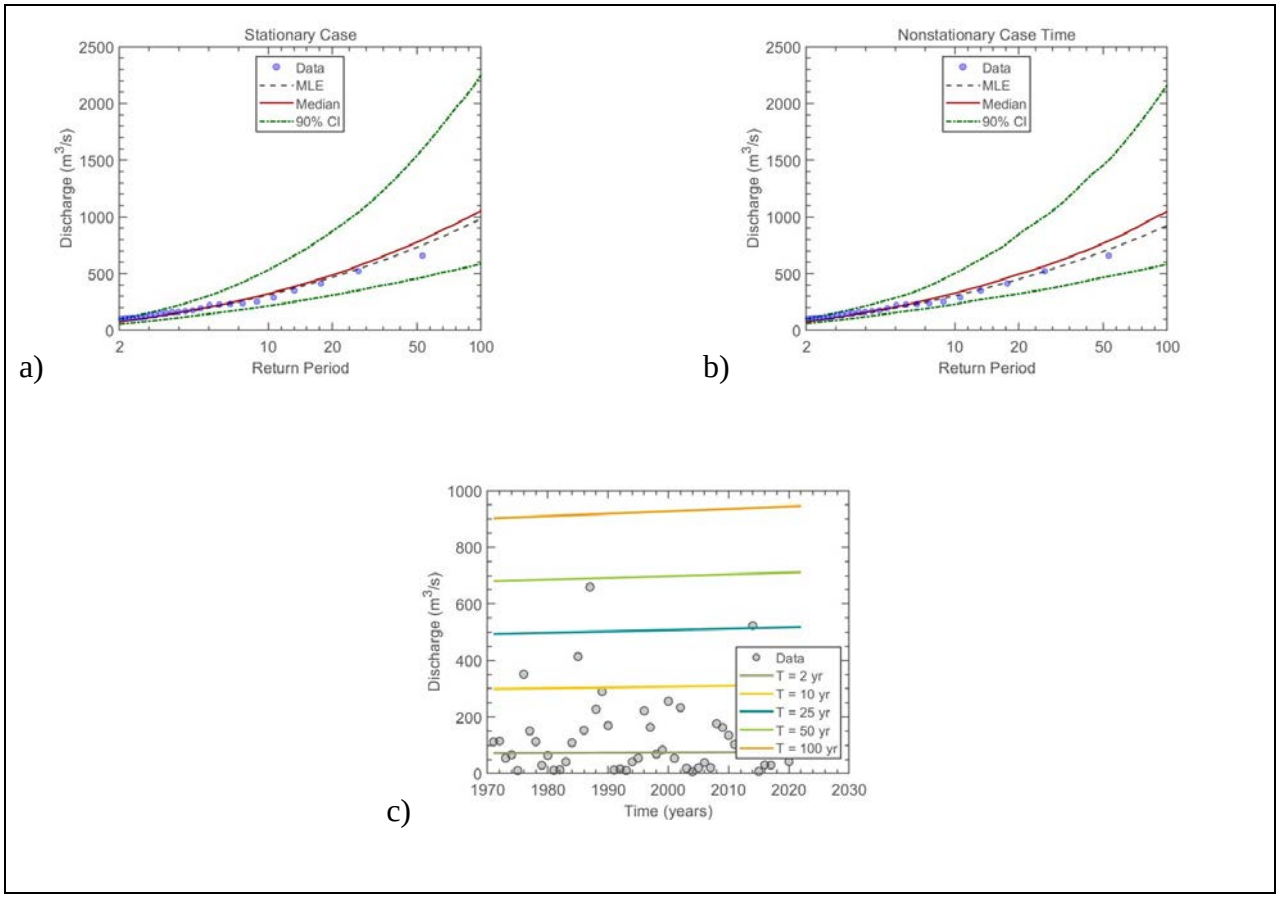

Figure 10.2 The LP3 (a) stationary model, (b) non-stationary model considering time as a covariate, and (c) effective return period as a function of time for Station: T5H012

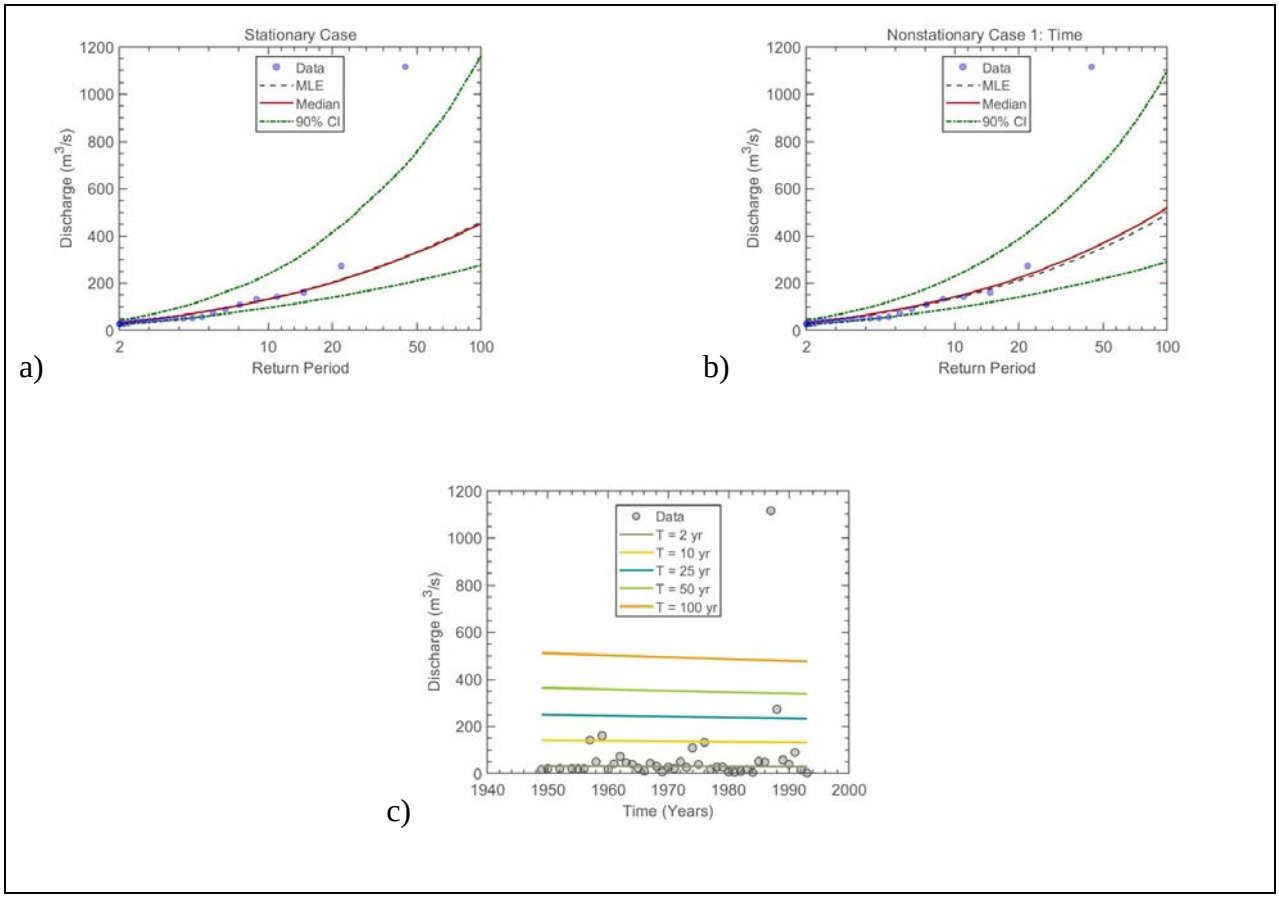

Figure 10.3 LP3 (a) stationary model, (b) non-stationary model considering time as a covariate, and (c) effective return period as a function of time for Station: U2H001

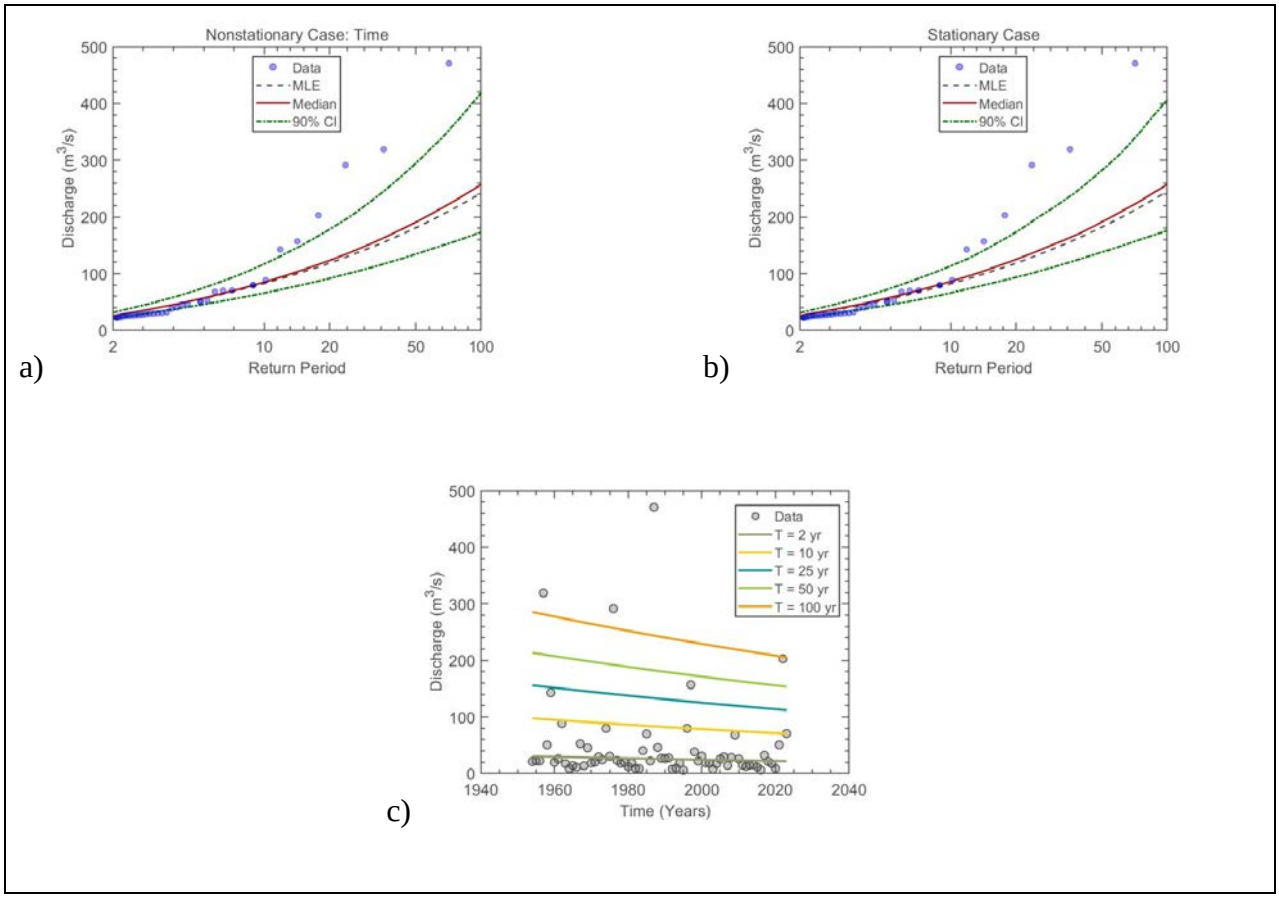

Figure 10.4 LP3 (a) stationary model, (b) non-stationary model considering time as a covariate, and (c) effective return period as a function of time for Station: U2H006

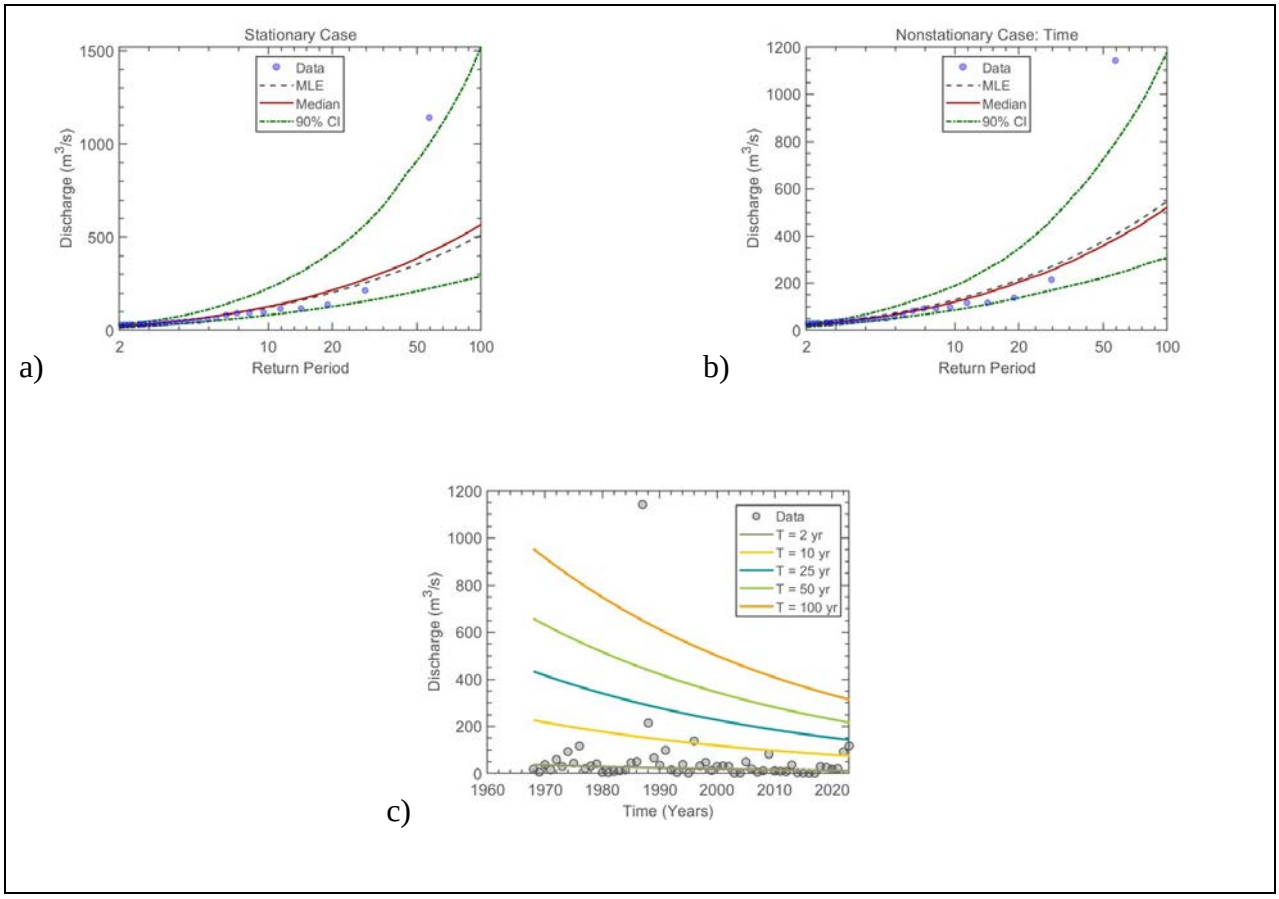

Figure 10.5 LP3 (a) stationary model, (b) non-stationary model considering time as a covariate, and (c) effective return period as a function of time for Station: U2H048

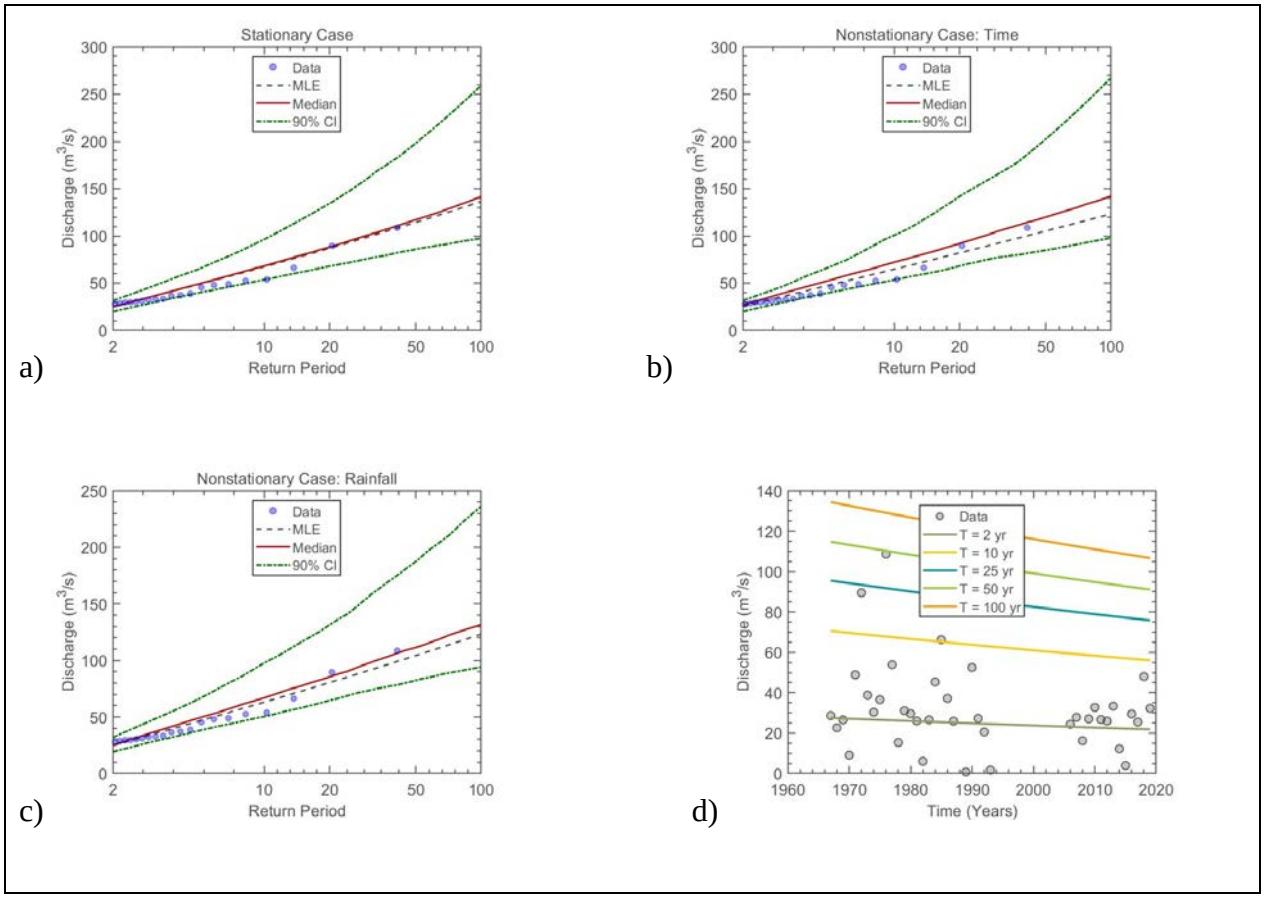

Figure 10.6 LP3 (a) stationary model, (b) non-stationary model considering time as a covariate, (c) non-stationary model considering rainfall as a covariate, and (d) effective return period as a function of time for Station:U3H001

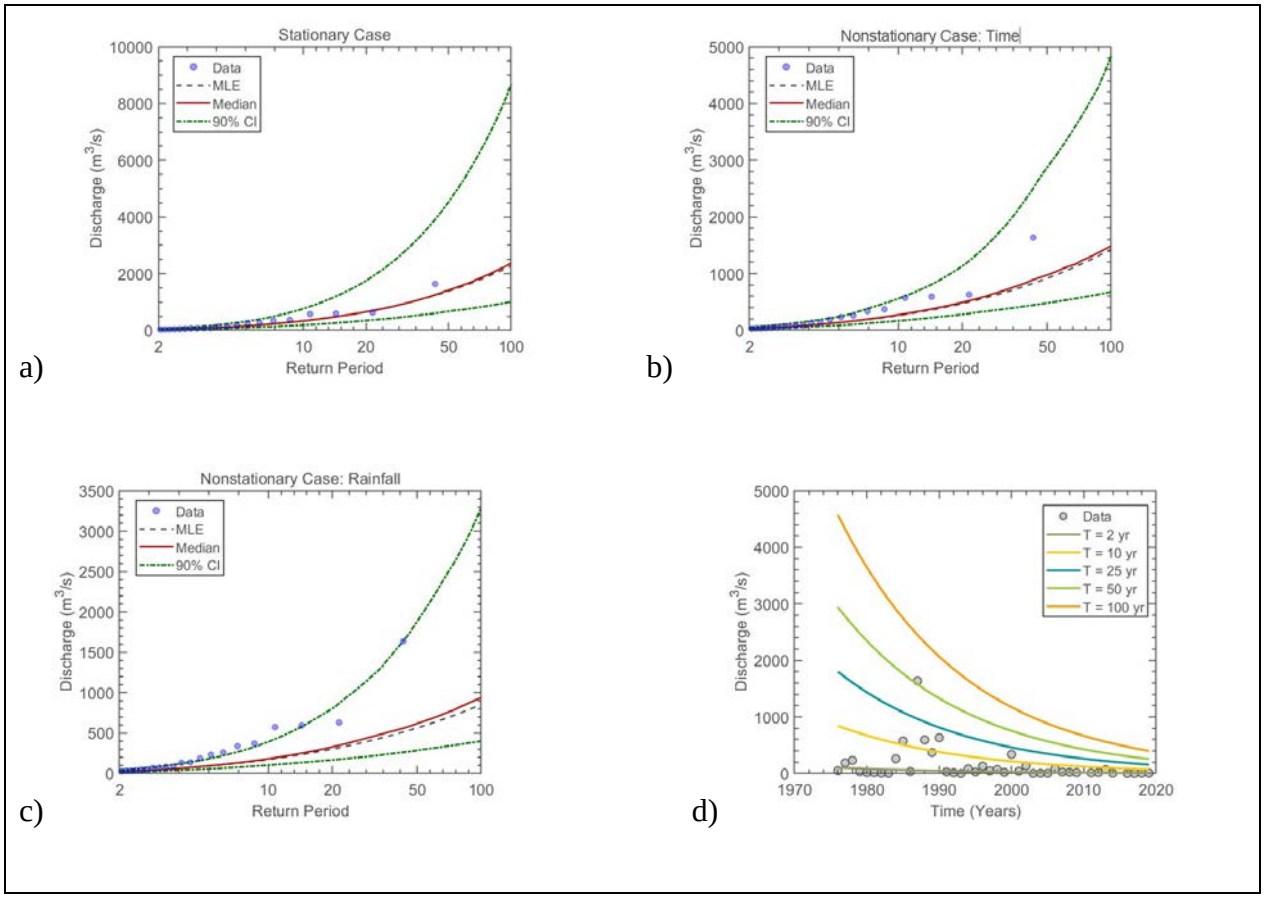

Figure 10.7 LP3 (a) stationary model, (b) non-stationary model considering time as a covariate, (c) non-stationary model considering rainfall as a covariate, and (d) effective return period as a function of time for Station:U3H005

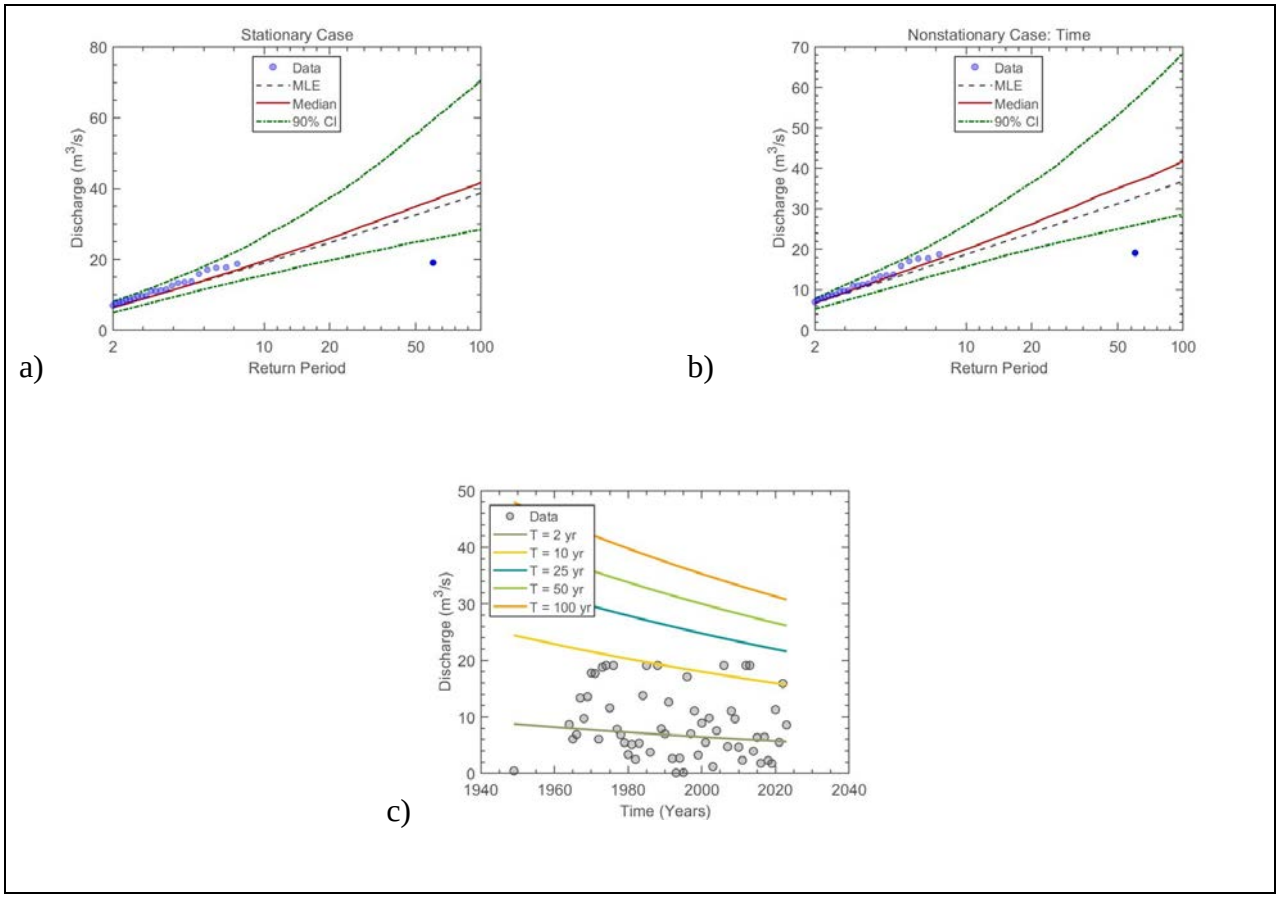

Figure 10.8 LP3 (a) stationary model, (b) non-stationary model considering time as a covariate, and (c) effective return period as a function of time for Station: U4H002

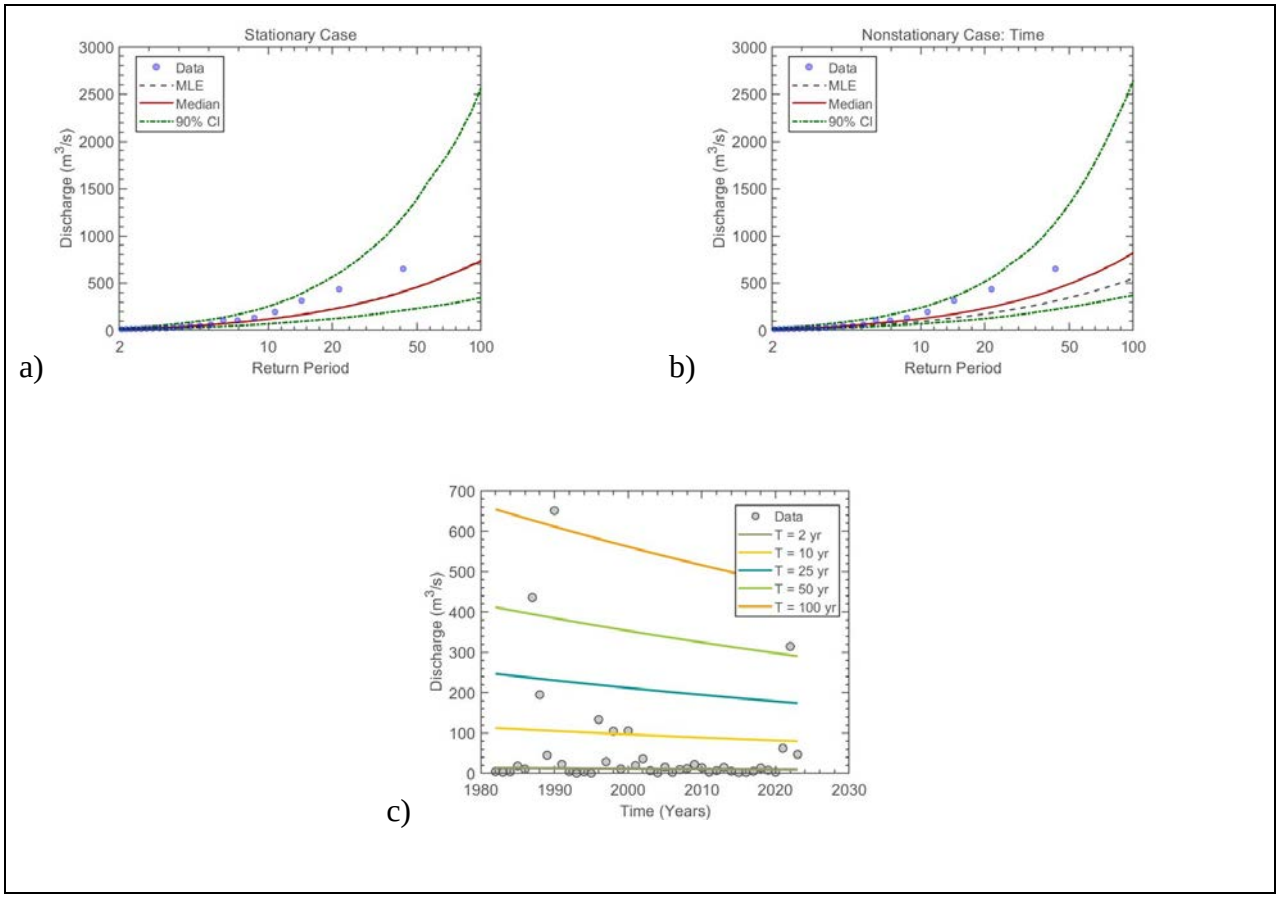

Figure 10.9 LP3 (a) stationary model, (b) non-stationary model considering time as a covariate, and (c) effective return period as a function of time for Station: U6H003

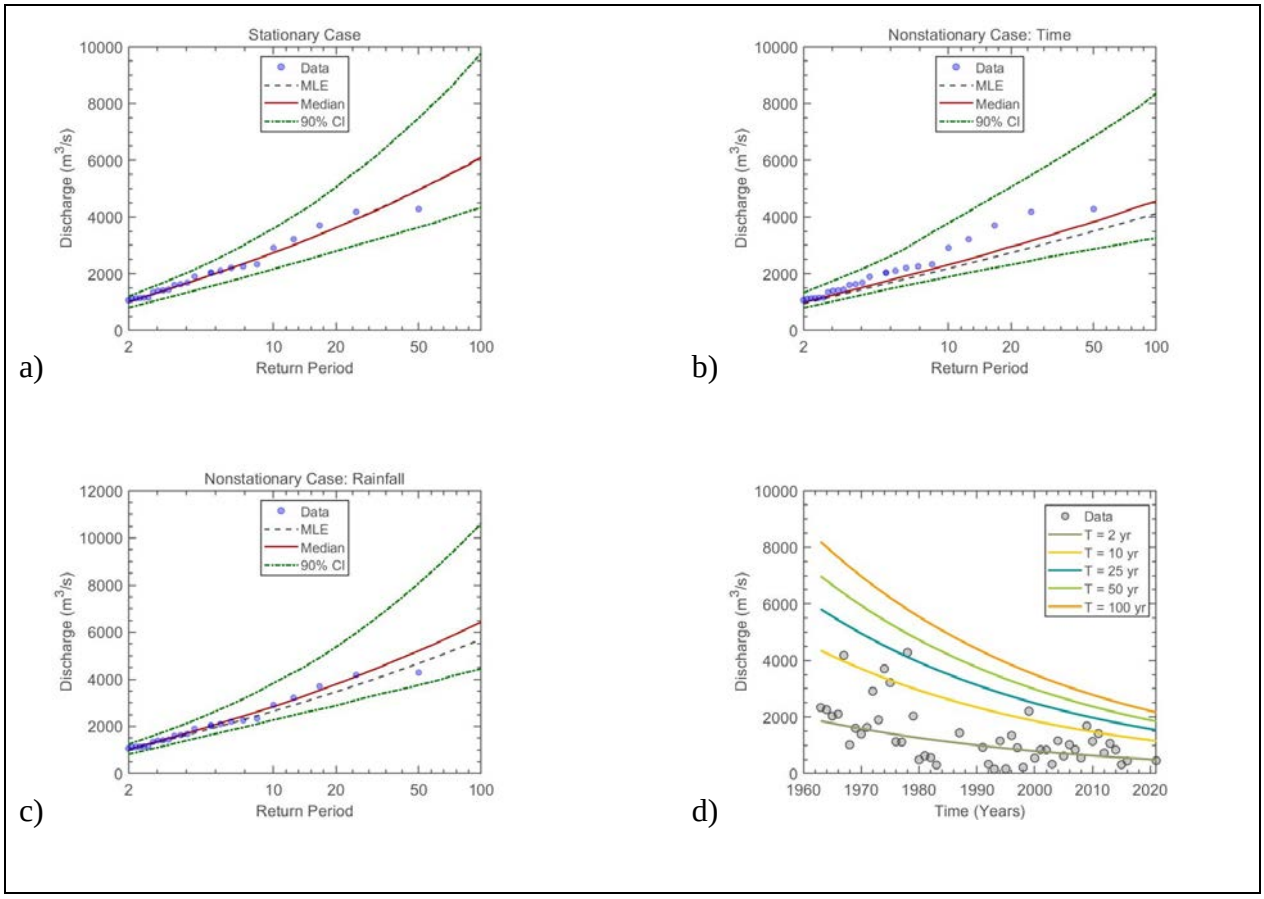

Figure 10.10 LP3 (a) stationary model, (b) non-stationary model considering time as a covariate, (c) non-stationary model considering rainfall as a covariate, and (d) effective return period as a function of time for Station:V5H002

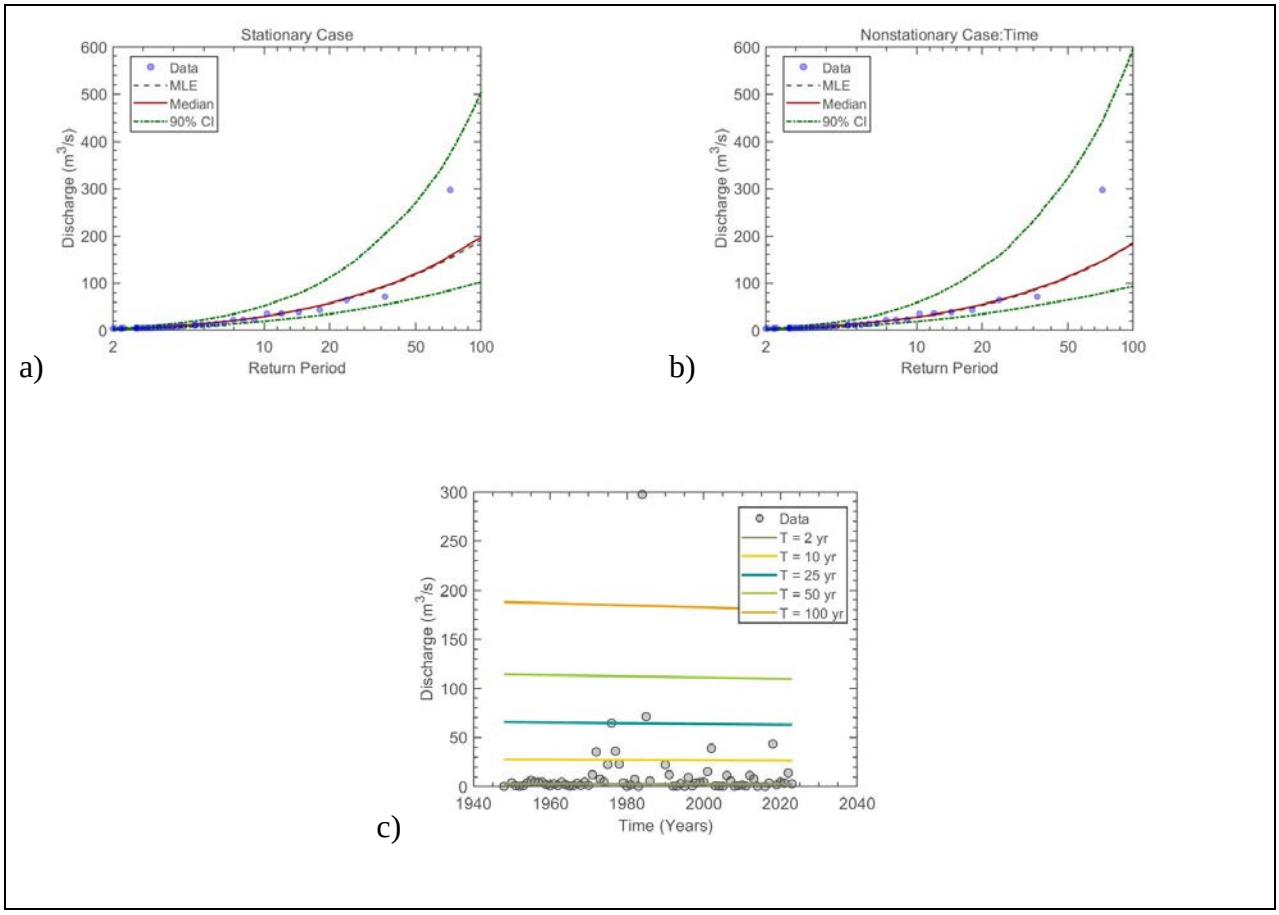

Figure 10.11 LP3 (a) stationary model, (b) non-stationary model considering time as a covariate, and (c) effective return period as a function of time for Station: W1H004

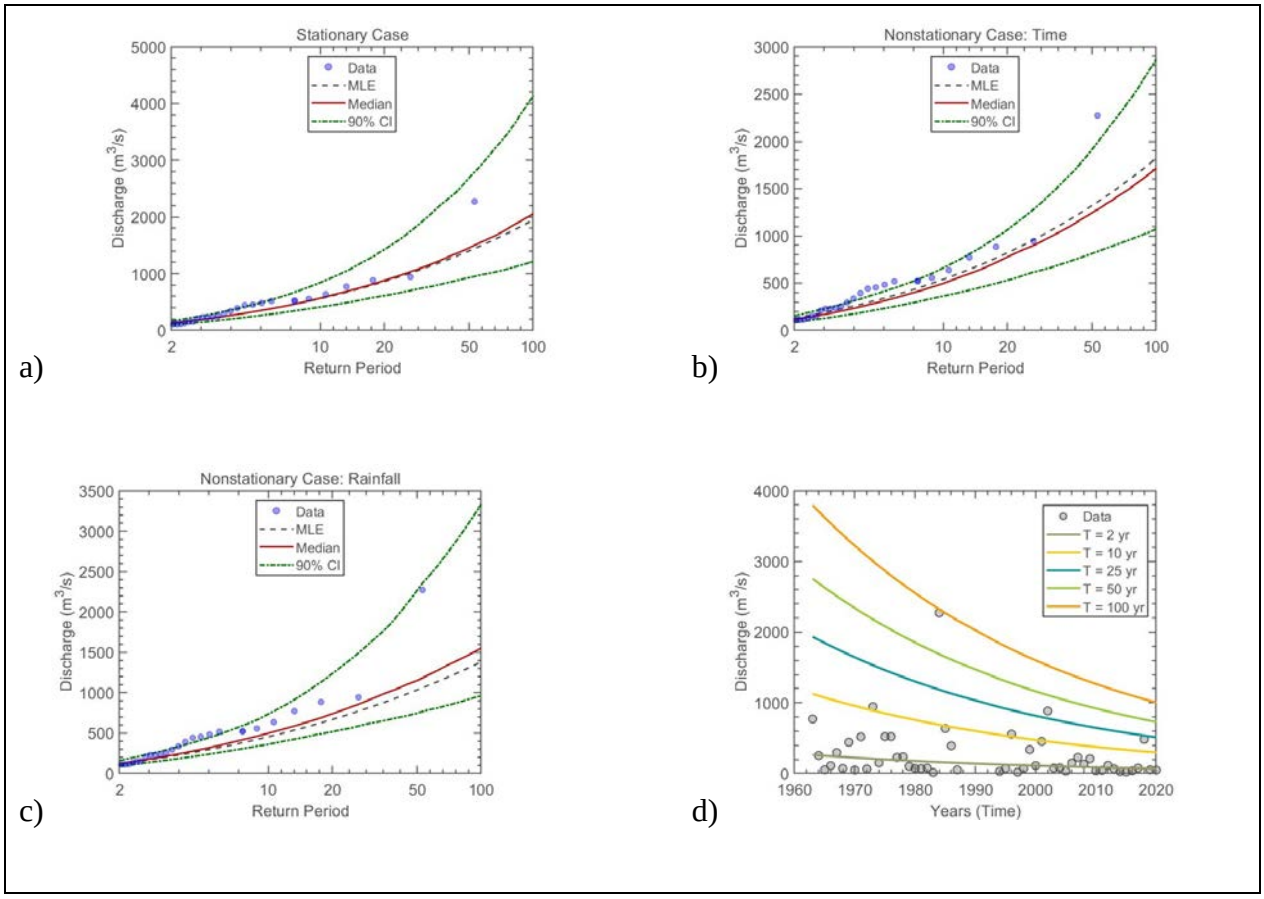

Figure 10.12 LP3 (a) stationary model, (b) non-stationary model considering time as a covariate, (c) non-stationary model considering rainfall as a covariate, and (d) effective return period as a function of time for Station:W1H009

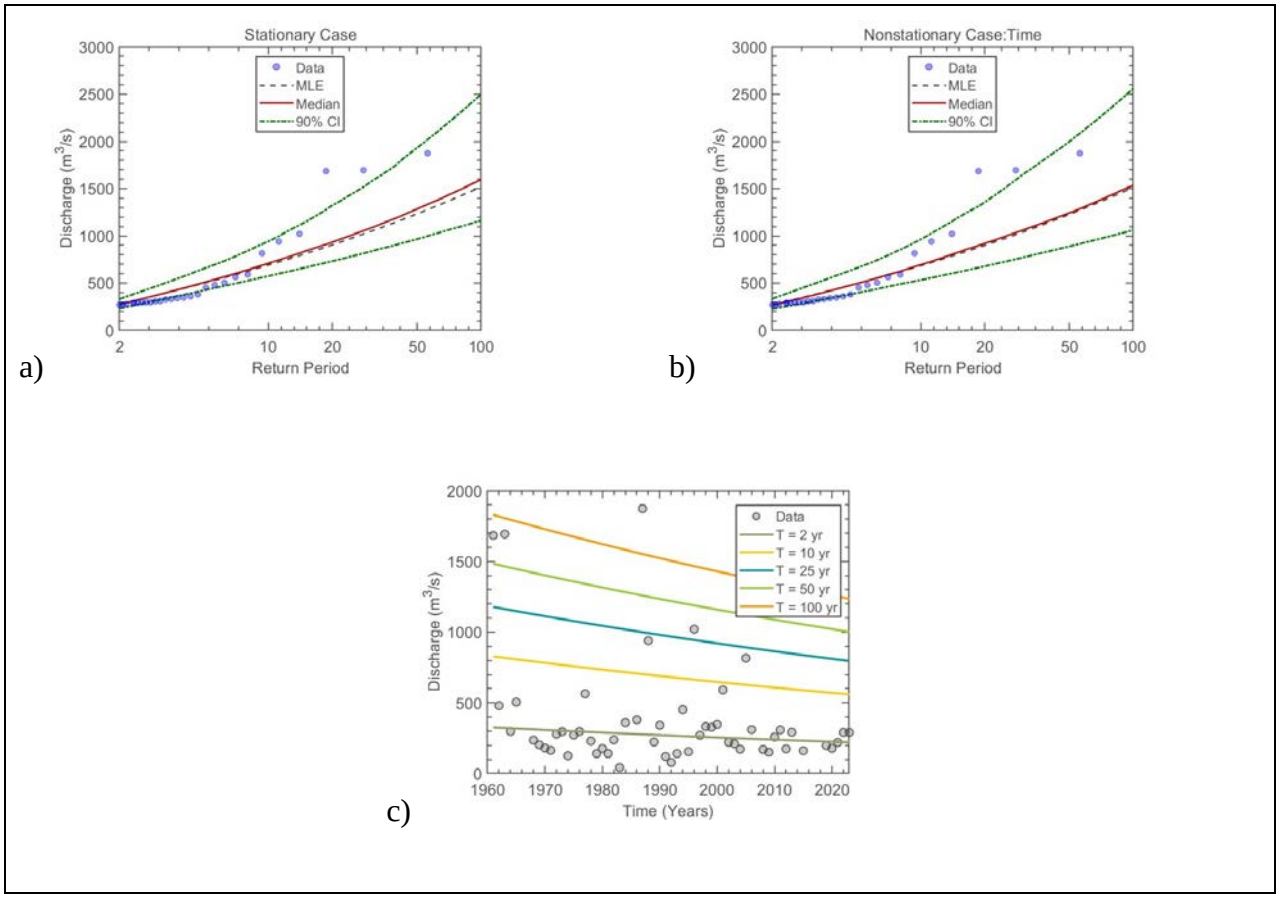

Figure 10.13 LP3 (a) stationary model, (b) non-stationary model considering time as a covariate, and (c) effective return period as a function of time for Station: W2H005

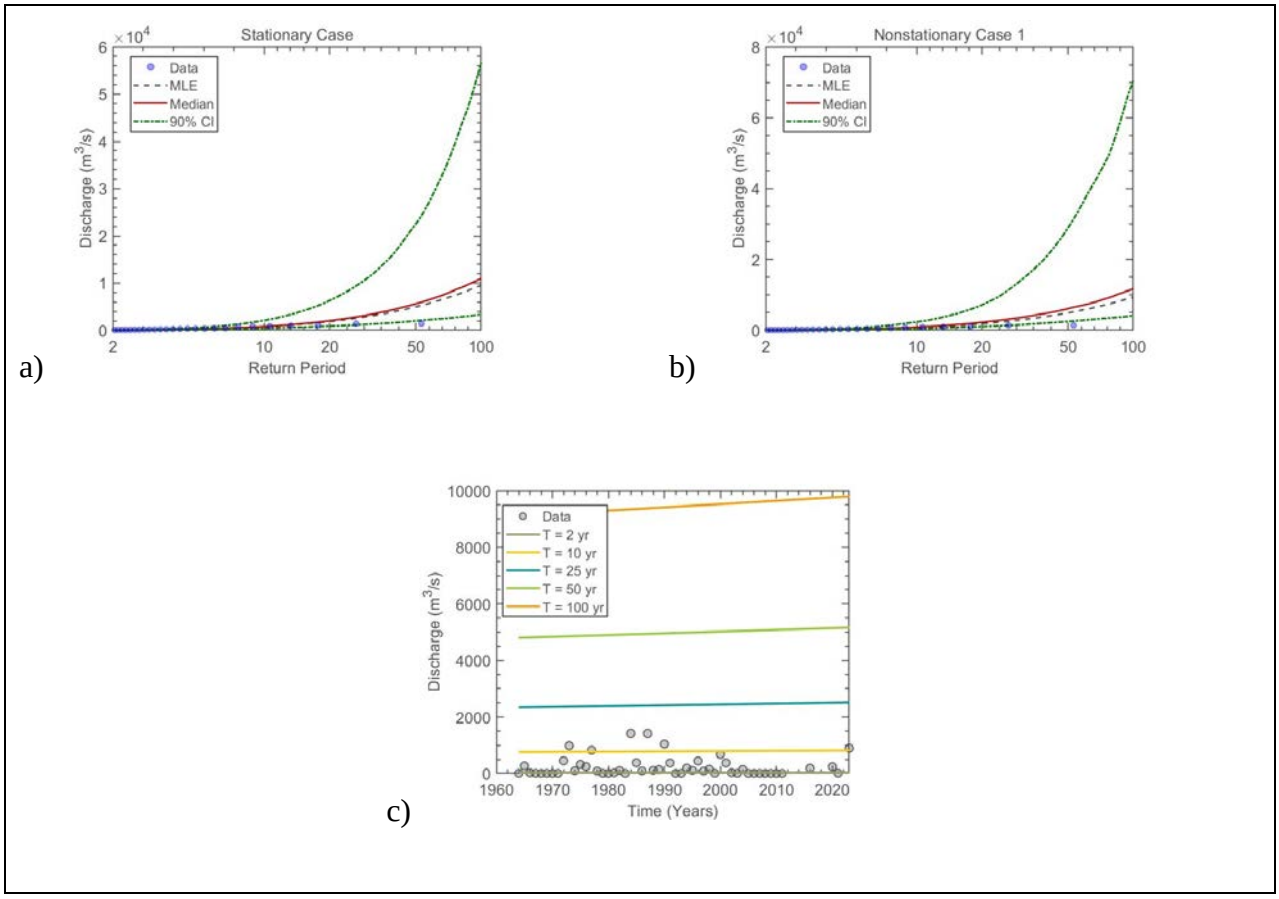

Figure 10.14 LP3 (a) stationary model, (b) non-stationary model considering time as a covariate, and (c) effective return period as a function of time for Station: W3H022

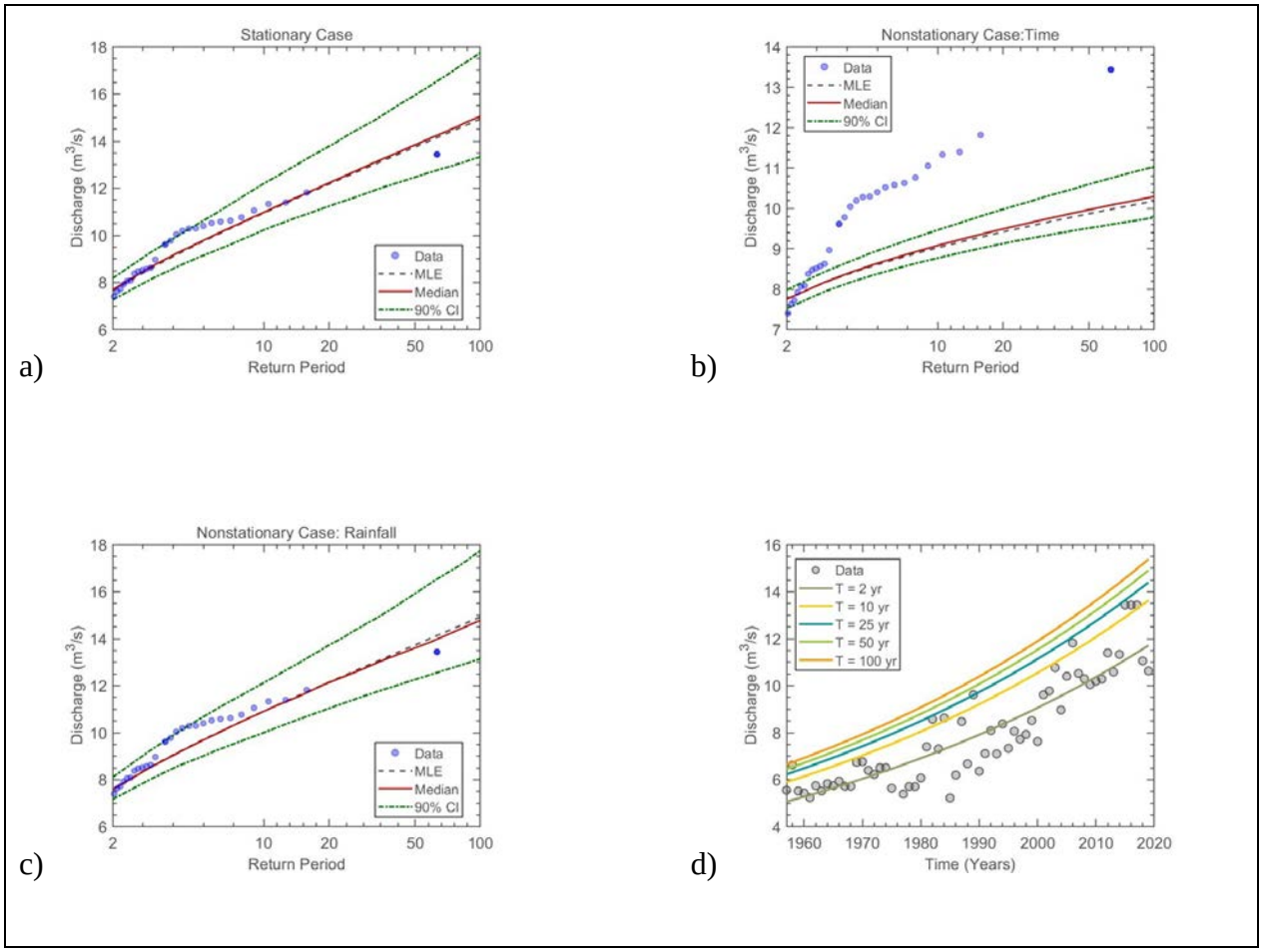

Figure 10.15 LP3 (a) stationary model, (b) non-stationary model considering time as a covariate, (c) non-stationary model considering rainfall as a covariate, and (d) effective return period as a function of time for Station:W4H012

Table 10.1 The LP3 statistical model performance criteria for all covariates

Station Number	Stationary			Non-Stationary Time			Non-Stationary Rainfall		
	AIC	BIC	RMSE	AIC	BIC	RMSE	AIC	BIC	RMSE
U3H001	107.06	**112.16***	19.71	**106.37***	113.12	**15.17***	107.83	114.59	20.74
U3H005	176.15	181.37	9782.30	168.51	175.45	404.24	**167.43***	**174.27***	**27.42***
V5H002	122.90	128.58	29.43	**108.19***	**115.76***	**11.72***	124.78	132.35	22.34
W1H009	168.59	174.44	32.37	164.98	172.80	**25.28***	**163.32***	**171.12***	641.57
W4H012	19.89	26.28	**22.27***	**-78.60***	**-70.09***	32.32	21.39	29.87	23.42

***Better performing model**